Assessing phytoplankton biogeography and photophysiology in the Atlantic Basin

Alex Robinson

A thesis submitted to the University of Oxford for the degree of Doctor of Philosophy in Earth Sciences

Supervised by Dr H. Bouman, Dr G. Tilstone & Dr S. Sathyendranath

Short abstract

Phytoplankton play a key role in the geochemical cycles of the Earth, are responsible for 50% of global carbon fixation, and through this, provide almost all of the energy for the entire marine trophic system. Understanding the dynamics of phytoplankton, and the species composition in relation to environmental factors is therefore of great importance. In this thesis a range of techniques to identify phytoplankton groups that use accessory pigment data obtained from high performance liquid chromatography are compared. While fixed indicator pigment:chl-*a* ratio approaches provide a quick and simple way of estimating phytoplankton distributions either on the basis of size-class or taxonomic group, the more sophisticated iterative approach of CHEMTAX divides the biomass into more categories and allows more flexibility to adapt to changes in indicator pigment:chl-*a* ratios caused by environmental variability. Combined with flow cytometric cell counts, depth-dependent trends in the intracellular concentration and composition of phytoplankton pigments can be identified. These data show an exponential decrease in the ratio of carbon-to-chlorophyll with depth, in response to decreasing light intensity. The relative as well as absolute concentrations of phytoplankton pigments are also seen to change with depth, particularly under stratified conditions, with the ratio of zeaxanthin to chlorophyll-*a* decreasing with increasing depth, and the ratio of chlorophyll-*b* to chlorophyll-*a* increasing. Cluster analysis is used to identify the main phytoplankton populations in the North West Atlantic, with communities of large, fucoxanthin-containing phytoplankton dominating in spring when mixing is strong, before being replaced by smaller cells upon the onset of stratification. The links between trends in phytoplankton photophysiology and abiotic conditions are also explored, with temperature being found to be the most important forcing factor. Size-class specific relationships between phytoplankton photosynthetic rates and temperature are identified, with the potential for use in remotely-sensed models of primary production.

Extended abstract

Photosynthesis by marine phytoplankton plays a key role in the carbon cycle, and is responsible for the fixing of around 50 Pg of carbon per year, around half of the global net primary production. Phytoplankton are exceedingly abundant, with a total population of approximately $2.9x10^{27}$ individuals (Whitman *et al.*1998), with some 5000 species identified (Sournia *et al.* 1991) and range in size from the cyanobacterium *Prochlorococcus* which have a diameter of less than 1 μm, to diatom species which can reach up to 1000 μm in length (Jiang *et al.* 2005).

The first two results chapters focus on determining what phytoplankton are present in a sample and the factors governing their successional dynamics, by using pigment-based methods of identification, or by gaining an understanding of the successional dynamics of an area. A range of techniques using the concentration of phytoplankton accessory pigments as measured by high performance liquid chromatography (HPLC) have been developed to estimate the taxonomic composition of natural samples. In Chapter 2, three different methods, two of which use fixed pigment:chl-*a* ratios and one which allows variable pigment:chl-*a* ratios, are compared using data from the Atlantic Gyres. Uitz *et al.* (2008) developed a simple and widely used method to divide the biomass of a sample into three size classes – microphytoplankton (> 20 μm), nanophytoplankton (2-20 μm) and picophytoplankton (<2 μm) using 7 diagnostic pigments (size-class approach). Since this method is so frequently used, it will be included in all chapters as the pigment standard against which more complex or specialised approaches are compared. The method of Bidigare & Ondrusek (1996) divides biomass into taxonomic groups (taxa-based approach) and represents an attempt at a more sophisticated approach, as an extra stage of calculation is included to try and counter the

problem of many indicator pigments appearing in more than one phytoplankton group. While the fixed pigment ratio approaches of Uitz *et al.* (2008) and Bidigare & Ondrusek (1996) may be simple to implement, they are unable to take into account changes in phytoplankton pigment ratios caused by variability in the physiochemical environment, and so may produce inaccurate results outside of the conditions for which they were configured. CHEMTAX uses iterative matrix factorisation to estimate the taxonomic composition of a sample, where at each iteration, the pigment:chl-*a* ratios are modified until the combination which leaves the smallest residual errors is found. Prior to analysis, samples were divided into high-light (HL) and low-light adapted (LL) samples on the basis of the zeaxanthin:chl-*a* ratio, which may be considered as indicator of the photoacclimatory status of the Subtropical Gyre populations. Overall correlations between the estimates of biomass distribution for the different methods are robust, though the size-class based approach appeared to overestimate the importance of microphytoplankton in highly oligotrophic waters, whereas the taxa-based approach produced a number of negative biomass estimates for the prokaryotic class. CHEMTAX also displayed potential errors, assigning a significant proportion of the total biomass to *Synechococcus* at depths where flow cytometry counts indicated their abundance to be low. Significant correlations between the chl-*a* biomass estimates for nanophytoplankton and eukaryotes as counted by flow cytometry were found for all methods, and light regimes. Significant relationships were also found between picophytoplankton biomass from Uitz *et al.* (2008) and prokaryote cell counts from flow cytometry (*Prochlorococcus* + *Synechococcus*) and between prokaryote biomass estimated using the taxa-based approach and prokaryote cell counts. CHEMTAX divides the prokaryote biomass into *Prochlorococcus* and *Synechococcus*, with significant correlations seen between *Prochlorococcus* biomass and cell counts for both HL and LL samples, but not for *Synechococcus* in either HL or LL samples. Depth-dependent trends in phytoplankton pigment concentrations were also observed, with the ratio of chl-*b* to

chl-*a* increasing with depth, and the carbon-to-chlorophyll ratio decreasing exponentially for *Prochlorococcus, Synechococcus* and picoeukaryotes.

While estimates of phytoplankton taxonomic distribution can be obtained using HPLC pigments, the ecological dynamics of phytoplankton are strongly influenced by the size structure of the population. Groups such as diatoms may have the same dominant pigments present in all species, but can vary widely in size and hence in ecological function. In Chapter 3 two possible approaches for estimating phytoplankton mean equivalent spherical diameter (MESD) are compared. Bricaud *et al.* (2004) adapted the size-class method used in Uitz *et al.* (2008) by assuming a MESD of 50 μm for microphytoplankton, 5 μm for nanophytoplankton and 1 μm for picophytoplankton to produce a rough estimate of sample MESD. Roy *et al.* (2011) used instead the ratio between the absorption of intact phytoplankton cells at a particular wavelength and the predicted absorption for the same concentration of pigments in solution to estimate the degree of pigment packaging and hence MESD. A strong correlation was seen between MESD as estimated by both the pigment- and absorption-based methods of estimating size, though the pigment-based approach resulted in a much higher overall MESD. Differences were also seen in the distribution of estimates of MESD, with the pigment-based approach resulting in a sharp peak between 40 and 50 μm, while the absorption-based method correlated more closely with the trends seen in previous studies, such as Irwin *et al.* (2006). Unsupervised hierarchical cluster analysis was used on chlorophyll-normalised pigment concentrations to identify successional trends amongst phytoplankton populations with respect to season, water-column stratification and temperature. Well-mixed conditions in spring and early summer were found to be associated with large cells, and high concentrations of fucoxanthin, and chlorophyll-*c1* and chlorophyll-*c2*. As stratification increased over the course of the summer these were replaced with populations dominated

by chlorophyll-*b*, 19'-hexanoyloxyfucoxanthin, 19'-butanoyloxyfucoxanthin and divinyl chlorophyll-*a,* whilst MESD decreased. As stratification decreased in autumn, MESD increased again, with high levels of alloxanthin indicating the presence of nanophytoplankton such as small flagellates and cryptophytes. A cluster dominated by peridinin was found to be present at relatively constant levels for all seasons. Differences in phytoplankton size and ecological function are also reflected in changes in phytoplankton photophysiology. Clusters dominated by large cells showed much shallower relationships between the mean absorption by phytoplankton averaged between 400 and 700nm and chlorophyll-*a* biomass than was seen for those dominated by small cells. From the cluster analysis on phytoplankton counts, different relationships were also seen between the slope of the photosynthesis-light response curve (α) and chlorophyll-*a* biomass and between the maximal photosynthetic rate (P_m) and chlorophyll-*a* biomass, with the large fucoxanthin-dominated populations displaying a shallow gradient, while the gradients of the relationships for clusters with a small MESD and highly stratified conditions were found to be much steeper. In contrast to previous studies, a strong positive correlation was seen between MESD and the maximal quantum yield of photosynthesis (φ_m) for all but one cluster.

As demonstrated in Chapter 3, phytoplankton physiology is strongly linked with size, therefore in Chapter 4, two different HPLC-based methods of identifying samples dominated by a single phytoplankton size-class were used in conjunction with the largest ever database of *in-situ* photosynthesis-irradiance (*PE*) measurements to derive size-class specific trends in *PE* parameters relative to abiotic forcing. The size-class approach of Uitz *et al.* (2008) was adapted by considering any sample with over 70% of biomass assigned to a single size class as dominated by that class. This approach was compared with the method of Sathyendranath *et al.* (2009), where a series of pigment-based criteria were applied to

identify and remove any samples with a mixed population. While the method of Uitz *et al.* (2008) performs well at apportioning biomass in mixed populations, it was less good at identifying samples dominated by a single phytoplankton size-class, and samples classified as picophytoplankton- or microphytoplankton-dominated occurring at much wider range of temperatures than using the approach of Sathyendranath *et al.* (2009). Both the maximal biomass-normalised photosynthetic rate (P_m^B) and the biomass-normalised initial slope of the photosynthesis-irradiance curve (α^B) were found to be strongly influenced by temperature, with little relationship observed with respect to nutrient concentrations, or average light within the mixed layer. An "envelope" approach was used to identify trends in phytoplankton photosynthetic parameters with the 10% and 90% quantiles being used to assess relationships with respect to temperature, where the 90% level representing the response to temperature under optimal conditions. Within-class relationships reveal that the size of the dominant phytoplankton group decreases as temperature increases, with microphytoplankton dominating in cold to temperate environments (below 7.5 ^{o}C), nanophytoplankton from 7.5 ^{o}C to 17.5 ^{o}C and picophytoplankton from 17.5 ^{o}C to the maximal temperature observed in this study of 26.3 ^{o}C. P_m^B for both nanophytoplankton- and microphytoplankton-dominated waters is strongly and positively correlated with temperature, whereas picophytoplankton display the opposite pattern. α^B displayed a positive relationship with temperature for microphytoplankton and a negative correlation for picophytoplankton. The light-saturation parameter E_k (defined as P_m^B / α^B) was positively correlated with temperature for all size classes. Principle component analysis (PCA) was used to assess the main abiotic forcings of the ecosystem on the photosynthetic parameters of the different size groups. Microphytoplankton were found to dominate in areas of high turbulence and nutrient concentrations positively correlating with chlorophyll concentration, whereas nano- or picophytoplankton were more abundant in stable stratified

zones with picophytoplankton abundance most closely linked with temperature and light, and nanophytoplankton abundance with P_m^B and α^B.

The results from this thesis will aid the use of pigment-based methods of identifying phytoplankton community structure, while the successional trends and physiological differences between phytoplankton populations identified in Chapter 3 can be used to help parameterise ecological models of phytoplankton distributions and energy flow. Given the importance understanding carbon fixation and energy flow in the marine system, the size-class dependent relationships between phytoplankton *PE* parameters and temperature are of great importance, as they will allow more accurate remote-sensing models of phytoplankton primary production and therefore promote understanding of the ecological dynamics of the open oceans.

Declaration

This thesis is the result of my own work. Any assistance and collaboration with others has been acknowledged. It does not exceed the page limit set out by the degrees committee and is not substantially the same as any work that has been, or is being submitted to any other university for any degree, diploma or other qualifications.

Alex Robinson

Acknowledgements

First and foremost I would like to thank my supervisors. Heather Bouman has been a constant source of inspiration and assistance during my time here and has guided me in terms of my analysis and writing, helping me to enjoy not only the world of phytoplankton, but also that of R. Essential aid in terms of the practical side of studying phytoplankton came from Gavin Tilstone, who also supervised me during data collection on the ECOMAR cruise and helped with advice and with my work down in Plymouth. Last but certainly not least, Shubha Sathyendranath has provided overall guidance for the project combined with an almost divine ability to instantly understand any scientific problem and suggest the best route forwards.

I would also like to thank those who have helped me with advice and data, in particular Jorn Bruggeman who provided climatological and modelling data for estimating irradiances and mixed layer depths, and Shovonlal Roy who helped with the mathematical side of my cell size calculations, who both never failed to be a source of cheerful advice. Data came from the Bedford Institute of Oceanography, the British Oceanographic Data Centre, Plymouth Marile Laboratory, and the Laboratoire d'Océanographie de Villefranche.

Finally I would like to give a big thank you to my family, Rachel and my friends for their love and support throughout my PhD and especially whilst writing up, restoring my confidence when the finished project seemed so far away, and to the Department of Earth sciences for being such a friendly and enjoyable place to be throughout my time here.

Contents

List of figures

List of tables

List of nomenclature

Pigments

19'-but:	19'-butanoyloxyfucoxanthin
19'-hex:	19'-hexanoyloxyfucoxanthin
allo:	Alloxanthin
β-car:	β-carotene
chl-*a*:	Chlorophyll-*a*
chl-*b*:	Chlorophyll-*b*
chl-*c1*:	Chlorophyll-*c1*
chl-*c2*:	Chlorophyll-*c2*
chl-*c3*:	Chlorophyll-*c3*
diad:	Diadinoxanthin
diat:	Diatoxanthin
DVchl-*a*:	Divinyl chlorophyll-*a*
DVchl-*b*:	Divinyl chlorophyll-*b*
fuc:	Fucoxanthin
HPLC:	High performance liquid chromatography
MVchl-*a*:	Monovinyl chlorophyll-*a*
MVchl-*b*:	Monovinyl chlorophyll-*b*
per:	Peridinin
viola:	Violaxanthin
wDP:	Weighted diagnostic pigment concentration. Used in the Uitz *et al.* (2008) size-based classification method, it is the weighted sum of all diagnostic pigments used.
zea:	Zeaxanthin

Photophysiology terms

α^B:	The initial slope of the photosynthesis-irradiance curve	[mg C mg Chl^{-1} hr^{-1} µmol photons]m^{-2}s^{-1}
E_k:	Light-saturation parameter	[µmol photons] m^{-2}s^{-1}
θ:	Carbon-to-chlorophyll ratio	[g/g]
φ_m:	The maximum realised quantum yield of photosynthesis	[mol C mol photons^{-1}]
PAR:	Photosynthetically-active radiation	[*E* m^{-1} d^{-1}]
P_m^B:	The maximum biomass-normalised photosynthetic rate	[mg C mg Chl^{-1} hr^{-1}]
***PE* parameters:**	Photosynthesis-irradiance parameters	

Absorption

a^*_{ci} **(676) :**	*In-vivo* absorption by chlorophyll at 676nm	[m^2 mg Chl-*a*$^{-1}$]
a^*_{cm}**(676):**	*In-vivo* absorption by cellular material at 676nm	[m^2 mg Pigment^1]
$a_d(\lambda)$ **:**	Detrital absorption at wavelength λ	[m^{-1}]
$a_p(\lambda)$ **:**	Particulate absorption at wavelength λ	[m^{-1}]
$\bar{a}^*_{ph}$:	Mean specific absorption by phytoplankton between 400 and 700nm	[m^2 mg Chl-*a*$^{-1}$]
Q^*_c **:**	Package effect index	[dimensionless]

Other biophysical variables

f_{micro}:	The proportion of phytoplankton biomass due to microphytoplankton	
HL:	High-light adapted samples	
LL:	Low-light adapted samples	
MESD:	Mean equivalent spherical diameter	[µm]
f_{nano}:	The proportion of biomass due to nanophytoplankton	

f_{pico}**:**	The proportion of biomass due to picophytoplankton	
δ*S*:	Stratification index	[°C m^{-1}]
***SI*:**	The size index (a rough estimate of the mean size of a population, obtained by assigning microphytoplankton a MESD of 50 μm, nanophytoplankton 5 μm and picophytoplankton 1 μm.)	[μm]

CHEMTAX

Ratio matrix:	The theoretical ratio of pigment to total chl-*a* for each group
Ratio limits matrix:	The amount by which each pigment ratio is allowed to vary
Epsilon limit:	Specifies the root mean square difference between measured and predicted pigment compositions during calculation. If the residual is less than this, the calculation is deemed to be complete
Iteration limit:	Maximum number of iterations
Cut-off step:	The calculation is deemed complete if the step size increases beyond this
Initial step size:	Indicates the amount to vary pigment ratio matrix with each iteration. E.g. value of 5 causes it to be varied by 1/5

Chapter 1: Introduction

1.1 The importance of phytoplankton

1.1.1 Phytoplankton and the carbon cycle

It is curious to think of our planet as "Earth" when over 70% of the surface is covered by water, containing up to 35,000 phytoplankton cells in a single drop (Gómez-Baena *et al.* 2008). Phytoplankton play a key role in linking marine productivity, ocean chemistry and atmospheric composition and are responsible for fixing 50 Pg C per year, around half of the net global carbon fixation by photosynthesis (Field *et al.* 1998), despite phytoplankton comprising only 0.2% of the global standing stock of photosynthetic biomass (Raven & Falkowski 2002). In addition to playing such a key role in the global carbon cycle, phytoplankton have dictated the composition of the atmosphere for the last 2.4 Ga (billion years ago). Before oxygenative photosynthesis evolved in cyanobacteria around 2.7 Ga, global rates of carbon fixation were around 450 to 4500 times lower than at present, and oxygen was almost completely absent from the atmosphere (Canfield 2005). Significant oxygenation of the surface waters had occurred by 2.4 Ga, and by 1.8 Ga the deep water systems were also oxygenic. Ever since this initial expansion of the phytoplankton resulted in the extinction of those species adapted to an anoxic lifestyle and their replacement with aerobic systems, phytoplankton have played a key role not only in providing the energy for marine ecosystems, but also in helping regulate global carbon fluxes.

1.1.2 Phytoplankton diversity and abundance

Marine phytoplankton are exceedingly numerous and diverse, with an estimated 5000 species globally (Sournia 1991), possibly far more if different strains of prokaryotic picophytoplankton are included (Pichard *et al.* 1997), and display a greater than 1500 fold range in size, with the smallest photosynthetic prokaryote *Prochlorococcus* being only 0.6 µm in diameter and the largest eukaryotes being over 1000 µm (Jiang *et al.* 2005). Such a range in lengths is comparable to that seen between a small ant and a human, so it is not surprising that the selective pressures acting on phytoplankton and their ecological functions vary greatly. Phytoplankton also contain some of the most abundant species on earth, with around 10^{23} individuals of the haptophyte *Emiliania huxleyi,* (Emiliani 1993) and a total of 10^{24} – 10^{25} nanophytoplankton (2-20 µm) and microphytoplankton (>20 µm) combined (Tett & Barton 1995). Prokaryotic groups are more numerous still, with around 10^{26} individuals of *Synechococcus* (Raven 1998), while *Prochlorococcus* is thought to be the single most abundant organism on the planet, capable of achieving densities of 700,000 /ml in the field, and with a possible worldwide population of around 10^{27} (Gómez-Baena *et al.* 2008). All these combine to give a worldwide total of all phytoplankton of up to 2.9×10^{27} individuals (Whitman *et al.* 1998). While it is through their vast abundance that such small organisms are of such global importance, their small size and rapid generation times make the study of phytoplankton physiology and ecology very challenging.

1.1.3 Phytoplankton and spatial scales

In addition to phytoplankton being highly diverse in terms of the number of species and size range, many key aspects of their ecology are very difficult to measure accurately. As cell sizes vary so widely, a uniform measure of biomass is required. In many ways cell carbon is highly suitable as it provides a good measure of energy flow in an ecosystem (Behrenfeld *et al.*

2005). In the context of phytoplankton however in practice it is very difficult to apply, since it is exceedingly difficult to distinguish between phytoplankton carbon, and that due to detritus or other heterotrophic species (Sathyendranath *et al.* 2009). Chlorophyll-*a* can be reliably and cost-effectively measured, can be sensed remotely, and is only associated with living cells (Mantoura & Llewellyn 1983). Chlorophyll is therefore used as a measure of biomass for the majority of phytoplankton studies, despite having a complex relationship with cell carbon as a function of photoacclimatory status, nutrient availability and cell size (Sathyendranath *et al.* 2009). Phytoplankton are also capable of very rapid generation times, with prokaryotes such as *Prochlorococcus* being capable of a generation time of less than a day in cultures (Partensky *et al.* 1999) and diatoms in culture being capable of dividing almost every 12 hours (Sunda & Huntsman 1997). In conjunction with the vast spatial scales over which ecological trends need to be considered, this makes accurate measurement of population dynamics far more difficult than for many terrestrial systems.

1.1.4 Phytoplankton and timescales

Despite the very short generation time of phytoplankton, it is important to consider all timescales on which phytoplankton have an effect. On very long geological timescales, the sinking of siliceous or calcareous phytoplankton is responsible for rock formation over large areas, and changes in the balance between siliceous and calcareous phytoplankton can have major impacts on the atmospheric CO_2 concentration (Murray & Wilson 1997). On shorter timescales, of thousands to hundreds of thousands of years, phytoplankton control a large fraction of the global fluxes in CO_2 and O_2, meaning that they dictate both atmospheric and ocean chemistry, as well as the long term global carbon cycle. Changes in atmospheric CO_2 concentrations can have major implications for climate and selective pressures on terrestrial

plants, while changes in ocean chemistry and pH strongly affect the selective pressures acting on a wide range of marine phytoplankton and fauna (Iglesias-Rodriguez *et al.* 2008). Certain phytoplankton affect regional climate even more directly, in the form of dimethyl sulphoxide (DMSO) production, which increases cloud formation (Charlson *et al.* 1987), and so decreases the amount of light reaching the surface. Understanding the variability in biomass, primary productivity and taxonomic groups present on a scale of days to years is vital for understanding trends higher up the trophic system, and management of key oceanic resources such as fishery stocks (Jennings & Brander 2010).

1.2 Studying phytoplankton

1.2.1 Growth and photosynthesis

Due to their small size, it is difficult to study the physiology of individual cells *in-situ*. Combined with the fact that many phytoplankton species are also very difficult to culture, in order to understand phytoplankton dynamics it is necessary to consider how mixed assemblages respond to environmental forcings. A range of approaches exist to assess phytoplankton production and growth. Growth rate (μ) is defined as the rate at which cells divide, usually expressed in divisions per day. This parameter is central to marine ecosystem models, but is very difficult to derive for natural populations. Moreover, as estimates of growth rate have dimensions of time they consequently do not provide any direct measure of fluxes of carbon or energy. For these reasons measurements of primary production are routinely made in the field. The first attempts to measure directly net photosynthetic rates compared changes in the concentration of oxygen in two identical samples of seawater, one subjected to light, the other in an opaque bottle (Gaarder & Gran 1927). For the most part

however this oxygen-based approach has been replaced with the more sensitive ^{14}C method first developed by Nielsen (1959). Samples are incubated with radio-labelled sodium bicarbonate, before being filtered, with the difference in the resultant level of radioactivity between the dark and light bottles providing a measure of light induced carbon fixation. ^{14}C incubations can be performed in a range of manners, either *in-situ* in the water-column, on deck or in, artificially-lit incubators.

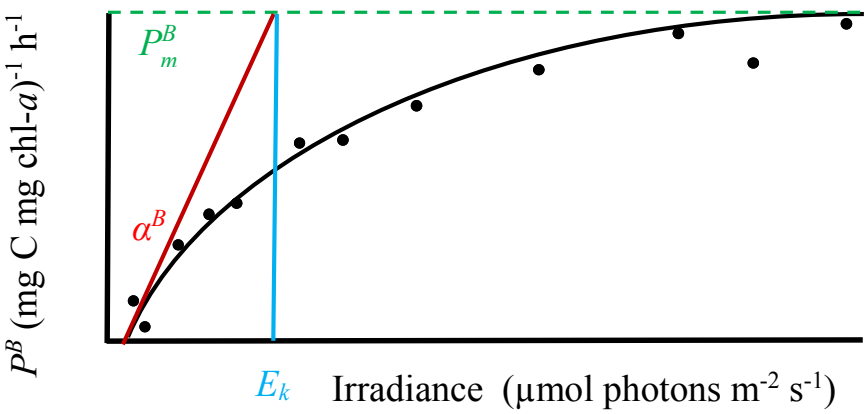

Fig 1.1. Simple photosynthesis - irradiance curve, showing maximal biomass-normalised photosynthetic rate (P_m^B), the biomass-normalised initial slope (α^B) and the light saturation onset parameter E_k. The curve is offset with respect to the origin due to the energetic costs of respiration.

The rate of production is closely linked with the light intensity to which the sample is subjected, initially showing a linear response before reaching a plateau (P_m^B) (Fig 1.1) (Platt & Jassby 1976). Very high irradiances can cause a decrease in the photosynthetic rate due to photoinhibition, as damage is done to the light-harvesting apparatus (MacIntyre *et al.* 2002). By normalising the *PE* parameters to biomass, samples from different regimes can be

compared, and secondary determinants of variability in phytoplankton primary productivity can be examined. To explain the energy flow through the marine system however, point measurements of the rate of primary production need to be linked not only with an understanding of phytoplankton distributions and dynamics, but also to how changes in the phytoplankton groups present can affect energy transfer to higher trophic levels

1.2.2 The effect of size

To accurately estimate marine primary production, spatial and temporal distribution patterns of the different phytoplankton groups need to be understood, as well as their biological responses to abiotic forcing. Even if reliable estimates can be made of both the phytoplankton biomass present and the rate of primary production, the fate of the fixed carbon can vary widely according to the size of the phytoplankton group responsible (Chisholm 1992). Large cells such as diatoms have a low surface-area-to-volume ratio, and hence following Stoke's law sink rapidly, and therefore form the majority of export to deep waters. Small cells such as cyanobacteria, conversely, have a very high surface area to volume ratio, and therefore have very low sinking rates (Bach *et al.* 2012). The slow rate of sinking means that their cellular contents are efficiently and rapidly remineralised and the carbon released, within the surface waters (Kiørboe 1993).

The size or taxonomic class of phytoplankton responsible for primary production has implications for energy flow to other trophic levels (Maury *et al.* 2007, Law *et al.* 2009). Biomass fixed by small cells tends to lead to a food web dominated by jellyfish and other macrozooplankton (Parsons & Lalli 2002), while that fixed by microphytoplankton favours zooplankton such as ciliates and fish larvae (Greve & Parsons 1977), meaning that even small seasonal or spatial changes in the distribution of differently sized phytoplankton can be of great importance in determining productivity and energy flow to higher trophic levels, such as

in determining fish recruitment (Platt & Fuentes-Yaco 2003). Once trends in phytoplankton distributions and productivity can be understood and monitored in the short term, this knowledge can then be used both to understand global fluxes of carbon and to predict the effects of altered CO_2 concentrations and climate change (Hays *et al.* 2005). Such effects can then be used to aid understanding in long-term models of water and atmospheric circulation and chemistry (Le Quéré *et al.* 2005). The challenges faced in understanding of trends in phytoplankton ecology and physiology occur at three stages. First, one must have the tools to measure accurately the phytoplankton biomass and taxa present at a given point in time and space. Second, using a large number of such observations, it is then necessary to identify the trends in phytoplankton distributions with respect to seasonality or physical forcing. Finally, once the distributions of the different phytoplankton groups are known, one can try to predict future physiological responses of different phytoplankton size or taxonomic classes to abiotic forcing.

1.2.3 Identifying phytoplankton – *in-situ* approaches

Unlike in many fields of terrestrial ecology, determining the species present in a water sample is far from a trivial problem due to the small size of phytoplankton cells. Initial studies such as Allen (1921) or Hardy *et al.* (1936) concentrated only on the largest diatoms and dinoflagellates, which could easily be sampled using a silk net. The Continuous Plankton Recorder (CPR) program, which has been running since 1931, provides a vast dataset of over 5 million miles of sampling and also uses silk nets with a mesh size of 270 μm. However this continuous sampling device is unable to capture many of the smaller phytoplankton (Warner & Hays 1994), which may range in size down to 0.6 μm (Raven 1998). Details about the phytoplankton population structure can also come from light microscopy. While this may allow for very precise identification (to species level) of certain phytoplankton groups, it is a

highly-skilled and time-consuming process. In addition, certain groups such as *Prochlorococcus* are too small to be identified using conventional light microscopy. Since *Prochlorococcus* is the most abundant organism on the planet (Raven 1998), such an omission is clearly a significant disadvantage. Finally, some groups such as nanoflagellates are destroyed during the fixing process and their omission further skews the resulting estimate of the phytoplankton taxonomic distribution (Bergesch & Odebrecht 2001). While using epifluorescence microscopy does allow the identification of prokaryotic phytoplankton, this process is even more time consuming than standard light microscopy analyses, and is not suitable for general application (Havskum *et al.* 2004).

If light microscopy is biased in favour of large cells and provides excessive detail at the cost of processing time, flow cytometry presents the opposite problems. Processing time is low, the degree of operator skill required is far lower than for microscope identification, and it is capable of distinguishing the main cyanobacterial genera from each other and eukaryotic cells. Unfortunately this method cannot enumerate large cells, with many flow cytometers having an upper size limit of 20 μm or less, and is unable to distinguish between various eukaryotic groups (Roy *et al.* 2011). Fluorescent *in-situ* hybridisation (FISH) probes have potential as all sizes of phytoplankton could be targeted equally, however doubts exist about the reliability of the method, since the efficiency of hybridisation may vary according to the phytoplankton group targeted (Nair *et al.* 2008).

Unlike either microscopy or flow cytometry, using High Performance Liquid Chromatography (HPLC) to measure the concentrations of key accessory pigments can be applied to all sizes of phytoplankton and used to estimate the taxonomic composition of the sample (Wright 2005). However, few phytoplankton groups possess unique indicator pigments, and when using this some assumptions are required in terms of the plasticity of pigment composition both within and between taxa (Gibb *et al.* 2001), rendering uncertainties

in its precision. A range of different methods have been devised to use HPLC pigment data, and some of these are considered in Chapter 2. In particular there is a trade-off between methods that are simple and widely used, and those which are more complex, potentially offering a more accurate and detailed assessment of the gross community structure of marine phytoplankton, at the cost of being more complicated to use and run the risk of introducing errors which are difficult to quantify. The simpler sort of approaches, such as those of Uitz *et al.* (2008), use fixed indicator pigment:chl-*a* ratios to estimate the chl-*a* biomass associated with a given concentration of an accessory pigment. More complex methods, such as CHEMTAX, use iterative routines to apportion the biomass due to different groups and are able to account for differing light regimes or other abiotic forcing factors such as nutrient availability which might alter pigment ratios, by using flexible accessory pigment:chl-*a* ratios.

1.2.4 Remote-sensing methods

i) Mapping phytoplankton distributions

The approaches described so far to assess phytoplankton distributions have all involved *in-situ* measurements of discrete water samples collected on-board scientific research vessels. Satellite remote sensing allows the distribution of phytoplankton to be monitored not only over a larger area, but at a higher temporal resolution. Since the launch of the Coastal Zone Colour Scanner (CZCS) in 1978, followed by the Sea-viewing WIde Field-of view Sensor (SeaWIFS) in 1997 and the MODerate-resolution Imaging Spectroradiometer (MODIS) in 1999, a range of algorithms have been developed to estimate phytoplankton biomass from ocean-colour observations. Estimates of surface chlorophyll concentration can be obtained from satellites, despite the water-leaving component of the signal reaching the sensor being as little as 5% of the total (Joint & Groom 2000). More recently, remote-sensing algorithms have been developed to detect key phytoplankton groups from satellite ocean-colour data (Alvain

et al. 2005, Sathyendranath *et al.* 2005).

ii) Mapping marine primary production

A range of models have also been developed to convert chlorophyll biomass estimates from satellites into rates of primary production (Carr *et al.* 2006, Friedriechs *et al.* 2009, Tilstone *et al.* 2009, Saba *et al.* 2010). The simplest models correlated surface chlorophyll concentration with ^{14}C analysis of depth-integrated production rates (Platt & Herman 1983). Empirical approaches were then developed using sea surface temperature to predict photosynthetic rate (e.g. Behrenfeld & Falkowski (1997a)). Semi-analytical wavelength-resolved models such as those of Platt & Sathyendranath (1988), Morel (1991), Longhurst *et al.* (1995), or Platt *et al.* (2008) use photosynthesis-spectral light relationships to predict photosynthetic rates either from sea surface temperature, or prior knowledge of P_m^B and α^B. Since phytoplankton size is so important in determining ecological function, the latest approaches such as that of Uitz *et al.* (2010) divide the overall estimate of primary production according to phytoplankton size-class.

1.2.5 Phytoplankton functional and ecological types

Before considering how changes in the abiotic conditions of the marine environment, e.g. nutrient concentrations, irradiance, temperature or the mixing regime, affect phytoplankton, it is important to consider the types of phytoplankton, their different responses to physical forcing and the ways in which their ecology varies. While size explains many of the differences between species, it is not responsible for variation. Despite the lack of physical barriers constraining the distribution of phytoplankton species, the taxonomic composition of field phytoplankton samples varies according to location and season. Given the large number of different species found globally, it is not possible to consider differences in their ecological

function independently, however macroecological patterns can be seen with respect to functional type, size or large-scale taxonomic group.

Functional type is defined in Nair *et al.* (2008) as a group of species that, irrespective of phylogeny, share similar traits, with silicifiers, calcifiers, dimethyl sulphoxide producers, nitrogen fixers and picophotoautotrophs being identified as the most important types. In the following section the key ecological properties of the main functional groups of phytoplankton are described.

Silicifiers

Silicifiers such as diatoms dominate the microphytoplankton (20 – 200 μm) size-class. By using silicate as opposed to organic cell walls, the cost of cell wall synthesis is greatly reduced (Raven 1982), allowing for increased growth rates, and a decrease in the energetic cost of forming large spines or other protuberances to increase apparent cell size as defence against predation (Hamm *et al.* 2003). The decreased strength of silicate cell walls per unit thickness as compared with those made of other substances (such as polyglycan) however means that they are thicker and so the overall density of the cell increases (Raven & Waite 2004). Combined with large mean cell sizes, the sinking rates for diatoms are very high. In stratified environments, this would constitute a major competitive disadvantage as cells are rapidly removed from the photic zone, however in highly turbulent areas this has been suggested as a possible competitive advantage since nutrient concentrations often increase with depth, and rapid re-suspension would counter the dangers of sinking (Raven & Waite 2004, Nair *et al.* 2008).

Calcifiers

The coccolithophores are a highly abundant group of prymnesiophytes and are characterised by external calcium carbonate plates. This group is responsible for the fixation of large quantities of carbonate from the water-column. They also sink rapidly due to their high

density, and as such are responsible for a large portion of the export of carbonate to the deep ocean, and play a key role in the long-term carbon cycle, and regulation of ocean acidity (Le Quéré *et al.* 2005). The energetic costs of calcification increase sharply as pH decreases (Riebesell *et al.* 2000), so given the current focus on the impact of increased atmospheric CO_2 concentrations understanding the global distributions of this group is of interest

DMS producers

Dimethyl sulphide acts as a cloud-nucleating agent and is released by a wide range of phytoplankton taxonomic groups (Nair *et al.* 2008). Phytoplankton are the main non-anthropogenic source of reduced sulphur in the atmosphere (Simó 2001), and hence play a major role in regulating ocean acidity. Since the albedo effect from clouds is an important aspect controlling global temperatures, the dynamics of DMS producers provide an important link between short-term phytoplankton ecology and long-term climatic trends (Charlson *et al.* 1987).

Nitrogen fixers

Nitrogen is frequently limiting in surface waters in the Atlantic (Barlow *et al.* 1993), hence any group capable of fixing dissolved N_2 into a biologically useful form will be at a significant competitive advantage, as well as having a major influence on the global nitrogen cycle (Gruber & Galloway 2008). The process is highly energy demanding, and very inefficient at low temperatures (Le Quéré *et al.* 2005) meaning that this group is predominantly found in warm, oligotrophic waters.

Picophotoautotrophs

This class includes all phytoplankton which are under 2 μm in diameter (Raven 1998), and includes both prokaryotic and eukaryotic species. Due to their very high surface-area-to-volume ratio, these small cells have a competitive advantage for acquisition of both light and nutrients compared to larger ones, as well as greater efficiencies of resource use (Raven

1998), though predation pressures are higher (Kiørboe 1993). The small size of picophotoautotrophs also means that sinking rates are very low, allowing them to remain in the photic zone for longer in low-turbulence waters, and that on death nutrients are rapidly remineralised as opposed to sinking out of the photic zone (Raven 1998).

1.3 Abiotic variables and phytoplankton distribution

1.3.1 Resource usage

Ancillary information on those abiotic factors that are known to govern the physiological ecology of phytoplankton groups is required to understand their biogeography whether they be categorised by their size-classes, taxonomic group or functional group. Margalef (1978) adapted the idea of *r*- and *K*-strategists to produce his mandala of phytoplankton ecological niches according to nutrient availability and turbulence, which has since been further used to describe global phytoplankton distributions (Estrada & Berdalet 1997, Bown 2005). *r*-strategists have evolved to be capable of very rapid reproduction in order to take advantage of episodic disturbances to the ecosystem. Turbulence in the water-column will result in deep, nutrient-rich water reaching the photic zone. Under nutrient replete conditions, inefficiencies of nutrient use do not constitute a selective disadvantage, so *r*-strategists or "opportunists" thrive, for example silicifiers such as diatoms. *K*-strategists or "gleaners" rely instead on very efficient use of resources, therefore favouring smaller cells with higher nutrient affinities (Tozzi *et al.* 2004). *K*-strategists are therefore found in more stratified, lower-nutrient conditions, and *r*-strategists in more mixed regions (Cermeño *et al.* 2008).

1.3.2 Size and selective pressures

The mean size and dominant functional type of phytoplankton in a sample is dictated by a combination of nutrient availability, predation and turbulence. In regions where mixing is strong and *r*-strategists are favoured, large cell size is a competitive advantage. Large organisms are rarer than small organisms in the marine system, both in terms of abundance, and biomass (Platt 1985), so as the size differential between zooplankton grazer and phytoplankton prey remains relatively constant across the size spectrum, steady-state predation pressures are lower for large cells (Kiørboe 1993). Large cells such as diatoms also possess vacuoles containing nutrient reserves, which can be filled during turbulent periods when nutrient concentrations are high (Falkowski & Oliver 2007). When light intensities increase as the depth of mixing decreases, conditions become favourable for growth leading to the formation of phytoplankton blooms (Sverdrup 1953). While relative growth rates decrease with increases in size for all plankton classes, the effect is greater for zooplankton than phytoplankton (Sheldon & Parsons 1967, Platt 1985). This will mean that the grazer population response time to a phytoplankton bloom will be greater as mean cell size increases, further increasing the competitive advantages for large cells (Ward *et al.* 2012). When stratification is strong and nutrients are scarce, *K*-strategists are favoured and the selective pressures acting on cell size instead benefit the smallest cells (Falkowski & Oliver 2007). Under nutrient-limiting conditions, the efficiency of nutrient uptake increases and the half-saturation constant decreases as the average cell size decreases (Kiørboe 1993). Sinking rate also decreases, which under stratified conditions offsets the increase in predation pressure conferred by small cell size (Kiørboe 1993).

1.3.3 Stratification and nutrients

Phytoplankton distributions often vary on a latitudinal or spatial basis, but are in fact controlled by abiotic forcing factors, in particular nutrients, light and stratification (Gibb *et al.* 2000, Marañon *et al.* 2000). The degree of stratification is dictated by the balance between solar heating and mixing, mainly by winds. A warm surface layer is formed which floats above the colder deep water, with the density difference preventing fluxes between the two water bodies. Since nutrients cannot be replenished from deep water reserves, they are rapidly depleted by phytoplankton. In tropical waters, the degree of solar heating is high and continues all year round, resulting in a deep and very strong permanent thermocline, meaning that nutrients lost cannot be replaced, resulting in a highly oligotrophic surface layer. In temperate latitudes, the strength of sunlight is weaker and more seasonal, meaning that during winter the thermocline breaks down and nutrient-rich water is brought to the surface. During late spring to summer, as the solar elevation increases, a stratified surface layer forms (though this is never as extreme as in tropical regions) before stratification breaks down again as the depth of mixing increases in autumn to winter. Such seasonal trends are considered in detail in Chapter 3. There are however certain exceptions to this general rule linking nutrient availability to season and latitude. Areas of upwelling, such as the western margins of continents or around the equator, can result in nutrient-rich deep waters being brought to the surface, even at low latitudes. In addition, coastal waters are strongly affected by riverine input, and arctic regions by ice melting. This thesis is focussed on open-ocean regions, however, and coastal and arctic conditions are not considered.

1.3.4 Light

Irradiance is strongly linked with latitude, depth and season, and controls the rate of photosynthesis. Below a threshold light intensity, the photosynthetic rate is directly and

linearly related to irradiance, before gradually reaching a plateau above this threshold (Platt & Jassby 1976). However, excessive light lowers the photosynthetic rate due to photoinhibition and leads to an increased investment in the synthesis of photoprotective pigments (Raven 2011). At high latitudes during the winter, mixing is strong, frequently extending below the photic zone, meaning that cell pigmentation is adapted to harvest a low photon flux density with high efficiency. Conversely, under very stratified tropical conditions, phytoplankton populations at different depths in the water-column are exposed to a range of light intensities. This is reflected in the depth-dependence of intracellular chlorophyll concentrations, with high chlorophyll per cell at the bottom of the photic zone and low chlorophyll per cell at the surface. Moreover vertical variability in the relative concentrations of photoprotective pigments is also seen, with surface samples having higher concentrations of photoprotective pigments such as zeaxanthin than deep samples (Bouman *et al.* 2000). The change in pigment composition may be the result of photoadaptation by the one strain of phytoplankton, or the replacement of one taxonomic group by another. Some situations are so stable and stratified that genetically distinct strains of the same species have evolved according to depth, even to the extent that the deep populations lose the ability to protect against damaging irradiances (Moore & Chisholm 1999). As with nutrient acquisition, light-harvesting efficiency increases as cell size decreases. This is due to the package effect, whereby decreased self-shading means lower intracellular chlorophyll concentrations are required (Morel & Bricaud 1981), further decreasing the energetic costs associated with small cells (Raven 1998).

1.3.5 Temperature

Temperature affects phytoplankton distributions and responses both directly and indirectly. Direct influence on phytoplankton photosynthetic rates comes from the effect of changing temperature on the rate of enzyme-catalysed reactions, where rates increase with rising

temperature (Raven & Geider 1988). A range of studies have demonstrated increases in photosynthetic rate as a function of temperature for both culture- (Eppley 1972, Geider *et al.* 1997) and field-based (Behrenfeld & Falkowski 1997a) studies. Temperature has also been found to affect the rate of nutrient uptake (Aksnes & Egge 1991), with increased rates being observed as temperature increases. In nature, however, the relationships between temperature and photosynthetic rate are far more complex, as temperature rarely varies independently from other forcing factors. Behrenfeld & Falkowski (1997a) observed that the optimal chlorophyll-normalised photosynthetic rate (P_{opt}^{B}) reached a maximum at around 25ºC, before decreasing sharply, and is due to the links between temperature and other abiotic variables such as irradiance and stratification. Fortunately, unlike the degree of stratification, temperature can be measured remotely by satellites, making it a very valuable variable for large scale modelling of phytoplankton dynamics.

1.4 Motivation for this study

The results presented in this thesis investigate large-scale trends in the distribution and physiology of phytoplankton in Atlantic Basin. In order to understand the ecological dynamics of a system, it is first necessary to identify the organisms present. Owing to the nature of phytoplankton such identification often represents a trade-off between the detailed taxonomic information provided using light microscopy and indices of the gross composition of phytoplankton cells using HPLC pigment-ratio methods. HPLC pigment approaches usually involve applying uniform ratios across vast areas of the global ocean (e.g. Uitz *et al.* 2010), despite known variations in pigment complement due to different species being present, nutrient status and photoacclimation. Yet, no matter how well suited a particular set

of fixed pigment-ratios may be for the initial calibration study, when applied to different areas significant errors in the estimation of taxa-specific biomass may arise. In Chapter 2, two widely-used fixed pigment-ratio approaches are compared with the far more complex CHEMTAX variable pigment-ratio method. Samples were taken from the Subtropical Gyres as the mean cell size is low in such areas, meaning flow cytometry counts of phytoplankton abundance can be used to estimate phytoplankton biomass in order to assess the performance of the various pigment-based methods. The aims for Chapter 2 are:

1. To assess which method of estimating phytoplankton groups using HPLC pigments provides the most accurate results.
2. To identify potential sources of error in each of the approaches and so aid their use in other studies.
3. To assess trends in phytoplankton intracellular pigment concentration and thereby assess the importance of photoacclimation in interpreting HPLC pigment data.

While the Subtropical Gyres of the Atlantic Basin are a stable system, with only a weak effect of seasonality, the North West Atlantic shows a high degree of temporal variability in physical forcing, and very strong successional pattern in species composition. In order to understand how the relative importance of different phytoplankton populations changes with time, cluster analysis on chlorophyll-normalised accessory pigments is used to identify the different phytoplankton populations present. Unlike the HPLC taxonomic approaches considered in Chapter 2, this method does not aim to identify the groups present, but to establish which samples are most similar to each other, allowing distinction between populations with different pigment signatures. The clusters identified are assessed as a function of seasonality, stratification and size. Since size is an important indicator of ecological function, an absorption- and a pigment-based approach to estimating phytoplankton size are compared. The aims for Chapter 3 are:

1. To identify distinct clusters of samples using HPLC pigments.
2. To compare estimates of mean phytoplankton size obtained using HPLC pigments and phytoplankton absorption.
3. To assess how phytoplankton succession and size are related to stratification.
4. To identify physiological and size-based differences between the different phytoplankton pigment clusters.

In order to parameterise the next generation of remote-sensing productivity models, and aid the understanding of energy flow through the marine ecosystem, it is necessary to identify the phytoplankton groups present at a given point and their contribution to primary production. Culture studies have shown that phytoplankton *PE* parameters are strongly linked with abiotic forcing (nutrients, light and temperature), yet the nature of these relationships will change according to the phytoplankton group in question. Since it is rare for a single phytoplankton group to dominate a sample in nature obtaining size-specific trends in phytoplankton *PE* parameters from mixed populations is difficult. This study uses a large database of phytoplankton *PE* parameters and HPLC pigment concentrations so two pigment-based approaches for identifying samples dominated by a single size class can be compared, and the relationships between the *PE* parameters and environmental variables such as temperature for a single size-class can be examined. These relationships can be used to aid parameterisation of remote-sensing models, and are an improvement on existing models which assign a single *PE* parameter to a phytoplankton group, regardless of the conditions. The aims for Chapter 4 are:

1. To compare two HPLC pigment-based approaches for identifying instances of dominance by a particular phytoplankton size- or taxonomic-class
2. To identify class-specific trends in phytoplankton *PE* parameters.
3. To determine relationships between phytoplankton *PE* parameters and abiotic variables according to size-class.

Chapter 2: A comparison of pigment-based methods of studying phytoplankton community structure in the Atlantic Subtropical Gyres

2.1 Abstract

Three different approaches based on HPLC accessory pigment concentrations were used to estimate the community structure of phytoplankton from the Atlantic Gyres. The effectiveness of the size-based and taxa-based fixed pigment:chl-*a* methods was compared with the more complex variable pigment:chl-*a* ratio approach of CHEMTAX (an iterative matrix factorisation Matlab routine). Samples were first separated into high-light adapted (HL) and low-light adapted (LL) on the basis of their zeaxanthin:chlorophyll-*a* ratio, before the biomass estimates from each method were compared with flow cytometry counts. LL samples were found to contain significantly more chlorophyll-*a* / cell than HL for all phytoplankton classes and for all three approaches. Significant correlations were seen between the combined biomass estimates for pico- and nanophytoplankton and picoeukaryotes as counted by flow cytometry for all approaches and depths. Unlike the other two methods, CHEMTAX divides the estimate of prokaryote biomass into *Prochlorococcus* and *Synechococcus*, with significant correlations seen for both HL and LL *Prochlorococcus*. No relationship was seen for *Synechococcus* in either HL or LL classified

samples. Significant differences in the biomass assigned to different phytoplankton classes according to method were seen, with the size-based method giving higher microphytoplankton estimates than CHEMTAX for HL and LL samples. Prymnesiophyte biomass was higher for the taxa-based method than from CHEMTAX for HL and LL samples, but HL and LL pelagophyte along with HL prokaryote biomass was found to be lower using the taxa-based approach. The ratio of chl-*b*:chl-*a* was found to increase as depth increased, while the ratio of carbon-to-chlorophyll decreased with increasing depth for *Prochlorococcus*, *Synechococcus* and eukaryotes.

2.2 Introduction

2.2.1 Phytoplankton distributions

Phytoplankton are known to vary widely, both in size and functional type. The combination of different sizes and classes is known to be a major determinant of the fluxes of fixed carbon, either by sinking, or via grazing and support of higher trophic levels (Greve & Parsons 1977). Phytoplankton found in the Atlantic Basin vary widely in both species, and size. The North Atlantic Gyre has been extensively studied, but understanding of the spatial and temporal variations in the size and taxonomic composition of phytoplankton communities is still limited (Marañon *et al.* 2001). Previous studies of the Atlantic Basin have identified trends in changing taxonomic composition of phytoplankton with respect to either latitude, mixing regime or biomass (Estrada & Berdalet 1997, Brown *et al.* 2002, Tarran *et al.* 2006). Large cells, such as diatoms, tend to dominate primary production in high-biomass, high-latitude areas (Estrada & Berdalet 1997). Such regions are associated with strong mixing and a weak, seasonal thermocline, while nutrient-poor strongly stratified areas such as the Subtropical Gyres are characterised by small prokaryotic species (Raven 1998, Marañon *et al.* 2001, Grob *et al.* 2007). On a large spatial scale, a cost-effective and accurate method of identifying phytoplankton groups would be of great use to biogeochemical modellers as it would facilitate the classification of samples according to the species present, which in turn can be used to derive group-specific characteristics such as photosynthetic rates. At a more regional level it could allow an in-depth understanding of key ecological and successional patterns. Due to these benefits, a wide range of approaches to identifying phytoplankton groups should be considered, since microscope-count data is limited in abundance and can only provide part of the picture.

2.2.2 Microscope-based taxonomic approaches, flow cytometry and genetic probes

Microscope taxonomy requires high levels of skill and is exceedingly time consuming and costly. Owing to the very short generation times of phytoplankton and large scale spatial variation it would not be possible to assess the phytoplankton dynamics of the Atlantic Basin using microscopy. As a further practicality, many groups are fragile and are damaged or destroyed in the fixing process, resulting in an incomplete representation of the biomass present (Bergesch & Odebrecht 2001). In particular small, phytoplankton (< 2 μm) are often responsible for a large proportion of production in open-ocean waters and are exceedingly difficult to identify by light microscopy owing to the lack of external morphological features, while electron microscopy based approaches are impractical for large numbers of samples (Partensky *et al.* 1999). Flow cytometry can rapidly enumerate the abundance of small cells, but is unable to give detailed taxonomic information on eukaryotic pico- and nanophytoplankton. Tools such as epifluorescence microscopy (Havskum *et al*. 2004) and fluorescence *in-situ* hybridisation (FISH) probes can also be used (Simon *et al.* 1995), but are also time consuming and costly. The absorptive properties of the sample can give an indication of the size structure but again less about the taxonomic composition (Ciotti *et al.* 2002), though some recent work has attempted to estimate pigment concentrations using a Gaussian decomposition of phytoplankton absorption spectra (Hoepffner & Sathyendranath 1993, Moisan *et al.* 2011).

2.2.3 Identifying phytoplankton using phytoplankton pigment data from HPLC

Phytoplankton pigments are routinely measured using High Performance Liquid Chromatography (HPLC) and are a cost-effective way of assessing community structure of a large number of samples. They have the further benefit that the analysis is quick and can be performed in a consistent manner, with a 7% variation in chl-*a* concentrations and 21.5% for

accessory pigments found in samples analysed by four laboratories using different pigment extraction methods (Claustre *et al.* 2004). A range of pigment-based approaches have been developed, (Gieskes *et al*. 1988, Everitt *et al*. 1990, Letelier *et al*. 1993, Mackey *et al.* 1996, Bidigare & Ondrusek 1996, Vidussi *et al.* 2001, Uitz *et al.* 2006, 2008, Van den Meersche 2008, Sathyendranath *et al*. 2009) by which HPLC data can be used to obtain taxonomic information about the phytoplankton groups present, including fragile groups such as flagellates or sub-micron ones such as *Prochlorococcus* (Gibb *et al.* 2001).

2.2.4 Phytoplankton accessory pigments

Different phytoplankton groups use a wide range of pigments, both for light-harvesting and photoprotection (Wright *et al.* 1997). For example, *Prochlorococcus* contains the divinyl form of chlorophyll-*a*, peridinin is a marker for dinoflagellates and alloxanthin occurs in cryptophytes. The relative importance of each taxonomic class can therefore be estimated using the ratio of key accessory pigments to chl-*a* (Gieskes *et al.* 1988). The approaches vary greatly in their complexity and in the number of diagnostic pigments used, but can be divided according to whether the ratios of accessory pigment to chl-*a* are fixed, or can be tuned to account for photoacclimatory changes in pigment composition. It is however difficult to estimate the contribution of a particular taxonomic class towards the total biomass with perfect accuracy whichever method is being used, as few phytoplankton groups possess unique marker pigments (Wright *et al*. 1997). For example, fucoxanthin is the main indicator pigment used for diatoms, but is also present in prymnesiophytes and chrysophytes. This problem is further compounded by the flexibility phytoplankton show with regard both to absolute intracellular pigment concentrations and to their relative abundances, with a large degree of variation being seen in the relative importance of different pigments within a phytoplankton group due to the light regime to which they are adapted (Partensky *et al.*

1996).

2.2.5 Light-dependent trends in phytoplankton pigment concentrations

Low-light adapted (LL) populations contain much higher quantities of chl-*a* / cell than high-light (HL) adapted ones, since as the photon flux density decreases greater intracellular pigment concentrations are required to harvest the same amount of light (Geider *et al.* 1997). Blanchot *et al.* (2001) reported an 11-fold increase in chl-*a* / cell for eukaryotes and a 4-fold increase in the concentration of divinyl chlorophyll-*a* (DVchl-*a*) per *Prochlorococcus* cell with decreasing light levels. Such variation in intracellular pigment concentrations causes the large range of carbon-to-chlorophyll ratios in natural samples (Llewellyn *et al*. 2005), and means comparison between carbon-based and chlorophyll-*a*-based estimates of phytoplankton biomass hard to make. The carbon-to-chlorophyll ratio (θ) is difficult to measure using direct approaches (Sathyendranath *et al*. 2009), and is key in converting biomass-normalised photosynthesis-irradiance parameters to phytoplankton growth rates and hence is of great interest to satellite oceanographers, as well as biogeochemical and ecological modellers.

2.2.6 Light-dependent trends in phytoplankton pigment composition

Changes in intracellular pigment composition with respect to light regime vary across different pigment groups. HL samples have much higher chlorophyll-normalised intracellular concentrations of non-photosynthetic pigments such as zeaxanthin, as compared with LL samples, with Babin *et al.* (1996) and Bouman *et al*. (2000) finding the chlorophyll-normalised zeaxanthin concentration to be inversely correlated with depth. The ratio of chlorophyll-*b* (chl-*b*) to chl-*a* is also seen to vary widely according to light regime (Bouman *et al.* 2000), with much higher levels seen in LL samples. Blanchot *et al.* (2001) reported a 4-fold increase in the ratio of chl-*b*:chl-*a* in picoeukaryotes, and a 14-fold increase in the ratio of

DVchl-*b*:DVchl-*a* in *Prochlorococcus* from the surface to 150 m. While in many groups these changes in intracellular pigment concentration and composition are a result of photoacclimation, in stable, stratified regions where the picocyanobacterium *Prochlorococcus* dominates, these vertical changes in intracellular pigment composition may be enhanced by the presence of genetically-distinct ecotypes (Moore *et al.* 1995, Moore *et al.* 1999). This study aims to assess the effectiveness of a range of pigment-based approaches used in chemotaxonomic studies outlined below in estimating phytoplankton taxonomic composition and size structure, and then to use these approaches to examine trends seen in the latitudinal distribution of phytoplankton across the Atlantic Subtropical Gyres.

2.2.7 Fixed pigment:chl-*a* ratio methods

2.2.7a Size-class method of Uitz *et al.* (2008)

Uitz *et al.* (2008) built on the model of Vidussi *et al*. (2001) to apportion biomass into 3 size-classes – microphytoplankton (>20 μm), nanophytoplankton (2-20 μm) and picophytoplankton (<2 μm). Thus, the approach can be classified as a size-based fixed pigment:chl-*a* ratio method. Seven diagnostic pigments are used, each with a weighting coefficient derived from a multiple linear regression analysis on a global dataset (Uitz *et al.* 2006). The proportion of chlorophyll biomass in each size-class is estimated by dividing the sum of the weighted accessory pigments associated with that class by the sum of all seven weighted diagnostic pigments. While this method is widely used as it is quick and simple to implement, it has certain drawbacks. In addition to the inherent limitations of fixed-pigment ratios, many taxonomic groups cover wide size ranges (Aiken *et al.* 2008), consequently care needs to be taken to ensure the resulting size classes are representative of the study area.

2.2.7b Taxonomic based method of Bidigare & Ondrusek (1996)

Although pre-dating the technique of Uitz *et al.* (2008), the method described by Bidigare & Ondrusek (1996) represents a more complex approach to assigning phytoplankton biomass, and produces taxonomic- rather than size-based groups (taxonomic-based fixed pigment:chl-*a* method). As with the size-based approach of Uitz *et al*. (2008), fixed ratios are used to convert concentrations of key indicator pigments into biomass estimates. The problem of pigments being found in more than one phytoplankton group is addressed using a second stage of calculation, in which the shared accessory pigments are assigned to phytoplankton classes, before using these new class-specific values to assign chl-*a* biomass. Both the methods of Uitz *et al.* 2008 and Bidigare & Ondrusek (1996) however depend on the fixed pigment:chl-*a* ratios being appropriate for a given dataset.

2.2.8 Variable pigment ratio methods - CHEMTAX

While fixed pigment-ratio methods may be simple to implement, they are limited either in terms of accuracy or scope. Variations observed in phytoplankton pigment ratios according to light regime or the changes in the species present mean for the approach to be entirely reliable calibration against microscope counts is required. CHEMTAX, a far more powerful and flexible approach to using pigment:chl-*a* ratios, was developed by Mackey *et al.* (1996), utilizing an iterative routine. Here matrix factorisation is used to estimate the contribution to total biomass of different phytoplankton taxa. An initial seed matrix of pigment:chl-*a* ratios is used to factorise a data matrix containing the observed pigment concentrations data into a matrix of the proportion of the total chlorophyll biomass due to each phytoplankton class. A refined pigment:chl-*a* matrix (output matrix) is then generated (Mackey *et al*. 1996). By accounting for both variations in pigment:chl-*a* ratios and the relative abundance of each phytoplankton group the residual unexplained errors are minimised. Moreover, allowing

different ratios of the same indicator pigments to be used for different phytoplankton classes, CHEMTAX avoids some of the problem caused by a lack of unique indicator pigments. As the matrix factorisation procedure of CHEMTAX is an iterative process, allowing the pigment:chl-*a* ratio to change, it is capable of self-tuning, and hence avoiding the need to tailor initial pigment:chl-*a* ratios for a particular set of environmental conditions. This flexibility is particularly useful when studying samples acclimated to a range of light intensities, as it can account not only for the increased concentration of light-harvesting pigments relative to chl-*a* for LL as compared with HL cells, but also the changes in the ratios of the accessory pigments (Moore *et al*. 1995, Bouman *et al*. 2000, Blanchot *et al*. 2001).

2.2.9 Limitations of CHEMTAX

Since CHEMTAX operates without any direct recourse to biological processes, care needs to be taken to ensure that spurious solutions are not produced, and may be the most significant drawback to this sort of "black box" process. A range of studies such as that of Latasa (2007) have tried to quantify the potential errors in biomass estimates from CHEMTAX. The risk of implausible results could be reduced if the input pigment:chl-*a* ratios were tightly constrained, but this would mean that the optimal solution would be unlikely to be found, and would compromise the scope for the approach to account for variability in the pigment:chl-*a* ratios caused by photoacclimation or a change in the community assemblage. In their initial study Mackey *et al.* (1996) suggested that variation in the pigment:chl-*a* ratio should be limited to ± 25% of initial values. Subsequent work has demonstrated that the approach displays considerably greater robustness and so wider tolerances should be allowed, with Gibb *et al.* (2001) and Veldhuis & Kraay (2004) allowing for a maximum of 500% change in pigment:chl-*a* ratio.

2.2.10 Validation

To test the effectiveness of any pigment-based approach to estimating phytoplankton taxonomy or size, an independent measure of group-specific biomass is required for comparison. While the abundance and distribution of microscope-counts data is sparse in publicly accessible databases for the Atlantic Subtropical Gyre, flow cytometry counts of marine phytoplankton are often routinely performed on research expeditions, and these data are available from international oceanographic data centres. Although flow cytometry data has the disadvantage that it is unable to register large cells such as diatoms and dinoflagellates, they are a small proportion of the total biomass (Marañon *et al.* 2001). In addition diatom and dinoflagellates species which are found in the Subtropical Gyres are smaller than those seen in more nutrient-rich, higher latitudes (Marañon *et al.* 2001), meaning that flow cytometry can be used to obtain a reliable picture of phytoplankton distribution and abundance for Gyre samples.

2.2.11 Chapter aims

This study aims to compare three different HPLC pigment-based approaches to estimating phytoplankton population structure and to determine if the increased complexity of the variable indicator pigment:chl-*a* method found in CHEMTAX produces better results than the simpler fixed pigment:chl-*a* approaches of Bidigare & Ondrusek (1996) and Uitz *et al.* (2008) using flow cytometry counts to validate the various models. Information on intracellular pigment concentrations will be used to divide the samples into high- and low-light adapted groups to account for changes in photo-acclimation. Once a reliable method has been determined, this will then be used to assess trends in the latitudinal distribution of phytoplankton groups within the Atlantic Gyre system and carbon-to-chlorophyll ratios in different phytoplankton groups.

2.3 Methods

2.3.1 Data sources

HPLC and flow cytometry data were obtained from the British Oceanographic Data Centre (BODC) across the Atlantic Basin for the AMT (Atlantic Meridional Transect) series of cruises between Great Britain (~50 ºN) and either the Falkland Islands, (~50 ºS), Cape Town (~30 ºS), Montevideo (~30 ºS) or Punta Arenas (~50 ºS). Samples from AMT cruises 3, 4, 6, 12, 13, 14, 15 and 18 were included in the analysis. Data were also obtained for EUMELI 3 and 4 performed as part of the JGOFS-France programme (http://www.obs-vlfr.fr/cd_rom_dmtt/eu_main.htm). To allow comparisons between biomass estimates from pigment concentrations and flow cytometric cell counts, only samples within the Oceanic Gyres were included, where it was assumed that the phytoplankton standing stock consists of cells < 20 μm in diameter. To determine which sampling stations were located within the Oceanic Gyres, the approach of Polovina *et al*. (2008) was followed, where samples with a total *in-situ* chl-*a* (monovinyl + divinyl) of greater than 70 ng/l for the shallowest depth measured were discarded. A total of 421 samples satisfy this criterion (Table 2.1).

Table 2.1: List of cruises included in analysis and the number of Gyre samples

Cruise	Start date	End date	n HPLC	n Flow cytometry
AMT-3	20/9/1996	25/10/1996	27	0
AMT-4	21/4/1997	27/5/1997	71	2
AMT-6	14/5/1998	15/6/1998	41	10
AMT-12	12/5/2003	17/6/2003	24	14
AMT-13	10/9/2003	14/10/2003	17	14
AMT-14	26/4/2004	2/6/2004	26	25
AMT-15	19/9/2004	29/10/2004	18	1
AMT-18	3/10/2008	10/11/2008	74	36
EUMELI 3	14/9/1991	24/10/1991	59	49
EUMELI 4	18/5/1992	30/6/1993	64	64
Total			421	215

Gyre stations ranged in latitude from 30.86 ºS to 41.38 ºN (Fig 2.1) and from the surface to 250 m in depth. Total chl-*a* values varied from 1.8 to 604 ng/l. For the 226 samples with flow cytometry counts *Prochlorococcus* counts ranged from 14 to 353300 cells/ml, *Synechococcus* from 0 to 42930 cells/ml and picoeukaryotes from 0 to 11750 cells/ml.

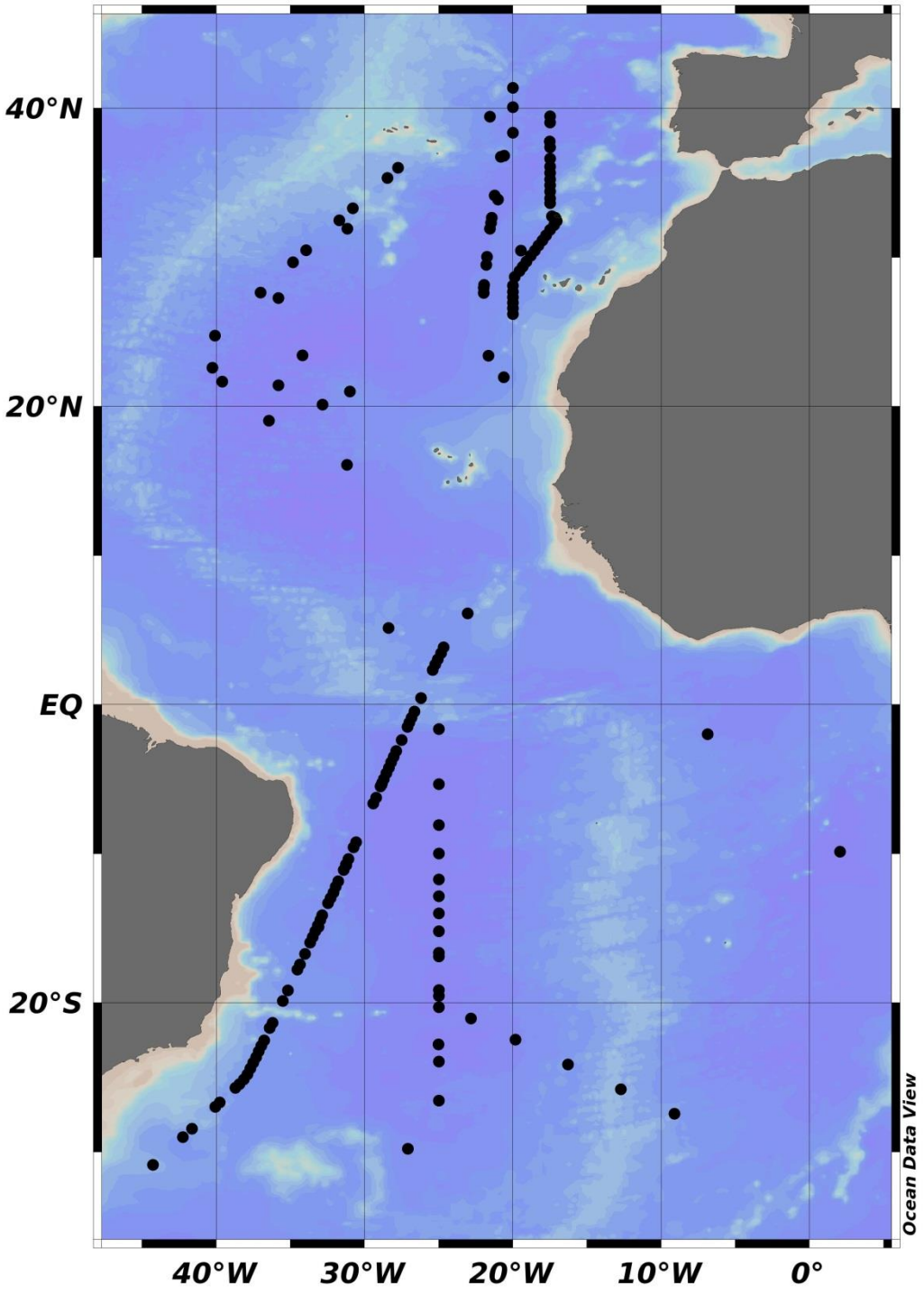

Fig 2.1: Map showing station locations. Stations selected on the basis that the surface concentration of total chl-*a* as measured by HPLC is less than 70 ng/l.

2.3.2 Flow cytometry

2.3.2a AMT cruises

For AMT cruises 3 - 6, seawater samples were collected from 10 depths (12 for AMT-4 (Zubkov *et al*. 2000)) at each station from 2 to 200 m using a Niskin bottle. Additional surface samples were collected every 4 hours for AMT-3 and every 2 hours for AMT-6 from the underway non-toxic supply (Zubkov *et al.* 1998). For flow cytometry two or three 0.9 ml subsamples (1.6 ml for AMT6) from the same sample were pooled in a polypropylene vial, fixed with 0.1-0.3% (final concentration) glutaraldehyde, frozen and kept either in liquid nitrogen or at -30 ^{o}C for 1-2 months before they were analysed. Samples were analysed using a FACSort flow cytometer (Becton Dickinson) equipped with a 15 mW laser exciting at 488 nm. Four major groups of picophytoplankton: *Prochlorococcus*, *Synechococcus,* picoeukaryotic and nanoeukaryotic cells, were characterised and enumerated using group-specific side-scatter and orange (585±21 nm) and red (>650 nm) autofluorescence properties (Zubkov *et al*. 1998, 2000). Methods for AMT-12, 13, 14 15 and 18 differed only in that samples were fixed instead with a 1% final concentration of paraformaldehyde (Heywood *et al.* 2006).

2.3.2b EUMELI cruises

Water collection for EUMELI 3 and 4 was performed using a rosette with 12 Niskin bottles. For EUMELI 3, a FACScan flow cytometer (Becton Dickinson) was used on-board in a thermostated room to count live picoplanktonic populations without fixation (Partensky *et al.* 1996) before analysis using CytoPC software (Vaulot *et al.* 1989). For EUMELI 4 samples were preserved in a final concentration of 0.5% paraformaldehyde for 10 – 15 minutes before being frozen in liquid nitrogen. Analysis was performed using an EPICS 541 flow cytometer

(Coultronics, Hialeah, FL), with a 6 W argon laser (Coherent, Paolo Alto, FL) exciting at 488nm, and a Micro-Sample Delivery System, using the optical configuration described in Vaulot *et al*. (1990). Owing to the very low levels of red-fluorescence in surface samples, *Prochlorococcus* abundance from the top 60 m was estimated from red fluorescence distributions, assumed to be log-normal (Partensky *et al.* 1996). Cell carbon estimates were obtained using carbon conversion factors from Grob *et al.* (2011), with high-light adapted *Prochlorococcus* at 35 fg/cell, low-light adapted *Prochlorococcus* 50 fg/cell, *Synechococcus* 60 fg/cell and picoeukaryotes 600 fg/cell.

2.3.3 HPLC pigment analysis

For the AMT cruises, HPLC analysis was performed as described in Barlow *et al*. (1997). Underway samples were taken every 2 hours, with between 0.5 and 4 l of water filtered through 25 mm GF/F filters from the non-toxic supply. For vertical profiling, samples were taken from the 10 l bottle on the CTD rosette system from as many as 9 depths from the surface to 200 m. Filters were then stored at -80 ºC until analysis. Pigments were extracted in acetone using ultrasonification before centrifuging to remove debris. Analysis was performed using a Shimadzu HPLC coupled to a Thermo Separations Products autosampler and a UV6000 diode-array absorbance detector. For the EUMELI cruises, 2 l of seawater was collected using Niskin bottles from between 4 and 11 depths from the surface to 150 m before being filtered onto GF/F filters, which were flash frozen using liquid nitrogen and stored. Pigments were then extracted using methanol following Mantoura & Llewellyn (1983), and detected using two LDC Milton Roy spectrophotometers in series, one at 440 nm for chlorophylls and carotenoids and one at 676 nm for chlorophylls and phaeopigments.

2.3.4 Size-fractionated chlorophyll measurements

Water samples were collected from Niskin bottles and 250 ml was used for sequential filtration through 20 µm, 2 µm and 0.2 µm polycarbonate filters before extraction in 90% acetone and storage at -20 °C. Chlorophyll concentration was determined using a 10AU Turner Designs Fluorometer, using the non-acidification technique of Welchsmeyer (1994).

2.3.5 Subdividing samples into high- and low-light adapted using pigment ratios

Phytoplankton display a large variation both in total pigment concentrations and in the relative importance of different pigments, with low-light adapted (LL) cells having much higher intracellular chlorophyll levels than high-light adapted (HL). While fixed pigment:chl-*a* ratio methods are not able to take this variation into account, CHEMTAX is capable of varying the relative concentration of different pigments. Dividing the samples into HL and LL categories will allow the ratios used in the analysis to be more representative of the intracellular pigment concentrations (Wright *et al.* 2010). Zeaxanthin (zea) is a major photo-protective pigment in prokaryotes, and a strong relationship is seen in zea:chl-*a* with respect to depth and light intensity (Fig 2.2a) (Babin *et al.* 1996, Bouman *et al.* 200, 2006). Therefore the zea:chl-*a* ratio was used to assess the light regime to which the samples are acclimated. Samples were defined as being LL if their zea:chl-*a* ratio was less than 0.3 by weight, and the sampling depth was greater than 40 m. This resulted in 130 samples being classified as LL and 291 as HL. The suitability of this split is confirmed by the tight correlation seen between the *Prochlorococcus* intracellular concentration of divinyl chlorophyll-*a* (DVchl-*a*) and zea:chl-*a* (Fig 2.2b) ($F_{1, 204}$= 167, $p < 0.0001$, $R^2 = 0.45$). Once samples were classified as HL- or LL-adapted, data were analysed using either the fixed pigment:chl-*a* or the variable pigment:chl-*a* ratio methods described below.

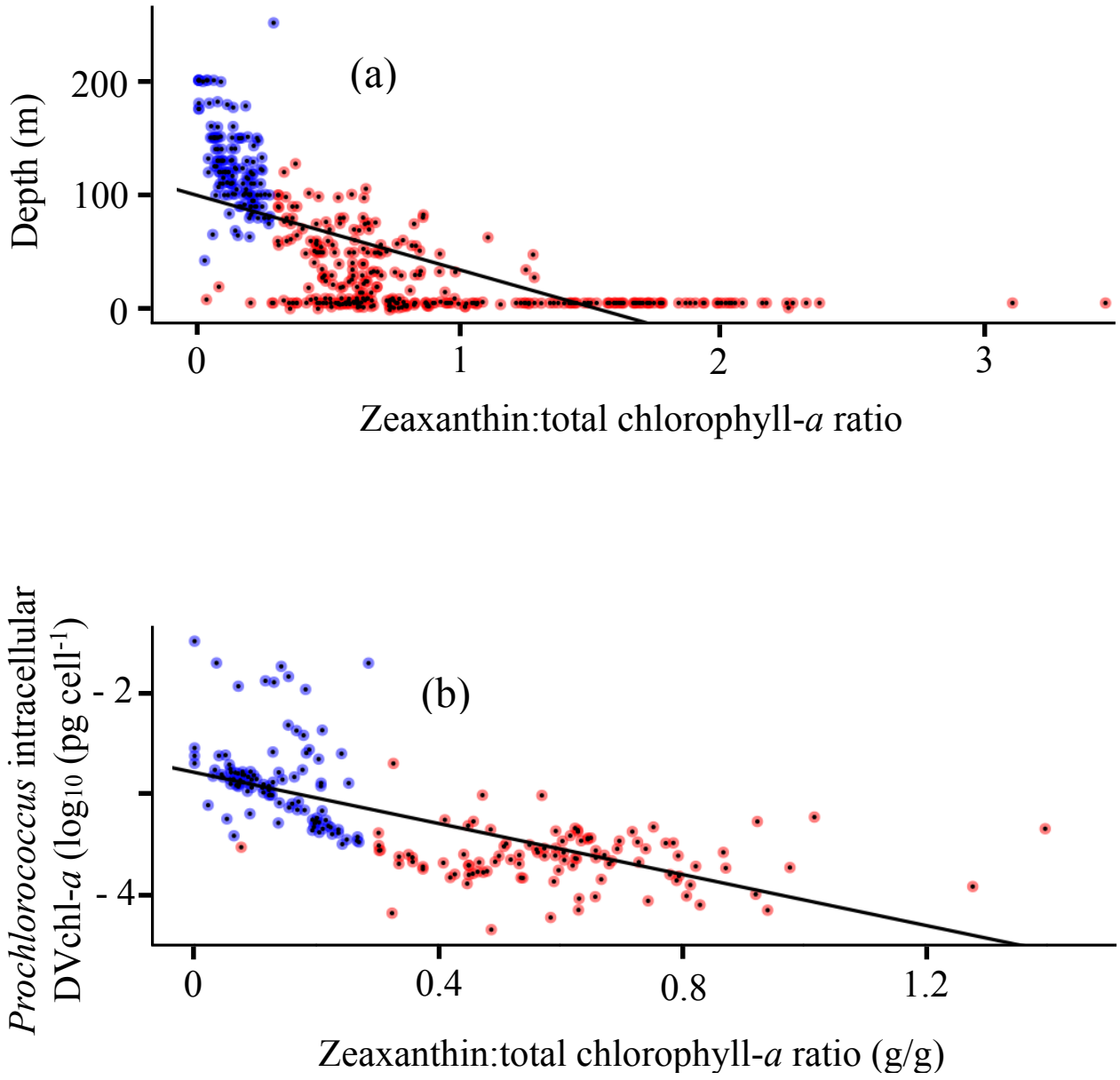

Fig 2.2: LL samples shown in blue, HL in red, showing: (a) Relationship between zeaxanthin concentration normalised to total chl-*a* concentration and depth, (y = - 65x + 99, $F_{1, 419}$= 336.2, p < 0.0001, R^2 = 0.44). (b) Chlorophyll-normalised zeaxanthin concentration as a function of DVchl-*a* per *Prochlorococcus* cell, (y = -1.3x - 2.8, $F_{1, 204}$= 167, p < 0.0001 R^2 = 0.45).

2.3.6 Pigment-based methods

For both the size-based fixed-pigment:chl-*a* method (Uitz *et al.* 2008) and the taxa-based fixed-pigment:chl-*a* approach (Bidigare & Ondrusek 1996), methods were followed as detailed in the respective papers, using the pigment:chl-*a* ratios as provided.

2.3.6a Fixed pigment:chl-*a* ratio methods

i) Uitz *et al.* (2008)

This approach divides the total chlorophyll-*a* into 3 size-classes (microphytoplankton > 20 μm, nanophytoplankton 2-20 μm, picophytoplankton < 2 μm) using seven diagnostic pigments. Fucoxanthin (fuc) and peridinin (per) are used as indicators of microphytoplankton, alloxanthin (allo), 19'-butanoyloxyfucoxanthin (19'-but) and 19'-hexanoyloxyfucoxanthin (19'-hex) for nanophytoplankton, with zea, and combined chlorophyll-*b* and divinyl chlorophyll-*b* (chl-*b*) representing picophytoplankton. Uitz *et al.* (2008) derived a weighted sum of these diagnostic pigments (wDP) as follows:

$$\text{wDP} = 1.41[\text{fuc}] + 1.41[\text{per}] + 0.6[\text{allo}] + 0.35[\text{19'-but}] + 1.27[\text{19'-hex}] + 0.86[\text{zea}] + 1.01[\text{chl-}b]. \quad (1)$$

The proportion of biomass due to each size-class is then calculated as follows, where f_{micro} is the proportion of microphytoplankton, f_{nano} the proportion of nanophytoplankton and f_{pico} the proportion of picophytoplankton.

$$f_{micro} = (1.41[\text{fuc}] + 1.41[\text{per}])/\text{wDP} \quad (2)$$

$$f_{nano} = (0.6[\text{allo}] + 0.35[\text{19'-but}] + 1.27[\text{19'-hex}])/\text{wDP} \quad (3)$$

$$f_{pico} = (0.86[\text{zea}] + 1.01[\text{chl-}b]) / \text{wDP} \quad (4)$$

These proportions can then be multiplied by the chl-*a* concentration to obtain a chlorophyll-based biomass estimate for each size-class. Since microphytoplankton are too large to be detected by flow cytometry, this class was not included for validation. The nanophytoplankton class was compared with picoeukaryote counts and the picophytoplankton class with combined *Prochlorococcus* and *Synechococcus* counts since the Uitz *et al.* (2008) approach uses pigment predominantly found in picocyanobacteria to define the picophytoplankton class and eukaryotic pigments for the nanophytoplankton class.

ii) Bidigare & Ondrusek (1996)

In the approach of Bidigare & Ondrusek, chlorophyll biomass is divided into 4 taxonomic classes of eukaryotes – prymnesiophytes, pelagophytes, dinoflagellates and diatoms, using 4 diagnostic pigments: 19'-but, 19'-hex, fuc, and per, as opposed to apportioning into size-classes as in Uitz *et al*. (2008). The chlorophyll-a biomass attributed to eukaryotic autotrophs was found by summing these groups, and the chlorophyll-a assigned to photosynthetic prokaryotes was calculated as the difference between the total chlorophyll-a concentration and that from photosynthetic eukaryotes. This method also differs in approach from Uitz *et al*. (2008) as it uses a two- stage process. Two constants, K and L, are used to estimate the proportion of the total 19'-hex which is from prymnesiophytes ($[19'\text{-hex}]_{prym}$) and the proportion of 19'-but from pelagophytes ($[19'\text{-but}]_{pel}$).

$$K = [19'\text{-hex}]_{prym} / [19'\text{-but}]_{prym} = 54.27 \quad (5)$$

$$L = [19'\text{-hex}]_{pel} / [19'\text{-but}]_{pel} = 0.14 \quad (6)$$

$$[19'\text{-hex}]_{prym} = (K/(K - L))\,([19'\text{-hex}]_{total} - ([19'\text{-but}]_{total}\, L)) \quad (7)$$

$$[19'\text{-but}]_{pel} = (K/(K - L))\,([19'\text{-but}]_{total} - ([19'\text{-hex}]_{total}/K)) \quad (8)$$

These group-specific accessory pigments are then used to calculate the chlorophyll biomass due to prymnesiophytes ([chl-*a*]$_{prym}$), pelagophytes ([chl-*a*]$_{pel}$), dinoflagellates ([chl-*a*]$_{dino}$) and diatoms ([chl-*a*]$_{diat}$).

Prymnesiophytes: $[\text{chl-}a]_{prym} = 1.3\ [19'\text{-hex}]_{prym}$ (9)

Pelagophytes: $[\text{chl-}a]_{pel} = 0.9\ [19'\text{-but}]_{pel}$ (10)

Dinoflagellates: $[\text{chl-}a]_{dino} = 1.5\ [\text{per}]$ (11)

Diatoms: $[\text{chl-}a]_{diat} = 0.8([\text{fuc}] - (0.02[19'\text{-hex}]_{prym} + 0.14[19'\text{-but}]_{pel}))$ (12)

Eukaryotic photoautotrophs: $[\text{chl-}a]_{euk} = [\text{chl-}a]_{prym + pel + dino + diat}$ (13)

Prokaryotic photoautotrophs: $[\text{chl-}a]_{prok} = [\text{chl-}a]_{total} - [\text{chl-}a]_{euk}$ (14)

For the purposes of flow cytometry validation, prokaryote biomass was compared with combined *Prochlorococcus* and *Synechococcus* flow cytometry counts, and prymnesiophytes and pelagophytes from the taxa-based method were combined for comparison with picoeukaryotes from flow cytometry.

2.3.6b Variable pigment:chl-*a* - CHEMTAX

The input ratio matrix was adapted from Gibb *et al.* (2001), omitting the violaxanthin term since this pigment was not measured for either EUMELI cruise (Table 2.2). Mackey *et al.* (1996) and Latasa (2007) state that analysis should be done in batches of around 50 samples, so within each light-regime (HL and LL) samples were randomised and divided into batches of between 45 and 55.

Table 2.2: Initial input pigment:chl-*a* ratio matrix for CHEMTAX phytoplankton chlorophyll biomass estimation adapted from Gibb *et al.* (2001). chl-*c3*: chlorophyll *c*-3; per: peridinin; 19'-but: 19'-butanoyloxyfucoxanthin; fuc: fucoxanthin; 19'-hex: 19'-hexanoyloxyfucoxanthin; allo: alloxanthin; zea: zeaxanthin; chl-*b*: the sum of mono and divinyl chlorophyll-*b;* DVchl-*a*: Divinyl chlorophyll-*a*; MV chl-*a*: monovinyl chlorophyll-*a*.

	chl-*c3*	**per**	**19'-but**	**fuc**	**19'-hex**	**allo**	**zea**	**chl-*b***	**DVchl-*a***	**MV chl-*a***
Input matrix										
Diatoms	0	0	0	0.76	0	0	0	0	0	1
Dinoflagellates	0	1.06	0	0	0.38	0	0	0	0	1
Prymnesiophytes	0.17	0	0.02	1.21	1.36	0	0	0	0	1
Chrysophytes	0.25	0	1.56	0.97	0	0	0	0	0	1
Chlorophytes	0	0	0	0	0	0	0.12	0.57	0	1
Cyanobacteria	0	0	0	0	0	0	0.59	0	0	1
Cryptophytes	0	0	0	0	0	0.23	0	0	0	1
Prochlorococcus	0	0	0	0	0	0	0.2	0.5	1	1

CHEMTAX uses a statistical fit to converge on the pigment:chl-*a* ratio matrix which explains the greatest proportion of the variance in the samples. It has however a limited capacity to adjust the ratios in a given run (Latasa *et al.* 2007) and the first run rarely renders the true value. Therefore following Wright & Van den Enden (2000), all samples were run through CHEMTAX twice, with the pigment:chl-*a* output ratio matrix from the first CHEMTAX run being used as the input pigment:chl-*a* ratio matrix for the second run. All data presented here

are therefore a result of the second CHEMTAX run. For validation against flow cytometry data, *Prochlorococcus* and *Synechococcus* chl-*a* biomass can be compared directly with cell counts measured by flow cytometry. Prymnesiophyte, chrysophyte, chlorophytes and cryptophytes chl-*a* biomass were combined for correlation against picoeukaryote counts.

Care must be taken to ensure that the degree to which the pigment:chl-*a* ratio matrix varies is suitable. If unconstrained, CHEMTAX can allow these ratios to change by up to 500% per run. If the analysis is too restrictive, there is a risk that either the ratios cannot be altered sufficiently to allow photoacclimatory trends to be fully taken into account, or that the analysis gets trapped in a localized minimum. To investigate the effect of constraining the pigment:chl-*a* ratios, two separate analyses were performed, chosen to represent two very different ways in which CHEMTAX could be configured (see Appendix to this chapter including Table 2.7). The results presented below use an epsilon limit of 0.0001 (the root mean square difference between the measured and predicted pigment compositions at which the calculation is deemed to be complete), an iteration limit of 1000, and a cut off step of 1000 (meaning that the calculation is complete when the pigment ratio matrix is varied by less than 1/1000 per iteration). Pigment:chl-*a* ratios were allowed to vary by 500%.

2.3.7 Data analysis and processing

All data and model outputs were analysed using R (R Development Core Team 2009), and plotted using package “ggplot2” (Wickham 2009). Wilcoxian rank sum statistical tests and the fitting of linear models were performed in R using the package “stats”. Fitting of quantiles and running means was performed using package “Rcmdr”. Contour plots were produced using Ocean Data View, version 4 (Schlitzer 2002).

2.4 Results

2.4.1 Comparison of CHEMTAX output with fixed-pigment ratio classification methods

In order to confirm that the non-constrained configuration of CHEMTAX is providing a realistic estimate of the biomass in each size or taxonomic class, a comparison was made with two fixed pigment-ratio approaches to estimating phytoplankton community structure.

2.4.1a Size-class based approach - Uitz *et al*. (2008)

A comparison of the outputs from the size-class based method and CHEMTAX when estimating the proportion of picophytoplankton reveals a strong positive correlation, (Fig 2.3a & Table 2.3) for both HL ($R^2 = 0.83$, $p < 0.0001$) and LL samples ($R^2 = 0.48$, $p < 0.0001$). Mean picophytoplankton biomass, however, is higher for the size-class based method at 36.7 and 95.7 ng chl-*a* for HL and LL samples, respectively, as compared with 35.6 and 86.3 ng chl-*a* from CHEMTAX. No significant difference between the mean picophytoplankton biomass as estimated using the size-class based approach and CHEMTAX was seen for either LL ($W = 9105$, $p = 0.28$) or HL samples ($W = 39078$, $p = 0.06$).

Significant correlations are also seen for the proportion of nanophytoplankton for HL samples ($R^2 = 0.74$, $p < 0.0001$) (Fig 2.3b), and LL samples ($R^2 = 0.55$, $p < 0.0001$). However the nanophytoplankton biomass is estimated to be significantly lower for LL samples using the size-class based method than from CHEMTAX, at 75 ng chl-*a*/l as compared with 93 ng chl-*a*/l ($W = 7176$, $p = 0.036$). There is no difference for HL samples at 18.9 and 19.1 ng chl-*a*/l for the size-class based method and CHEMTAX respectively ($W = 43812$, $p = 0.38$).

Microphytoplankton (Fig 2.3c) also display a positive correlation between the two

methods of assigning phytoplankton biomass for both HL (R^2 = 0.79, p < 0.0001) and LL samples (R^2 = 0.95, p < 0.0001). There is however a large systematic difference in the proportion of biomass ascribed to this class. While this effect is linear, the size-class based method ascribes a far greater proportion of the biomass to microphytoplankton than seen from CHEMTAX, although the overall percentage is still low. HL samples show significant differences in the mean according to the method used, at 6.1 and 2.9 ng chl-*a*/l for the size-class based method and CHEMTAX respectively (W = 58887, p < 0.0001), while the difference in means was even greater for LL samples at 16.2 and 7.4 ng chl-*a*/l (W = 12559, p < 0.0001). In addition, the size-class based approach gives a considerable spread in the proportion of microphytoplankton for samples where CHEMTAX suggests this size-class is absent.

2.4.1b Taxa-based method - Bidigare & Ondrusek (1996)

There is a strong positive correlation between prokaryote biomass as estimate by CHEMTAX and prokaryote biomass from the taxa-based method (Fig 2.3d, Table 2.3) for both HL (R^2 = 0.83, p < 0.0001) and LL samples (R^2 = 0.61, p < 0.0001). A significant difference in means for the two methods was seen for HL samples (W = 32238, p < 0.0001), with an estimate of 28.7 ng chl-*a* /l for the taxa-based method and 35.6 ng chl-*a*/l for CHEMTAX, though there was no significant difference seen for LL samples (W = 8398, p = 0.93) with CHEMTAX assigning a mean biomass of 86.3 ng chl-*a*/l to this size-class, as compared with 87.3 ng chl-*a*/l for the taxa-based method.

The relationship with respect to diatom biomass is also strong (Fig 2.3e), with a very significant correlation seen for HL (R^2 = 0.69, p < 0.0001) and LL samples (R^2 = 0.96, p < 0.0001). The difference in mean diatom biomass is significant for LL samples (W = 7046, p = 0.02) with CHEMTAX estimating 3.4 ng chl-*a*/l and the taxa-based method giving 2 ng chl-

a/l. Possibly owing to the greater sample size, an even more significant difference in mean values is seen for HL samples (W = 54236, $p < 0.0001$) with the taxa-based method again giving a mean of 2.1 ng chl-*a*/l and CHEMTAX an estimate of 1.5 ng chl-*a*/l.

Estimates of dinoflagellate biomass show a strong linear correlation, though the relationship is offset compared to 1:1 (Fig 2.3f), for both HL (R^2 = 0.97, $p < 0.0001$) and LL samples (R^2 = 0.97, $p < 0.0001$). No significant difference in mean values was seen for HL samples (W = 23361, p = 0.51) with CHEMTAX giving a mean dinoflagellate biomass of 1.4 ng chl-*a*/l and the taxa-based method 2.13 ng chl-*a*/l. Both approaches resulted in higher biomass estimates for LL samples than for HL samples, with the taxa-based method estimating 5.4 ng chl-*a*/l (W = 13247, $p < 0.0001$) and CHEMTAX 4.0 ng chl-*a*/l (W = 12629, $p < 0.0001$), however the difference between methods is not significant (W = 9190, p = 0.22).

A significant correlation is observed for prymnesiophyte biomass between the two classification methods (Fig 2.3g), for HL (R^2 = 0.39, $p < 0.0001$) and LL samples (R^2 = 0.9, $p < 0.0001$), although there is a difference seen in the mean prymnesiophyte biomass as calculated by the two methods. For HL samples, the taxa-based method results in a mean of 20.1 ng chl-*a*/l, as compared with 10.3 ng chl-*a*/l from CHEMTAX (W = 66825, $p < 0.0001$). For LL samples, the taxa-based method estimates 62.5 ng chl-*a*/l, while CHEMTAX gives 35.9 ng chl-*a*/l (W = 12671, $p < 0.0001$). The difference in mean biomass according to light regime is significant for both the taxa-based method (W = 4192, $p < 0.0001$) and CHEMTAX (W = 4646, $p < 0.0001$).

Significant correlations are also seen between the taxa-based approach and CHEMTAX for classifying pelagophytes biomass (Fig 2.3h) for both HL samples (R^2 = 55, $p < 0.0001$) and LL samples (R^2 = 0.58, $p < 0.0001$). The mean HL biomass estimates differ significantly, however, with the taxa-based method estimating 5 ng chl-*a*/l, whereas CHEMTAX gives 8.8 ng chl-*a*/l (W = 35437, p = 0.001). The same trend is seen again for the

LL samples at 29.3 ng chl-*a*/l and 57 ng chl-*a*/l for the taxa-based approach and CHEMTAX respectively, and again the difference is highly significant (W = 5136, $p < 0.0001$). The difference in pelagophyte biomass between HL and LL samples is significant for both the taxa-based method (W = 2595, $p < 0.0001$) and CHEMTAX (W = 2758, $p < 0.0001$).

Table 2.3: Comparison of fixed pigment:chl-*a* ratio methods with CHEMTAX. Wilcoxian tests were used to determine if the mean biomass as estimated by each method was significantly different. Linear least squares regression was used to determine the correlation between the methods, the coefficient of determination, and the significance of this relationship. * > 0.05, ** > 0.01, *** > 0.001.

Method	Light regime	Class	Mean biomass (ng / l)	CHEMTAX mean biomass (ng /l)	Significance of difference between CHEMTAX and fixed pigment:chl-*a* mean biomass estimates		Correlation	R^2	Significance of regression between CHEMTAX and fixed pigment:chl-*a* biomass estimates	
Uitz *et al.* (2008)	**HL**	**Pico**	34.7	35.8	$W = 39078$, $p = 0.06$		y = 1.00x + 2.8	0.83	$F_{1, 287} = 1377$, $p < 0.0001$	***
		Nano	18.9	19.1	$W = 43812$, $p = 0.38$		y = 0.99x + 0.4	0.74	$F_{1,287} = 828$, $p < 0.0001$	***
		Micro	6.1	2.9	$W = 58887$, $p < 0.0001$	***	y = 0.51x – 0.2	0.79	$F_{1,287} = 287$, $p < 0.0001$	***
	LL	**Pico**	95.7	86.3	$W = 9105$, $p = 0.28$		y = 0.70x + 19.8	0.48	$F_{1,128} = 118$, $p < 0.0001$	***
		Nano	74.9	93.0	$W = 7176$, $p = 0.036$	*	y = 1.02x + 16.6	0.55	$F_{1,128} = 159$, $p < 0.0001$	***
		Micro	16.2	7.4	$W = 12559$, $p < 0.0001$	***	y = 0.58x – 2.1	0.95	$F_{1,128} = 242$, $p < 0.0001$	***
Bidigare & Ondrusek (1996)	**HL**	**Prokaryotes**	28.7	35.6	$W = 32238$, $p < 0.0001$	***	y = 0.89x + 10.4	0.83	$F_{1, 287} = 1458$, $p < 0.0001$	***
		Diatoms	2.1	1.5	$W = 54236$, $p < 0.0001$	***	y = 0.96x – 0.5	0.69	$F_{1,287} = 636$, $p < 0.0001$	***
		Dinoflagellates	2.1	1.4	$W = 23361$, $p = 0.51$		y = 0.72x – 0.1	0.97	$F_{1,287} = 9224$, $p < 0.0001$	***
		Prymnesiophytes	20.0	12.3	$W = 66825$, $p < 0.0001$	***	y = 0.45x + 1.3	0.39	$F_{1, 287} = 188$, $p < 0.0001$	***
		Pelagophytes	5.0	8.8	$W = 35437$, $p = 0.001$	**	y = 1.78x – 0.04	0.55	$F_{1,287} = 351$, $p < 0.0001$	***
	LL	**Prokaryotes**	87.4	86.3	$W = 8398$, $p = 0.93$		y = 0.74x + 21.5	0.61	$F_{1,128} = 201$, $p < 0.0001$	***
		Diatoms	2.0	3.4	$W = 7046$, $p = 0.02$	*	y = 1.53x + 0.3	0.96	$F_{1,128} = 2743$, $p < 0.0001$	***
		Dinoflagellates	5.4	4.0	$W = 9190$, $p = 0.22$		y = 0.74x – 0.02	0.97	$F_{1,128} = 3920$, $p < 0.0001$	***
		Prymnesiophytes	62.5	35.9	$W = 12671$, $p < 0.0001$	***	y = 0.56x + 0.9	0.90	$F_{1,128} = 1206$, $p < 0.0001$	***
		Pelagophytes	29.4	57.1	$W = 5163$, $p < 0.0001$	***	y = 2.1x – 5.2	0.58	$F_{1,128} = 181$, $p < 0.0001$	***

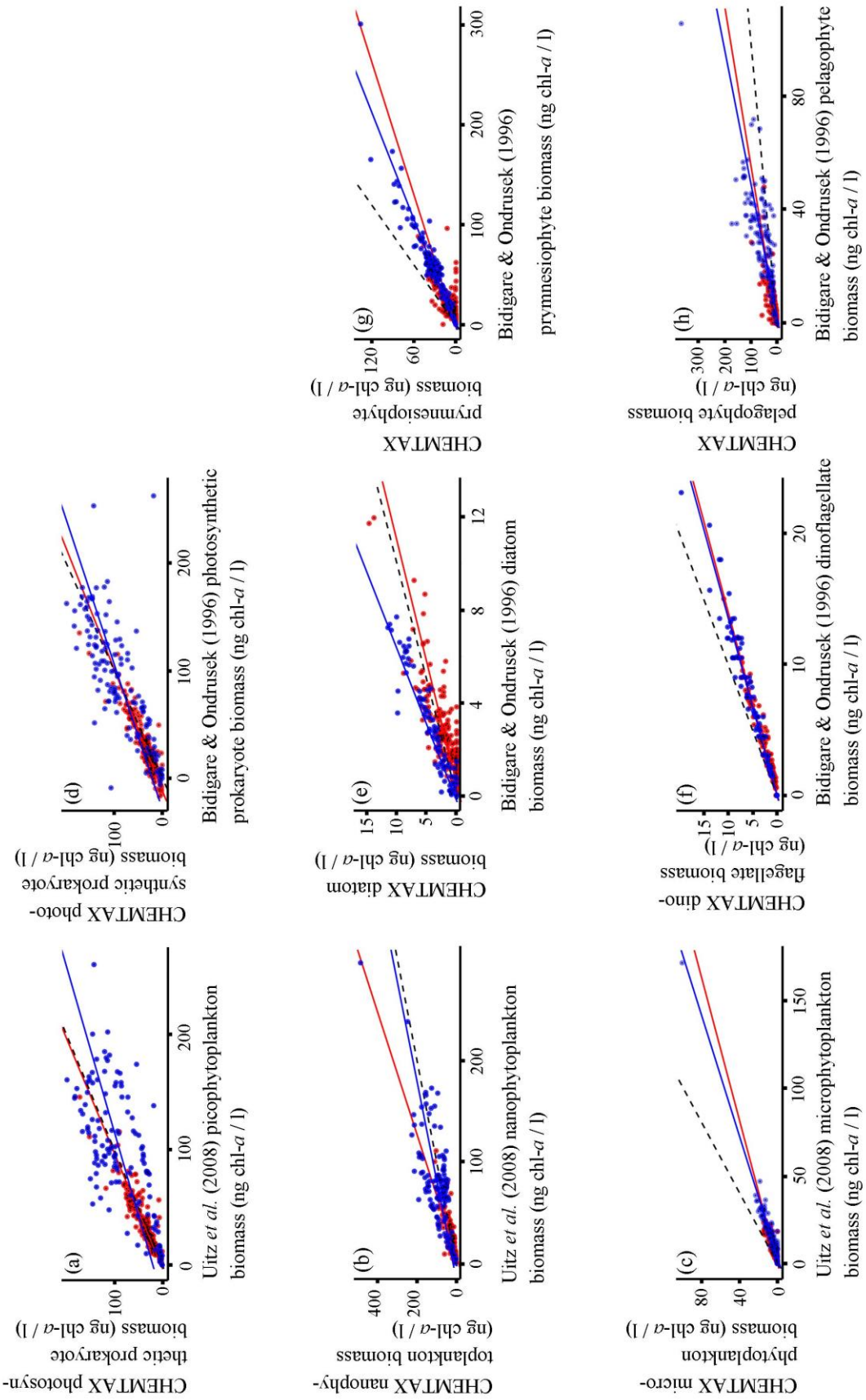
(a)
CHEMTAX photosynthetic prokaryote biomass (ng chl-a / l)
Uitz et al. (2008) picophytoplankton biomass (ng chl-a / l)
(b)
CHEMTAX nanophytoplankton biomass (ng chl-a / l)
Uitz et al. (2008) nanophytoplankton biomass (ng chl-a / l)
(c)
CHEMTAX microphytoplankton biomass (ng chl-a / l)
Uitz et al. (2008) microphytoplankton biomass (ng chl-a / l)
(d)
CHEMTAX photosynthetic prokaryote biomass (ng chl-a / l)
Bidigare & Ondrusek (1996) photosynthetic prokaryote biomass (ng chl-a / l)
(e)
CHEMTAX diatom biomass (ng chl-a / l)
Bidigare & Ondrusek (1996) diatom biomass (ng chl-a / l)
(f)
CHEMTAX dinoflagellate biomass (ng chl-a / l)
Bidigare & Ondrusek (1996) dinoflagellate biomass (ng chl-a / l)
(g)
CHEMTAX prymnesiophyte biomass (ng chl-a / l)
Bidigare & Ondrusek (1996) prymnesiophyte biomass (ng chl-a / l)
(h)
CHEMTAX pelagophyte biomass (ng chl-a / l)
Bidigare & Ondrusek (1996) pelagophyte biomass (ng chl-a / l)

Fig 2.3. Relationship between biomass estimates for different size classes following methods of Uitz *et al.* (a-c), and Bidigare & Ondrusek (1996) (d-h) against CHEMTAX. Picophytoplankton < 2 μm, nanophytoplankton 2—20 μm, microphytoplankton > 20 μm. HL samples shown in red, LL samples in blue. Dashed line shows the 1:1 ratio. (a) Picophytoplankton biomass from Uitz *et al.* (2008) and CHEMTAX, showing significant correlation for both HL and LL adapted samples. No significant difference in the biomass estimate according to method for either HL or LL samples. (b) Nanophytoplankton biomass from Uitz *et al.* (2008) and CHEMTAX, with significant relationship for both HL and LL samples. No difference was seen in biomass estimates according to method for HL samples, however the biomass estimate from CHEMTAX was significantly higher for LL samples. (c) Microphytoplankton biomass from Uitz *et al.* (2008) and CHEMTAX, with significant correlations for HL and LL samples. Mean microphytoplankton biomass was significantly higher following Uitz et al (2008) for both HL and LL. (d) Bidigare & Ondrusek (1996) photosynthetic prokaryote biomass, showing significant correlation for both HL and LL samples. The Bidigare & Ondrusek (1996) method gives a significantly lower biomass estimate for HL samples than CHEMTAX, though there is no difference for LL samples. (e) Diatom biomass as estimated by Bidigare & Ondrusek (1996) and CHEMTAX. Significant correlations are seen for both HL and LL samples. The Bidigare & Ondrusek (1996) approach gives a significantly higher biomass estimate for LL samples, and a significantly lower estimate for HL samples than CHEMTAX. (f) Dinoflagellate biomass according to Bidigare & Ondrusek (1996) and CHEMTAX, with a significant correlation for both HL and LL samples. There is no significant difference in biomass estimates according to classification method. (g) Prymnesiophytes biomass from Bidigare & Ondrusek (1996) and CHEMTAX, with significant correlations for both HL samples and LL samples. The Bidigare & Ondrusek (1996) method gives significantly higher biomass for both HL and LL samples than CHEMTAX. (h) Pelagophyte biomass according to Bidigare & Ondrusek (1996) and CHEMTAX, with a strong correlation for both HL adapted samples and LL samples. The Bidigare & Ondrusek (1996) method gives significantly lower biomass for both HL and LL samples.

2.4.1c Latitudinal variations in estimates of phytoplankton biomass

Gridded field plots reveal spatial patterns with respect to the difference in the proportion of biomass assigned to each size-class by CHEMTAX and the size-based approach (Fig 2.4). The two methods are in relatively tight agreement for the proportion of microphytoplankton at around 20 ^{o}S, and for deep samples around 20 ^{o}N (Fig 2.4a). For the remainder of the dataset, the size-based approach assigns a greater proportion of the total biomass to the microphytoplankton class, particularly for surface samples just north of the equator. In the nanophytoplankton size-class, CHEMTAX biomass estimates are much lower for deep samples around 20 ^{o}S, and higher than the size-based method for deep samples at 20 ^{o}N, and around the equator for all depths (Fig 2.4b). The differences in the proportion of biomass assigned to the picophytoplankton size-class show the opposite trend to that for nanophytoplankton, with CHEMTAX producing a much higher estimate for deep samples around 20 ^{o}S, and at around 35 ^{o}N, and a much lower estimate than the size-based method for deep samples at 20 ^{o}N (Fig 2.4c).

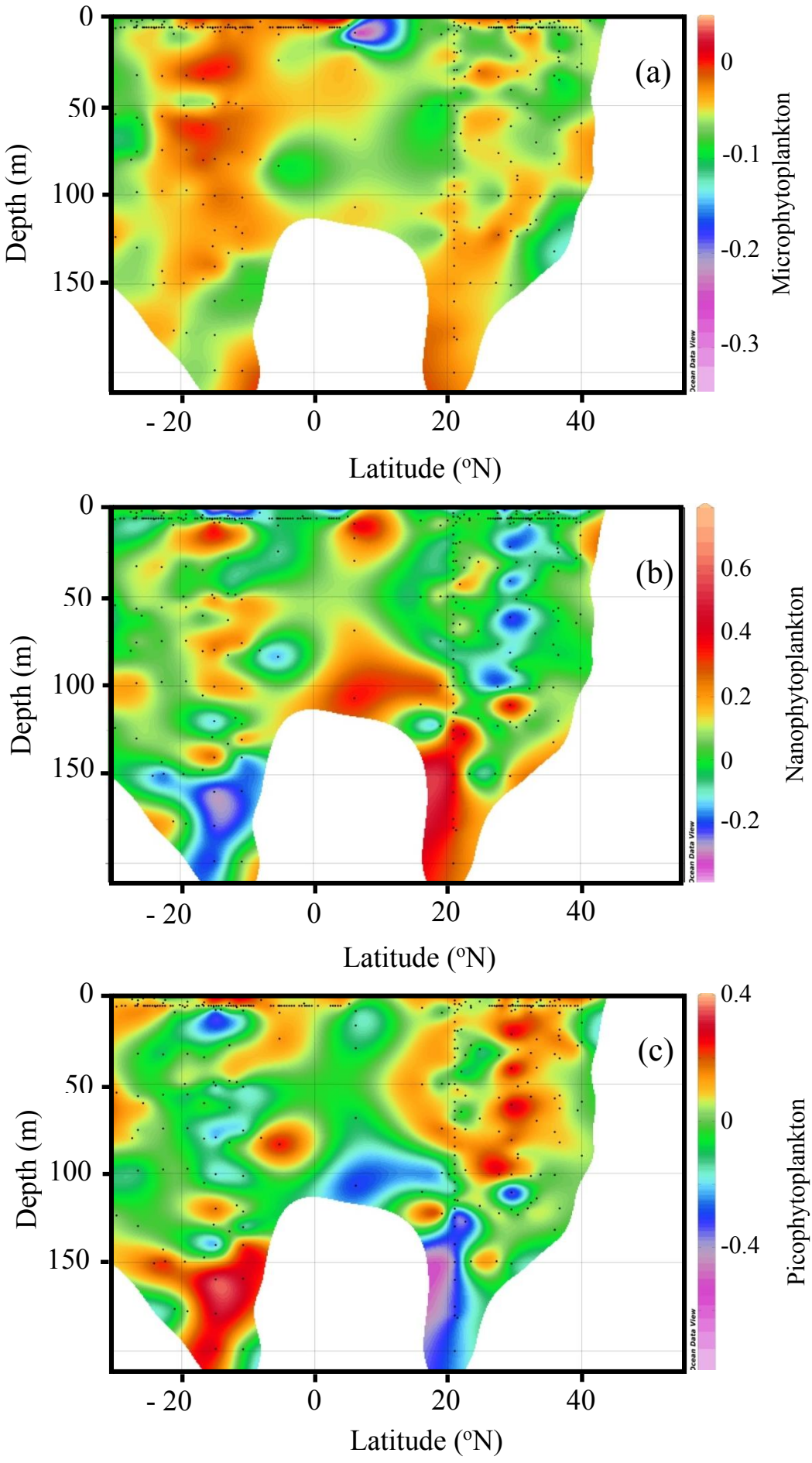
(a)
Depth (m)
0
50
100
150
- 20
0
20
40
Latitude (°N)
0
-0.1
-0.2
-0.3
Microphytoplankton
(b)
Depth (m)
0
50
100
150
- 20
0
20
40
Latitude (°N)
0.6
0.4
0.2
0
-0.2
Nanophytoplankton
(c)
Depth (m)
0
50
100
150
- 20
0
20
40
Latitude (°N)
0.4
0
-0.4
Picophytoplankton

Fig 2.4: Spatial differences in biomass estimates from the size-class method and CHEMTAX as a function of latitude. The colour shows the proportion of biomass as estimated using the size-class fixed pigment:chl-*a* method (Uitz *et al.* 2008) subtracted from that estimated using CHEMTAX (run under lax criteria). (a) Microphytoplankton showing the consistently higher biomass estimated from the size-class based approach. (b) Nanophytoplankton, with the size-class based approach estimating greater nanophytoplankton dominance at 15 ^{o}S and picophytoplankton at 20 ^{o}N as compared with CHEMTAX. (c) Picophytoplankton again showing the divergence in biomass estimates for the two methods at 15 ^{o}S and 20 ^{o}N.

2.4.2 Validating biomass estimates with flow cytometry counts

A possible obstacle to using flow cytometry data to evaluate biomass estimates is that flow cytometry is unable to measure large cells. Microphytoplankton however appear to constitute only a minor component of the Gyres biomass for most samples, with size-fractionated chlorophyll measurements giving a mean microphytoplankton component of 1.7% (Fig 2.5), meaning that, flow cytometry counts can be used to validate the different methods of estimating size-specific biomass in this situation.

Since divinyl chlorophyll-*a* occurs solely in *Prochlorococcus,* DVchl-*a* concentration and *Prochlorococcus* cell abundance (Fig 2.6a) can be compared directly. Significant correlations are seen for both LL ($F_{1, 103}$ = 60.7, $p < 0.0001$, $R^2 = 0.36$), and HL samples ($F_{1, 109}$ = 22.8, $p < 0.0001$, $R^2 = 0.17$) (Table 2.4).

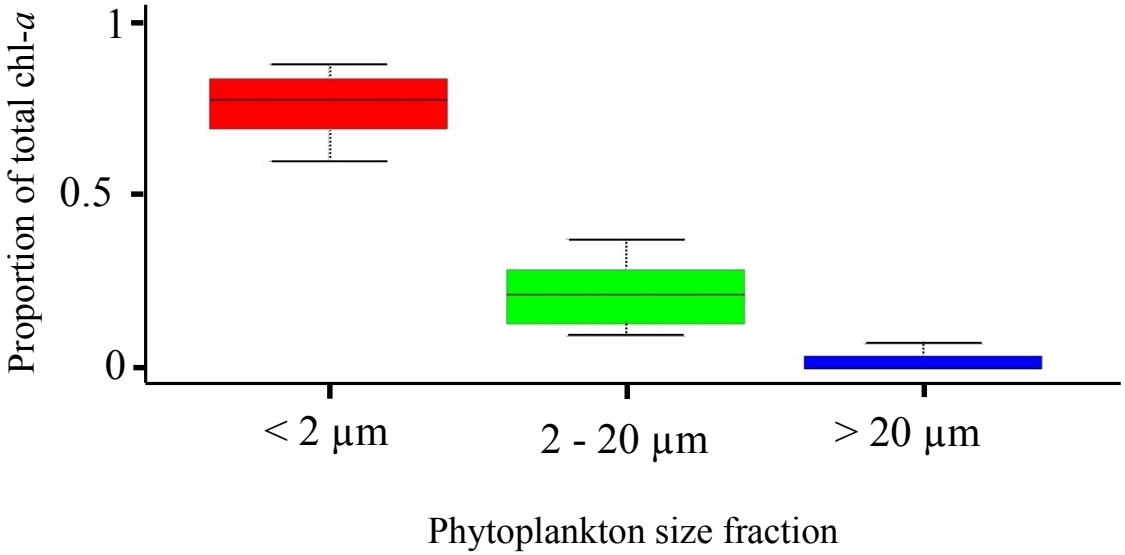

Fig 2.5: The proportion of the total chl-*a* by size class according to size fractionated HPLC. Data from all depths from the AMT-3 cruise.

2.4.3 Fixed pigment:chl-*a* methods

2.4.3a Size-class based – Uitz *et al.* (2008)

Since this analysis is using a dataset containing a large number of flow cytometry counts, it is possible to validate these pigment-based classification methods. When comparing size-class based estimates of chl-*a* due to picophytoplankton with total photosynthetic prokaryote counts (*Prochlorococcus* + *Synechococcus*) from flow cytometry, a significant relationship is seen for both HL samples and LL samples (Fig 2.6b, Table 2.4), with HL prokaryotes containing a significantly lower mean quantity of chlorophyll-*a* per cell at 0.39 fg chl-*a* / cell as compared with 9.1 fg chl-*a* / cell for LL prokaryotes ($W = 985$, $p < 0.0001$) (Table 2.5).

A significant positive relationship is also seen between the proportion of chlorophyll due to nanophytoplankton and picoeukaryote cell counts (Fig 2.6c, Table 2.4) for HL and LL samples, though there is a considerable spread in biomass estimates at stations where very few cells are detected. This is particularly pronounced for LL samples. HL cells have significantly

less chlorophyll than LL, with a mean of 24.9 fg chl-*a* per picoeukaryote cell for HL samples and 345 fg chl-*a* per picoeukaryote cell for LL samples ($W = 1843$, $p < 0.0001$) (Table 2.5).

2.4.3b Taxa-based - Bidigare & Ondrusek (1996)

A significant correlation between autotrophic prokaryote cell counts from flow cytometry and autotrophic prokaryote chl-*a* biomass as estimated by the taxa-based classification method for LL samples was observed (Fig 2.6d, Table 2.4). The relationship is even more significant when considering HL samples, giving an estimate of 0.39 fg chl-*a* / cell for HL samples and 8.2 fg chl-*a* / cell for LL samples, which is significantly different ($W = 1143$, $p < 0.0001$) (Table 2.5).

A tighter relationship is seen between the combined prymnesiophyte and pelagophyte biomass from the taxa-based pigment method and picoeukaryotes from flow cytometry (Fig 2.6e, Table 2.4) than was observed when using the size-based approach, with significant correlations for both HL and LL samples. This gives an estimate of 28.8 fg chl-*a* / cell for HL samples and 404 fg chl-*a* / cell for LL samples, which is significantly different ($W = 1287$, $p < 0.0001$) (Table 2.5).

2.4.4 Validating CHEMTAX biomass estimates with flow cytometry

Unlike the other pigment-based approaches CHEMTAX separates the photosynthetic prokaryote biomass into the two globally significant picocyanobacterial genera, *Prochlorococcus* and *Synechococcus*. A significant correlation between *Prochlorococcus* biomass and flow cytometry counts is observed for HL samples (Fig 2.7a, Table 2.4), despite the correlation explaining a low proportion of the total variance, with an even stronger correlation between flow cytometry counts and *Prochlorococcus* biomass being observed for LL. HL samples average 0.14 fg chl-*a* / cell and LL samples 2.4 fg chl-*a* / cell, which is a

highly significant difference ($W = 495$, $p < 0.0001$) (Table 2.5). *Prochlorococcus* as measured by flow cytometry is highly abundant at a depth of 150 m, and still present in significant numbers at 200m (Fig 2.8a), and is also reflected in the trends seen in *Prochlorococcus* chl-*a* biomass as estimated by CHEMTAX (Fig 2.8b).

Trends in *Synechococcus* biomass prove difficult to identify using accessory pigments (Fig 2.7b, Table 2.4), with no significant correlations between biomass estimates from CHEMTAX and flow cytometry counts found for HL samples or LL samples, although this may be heavily affected by a small number of outlier points. A significant difference is seen in the mean chl-*a* / cell for HL (14.3 fg chl-*a* / cell) and LL samples (215.6 fg chl-*a* / cell) ($W = 3825$, $p = 0.003$) (Table 2.5). It is also interesting to note the large number of LL samples where flow cytometry finds few or no *Synechococcus* cells, whereas CHEMTAX produces large biomass estimates. The effect is seen even more strongly when comparing the depth profiles of biomass distribution from the two methods. *Synechococcus* as counted by flow cytometry is rare below 100 m, and almost completely absent below 120 m (Fig 2.8c). If *Synechococcus* biomass is estimated using CHEMTAX, the group remains a major contributor to phytoplankton biomass at depths of almost 200 m (Fig 2.8d).

Highly-significant correlations are seen however between picoeukaryotes, as measured by flow cytometry and the combined biomass estimates from CHEMTAX for prymnesiophytes, chlorophytes, cryptophytes and chrysophytes (Fig 2.7c, Table 2.4) for both HL samples and LL samples, leading to an estimate of 26.1 fg chl-*a* / cell for HL populations and 334.4 fg chl-*a* / cell for LL populations, a significant difference ($W = 1005$, $p < 0.0001$) (Table 2.5).

(a)
(b)
(c)
(d)
(e)
HPLC DVchl-a (ng/l)
Prochlorococcus counts from flow cytometry (cells / ml)
Uitz et al. (2008) picophytoplankton biomass (ng chl-a/l)
Picophytoplankton counts from flow cytometry (cells / ml)
Uitz et al. (2008) nanophytoplankton biomass (ng chl-a/l)
Eukaryote counts from flow cytometry (cells / ml)
Bidigare & Ondrusek (1996) photosynthetic prokaryote biomass (ng chl-a/l)
Photosynthetic prokaryote counts from flow cytometry (cells / ml)
Bidigare & Ondrusek (1996) nanophytoplankton biomass (ng chl-a/l)
Eukaryote counts from flow cytometry (cells / ml)

Fig 2.6: Relationship between biomass estimates for different size-classes from fixed pigment:chl-*a* ratio methods of chemotaxonomy and flow cytometry counts. In all cases relationships are significant at the level of $p < 0.0001$. Picophytoplankton < 2 μm, nanophytoplankton 2—20 μm, microphytoplankton > 20 μm. HL samples shown in red, LL in blue. (a) Relationship between HPLC divinyl chlorophyll-*a* and *Prochlorococcus* flow cytometry counts. (b) Relationship between picophytoplankton flow cytometry counts and prokaryote chl-*a* as estimated using the Uitz *et al.* (2008) approach. (c) Relationship between eukaryote flow cytometry counts and chl-*a* as estimated using the Uitz *et al.* (2008) approach. (d) Relationship between photosynthetic prokaryote flow cytometry counts and prokaryote chl-*a* as estimated using the Bidigare & Ondrusek (1996) approach. (e) Relationship between eukaryote flow cytometry counts and combined chl-*a* for prymnesiophytes and pelagophytes as estimated using the Bidigare & Ondrusek (1996) approach.

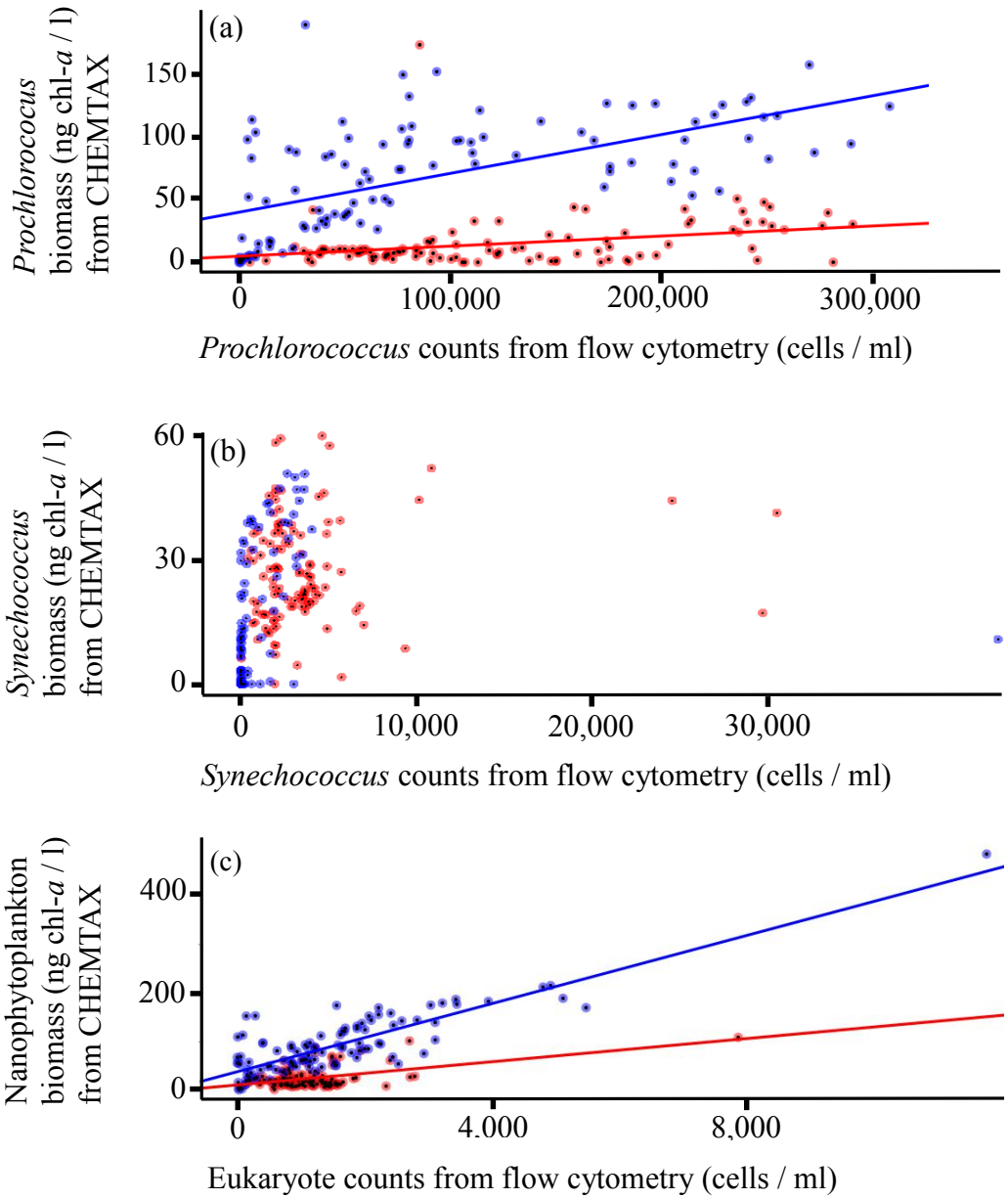

Fig 2.7. Relationship between biomass estimates for different classes from CHEMTAX and flow cytometry counts. HL samples shown in red, LL in blue. (a) Relationship between *Prochlorococcus* flow cytometry counts and *Prochlorococcus* biomass as estimated by CHEMTAX. Significant correlations for LL samples ($y = 8*10^{-5}x + 4.8$, $F_{1, 103} = 59$, $p < 0.0001$, $R^2 = 0.36$), and HL samples ($y = 3*10^{-5}x + 40$, $F_{1, 106} = 10.4$, $p = 0.017$, $R^2 = 0.08$) . (b) *Synechococcus* flow cytometry counts and *Synechococcus* biomass as estimated by CHEMTAX. Neither LL samples ($F_{1, 117} = 2.3$, $p = 0.13$, $R^2 = 0.01$), nor HL samples ($F_{1, 117} = 2.3$, $p = 0.13$, $R^2 = 0.01$) display significant correlations. (c) Eukaryote flow cytometry counts and chl-*a* as estimated by CHEMTAX. LL samples ($y = 0.035x + 39$, $F_{1, 104} = 128$, $p < 0.0001$, $R^2 = 0.55$), and HL samples ($y = 0.011x + 11.9$, $F_{1, 118} = 43$, $p < 0.0001$, $R^2 = 0.26$) show significant correlations.

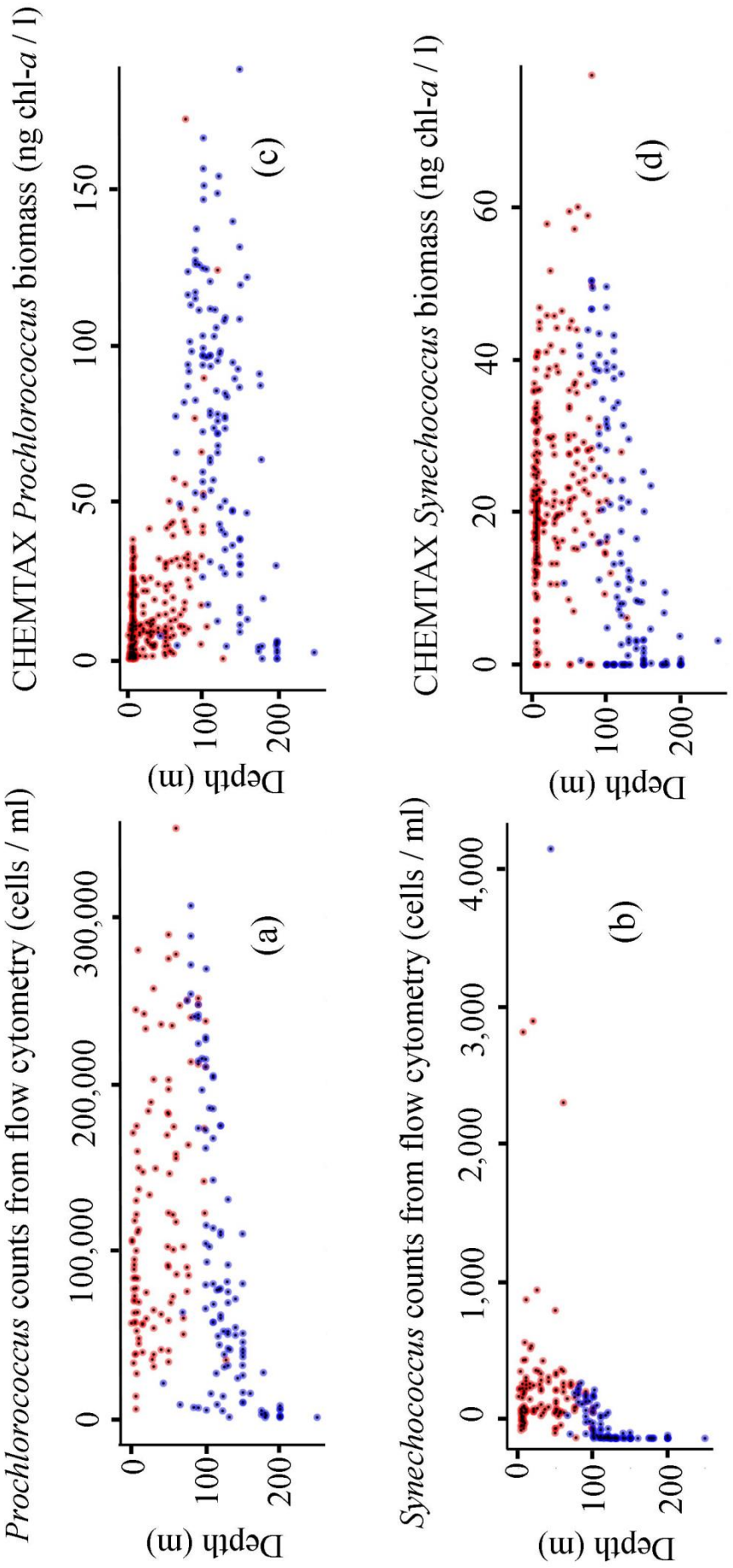

Fig 2.8: Depth-dependent distributions of *Prochlorococcus* and *Synechococcus*. High-light adapted points shown in red, low-light adapted in blue. (a) Relationship between the abundance of *Prochlorococcus* from flow cytometry counts and depth. (b) Trends with respect to *Synechococcus* counts and depth. (c) *Prochlorococcus* chl-*a* biomass as estimated by CHEMTAX against depth. (d) *Synechococcus* chl-*a* biomass as estimated by CHEMTAX with respect to depth.

Table 2.4: Relationships of group-specific biomass against flow cytometry counts. Regressions shown for the size-based classification method (Uitz *et al.* 2008), the taxa-based method (Bidigare & Ondrusek 1996) and CHEMTAX. For size-class approach, picoeukaryotes counts are compared with the nanophytoplankton size-class. For the taxa-based approach, picoeukaryotes are compared with the combined chl-*a* biomass of prymnesiophytes and pelagophytes. For CHEMTAX, picoeukaryotes are compared with the combined chl-*a* biomass of prymnesiophytes, cryptophytes, chlorophytes and chrysophytes. CHEMTAX is run under lax and strict criteria (See appendix for details. All results presented in this chapter are using the lax criteria). * < 0.05, ** < 0.01, *** < 0.001.

		Regression of biomass estimates against flow cytometry counts					
Method	**Light regime**	**Class**	**x**	**Intercept**	***p***	**R^2**	**Significance**
HPLC DVchl-*a*	HL	*Prochlorococcus*	0.00011	10.9	< 0.0001	0.17	***
	LL	*Prochlorococcus*	0.00029	47.6	< 0.0001	0.36	***
Uitz *et al.* 2008	HL	Pico	0.00012	22.56	< 0.0001	0.21	***
		Nano	0.01023	12.36	< 0.0001	0.23	***
	LL	Pico	0.00033	66.05	< 0.0001	0.29	***
		Nano	0.01897	41.09	< 0.0001	0.45	***
Bidigare & Ondrusek 1996	HL	Pico	0.00015	49.39	< 0.0001	0.28	***
		Nano	0.01321	51.66	< 0.0001	0.26	***
	LL	Pico	0.00042	4.83	< 0.0001	0.42	***
		Nano	0.02273	23.95	< 0.0001	0.55	***
CHEMTAX – Lax	HL	*Prochlorococcus*	0.00008	3.79	0.0017	0.08	***
		Synechococcus	0.00040	39.69	0.13	0.01	
		Nano	0.01192	11.90	< 0.0001	0.21	***
	LL	*Prochlorococcus*	0.00031	39.69	< 0.0001	0.36	***
		Synechococcus	0.00064	14.14	0.097	0.02	
		Nano	0.03502	39.01	< 0.0001	0.73	***
CHEMTAX - Strict	HL	*Prochlorococcus*	0.00010	4.98	0.0003	0.11	***
		Synechococcus	0.00010	30.41	0.071	0.02	
		Nano	0.00054	10.24	< 0.0001	0.15	***
	LL	*Prochlorococcus*	0.00041	52.08	<0.0001	0.42	***
		Synechococcus	0.00045	12.00	0.23	0.005	
		Nano	0.03478	24.31	< 0.0001	0.68	***

Table 2.5: Chlorophyll-*a* content per cell for *Prochlorococcus, Synechococcus* and picoeukaryotes, with cell counts obtained from flow cytometry. For size-class approach, picoeukaryotes are considered equivalent to nanophytoplankton class. For the taxa-based approach, picoeukaryotes represent the combined chl-*a* biomass of pelagophytes and prymnesiophytes. For CHEMTAX, picoeukaryotes represent combined chl-*a* biomass of prymnesiophytes, cryptophytes, chlorophytes and chrysophytes. * < 0.5, ** < 0.01, *** < 0.001

		Pigment / cell (fg chl-*a*/cell)			
Method	**Class**	**Mean HL**	**Mean LL**	**Difference according to depth**	
Size-class based (Uitz *et al.* 2008)	Pico	0.32	9.1	$W = 937,\ p < 0.0001$	***
	Picoeukaryotes	24.9	345	$W = 1601,\ p < 0.0001$	***
Taxa-based (Bidigare & Ondrusek 1996)	Prokaryote	0.39	8.2	$W = 1116,\ p < 0.0001$	***
	Picoeukaryotes	28.8	404	$W = 1137,\ p < 0.0001$	***
CHEMTAX	*Prochlorococcus*	0.142	2.43	$W = 495, p < 0.0001$	***
	Synechococcus	14.3	215.6	$W = 3825, p = 0.003$	**
	Picoeukaryotes	26.1	334.4	$W = 1005, p < 0.0001$	***

2.4.5 Depth-dependent trends in phytoplankton pigments

Depth-dependent trends in zea:chl-*a* ratios have already been demonstrated (Fig 2.2) and used to divide samples according to light regime. A significant relationship is also seen in the ratio of chl-*b*:chl-*a* with respect to depth (*z*) (Fig 2.9a).

$$\text{Chl-}b\text{:chl-}a = 0.0288 + 0.0024\, z,\ (F_{1,\,419} = 301,\ p < 0.0001,\ R^2 = 0.42). \quad (14)$$

The CHEMTAX biomass estimates can be used to study variations in intracellular pigment concentration as a function of depth. The estimated group specific outputs of chlorophyll biomass using CHEMTAX are approximations, and in situations where a group is absent, a non-zero, and sometimes very small negative value can be generated (ranging from 0 to -3.3 x 10^{-14}), preventing the use of logarithms in the analysis of the CHEMTAX outputs. All samples with negative biomass estimates were excluded from the dataset for this part of the analysis (n = 5 for *Prochlorococcus*, n = 36 for *Synechococcus*). A strong linear relationship is seen between the log of the intracellular chl-*a* concentration and depth for *Prochlorococcus* (Fig 2.9b, Table 2.4), with a mean of 0.14 fg / cell for HL samples and 2.4 fg / cell for LL. *Synechococcus* also shows a strong correlation (Fig 2.9c) with a mean HL pigment content of 1.4 fg / cell and 216 fg / cell for LL. Eukaryotes also show a significant relationship (Fig 2.9d), with mean of 26 fg / cell for HL and 334 fg / cell for LL.

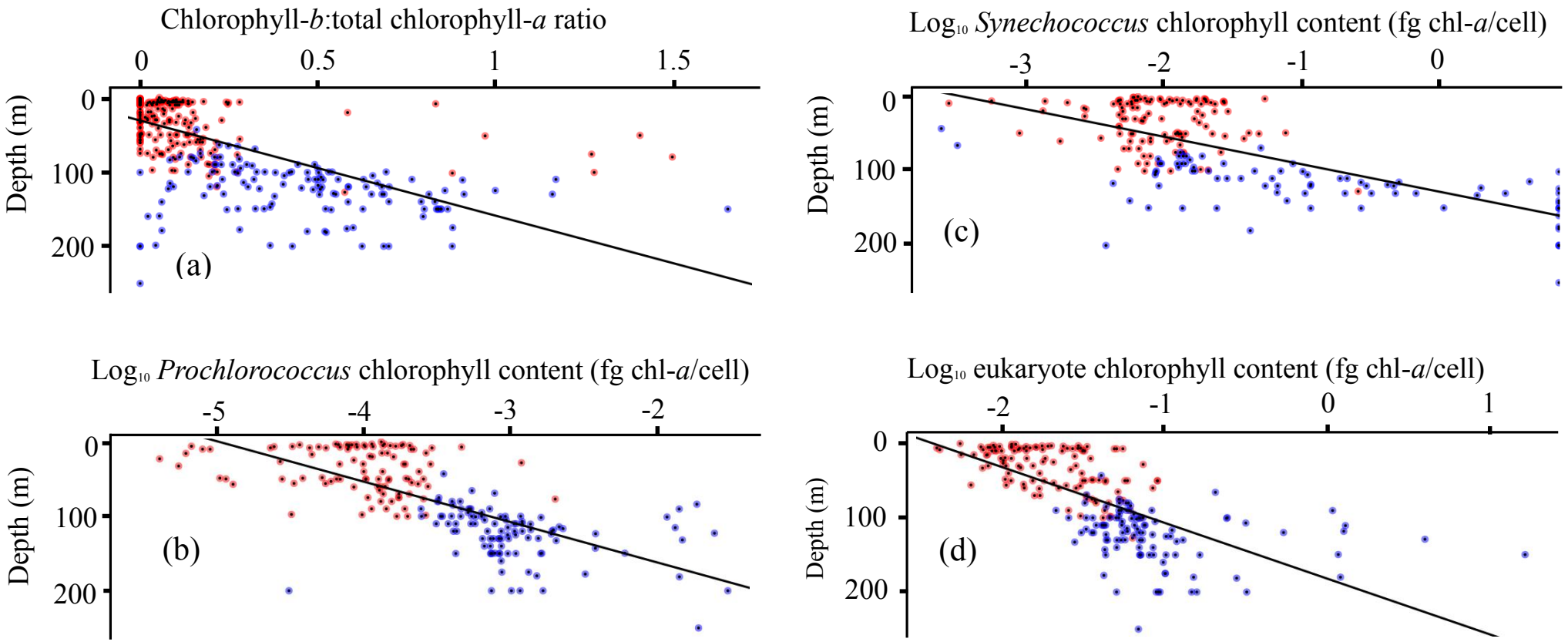

Fig 2.9: Relationships between phytoplankton chlorophyll-*a* content and depth. HL samples in red, LL in blue. (a) Changes in the ratio of chl-*b* to chl-*a* with respect to depth. (b) *Prochlorococcus* chl-*a* / cell as a function of depth. (c) *Synechococcus* chl-*a* / cell as a function of depth. (d) Eukaryote chl-*a* / cell as a function of depth; note some very high pigment / cell values for some deep samples, possibly due to low sample volumes being counted.

2.4.6 Depth-dependent trends in carbon-to-chlorophyll ratio

By using literature estimates of cell carbon from Grob *et al.* 2011 it is also possible to consider these trends in terms of changes in the carbon-to-chlorophyll ratio (θ) (Table 2.6). A strong logarithmic trend with respect to depth is seen in θ for *Prochlorococcus* ($F_{1,86} = 94$, $R^2 = 0.52$, $p < 0.0001$), giving a theoretical surface θ of 1110 g/g (Fig 2.10a), a mean for HL samples of 384 g/g, for LL of 81 g/g and a mean of 225 g/g over the entire water-column. A significant exponential decay relationship between θ and depth is also observed for *Synechococcus* (Fig 2.10b) ($F_{1,181} = 73$, $R^2 = 0.28$, $p < 0.0001$), giving a theoretical surface θ of 168 g/g, a mean for HL samples of 14 g/g, 9 g/g for LL and 11 g/g for the whole water-column. The proportion of variance explained however is smaller than seen for *Prochlorococcus*. The relationship between θ and depth for picoeukaryotes is again an exponential decay, and is highly significant (Fig 2.10c) ($F_{1,220} = 183$, $R^2 = 0.45$, $p < 0.0001$). The regression of this relationship gives a theoretical value of 155 g/g at the surface. The mean for all HL samples is 38 g/g, and 9 g/g for LL, with an overall water-column mean of 24 g/g. There are several points which may represent either an underestimate of cell abundances or an over estimate of picoeukaryote biomass since values of θ below 1 are not possible (Taylor *et al*. 1997).

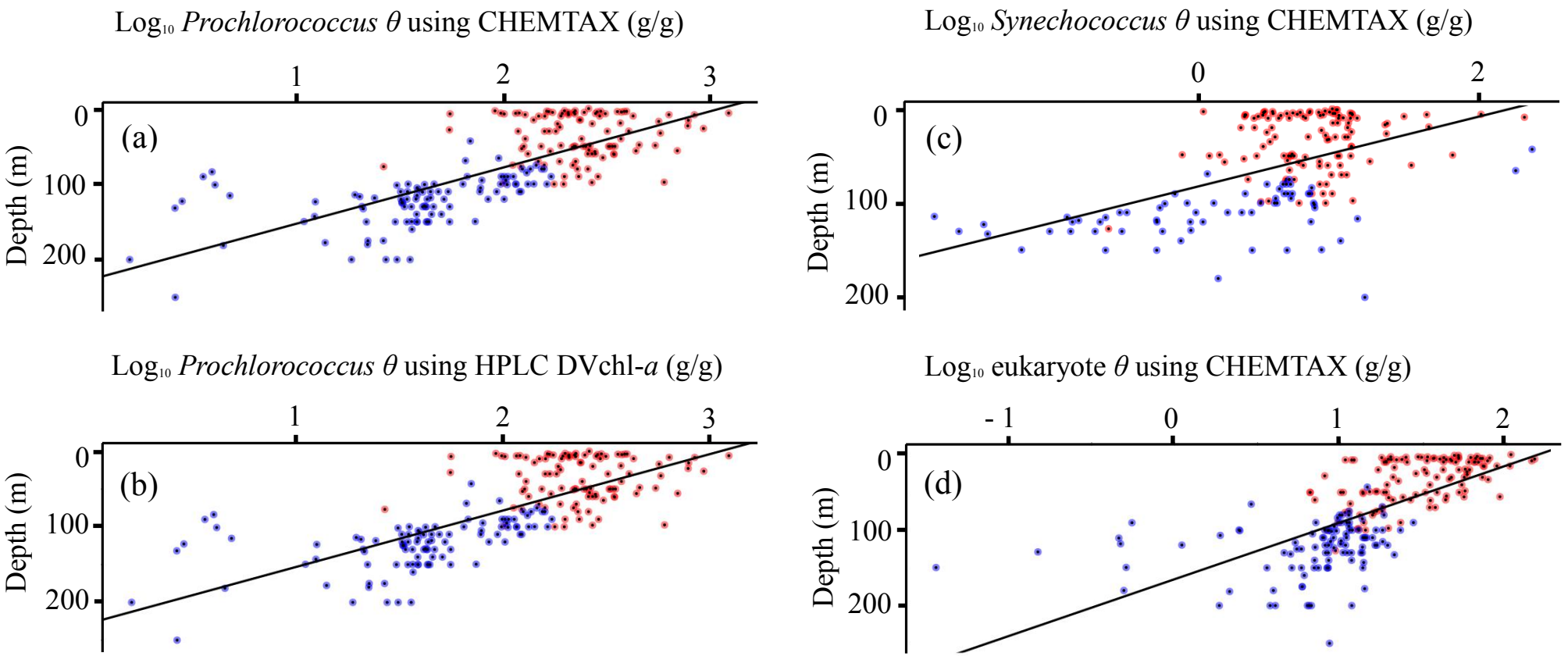

Fig 2.10: Relationships between carbon-to-chlorophyll ratio (θ) and depth for different phytoplankton groups. Cell carbon estimated from flow cytometry counts and cell carbon c from Grob *et al.* (2011). HL samples in red, low light adapted in blue. (a) *Prochlorococcus* using chlorophyll estimate from CHEMTAX, showing the strong trend between θ of 10 and 1000, yet potential scatter outside this range. (b) *Prochlorococcus* using HPLC DVchl-*a*. (c) *Synechococcus* using biomass from CHEMTAX. (d) Picoeukaryotes, using chlorophyll from CHEMTAX.

Table 2.6: Carbon-to-chlorophyll ratios with respect to depth for *Prochlorococcus, Synechococcus* and picoeukaryotes. Group-specific biomass from lax CHEMTAX analysis, carbon estimates converted from flow cytometry cell counts and cell-specific carbon conversion factors from Grob *et al.* 2011.

Carbon-to-chlorophyll ratio (g/g)									
Class	**Surface**	**Mean HL**	**Mean LL**	**Whole water-column**	**Relationship with depth (*z*)**	**F statistic**	***p***	**R^2**	
Prochlorococcus (HL 35 fg/cell, LL 50 fg/cell)	1110	384	81	225	$y = 10^{((231-z)/67.8)}$	$F_{1,86} = 94$	< 0.0001	0.52	***
Synechococcus (60 fg /cell)	168	14	9.16	11	$y = 10^{((82.6-z)/37.1)}$	$F_{1,181} = 73$	< 0.0001	0.28	***
Picoeukaryotes (600 fg /cell)	155	38	9.3	24	$y = 10^{((165 - z)/75.3)}$	$F_{1,220} = 183$	< 0.0001	0.45	***

2.5 Discussion

2.5.1 Comparison between pigment-based approaches

To consider the suitability of CHEMTAX as a tool for separating chl-*a* standing stock into various phytoplankton classes, it is necessary to assess its performance relative to simpler pigment-based methods. As an iterative empirical approach, CHEMTAX involves a degree of uncertainty in the outcome (Latasa *et al*. 2007). As the pigment:chlorophyll-*a* ratios used are allowed to vary, if unconstrained, it is possible for a mathematically-optimal solution of the relative contribution of different groups to be unrelated to those actually present in the sample (Latasa *et al.* 2007). Conversely, for a highly-constrained analysis to apportion biomass accurately, the pigment:chl-*a* ratios must be assigned based on knowledge of the geographic location and sampling depth.

2.5.1a Size-based method – Uitz *et al*. (2008)

Strong correlations between the picophytoplankton output from the size-based approach and cyanobacterial biomass from CHEMTAX are observed, for both HL and LL samples (Fig 2.3a). While there is some scatter seen around the 1:1 relationship, in the absence of any independent data on the fractional contribution of picophytoplankton to total biomass, it is difficult to know which approach is closer to the truth.

A difference in biomass estimates using the Uitz *et al.* (2008) approach and CHEMTAX for the nanophytoplankton class (Fig 2.3b) has important implications for assessing the global distribution of this group using pigments. Given that the dataset used in this study consists entirely of samples defined as originating from the Gyres (Polovina *et al.* 2008), one would expect the combined biomass of small eukaryotes such as prymnesiophytes,

chlorophytes, cryptophytes and chrysophytes is likely to form a major portion of the total (Raven *et al*. 1998) as confirmed by studies such as that of Grob *et al.* (2011). The oligotrophic gyres are typically stratified systems with relatively shallow mixing (Marañon 2005), allowing for populations at different depths to acclimate to the prevailing light conditions. That the biomass for nanophytoplankton as estimated by the size-based classification method is lower than that from CHEMTAX is likely to be due to the inflexibility of a fixed pigment:chl-*a* approach to classification. Unlike CHEMTAX the Uitz *et al.* (2008) method uses a single pigment-ratio for both HL and LL samples, despite the large differences in photoacclimatory status and taxonomic composition of phytoplankton cells between surface and deep assemblages seen by a range of other studies (Rodriguez *et al*. 2006, Veldhuis & Kraay 2004). The size-based classification method was developed from work by Claustre (1994), Vidussi *et al*. (2001), and the pigment:chl-*a* ratios were derived from a global study (Uitz *et al.* 2006), and has a bias towards high chlorophyll regions, where the proportion of large microphytoplankton is much higher than in the Subtropical Gyres. The diagnostic pigment for microphytoplankton used in Uitz *et al.* (2008) is fucoxanthin which can be a major pigment of prymnesiophytes and chrysophytes as well as some dinoflagellates (Wright *et al*. 1997). Therefore it is possible that fucoxanthin associated with smaller eukaryotes in the size-based classification method is instead assigned to the microphytoplankton, causing a lower estimate of nanophytoplankton biomass (Uitz *et al* 2009).

The potential shortcomings of using fixed pigment:chl-*a* ratios, and allowing each diagnostic pigment to appear in only one size-class, are seen again when considering the microphytoplankton size class (Fig 2.3c). CHEMTAX estimates the biomass due to microphytoplankton to be less than half of that found using the size-based method of classification, for both HL and LL samples. Microphytoplankton are predicted to be scarce in

the oligotrophic ocean (Le Bouteiller & Blanchot 1991, Marañon *et al*. 2001), particularly in HL samples, as confirmed by size fractionated chl-*a* analysis. The difference in mean microphytoplankton biomass may therefore reflect the self-tuning aspect of CHEMTAX, with CHEMTAX assigning much of the biomass associated with fucoxanthin to prymnesiophytes, which are known to be dominant in the open ocean, low-chlorophyll regions of this study.

Alternatively, since HL and LL samples are considered separately, the output from CHEMTAX may reflect the very high intracellular pigment concentrations seen in microphytoplankton, deep in the water-column resulting from acclimation to very low irradiances.

2.5.1b Taxa-based approach (Bidigare & Ondrusek 1996)

This classification method was developed in the central equatorial Pacific, and while it only uses 4 diagnostic pigments, as compared with the 7 from the size-based classification method of Uitz *et al.* (2008), or 10 as used in this CHEMTAX analysis, it is of considerable interest given the two stage approach to allocating 19'-hex and 19'-but, and important since it may be used in studies where the full array of accessory pigments is not available. For the Gyres however the method is at a disadvantage as the contribution to the total biomass from picophytoplankton, typically the most important contributor to total phytoplankton biomass (Fig 2.5), is not calculated directly, but instead is estimated from the difference between the total chl-*a* and that ascribed to the various eukaryotic groups. This aspect of the method can be regarded as a major drawback, since some samples are assigned a negative picophytoplankton biomass (Fig 2.3d).Such negative biomass estimates prevent a range of further analyses, such as pigment per cell calculations. This “reverse” approach of estimating biomass for picophytoplankton also leads to lower contributions for LL samples than that obtained using CHEMTAX.

A very close correlation is seen between dinoflagellate biomass as estimated by CHEMTAX and the taxa-based classification method (Fig 2.3f). This correlation is despite the latter only using peridinin as a diagnostic pigment, as compared with peridinin and 19'-hex for CHEMTAX. Such a close fit may be due to the intermediate step used in the taxa-based method of Bidigare & Ondrusek (1996) to calculate prymnesiophyte 19'-hex.

However, major differences in the contribution to total chl-*a* of the other eukaryotic groups as estimated by the taxa-based approach and CHEMTAX are seen. The taxa-based classification approach allocates far more biomass to prymnesiophytes and less to diatoms for both HL and LL samples than CHEMTAX (Fig 2.3e & 2.3g). Large differences are also observed for HL samples for both taxonomic groups, where the taxa-based method gives a wide range of biomass estimates for diatoms and prymnesiophytes, for samples where CHEMTAX finds them both to be absent. Previous studies such as Maranon *et al*. (2000) and Le Bouteiller *et al*. (2001), found neither group to be present in large numbers in surface Gyre waters, thus illustrating a major drawback of fixed pigment:chl-*a* ratio approaches to estimating community structure, and demonstrating the greater flexibility afforded by CHEMTAX. This flexibility is of particular use when the method is being applied to areas outside that where the pigment:chl-*a* ratios were first calculated. Since the major benefit of pigment-based methods of classification is that it should be possible to apply them consistently in studies where flow cytometry or microscope data is not available, this result alone does much to justify the extra complexity that CHEMTAX entails.

It is not surprising that pelagophytes biomass from the taxa-based approach does not compare well with the output from CHEMTAX (Fig 2.3h), with the CHEMTAX output being significantly higher for both HL and LL pelagophytes samples. Since the taxa-based method only assigns biomass to 4 eukaryotic phytoplankton groups, the category of pelagophytes must be compared with the sum of the CHEMTAX biomass estimates for all eukaryotic

groups apart from diatoms, dinoflagellates and prymnesiophytes, in this case chlorophytes, cryptophytes and chrysophytes. As well as offering valuable information as to how this biomass is further divided into other classes of phytoplankton, CHEMTAX may offer more robust estimates due to the higher number of indicator pigments used in the analysis.

2.5.2 Spatial comparisons of size-class based method and CHEMTAX

Differences in the proportion of biomass assigned to each group also reveal interesting trends when considered spatially. The size-based approach consistently places a greater proportion of the total biomass in the microphytoplankton group than CHEMTAX, for reasons discussed above (Fig 2.4a). The difference in the proportion of the biomass due to nanophytoplankton and picophytoplankton according to the size-based approach of Uitz *et al.* (2008) and CHEMTAX(Fig 2.4b&c) show a very interesting localised effect. The size-based approach results in much higher proportions of picophytoplankton than CHEMTAX at 20 ^{o}N while resulting in a much lower proportion at the same latitude in the southern hemisphere. CHEMTAX allocates this biomass to the nanophytoplankton, resulting in the reverse pattern. This demonstrates the drawbacks of allowing a single pigment to be used as an indicator for only a single phytoplankton class, and may result in an overestimation of the global standing stock of microphytoplankton when such pigment methods are combined with satellite maps of chlorophyll.

As well as overall correlation between biomass as estimated by different methods, it is important to establish whether the differences seen are as a result of random scatter or systematic bias. Of interest is the spread of points observed in estimated microphytoplankton biomass, with 4 samples giving values of over 100 ng/l microphytoplankton chl-*a*, all from the top 50 m of the water-column and with a maximum of 171.4 ng/l microphytoplankton chl-*a*. In general the size-class based method consistently results in a higher

microphytoplankton biomass estimate for almost all samples (Fig 2.4a). While there is some large-scale patchiness visible, there does not appear to be a consistent depth- or latitude-dependent trend. In the case of nanophytoplankton (Fig 2.4b) and picophytoplankton (Fig 2.4c), a more systematic bias is seen, particularly around 20^{o} North and South. The size-class based method estimates the proportion of biomass due to nanophytoplankton to be almost half of that as estimated using CHEMTAX for the stations at 21 ^{o}N (EUMELI), while resulting in much higher proportional estimates for stations at 15 ^{o}S. The opposite pattern is then seen for the proportion of picophytoplankton.

2.5.3 Validation against flow cytometry counts

Due to the highly variable nature of phytoplankton photoacclimation, no pigment-based method of estimating biomass can explain all the variability in cell abundance measured by flow cytometry (Figs 2.6 & 2.7), since the conditions to which the samples are adapted vary widely. Studies such as Gieskes & Kraay (1986) and Partensky *et al.* (1999) have tried to quantify intracellular chlorophyll concentrations, but this is dependent on the light regime, nutrient availability and the species present. Given that Blanchot *et al*. (2011) identified an 11-fold difference in intracellular chl-*a* concentration according to light regime, it was decided that any attempts at converting counts to chlorophyll estimates would result in large errors, and potentially mask more fundamental trends or biases relating to differences in the methods themselves.

Since large cells (microphytoplankton) cannot be counted using flow cytometry, validation of biomass estimates for this size-class was not possible. This study however was limited to data from gyres, and the proportion of the total biomass due to microphytoplankton was low, as seen from size-fractionated chl-*a* analysis (Fig 2.5), all the pigment-based chemotaxonomic approaches, and previous studies in similar areas Herbland *et al.* (1985) and

Marañon *et al.* (2003), so biomass estimates for this size-class will not be considered for validation.

For all size-classes and classification approaches there was a positive offset for LL samples, where the pigment-based approaches resulted in high biomass estimates, and few or no cells were counted using flow cytometry. In the case of the eukaryotes, this is likely to be due to their low abundance, and the low volumes being measured, since a small absolute error combined with a low total count will result in a large proportional error (Shalapyonok *et al.* 2001). Correlations seen are very similar for the size-based classification method, the taxa-based classification method and for CHEMTAX (Figs 2.6 & 2.7, Table 2.4).

When considering the picophytoplankton group from the size-based approach or the prokaryote group from the taxa-based approach, *Prochlorococcus* has a mean abundance 40 times higher than *Synechococcus* and hence trends in the combined abundance reflect those in *Prochlorococcus*. The offset seen for LL *Prochlorococcus* could be caused by the presence of two separate deep populations, with different photoacclimatory responses (Fig 2.7). This second population, with cell counts of greater than 150,000/ml yet low biomass estimates from CHEMTAX appears to have an intracellular DVchl-*a* concentration more similar to that seen in the HL samples, than the remaining LL samples. Moore *et al.* (1995) and Partensky *et al.* (1999) found that DVchl-*b* was an important accessory pigment for certain *Prochlorococcus* ecotypes and so the surprisingly low pigment values may represent a switch from DVchl-*a* to DVchl-*b* as a major light-harvesting pigment. Since these samples are almost exclusively from the EUMELI series of cruises, where DVchl-*b* was not separated from MVchl-*b*, it is not possible to reach any firm conclusions. An alternative explanation is that these LL samples could represent a HL population, being incorrectly classified as LL, although as they have a mean depth of 96 m, this is unlikely. From absorption by water alone, using the value for K_w from Platt *et al*. (2003), irradiance at this depth will be 1.6% of that at

the surface. Given however the lack of any confirmed reason for omitting them from the analysis however, they were included in all statistical analysis as LL samples.

There are also potential problems in obtaining accurate flow cytometry data for samples subjected to high surface irradiances. Studies such as Partensky *et al.* (1999) have reported difficulties in counting HL *Prochlorococcus* cells due to their very low fluorescence values. This explains the high degree of scatter relative to the changes in pigment concentration due to changes in cell abundance, meaning that correlations are tighter and a greater proportion of total variance is explained for LL samples than in the HL samples for *Prochlorococcus* for all methods.

Relationships between biomass estimates and flow cytometry counts for *Synechococcus* are less clear than for either eukaryotes or *Prochlorococcus* (Fig 2.7b). This may be due in part to the range of cell abundances recorded by flow cytometry. 95% of samples have *Synechococcus* abundances ranging from 0 to 5679 cells/ml, leading to correlations being heavily influenced by a small number of samples with very high abundances (up to 43000 cells/ml). Despite the benefits of CHEMTAX, the method has certain important drawbacks when estimating *Synechococcus* abundance and is highlighted by the presence of LL samples where *Synechococcus* biomass is estimated to be high by CHEMTAX, yet is absent or very scarce according flow cytometry data. Studies have shown that *Synechococcus* is generally rare in deep samples (Moore *et al*. 1995, Partensky *et al*. 1999), which suggests that the high biomass predicted by CHEMTAX is a result of the lack of a unique pigment to identify *Synechococcus*. The CHEMTAX biomass estimate for *Synechococcus* is based solely on zeaxanthin concentration, a pigment also found in significant quantities in *Prochlorococcus, Trichodesmium* and other cyanobacteria not enumerated by flow cytometry. Ambiguity as to the source of zeaxanthin may potentially leading to false correlations between *Prochlorococcus* and *Synechococcus* biomass, as seen in

Fig 2.8, where *Synechococcus* is almost absent below 120 m according to flow cytometry data, whereas the output from CHEMTAX would suggest it is abundant to a depth of almost 200 m.

The relationship between eukaryotes as measured by flow cytometry and nanophytoplankton is strong for all three approaches (Fig 2.6c, e, 2.7c) for HL samples. This reflects the trend that within a phytoplankton group, species found in gyres are often smaller than those found in higher-biomass regions (Chavez *et al.* 1996, Vidussi *et al*. 2001, Uitz *et al.* 2006) and confirms the results shown in Fig 2.4, where the biomass measured from size-fractionated chl-*a* as determined by fluorometry is smaller than the pigment-based methods would predict. The gradient of the regressions is very similar across the methods for HL samples, while for LL samples it is considerably higher from CHEMTAX as a result of the pigment:chl-*a* ratio being increased to account for photoacclimation.

It is difficult to distinguish the different methods using their regressions against flow cytometry counts, since all three approaches find significant correlations between estimated chlorophyll biomass and flow cytometry counts for photosynthetic prokaryotes and picoeukaryotes (Figs 2.6 & 2.7, Table 2.4). Despite not explaining significantly more variation when validated against flow cytometry, CHEMTAX has certain very important benefits. The taxa-based approach is not appropriate for this study area, due to the manner in which prokaryotic biomass is calculated as the difference between the total and that assigned to the various eukaryotic groups. Given the importance of prokaryotes in warm, nutrient-poor waters (Raven 1998), a method where a substantial number of negative biomass estimates is not appropriate, since this implies that there may be a systematic bias in the estimation of this size-class and serious and undetectable errors in other samples. The size-based approach, while quick and simple to implement, is limited in output to three size-classes by the low number of indicator pigments used and the fixed nature of the pigment:chl-*a* ratios, whereas

by contrast CHEMTAX provides estimates for 8 groups, with HL and LL samples considered separately for each, allowing a more detailed understanding of how the biomass in a sample is divided.

2.5.4 Depth-dependent trends in pigment concentrations

That the ratio of chl-*b*:chl-*a* increases with depth is consistent with the trends reported by McManus & Dawson (1994), Bouman *et al.* (2000), Blanchot *et al.* (2001), Barlow *et al.* (2002) and Veldhuis & Kraay (2004) (Fig 2.9). The magnitude of this effect seen in this study however is far larger than seen by Blanchot *et al.* (2001), where chl-*b* was never more abundant than chl-*a*, and is instead similar to the trends seen in Bouman *et al.* (2000) where ratios of greater than 1 were reported. The increased importance of chl-*b* relative to chl-*a* as depth increases fits with the vertical profiles of *Prochlorococcus* from flow cytometry, and estimated using CHEMTAX (Fig 2.8). Increases in the chl-*b*:chl-*a* ratio are also seen as a photoacclimatory response of *Prochlorococcus* in field studies (Bouman *et al.* 2000) and in cultures (Partensky *et al.* 1993), meaning that the intracellular chl-*a* content of cells can be used under stratified conditions to provide an estimate of the light regime to which a population is acclimated.

The output from CHEMTAX can be used in conjunction with the flow cytometry counts to consider photoacclimation in the form of depth-dependent trends in pigment per cell (Fig 2.9, Table 2.5) A robust understanding of how intracellular concentrations of phytoplankton pigments change according to depth or cell size will aid comparisons between chlorophyll-based estimates of biomass such as from size-fractionated HPLC measurements and carbon-based approaches such as flow cytometry or microscopy. Larger cells contain a greater quantity of pigment, and displayed less variation with respect to depth. All size-classes for all methods displayed a strong positive correlation with respect to depth, demonstrating

the effects of photoacclimation. For eukaryotes the estimated chl-*a* / cell was very similar for all three approaches for both HL and LL samples. Cell chlorophyll estimates for picophytoplankton according to the size-based approach and prokaryotes from the taxa-based approach were far closer to those for *Prochlorococcus* than *Synechococcus* from CHEMTAX, reflecting the far greater *Prochlorococcus* abundances, despite the larger size of *Synechococcus* cells. Errors were observed in the estimates of cell biomass for high light-adapted *Prochlorococcus* populations, possibly due to the extremely low pigment concentrations at the sea surface, leading to implausibly low intracellular pigment concentrations. Interestingly, greater scatter on the relationship between intracellular pigment concentration and depth was seen for the LL eukaryote samples, perhaps demonstrating the range in pigment concentrations seen for a given depth due to the diverse taxonomic make up of this group.

2.5.5 Carbon-to-chlorophyll as a function of depth

The relationships observed between intracellular pigment concentrations and depth can also be considered in terms of trends in the carbon-to-chlorophyll ratio (θ) (Fig 2.10, Table 2.6). θ is a parameter used by ocean modellers, to convert elemental currencies of phytoplankton biomass such as carbon or nitrogen content into estimates of chl-*a* to compare with satellite ocean-colour data, and can be used to estimate growth rates using biomass-normalised photosynthetic rates measured in the field (Eppley 1972). This permits carbon-based models of carbon flux to be linked with remotely-sensed chlorophyll-based models of photosynthesis. All phytoplankton primary production models may be parameterized using a combination of 4 terms: the initial slope of the photosynthesis-irradiance curve, the light saturation parameter of the curve, the specific absorption by phytoplankton and θ (Sathyendranath *et al*. 2009), with trends in θ the most poorly understood (Taylor *et al*. 1997). The carbon-to-chlorophyll ratio is

also very difficult to measure in natural assemblages as the inclusion of dead or non-photosynthetic material is inevitable (Sathyendranath *et al.* 2009). As the variation in cell pigment content with depth is much greater than that seen in cell carbon, robust carbon estimates were obtained from applying the values from Grob *et al*. (2011). Despite this, a range of implausible values for θ are seen, perhaps due to either the HPLC-measured pigment biomass being low, or the volume counted using the flow cytometer being low, both potentially increasing the relative errors (Fig 2.10). It is also important to note the possible bias introduced in cell counts of surface populations of *Prochlorococcus* (< 60 m) that are exposed to very high growth irradiances, since their red fluorescence values are so low that accurate counting is difficult (Partensky *et al.* 1999)and this could be a possible explanation for the very high estimates for surface θ, which is far higher than seen in previous studies (Veldhuis & Kraay 2004). Values of average water-column θ were still higher than those for Veldhuis & Kraay (2004) by a factor of about 2, but are well within the range reported in previous studies (Redalje & Laws 1982, Goericke & Welschmeyer 1993, Buck *et al.* 1996). The estimates of water-column θ for this study may also be elevated by the very high number of surface samples included in the analysis.

Significant trends in θ for *Synechococcus* were also seen. The surface value predicted for θ for *Synechococcus* is lower than seen for *Prochlorococcus*, at 168 g/g. The lower θ reflects the decreased efficiency in light-harvesting for *Synechococcus* as compared with *Prochlorococcus* due to the package effect (Duysens 1956, Morel & Bricaud 1981, Sathyendranath *et al.* 1987, Key *et al*. 2010). Package effect is such that, for a given intracellular pigment concentration, a large cell will be able to harvest proportionally less light than a smaller one, for the same concentrations of chl-*a* due to self-shading, leading to higher intracellular concentrations of chl-*a* and hence a decrease in θ as cell size increases. Of interest however is the effect on the regression of LL samples at implausibly low values of

θ, possibly representing an overestimation of the contribution from *Synechococcus* to the total biomass.

The estimates of picoeukaryote θ also correspond well with previous studies with a mean water-column value of 24. This is a result of their larger cell size and hence decreased efficiency of light-harvesting, as noted by Finkel (2001) and references within. Veldhuis & Kraay (2004) reported the rate at which θ changed with respect to depth was lower for picoeukaryotes than smaller cells which is consistent with the results found in this study, although the values observed by Veldhuis Kraay (2004) were higher than in this study (water-column means ranging from 35 to 58 g/g)

2.6 Conclusions

When comparing the two fixed pigment:chl-*a* approaches with CHEMTAX it is important to note the general correlation seen in the division of biomass into phytoplankton groups across the different methods, although certain important differences were seen. CHEMTAX displayed greater flexibility than either the size-based approach or the taxa-based one, in particular with respect to depth-dependent effects, since the scope for self-tuning means the different pigment complements seen for HL and LL samples can be accounted for. The ability to separate the two cyanobacterial genera *Synechococcus* and *Prochlorococcus* is also potentially of use for studies wanting to understand the ecological dynamics of picophytoplankton populations in the Subtropical Gyres. However, when using CHEMTAX care needs to be taken to avoid false correlations between the two genera. In particular, the size-based approach appeared to overestimate the proportion of biomass due to microphytoplankton based on the size-fractionated estimates of chl-*a* for the study region. The taxa-based method, however, produced negative estimates of prokaryotic biomass for some samples, likely caused by the way the method defined the prokaryotic contribution as the difference between the total and that of the various eukaryotic groups estimated by diagnostic pigment ratios, which may not be suitable for Gyre conditions.

This study has clearly identified at least two separate populations of phytoplankton, with different pigment suites, both in terms of intracellular concentration and type. HL and LL populations could be separated according to the chlorophyll-normalised concentration of zeaxanthin, one of the key photoprotective pigments. Differences in photoacclimatory status between HL and LL populations were confirmed by similar trends in the intracellular concentration of DVchl-*a* in *Prochlorococcus* and the depth-dependent changes in chl-*a*:chl-*b*

ratio. A possible exception comes from a second deep population of *Prochlorococcus* at 21°N, with much lower intracellular concentrations of divinyl chl-*a*, possibly due to an increased dependence on other photosynthetic pigments.

Given the degree to which the ecological function of phytoplankton varies according to the taxa present, reliable methods of estimating community structure using HPLC pigments are essential for assessing trends in phytoplankton distribution across large spatial scales. Since a wide variety of approaches exist, it is very important that large-scale studies evaluate the performance of the different methods, not only to assess which provides the best results, but also in order to identify particular drawbacks or weaknesses of each approach.

CHEMTAX has been one of the most widely-used methods of assessing phytoplankton community structure using diagnostic pigments, despite the initial setup of the input data matrices requiring consideration of the geographical region, the dominant phytoplankton groups present and photoacclimatory changes. CHEMTAX has been shown to be robust due to the flexibility in adjusting the initial pigment:chl-*a* ratios, allowing for the method to be applied using the same initial conditions over a wide area, in this case the Subtropical Gyres. While previous studies have shown that the pigment:chl-*a* ratio needs to be tightly constrained, here we demonstrate that even when the ratios are allowed to vary freely, accurate and reliable outputs may be produced, which suggests that using CHEMTAX reliable depth-specific relationships can be obtained for both the carbon-to-chlorophyll ratios for different phytoplankton groups, and for intracellular pigment concentration. Depth dependent trends in carbon-to-chlorophyll ratios can be used in future studies both to allow conversion between carbon- and chlorophyll-based models of primary production, and between biomass normalised photosynthetic rates and growth rates.

2.7 Appendix: – CHEMTAX configuration

2.7.1 CHEMTAX definitions

Ratio matrix: The theoretical ratio of pigment to total chl-*a* for each group.

Ratio limits matrix: The amount by which each pigment ratio is allowed to vary.

Epsilon limit: Specifies the root mean square difference between measured and predicted pigment compositions during calculation. If the residual is less than this, the calculation is deemed to be complete.

Iteration limit: Maximum number of iterations.

Cut-off step: The calculation is deemed complete if the step size increases beyond this.

Initial step size: Indicates the amount to vary pigment ratio matrix with each iteration. E.g. value of 5 causes it to be varied by 1/5.

2.7.2 Division of samples for analysis

How the samples are divided for analysis is key when using CHEMTAX as while the output for a given sample is determined by the pigment:chl-*a* matrix, the matrix is in turn affected by the pigments present in the other samples in the batch. Many studies using CHEMTAX use samples from a single depth (Mendes *et al.* 2011, Eker-Develi *et al.* 2012) meaning that the photoacclimatory status of samples need not be considered. Others such as Mackey *et al.* (1996), Bel Hassen *et al.* (2008) and Wright *et al.* (2010) sorted the samples by depth before dividing into batches for analysis. This study however aims to characterize two phytoplankton populations, and it would not have been possible to consider the physiological differences of high- and low-light adapted populations had the data been divided into 8 depth bands. The relationship between depth and light depends on the attenuation of downwelling irradiance,

which in the open ocean can be considered to be a function of chlorophyll biomass (Kirk 2011), meaning that depth alone cannot be used as a measure of phytoplankton photoacclimation, particularly for studies covering very large areas. Photoacclimatory status is not the source of changes in the relative abundances of phytoplankton pigments, with variations also being seen according to biomass and season. A test was performed using a dataset with a 40-fold range of chlorophyll concentrations to examine for biomass-related sensitivity in the pigment ratios. Great consistency in the pigment:chl-*a* ratios which CHEMTAX converged on was seen across the range of chlorophyll concentrations, with no significant biomass-dependent relationship, supporting the approach of dividing samples for analysis according to light regime as opposed to biomass.

2.7.3 Strict and lax criteria

Under the "strict" criteria, pigment:chl-*a* ratios were tightly constrained, only being allowed to vary by 25% from their initial value (*r*) with each run. For the "lax" configuration the pigment:chl-*a* ratios were allowed vary by 500% (from *r*/5 to 5*r*) to find the mathematically-optimal solution. In each case, CHEMTAX was run twice, and as computational time was not limited the settings were chosen to try and reach as precise a result as possible, with the epsilon limit set to 0.0001, the iteration limit 1000, and the cut-off step 1000. No sub-iterations were used, with all pigments being varied independently with each iteration. The pigment:chl-*a* ratio output matrices for each analysis are shown in Table 2.7. See Table 2.8 for details of group-specific biomass from each analysis.

Table 2.7: Pigment:chl-*a* ratios for CHEMTAX. (A) Input matrix from Gibb *et al.* 2001. (B) Output ratios for HL samples after 2 runs under "strict" configuration with ratios allowed to vary by 25% per run. (C) Output ratios for LL samples after 2 runs under the "strict" configuration. (D) Output ratios for HL samples after 2 runs with "lax" settings with ratios allowed to vary by 500% per run. (E) Output ratios for LL samples after 2 runs under the "lax" configuration.

	chl-*c3*	**per**	**19'-but**	**fuc**	**19'-hex**	**allo**	**zea**	**chl-*b***	**DVchl-*a***	**MV chl-*a***
(A) Input matrix										
Diatoms	0	0	0	0.76	0	0	0	0	0	1
Dinoflagellates	0	1.06	0	0	0	0	0	0	0	1
Prymnesiophytes	0	0	0.02	1.21	0.38	0	0	0	0	1
Chrysophytes	0.17	0	1.56	0.97	1.36	0	0	0	0	1
Chlorophytes	0.25	0	0	0	0	0	0.12	0.57	0	1
Synechococcus	0	0	0	0	0	0	0.59	0	0	1
Cryptophytes	0	0	0	0	0	0.23	0	0	0	1
Prochlorococcus	0	0	0	0	0	0	0.2	0.5	1	1
(B) Strict HL output matrix										
Diatoms	0	0	0	0.76	0	0	0	0	0	1
Dinoflagellates	0	1.06	0	0	0	0	0	0	0	1
Prymnesiophytes	0.19	0	0.02	0.80	0.41	0	0	0	0	1
Chrysophytes	0.34	0	1.66	0.59	1.74	0	0	0	0	1
Chlorophytes	0	0	0	0	0	0	0.12	0.58	0	1
Synechococcus	0	0	0	0	0	0	1.03	0	0	1
Cryptophytes	0	0	0	0	0	0.23	0	0	0	1
Prochlorococcus	0	0	0	0	0	0	0.23	0.54	1.71	1
(C) Strict LL output matrix										
Diatoms	0	0	0	0.76	0	0	0	0	0	1
Dinoflagellates	0	0.93	0	0	0.41	0	0	0	0	1
Prymnesiophytes	0.17	0	0.02	1.13	1.44	0	0	0	0	1
Chrysophytes	0.38	0	1.78	0.62	0	0	0	0	0	1
Chlorophytes	0	0	0	0	0	0	0.11	0.79	0	1
Synechococcus	0	0	0	0	0	0	0.59	0	0	1
Cryptophytes	0	0	0	0	0	0.23	0	0	0	1
Prochlorococcus	0	0	0	0	0	0	0.26	0.70	1.56	1
(D) Lax HL output matrix										
Diatoms	0	0	0	0.76	0	0	0	0	0	1
Dinoflagellates	0	1.06	0	0	0.38	0	0	0	0	1
Prymnesiophytes	0.22	0	0.02	0.27	1.47	0	0	0	0	1
Chrysophytes	0.31	0	1.92	0.48	0	0	0	0	0	1
Chlorophytes	0	0	0	0	0	0	0.16	0.73	0	1
Synechococcus	0	0	0	0	0	0	1.49	0	0	1
Cryptophytes	0	0	0	0	0	0.23	0	0	0	1
Prochlorococcus	0	0	0	0	0	0	0.57	0.56	3.05	1
(E) Lax LL output matrix										
Diatoms	0	0	0	0.76	0	0	0	0	0	1
Dinoflagellates	0	1.06	0	0	0.38	0	0	0	0	1
Prymnesiophytes	0.17	0	0.02	0.12	1.77	0	0	0	0	1
Chrysophytes	0.53	0	1.98	0.17	0	0	0	0	0	1
Chlorophytes	0	0	0	0	0	0	0.10	1.04	0	1
Synechococcus	0	0	0	0	0	0	0.60	0	0	1
Cryptophytes	0	0	0	0	0	0.23	0	0	0	1
Prochlorococcus	0	0	0	0	0	0	0.51	1.48	3.06	1

Table 2.8: Proportions of biomass due to each phytoplankton group, as estimated by CHEMTAX run under either strict or lax conditions.

	Lax		**Strict**	
Group	Mean % of biomass – HL	Mean % of biomass – LL	Mean % of biomass – HL	Mean % of biomass – LL
Prochlorococcus	27.3	35.6	26.8	46
Synechococcus	36.7	7.1	37.4	6.6
Prymnesiophytes	18.4	20.2	18.5	1.42
Chrysophytes	7.7	14.0	8.1	14.5
Chlorophytes	4.6	19.1	4.4	28.4
Cryptophytes	0.7	0.5	0.7	0.6
Dinoflagellates	2.1	1.9	2.2	2.2
Diatoms	2.6	1.6	2.1	0

2.7.4 Correlations between strict and lax outputs

The study by Gibb *et al.* 2001 used surface data from the North Atlantic, and found chl-*a* concentrations below 50 ng/l, meaning that the pigment:chl-*a* ratio matrix is appropriate for all the HL samples. While photoacclimation and changes in the relative importance of different light-harvesting pigments mean that these ratios are likely to be inappropriate for some of the LL samples, the lax approach will allow the pigment ratios to alter sufficiently to be appropriate. The limit of 25% change per run for the strict configuration however might mean that insufficient adjustment to the ratios will be possible, and an incorrect pigment:chl-*a* ratio may be returned.

In some cases, such as for *Prochlorococcus* (Fig 2.11a), there was a very tight correlation between the proportion of the total biomass as estimated by the two approaches, with the dashed line representing a 1:1 ratio and the solid line the linear regression on the data. ($F_{1, 417}$ = 5338, $p < 0.0001$, $R^2 = 0.93$). There is however a significant difference in mean biomass, at 0.30 and 0.35 μg/l chl-*a* for the lax and strict approaches respectively (W =

77099, $p = 0.0016$), with the dashed line representing a 1:1 ratio and the black line the linear regression on the data. This difference is due to the strict approach consistently assigning a greater proportion of biomass to this group in LL samples. In other cases, such as the diatoms (Fig 2.11b), there were important differences. Despite a highly significant correlation ($F_{1, 417} = 73$, $p < 0.0001$, $R^2 = 0.15$), there is a significant difference in means with CHEMTAX giving a mean estimated biomass fraction of 0.001 for the strict run as compared with 0.023 for the lax approach ($W = 134498$, $p < 0.0001$). For the majority of samples, the strict criteria found almost no diatom biomass at all, whereas the lax approach returned a wide spread. This may represent CHEMTAX being unable sufficiently to alter pigment:chl-*a* ratio to take into account photoacclimation. A similar effect is seen when considering prymnesiophytes (Fig 2.11c). Although the correlation is significant ($F_{1, 417} = 58$, $p < 0.0001$, $R^2 = 0.12$), the less constrained approach results in higher biomass estimates for deep samples, with a highly significant difference at 0.19 and 0.09 μg/l chl-*a* for the lax and strict approaches respectively ($W = 141783$, $p < 0.0001$). The two approaches give similar results under shallow conditions though there is a very large difference for the deeper samples, with the strict criteria finding almost no prymnesiophyte biomass whereas the lax method produces up to 40% prymnesiophytes, again perhaps due to the inability of the strict method fully to take photoacclimation in LL samples into account, the lowest residuals resulting from this biomass being assigned to a different phytoplankton group.

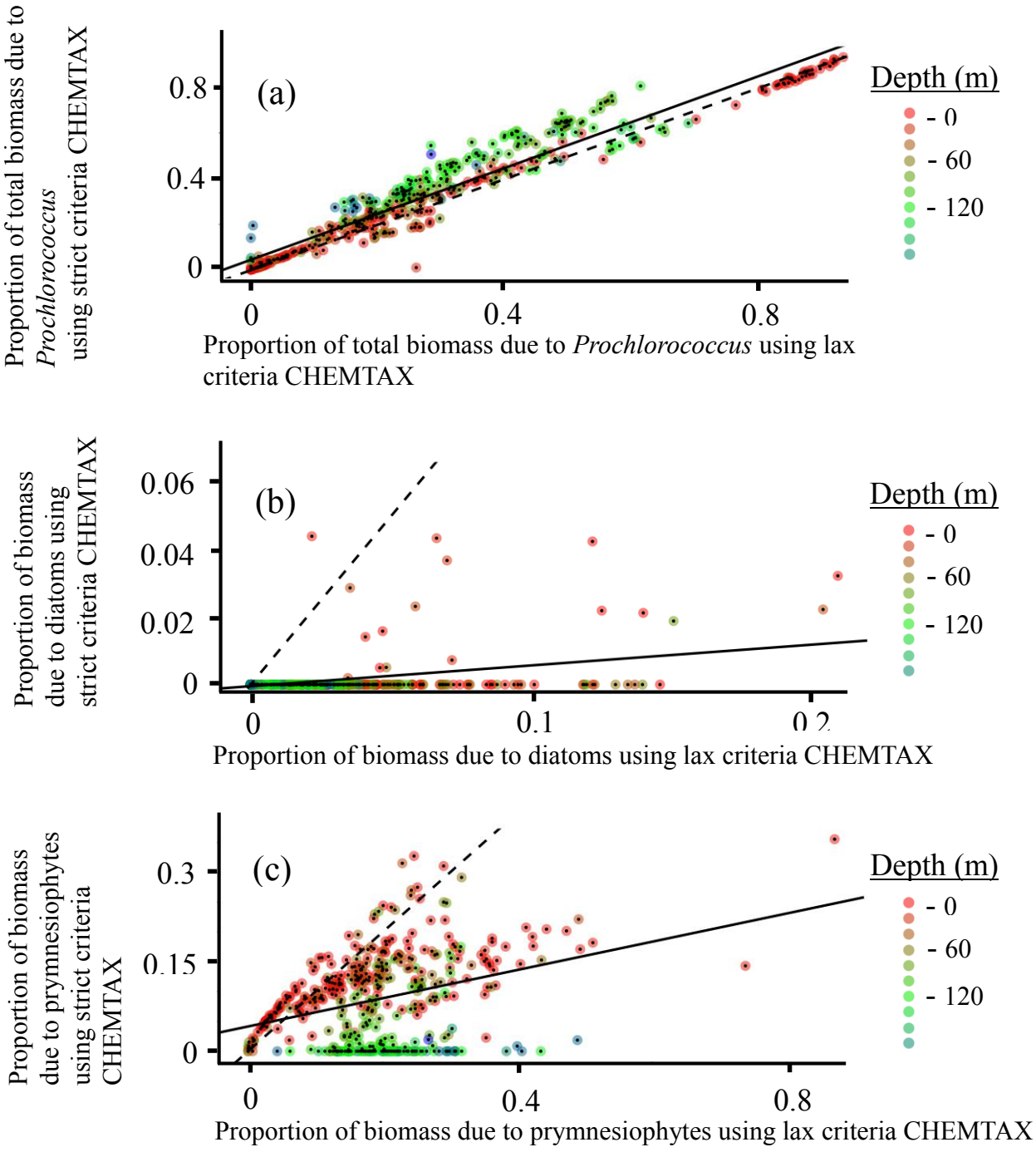

Fig 2.11: Showing differences in the proportion of biomass ascribed to different groups when CHEMTAX is run either with very strict constraints on the pigment:chl-*a* ratio, only allowing a change of ±25% with each run, or lax criteria where the pigment:chl-*a* ratio is allowed to vary freely, by up to ± 500% with each run. (a) *Prochlorococcus*, dashed line 1:1, solid line regression from data (y = 1.01x + 0.45, $F_{1, 417}$ = 5338, $p < 0.0001$, $R^2 = 0.93$). (b) Diatoms, dashed line 1:1, solid line regression from data (y = 0.06x - 0.0005, $F_{1, 417}$ = 73, $p < 0.0001$, $R^2 = 0.15$). (c) Prymnesiophytes, dashed line 1:1, solid line regression from data. (y = 0.24x + 0.04, $F_{1, 417}$ = 58, $p < 0.0001$, $R^2 = 0.12$)

2.7.5 Spatial differences between configurations

Differences in output can also be considered spatially. For *Synechococcus* (Fig 2.12a) the differences in the percentage of total biomass are small and very patchily distributed, implying that while the estimates from both methods are likely to have errors they appear to be randomly distributed, and do not show a systematic dependency on depth or latitude. Diatoms (Fig 2.12b), however, show a strong systematic effect from latitude, with the lax approach finding significant biomass around 20 ^{o}S and 25 ^{o}N, where the strict approach found very little diatom biomass. In the case of *Prochlorococcus* (Fig 2.12c) another systematic difference is seen, this time with respect to depth as opposed to latitude. The two configurations show close agreement for the majority of the study area, including the very heavily sampled section at 20 ^{o}N for shallow samples above 100 m, though the strict method produces consistently higher estimates below this depth. There is however a large disparity for deep samples at 15 ^{o}S, with the strict configuration resulting in an estimate of a considerably higher *Prochlorococcus* biomass. A comparison of the two configurations for prymnesiophytes, however, (Fig 2.12d) again shows a depth-dependent trend. For deep samples the strict approach estimates this group to be almost completely absent while the lax approach results in prymnesiophytes being one of the most abundant groups at depth of 100 to 200 m, despite a tight agreement for more shallow samples.

Given that previous studies have identified prymnesiophytes as one of the most abundant groups around the deep chlorophyll maximum (Gibb *et al.* 2001), this would appear to be a serious failing of the strict approach. Such systematic biases are far more problematic than more random errors and have the potential seriously to skew any analysis using pigment-based systems of estimating sample taxonomic composition.

Depth (m)
0
50
100
150
200
- 20
0
20
40
Latitude (° N)
(a)
0.2
0
-0.2
-0.4
Difference in the proportion of *Synechococcus* between lax and strict CHEMTAX

Depth (m)
0
50
100
150
200
- 20
0
20
40
Latitude (° N)
(c)
0.15
0.1
0.05
0
Difference in the proportion of diatoms between lax and strict CHEMTAX

Depth (m)
0
50
100
150
200
- 20
0
20
40
Latitude (° N)
(b)
0.2
0
-0.2
Difference in the proportion of *Prochlorococcus* between lax and strict CHEMTAX

Depth (m)
0
50
100
150
200
- 20
0
20
40
Latitude (° N)
(d)
0.4
0.2
0
Difference in the proportion of prymnesiophytes between lax and strict CHEMTAX

Fig 2.12: Spatial differences in CHEMTAX outputs according to strict or lax criteria. Gridded field plot showing the proportion of biomass as estimated by CHEMTAX using a strict parameter configuration subtracted from that estimated using CHEMTAX run under lax criteria as a function of latitude. (a) *Synechococcus*, showing not only a tight agreement for the majority of samples, but again the lack of a clear depth or latitude dependency. (b) Diatoms, showing the lack of a clear depth dependency but a strong latitudinal effect. (c) *Prochlorococcus*, demonstrating a tight agreement for the majority of samples, but also a large difference for deep stations, and those around 15 ^{o}S. (d) Prymnesiophytes, with a strong agreement for shallow samples and a much lower proportion of biomass for deep samples using the strict criteria.

2.7.6 Errors and residuals

The outputs from CHEMTAX itself can also be used to consider possible errors, including the percentage change in the pigment:chl-*a* ratio. Despite the apparent inability of the strict analysis sufficiently to alter the pigment:chl-*a* ratios, at no point is the full 25% change in mean row normalized pigment:chl-*a* ratio seen (Table 2.7). This might be interpreted as 25% being an adequate degree of flexibility, despite some ratios varying by up to 83% for the lax configuration, were it not for previous studies suggesting that the phytoplankton distributions generated were ecologically implausible. Further potential for error comes from a comparison of the residuals for both methods (Table 2.8) While the residuals are higher for the strict configuration, for both HL and LL samples, the difference is small, with the fit appearing to be better for the strict LL samples than the strict HL, despite the output from the strict analysis being biologically implausible.

Validation can be done using flow cytometry counts. As seen in Table 2.4, significant correlations between flow cytometry counts and CHEMTAX are seen for *Prochlorococcus* and nanophytoplankton for HL and LL samples, for both the lax and strict approaches, with little difference seen either in the overall significance of the correlations or the values for R^2.

Since these are field data it is difficult to state with certainty that one configuration is more accurate than the other, however previous studies highlighting the degree to which phytoplankton pigment:chl-*a* ratios change with respect to depth indicate that using CHEMTAX under the strict format with the same initial values for pigment:chl-*a* ratios for both HL and LL samples is inappropriate. This is confirmed by the combination of the absence of prymnesiophytes from the deep chlorophyll maximum, and the higher residuals seen, meaning that the lax approach was found to be more suitable, and will be used when comparing CHEMTAX with other pigment-based methods of taxonomy.

Table 2.7: Percentage changes in indicator pigment:chl-*a* ratios (normalised to total pigments) for samples analysed using the lax criteria, where ratios were allowed to vary by up to 500%. (A) HL samples, first run, (B) HL samples, second run, (C) LL samples, first run, (D) LL samples, second run.

	Percentage change in pigment : chl-*a* ratio									
	chl-*c3*	**per**	**19'-but**	**fuc**	**19'-hex**	**allo**	**zea**	**chl-*b***	**DVchl-*a***	**MVchl-*a***
(A) HL samples First run										
Diatoms	0	0	0	0	0	0	0	0	0	0
Dinoflagellates	0	0	0	0	0	0	0	0	0	0
Prymnesiophytes	34.0	0	20.6	-43.4	18.1	0	0	0	0	19.6
Chrysophytes	31.4	0	19.3	-40.2	0	0	0	0	0	7.0
Chlorophytes	0	0	0	0	0	0	13.2	13.2	0	-9.16
Synechococcus	0	0	0	0	0	0	61.0	0	0	-36.0
Cryptophytes	0	0	0	0	0	0	0	0	0	0
Prochlorococcus	0	0	0	0	0	0	20.8	-36.0	59.5	-45.7
(B) HL samples Second run										
Diatoms	0	0	0	0	0	0	0	0	0	0
Dinoflagellates	0	0	0	0	0	0	0	0	0	0
Prymnesiophytes	22.0	0	13.6	-42.2	16.6	0	0	0	0	7.9
Chrysophytes	-5.2	0	5.5	5.5	0	0	0	0	0	-5.2
Chlorophytes	0	0	0	0	0	0	0	0.63	0	-1.4
Synechococcus	0	0	0	0	0	0	0	0	0	0
Cryptophytes	0	0	0	0	0	0	0	0	0	0
Prochlorococcus	0	0	0	0	0	0	18.1	-12.9	-0.5	-6.4
(C) LL samples First run										
Diatoms	0	0	0	0	0	0	0	0	0	0
Dinoflagellates	0	0	0	0	0	0	0	0	0	0
Prymnesiophytes	14.4	0	14.4	-30.4	14.4	0	0	0	0	14.4
Chrysophytes	84.5	0	23.3	-83.2	0	0	0	0	0	23.3
Chlorophytes	0	0	0	0	0	0	-2.2	17.7	0	-9.8
Synechococcus	0	0	0	0	0	0	0	0	0	0
Cryptophytes	0	0	0	0	0	0	0	0	0	0
Prochlorococcus	0	0	0	0	0	0	7.6	7.6	7.6	-13.0
(D) LL samples Second run										
Diatoms	0	0	0	0	0	0	0	0	0	0
Dinoflagellates	0	0	0	0	0	0	0	0	0	0
Prymnesiophytes	8.4	0	8.4	-82.8	39.2	0	0	0	0	8.4
Chrysophytes	16.4	0	5.9	5.9	0	0	0	0	0	-16.7
Chlorophytes	0	0	0	0	0	0	-33.7	21.4	0	-13.5
Synechococcus	0	0	0	0	0	0	0.5	0	0	-0.3
Cryptophytes	0	0	0	0	0	0	0	0	0	0
Prochlorococcus	0	0	0	0	0	0	4.5	24.1	28.3	-44.9

Table 2.8: Mean residual errors for each pigment after CHEMTAX analysis (at the end of the second run of CHEMTAX) according to light regime and CHEMTAX configuration.

	chl-*c3*	**per**	**19'-but**	**fuc**	**19'-hex**	**allo**	**zea**	**chl-*b***	**DVchl-*a***	**MVchl-*a***	**Mean for all pigments**
Strict HL	0.0359	0.0004	0.0112	0.0142	0.0754	0.0011	0.1336	0.0346	0.0819	0.1628	0.0551
Strict LL	0.0220	0.0005	0.0262	0.0098	0.1345	0.0004	0.0203	0.0626	0.0327	0.1088	0.0418
Lax HL	0.0309	0.0003	0.0065	0.0061	0.0583	0.0007	0.0889	0.0250	0.0737	0.1125	0.0403
Lax LL	0.0105	0.0001	0.0233	0.0044	0.0257	0.0004	0.0133	0.0492	0.0203	0.0676	0.0302

Chapter 3: Phytoplankton size and succession in the North Atlantic and its relationship to photophysiology

3.1 Abstract

The biological dynamics of pelagic marine ecosystems are strongly influenced by the size structure and ecological succession of phytoplankton. Here two possible approaches to estimating the mean equivalent spherical diameter (MESD) of phytoplankton are compared and hierarchical cluster analysis on chlorophyll-normalised high performance liquid chromatography (HPLC) pigment concentrations is employed to identify successional trends amongst phytoplankton populations, with respect to season, water-column stratification and temperature in the North Atlantic Basin. Similar trends with respect to MESD were found for both the pigments-based approach of Bricaud *et al.* (2004) and the absorption-based method of Roy *et al.* (2011); although the distribution of estimated MESD produced using the absorption-based approach corresponded more closely with previous studies. Well-mixed conditions in spring to early summer were found to be associated with populations of large cells containing high concentrations of fucoxanthin, chlorophyll-*c*1 and chlorophyll-*c*2 relative to chlorophyll-*a*. As stratification increased over the course of the summer, these cells were replaced by populations dominated by chlorophyll-*b*, 19'-hexanoyloxyfucoxanthin, 19'-butanoyloxyfucoxanthin and divinyl chlorophyll-*a,* indicative

of small picophytoplankton including *Prochlorococcus*. As stratification decreased in autumn, MESD increased with alloxanthin increasing in importance, suggesting the presence of nanophytoplankton, such as small cryptophytes. A cluster dominated by peridinin was found to be present at relatively constant levels in all seasons. Differences in bio-optical properties were seen between the clusters; for those clusters dominated by large cells, the slope between the mean absorption of phytoplankton averaged between 400 and 700 nm and chlorophyll-*a* concentration was much shallower than for those dominated by small cells. Differing relationships were also seen between the initial slope of the photosynthesis-light response curve (α) and chlorophyll-*a* biomass, and between the maximal photosynthetic rate (P_m) and chlorophyll-*a* biomass according to the phytoplankton cluster, with the fucoxanthin-dominated populations of large cells again displaying a shallow gradient, whereas the corresponding gradients were higher for clusters with a small MESD from stratified areas. In contrast to previous studies, a strong positive correlation was seen between MESD and the maximal quantum realised yield of photosynthesis (φ_m) for all clusters except for one.

3.2 Introduction

The ecological functioning of marine phytoplankton communities is strongly influenced by the species present in the population, and globally almost 5000 species of marine phytoplankton have been identified (Sournia *et al.* 1991). One of the most important differences between phytoplankton species is their size, (Chisholm 1992, Raven 1998), with a 1000 fold range seen in cell size (Jiang *et al.* 2005), from ~0.6 μm to greater than 1000 μm. To understand the dynamics of a complex marine ecosystem such as the North Atlantic Basin, it is important to understand the ecological implications of cell size with respect to nutrient uptake, light-harvesting, growth and losses due to grazing or sinking.

In addition to the effects of size on phytoplankton physiology and photosynthetic rate, cell size dictates the fate of the carbon fixed. Small cells sink slowly (Fogg 1986, Legendre & Rassoulzadegan 1995, Raven 1998), such that nutrients are efficiently remineralised in the surface waters in a tight microbial loop (Azam *et al.* 1983, Fenchel 2008). Even when chlorophyll-normalised photosynthetic rates are high, the phytoplankton biomass is low in small-cell dominated areas of the ocean, as are the rates of carbon export (Raven 1998). In contrast, large cells form blooms and sink rapidly, leading to relatively high export fluxes to deep waters (Laws *et al.* 2000). The higher trophic systems supported by marine photoautotrophs also differ widely according to phytoplankton size (Ryther 1969, Landry 1977, Irwin *et al.* 2006). The efficient cycling of nutrients in a microbial-loop-dominated system leads to low energy transfer to higher trophic levels, compared with the classic phytoplankton-zooplankton–nekton food chain found in systems dominated by large phytoplankton species (Fenchel 1988), with implications for the types and quantity of biomass supported at higher trophic levels. Thus, understanding patterns of phytoplankton

biogeography can aid our understanding of the fate of fixed carbon, with respect to the transfer of energy to higher trophic levels and the global carbon cycle.

The link between cell size, nutrient uptake and ecological function has long been known (Margalef 1978, Key *et al.* 2010). Small cells have a higher efficiency when taking up nutrients (Fogg 1986, Raven 1998), owing to their high surface-area-to-volume ratio. However, under high-nutrient conditions, the high efficiencies do not confer a competitive advantage since growth is not limited by nutrient supply. Intracellular nutrient demands scale according to the same allometric rule as nutrient uptake, so a large cell size is not a competitive disadvantage when nutrients are replete (Kiørboe 1993). Under nutrient-limiting conditions, however, the potential uptake rate exceeds the rate of diffusion towards the cell, creating a depleted region around the cell, such that the rate of uptake is no longer dependent on surface area (Kiørboe 1993). Instead, nutrient assimilation rate is dictated by the rate of diffusion towards the cell, which is in turn inversely proportional to the square of the cell's radius, conferring a major advantage on small cells (Kiørboe 1993, Raven 1998), with the efficiency with which phytoplankton are able to take up nutrients having implications for their photosynthetic rates.

3.2.1 Size and primary production

The photosynthetic response of phytoplankton to irradiance can be described using two parameters in the absence of photoinhibition: the maximum biomass-normalised photosynthetic rate (P_m^B) and initial slope of the photosynthesis-irradiance (PE) curve (α^B), where B is typically represented in units of chlorophyll concentration. Models of primary production require accurate assignments of both PE parameters (Platt & Sathyendranath 1988, Geider *et al.* 1997). Various studies have found links between size and P_m^B (Bouman *et al.* 2005, Geider *et al.* 1997), with higher values of P_m^B recorded for small cells, presumably as a

result of their more efficient nutrient uptake. Others, such as Behrenfeld *et al.* (2008), have suggested that the greater efficiency of light-harvesting as cell size decreases can also result in increases in P_m^B due to lower investment in energetically-costly, light-harvesting pigments. By definition (Platt & Jassby 1976), α^B is a function of the chlorophyll-normalised absorption by phytoplankton between 400 and 700 nm ($\bar{a}_{ph}^*$) and the maximum quantum yield (φ_m):

$$\alpha^B = \varphi_m \, \bar{a}_{ph}^*. \quad (1)$$

Various studies (Hoepffner & Sathyendranath 1992, Kiørboe 1993, Babin *et al.* 1996, Sosik 1996) have found both $\bar{a}_{ph}^*$ and φ_m to vary widely in natural assemblages due to environmental factors such as nutrient availability, light intensity, and species composition. To understand the sources of variability in α^B, it is important to know the factors responsible for changes in light harvesting and utilisation by phytoplankton, and how the phytoplankton responses to these factors may differ between populations.

Size-dependent trends in α^B are well documented, with smaller cells benefiting, as noted earlier, from low costs of nutrient uptake (Howarth *et al.* 1988), as well as high efficiency of light harvesting due to minimal package effect (Duysens 1956, Morel & Bricaud 1981, Sathyendranath *et al.* 1987, Key *et al*. 2010). Package effect is such that, for a given intracellular pigment concentration, a large cell will be able to harvest proportionally less light than a smaller one because of self-shading, leading to a competitive advantage for the latter at limiting light levels (Sosik & Mitchell 1994). Size-dependent phytoplankton losses such as predation and sinking also determine the size structure of phytoplankton assemblages.

3.2.2 Size and predation

Gape-limitation of predators gives large cells an advantage when it comes to predation. To ingest a prey, zooplankton need to be larger than the phytoplankton they consume. Kiørboe (1993) reported a constant predator-prey size ratio across a wide range of phytoplankton sizes. The abundance of organisms per unit volume is inversely exponentially related to organism size such that the prey-predator ratio is larger for large phytoplankton than for small ones (Kiørboe 1993), and hence the predation pressure on large cells is lower than on small cells. The decrease in the surface-area-to-volume ratio with increased cell size, however, also results in greatly increased sinking rates for large cells and hence higher losses in non-turbulent environments (Jiang *et al.* 2005).

3.2.3 Estimating phytoplankton size

3.2.3a Optical and molecular approaches

Obtaining an accurate measure of phytoplankton size over basin scales is difficult. Very detailed assessment of the size structure of large phytoplankton may be provided by microscopic analysis at point locations. However, because this approach is labour intensive, it is not feasible to assess large-scale trends in this manner (Nair *et al.* 2008), and it is not possible to detect small cells such as *Prochlorococcus* using conventional light microscopy, though this can be overcome by using epifluorescence microscopy (Havskum *et al.* 2004). Moreover, microscopic analysis may be biased due to problems of preservation. Flow cytometry can provide rapid assessment of phytoplankton size for some samples, but standard instruments have a restricted size range, being usually designed for enumeration of cells of size between 1 and 10 or 20 μm (Moore *et al.* 2009). FlowCAM is capable of measuring larger cells; however it is costly, and not capable of measuring the full range of phytoplankton sizes simultaneously (Alvarez *et al.* 2011). Alternatively, indirect measurements of size can

be made by identifying phytoplankton taxonomic groups, and then using data from the literature to obtain mean cell sizes using fluorescence *in-situ* hybridisation (FISH) probes (Groben *et al*. 2004), but again these are time consuming and costly.

3.2.3b Estimating size from HPLC pigments

Another approach for identifying phytoplankton taxonomic groups and hence mean cell size is to use information about the relative concentrations of key indicator pigments (Bricaud *et al*. 2004). High performance liquid chromatography (HPLC) is routinely used to measure phytoplankton pigments, which can serve as markers for various phytoplankton classes (Gieskes *et al.* 1988, Everitt *et al.* 1990, Letelier *et al*. 1993, Mackey *et al*. 1996, Bidigare & Ondrusek 1996, Vidussi *et al*. 2001, Uitz *et al*. 2006, 2008, Van den Meersche *et al.* 2008, Sathyendranath *et al*. 2009), including sub-micron groups too small to be identified using conventional light microscopy (Gibb *et al*. 2001). Uitz *et al*. (2008) refined the model of Vidussi *et al.* (2001) which divides the chlorophyll-*a* pigment biomass into three size-classes; picophytoplankton (<2 μm), nanophytoplankton (2-20 μm) and microphytoplankton (>20 μm) using seven diagnostic pigments. This diagnostic-pigment approach was adapted to produce estimates of the mean phytoplankton size (Bricaud *et al*. 2004) and has been used in a wide range of studies (Claustre *et al.* 2005, Bricaud *et al*. 2010, Roy *et al*. 2011, Organelli *et al.* 2011).

Phytoplankton populations in the field rarely, if ever, consist of monocultures of a single size. Therefore, the approach of calculating the mean equivalent spherical diameter (MESD) of the population allows samples containing a range of phytoplankton sizes to be compared. Although the method of Bricaud *et al.* (2004) is relatively easy to implement, it does have certain drawbacks. Few phytoplankton groups have unique indicator pigments. For example, fucoxanthin, which the method of Bricaud *et al.* (2004) assigns solely to the

microphytoplankton, is also found in chrysophytes and prymnesiophytes (Vidussi *et al*. 2001). This problem is compounded by the flexibility phytoplankton groups show in both their absolute intracellular pigment concentrations, and the ratios between diagnostic pigment concentrations. Many phytoplankton groups also vary widely in size (Aiken *et al*. 2008) with diatoms being known to span almost 9 orders of magnitude in cell volume (Litchman & Klausmeier 2008), such that even if a method could accurately assess the taxonomic composition of a sample, this may not result in a valid estimate of phytoplankton size. Diatoms are routinely classified as microphytoplankton (Uitz *et al.* 2008), yet species such as *Minidiscus* may be as small as 2.5 μm (Quiroga & Chrétiennot-Dinet 2004), nearer to the picophytoplankton than microphytoplankton size range. Very large species are also known with the largest species having volumes in excess of 10^9 μm^3 (Litchman *et al.* (2009) which would correspond to a MESD of greater than 1500μm, meaning the maximum possible size estimate of 50 μm that the Bricaud *et al.* 2004 method can produce may be too small to describe either the largest diatoms or dinoflagellates (Hasle & Booth 1984).

3.2.3c Estimating size from the specific absorption coefficient of marine phytoplankton at 676nm

An alternative measure of phytoplankton size can be obtained from the specific absorption coefficient of phytoplankton (Roy *et al*. 2011). Light absorption by phytoplankton is a function of the intracellular pigment concentration, the types of pigment present and cell size (Yentsch & Phinney 1989). The effect of particle size comes from self-shading of chlorophyll and all other pigments within cells, such that absorption will be higher for a given quantity of pigment if it is contained in many small cells rather than few large cells. This is known as the package effect (Duysens 1956). At 676 nm Bidigare *et al.* (1990) found that all absorption by phytoplankton is due to various chlorophylls, with that due to chlorophyll-*a* (chl-*a*)

dominating. The degree of packaging can therefore be found from the ratio between the measured absorption by phytoplankton cells (*in-vivo*) and the predicted absorption by chl-*a* in solution (*in-vitro*), with the concentration determined by HPLC. A lookup table can then be used to estimate the MESD of the population (Cheung *et al.* unpublished).

3.2.4 Environmental control of phytoplankton community structure

This study focusses on the open-ocean North Atlantic, with widespread differences in the size and taxonomic structure of phytoplankton seen both spatially and seasonally. In temperate regions, phytoplankton size and taxonomic structure and nutrient availability vary on a seasonal basis (Anderson 2005, Alvain *et al.* 2008). The North Atlantic is characterised by strong winter mixing, which breaks down any seasonal thermocline that was formed during the previous spring-summer season, leading to high surface nutrient concentrations at the end of winter. Upon the onset of stratification in spring a bloom dominated by large diatoms results, before this assemblage is replaced by dinoflagellates and smaller cells as the strength of stratification increases, and the nutrient availability in the surface layer decreases (Dandonneau *et al*. 2004). Stratification is a valuable proxy for nutrient fluxes from deep water below the photic zone, which are difficult to measure directly. The strength of water-column stratification can be used to explain the successional trends seen with respect to both phytoplankton size and ecological function (Smayda & Reynolds 2001). Since the onset of stratification is earlier at lower latitudes than at high latitudes, the spring diatom bloom initiates at low latitudes before progressing north, such that stratification also dictates to a large extent latitudinal succession in phytoplankton (Sieracki *et al.* 1993).

3.2.5 Ecological effect of differences in the phytoplankton community structure

The different populations observed under different degrees of water-column stratification represent very different ecological strategies. Margalef (1978) first applied the concept of *r*- and *K*-strategists to marine phytoplankton. The *r*-strategists focus on rapid growth and reproduction, being able to dominate quickly an environment after a disturbance (Follows & Dutkiewicz 2011). The *K*-strategists, on the other hand, are adapted to more stable systems instead, gaining a competitive advantage from their more efficient use of resources, albeit at the cost of decreased reproductive rate, with a direct trade-off between the two approaches being seen in phytoplankton physiology (Litchman & Klausmeier 2007). Diatoms (typically larger cells) fill the *r*-strategist role as they are capable of very rapid growth and are able to take advantage swiftly of new sources of nutrients (Margalef 1978). However, as they are non-motile and large, diatoms are at a disadvantage as the system becomes more stable and stratified and nutrients are depleted due to losses caused by sinking and grazing (Cullen *et al.* 2002). The dinoflagellates and picophytoplankton that follow the diatom bloom represent two different *K*-strategist approaches to the conditions (Cullen *et al.* 2002). Dinoflagellates are able to regulate their position within the water-column (Estrada & Berdalet 1997) and hence both avoid losses due to sinking, and migrate to acquire nutrients, offsetting their lower growth rates. Picophytoplankton (cells < 2 μm) sink very slowly due to their small size and have a competitive advantage for nutrient assimilation due to their very high surface-area-to-volume ratio (Kiørboe 1993).

3.2.6 Chapter aims

The aim of the research presented in this chapter was to identify trends in distribution and succession in phytoplankton populations in the North Atlantic. Given the importance of cell size with respect to the ecological functioning of phytoplankton, a comparison will be made

between estimates of cell size obtained using phytoplankton absorption, and those from pigment- and taxonomic-based approaches. Since phytoplankton pigments differ between taxonomic and functional groups, variations in the chlorophyll-normalised concentration of different indicator pigments can be used to identify distinct phytoplankton populations. Unsupervised hierarchical cluster analysis will therefore be used to identify distinct phytoplankton populations, so that seasonal trends in size and taxonomic composition can be linked to the absorptive and photosynthetic properties of the different phytoplankton assemblages.

3.3 Methods

3.3.1 Study area

The study is based on data from several cruises in the North Atlantic. See Fig 3.1 for a map of station locations. Stations are predominantly from the North West Atlantic Shelf Province as defined by Longhurst *et al.* (1995), where water movements are significantly affected by the proximity to the coastline, although the water is anomalously deep for a continental shelf. The next most abundant set is from the polar regions, with a seasonal influence from ice cover where stratification caused by brackish meltwater may contribute to the onset of the spring bloom, and ice cover is present for a large portion of the year (Longhurst *et al.* 1995). Another group of data comes from the Westerlies Domain and is associated with strong seasonal mixing and high winter nitrate concentrations. Finally samples from the Caribbean are defined as part of the Trade Winds Regime, which are typically warm and highly stratified.

Sampling:

Vertical profiles of temperature were obtained from CTD casts. Water samples were obtained using Niskin bottles from the surface to a maximum depth of 170 m, with 95% from depths of 50 m or less for measurements of biological, physiological and optical properties of phytoplankton.

3.3.2 Climatological estimates of water-column properties

Estimates of photosynthetically-active radiation (PAR) averaged over the mixed layer were obtained from the World Ocean Atlas (WOA) for samples collected above the seasonal mixed-layer depth. The degree of stratification was estimated by taking the difference

between the sample temperature and the estimated temperature at 100 m from WOA data and dividing by the difference in depths. The depth of 100 m was selected as it is below both the climatological mixed-layer depth for almost all stations and the 1% light level. Li (2002) used differences in density to assess the degree of stratification. However, since density was not recorded in this data set, using *in-situ* measurements of temperature was preferable to using climatological estimates of density. Therefore:

$$\delta S = (T_s - T_{100}) / (100 - z_s) \quad (2)$$

Where δS is the stratification index, T_s is the temperature of a sample, T_{100} is the climatological temperature of the sample at 100m, and z_s the depth of the sample.

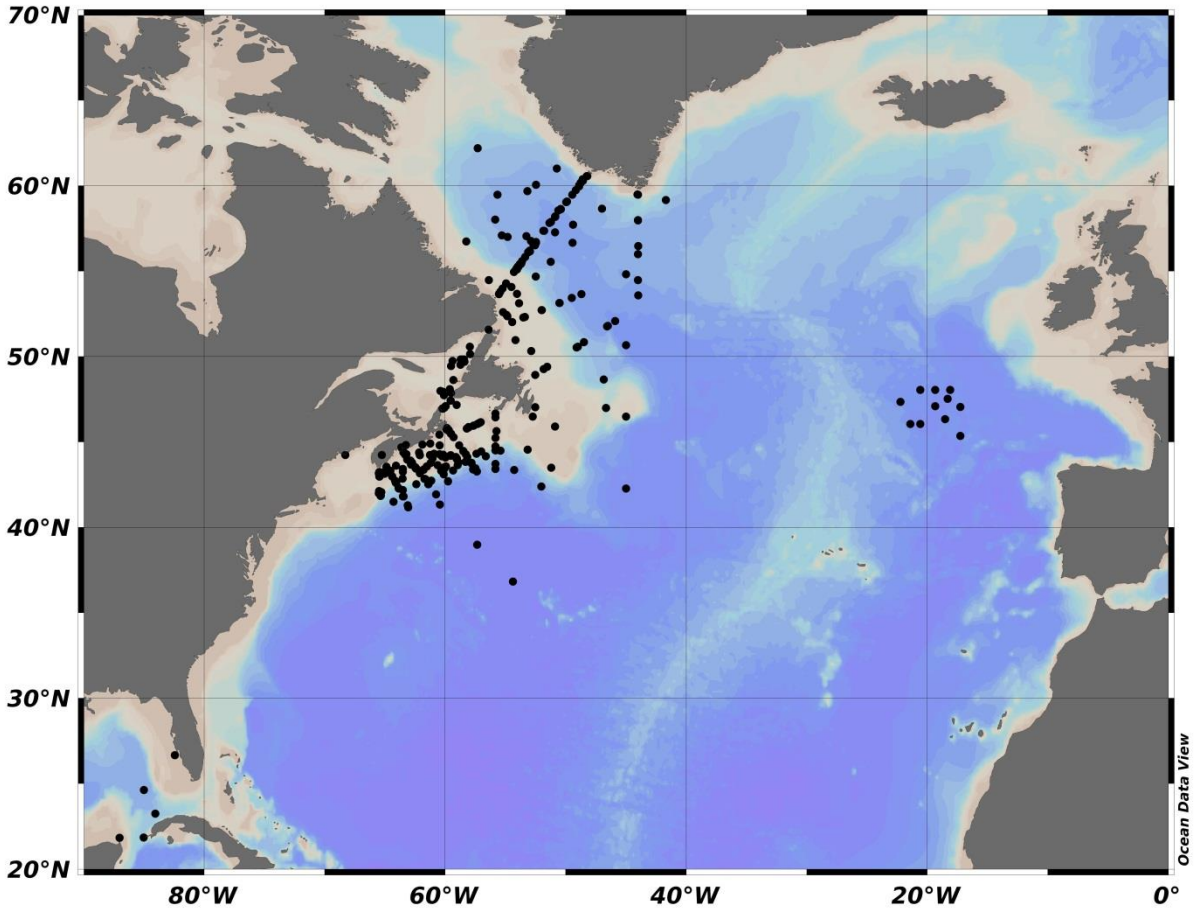

Fig 3.1: Map showing station locations in the North Atlantic with the full suite of HPLC pigment data for cluster analysis.

3.3.3 HPLC pigments

Chlorophyll-*a* and accessory pigment concentrations were measured using HPLC following the procedure of Head & Horne (1993). Water samples were filtered onto GF/F filters before being either analysed immediately or flash frozen in liquid nitrogen at -80ºC until analysis. Frozen filters were homogenised in 1.5 ml of 90% acetone, centrifuged and diluted with 0.5 M ammonium acetate at a ratio of 2:1 before being run on a Beckman C18 reverse-phase, 3 µm Ultrasphere column (Sathyendranath *et al*. 2005). Pigment peaks were identified for chlorophyll-*a* (chl-*a*), divinyl chlorophyll-*a* (DVchl-*a*), chlorophyll-*b* (chl-*b*), (including divinyl chlorophyll-*b* (DVchl-*b*) and monovinyl chlorophyll-*b* (MVchl-*b*), combined

chlorophyll-*c1* (chl-*c1*) and chlorophyll-*c2* (chl-*c2*), chlorophyll-*c3* (chl-*c3*), peridinin (per), 19'-butanoyloxyfucoxanthin (19'-but), 19'- hexanoyloxyfucoxanthin (19'-hex), fucoxanthin (fuc), violaxanthin (viola), diadinoxanthin (diad), alloxanthin (allo), diatoxanthin (diat), zeaxanthin (zea), and β-carotene. Samples lacking any of the 17 pigments mentioned above were discarded from the analysis, leaving a total of 1397 samples that were used out of a total of 2950.

3.3.4 Measuring phytoplankton spectral absorption

Particulate absorption samples were collected on GF/F filters, and analysed as described in Stuart *et al.* (1998, 2000). Absorption by particulate matter ($a_p(\lambda)$) on wetted filters was measured between 400 and 750 nm relative to a blank saturated in filtered seawater, using a dual-beam Shimadzu UV-2101 PC scanning spectrophotometer with an integrating sphere (Stuart *et al.* 2000). Optical density measurements were divided by the geometrical path length (volume filtered divided by the clearance area of the filter) and multiplied by a factor of 2.3 to convert from decimal to natural logarithms. Detrital absorption, $a_d(\lambda)$, was estimated following the method of Kishino *et al.* (1985), as modified by Stuart *et al.* (1998). Pigments were extracted using 20 ml of a 6:4 (vol:vol) 90% acetone and dimethyl sulfoxide (DMSO), followed by 10 ml of filtered seawater to remove any residual solvents (Stuart *et al.* 1998), before the absorption by the extracted filters was measured. Since water-soluble phycobiliproteins are not readily extracted using this method, a correction was applied to avoid underestimation of the absorption by phytoplankton. The detrital absorption spectrum was deconstructed into a series of Gaussian curves superimposed onto an exponential curve at the wavelengths of the peak absorption by the non-extracted pigments (420 and 666 nm for phaeopigments and 510, 550 and 590 nm for the biliproteins). The Marquardt-Levenberg

algorithm was used to determine the parameters which minimise the sum of squares between the estimated and observed variables, giving a very good fit ($R^2 \sim 0.99$), before using the fitted exponential as the measure for detrital absorption. Absorption coefficients were calculated by subtracting the optical density at 750 nm from all other wavelengths, dividing by the geometrical path length (volume filtered divided by the clearance area of the filter) and adjusting for path length amplification due to scattering by the filter. Absorption by phytoplankton was calculated by subtracting $a_d(\lambda)$ from $a_p(\lambda)$. The mean-specific absorption coefficient ($\bar{a}^*_{ph}$) was calculated by taking an average for all values of a_{ph} between 400 and 700 nm and dividing by the chl-*a* concentration measured by HPLC.

3.3.5 Photosynthesis-irradiance (*PE*) parameters

The protocol for the determination of *PE* parameters is described in full in Bouman *et al.* (2005). In brief, seawater samples were collected at the surface and at the chlorophyll maximum based on the *in vivo* fluorescence profile obtained from CTD casts. Thirty bottles were inoculated with 185 to 370 kBq (5 to 10 µCi) of ^{14}C-labelled bicarbonate and incubated for 2-3 hours. After the incubation, the seawater was filtered through 25 mm glass fibre filters (Whatman GF/F) at a vacuum pressure of < 200 mm Hg. The filters were exposed to concentrated HCl fumes to remove any inorganic carbon present, immersed in scintillation cocktail and the disintegration time per minute of ^{14}C was counted on a liquid scintillation counter. The *PE* parameters, P_m^B and α^B, were estimated by fitting the data to the model of Platt *et al.* (1980). The quantum yield of photosynthesis (φ_m) was calculated as:

$$\varphi_m = 0.0231\, \alpha^B / \bar{a}^*_{ph\,(400\text{-}700)}, \qquad (3)$$

where $\bar{a}^*_{ph\ (400\text{-}700)}$ is the mean chlorophyll-specific absorption coefficient of phytoplankton, between 400 and 700 nm, and the constant 0.0231 in the numerator converts grams to moles and hours to seconds.

3.3.6 Estimation of mean equivalent spherical diameter (MESD)

3.3.6a HPLC pigment-based method

The proportion of biomass due to microphytoplankton (>20 μm), nanophytoplankton (2-20 μm) and picophytoplankton (<2 μm) was estimated using the method of Uitz *et al*. (2008) using 7 diagnostic pigments (fucoxanthin, peridinin, alloxanthin, 19'-butanoyloxyfucoxanthin, 19'-hexanoyloxyfucoxanthin, zeaxanthin and total monovinyl and divinyl chlorophyll–*b* (chl-*b*)). Uitz *et al.* (2006, 2008) used multiple-linear regression to calculate the ratio of each pigment to chl-*a,* with a weighted sum of these diagnostic pigments (wDP) calculated as follows:

$$\text{wDP} = 1.41[\text{fuc}] + 1.41[\text{per}] + 0.6[\text{allo}] + 0.35[\text{19'-but}] + 1.27[\text{19'-hex}] + 0.86[\text{zea}] + 1.01[\text{chl-}b], \quad (4)$$

where [pigment] is the concentration of the pigment measured by HPLC. The ratio of the weighted sum of group-specific diagnostic pigments within a size class to wDP provides the proportion of biomass in each size-class (Uitz *et al.* 2006, 2008), in chlorophyll units.

$$f_{micro} = (1.41[\text{fuc}] + 1.41[\text{per}])/\text{wDP} \quad (5)$$

$$f_{nano} = (0.6[\text{allo}] + 0.35[\text{19'-but}] + 1.27[\text{19'-hex}])/\text{wDP} \quad (6)$$

$$f_{pico} = (0.86[\text{zea}] + 1.01[\text{chl-}b])/\text{wDP} \quad (7)$$

The method of Bricaud *et al.* (2004) was then used to generate a size index (*SI*) by converting these proportions into an estimate of MESD in μm, by assuming that picophytoplankton have an MESD of 1μm, nanophytoplankton of 5 μm and microphytoplankton of 50 μm:

$$SI = (f_{pico} + 5\, f_{nano} + 50\, f_{micro}) \quad . \tag{8}$$

3.3.6b Absorption-based method

The method of Roy *et al.* (2011) as modified by Cheung *et al.* (unpublished) was followed to estimate MESD using measurements of phytoplankton absorption (a_{ph}) using the filter pad method and pigment concentrations from HPLC. In brief, the degree of packaging was calculated by comparing the absorption by phytoplankton cells at 676 nm with the estimated absorption at 676 nm from the same chlorophyll concentration in a hypothetical solution. A lookup table was then used to convert this measure of packaging into MESD. See Appendix 3.1 or Roy *et al.* (2011) for details.

3.3.7 Calculating mixed-layer irradiance

Average surface irradiance was estimated using MODIS-Aqua monthly climatology (OceanColour level 3) which was combined with estimates of the vertical attenuation coefficient from chl-*a* and seawater from Platt *et al.* (2003) to obtain estimates of photosynthetically-active radiation (PAR) within the mixed layer. Mixed-layer depths, temperature (Locarnini *et al.* 2010), and salinity (Antonov *et al.* 2010) came from the World Ocean Atlas 2009 and potential density was taken from Jackett *et al.* (2006). Linear interpolation was used to derive estimates of daily irradiance from the monthly climatology. Natural-neighbour interpolations were used to estimate mixed-layer depth.

3.3.8 Statistical analysis

To examine physiological and ecological trends of phytoplankton communities, hierarchical cluster analysis was carried out using HPLC indicator pigment data using Ward's minimum variances clustering implemented in the statistical software R via the function "hclust" as part of the "stats" package 2.5.1 (http://cran.r-project.org). Effects of variations in total biomass were eliminated by using chlorophyll-normalised pigment concentrations. Data were plotted using package "ggplot2" version 0.8.9, and mapping package "Ocean data view" version 4.

3.4 Results

3.4.1 Summary of environmental and biological variables

The sample locations are shown in Fig 3.1, and are predominately from the North West Atlantic, with the majority of stations falling within the North West Coastal Shelves Province as defined by Longhurst *et al.* (1995). Latitude ranges from 21.8 º N to 62.2 º N, with 50% of samples from 43.2 º N to 48.6 º N. Sample temperatures varied between -1.6 ºC and 26.3 ºC with a mean of 7.9 ºC. Total HPLC chl-*a* ranged from 0.014 µg/l to 26.3 µg/l with a mean of 1.40 µg/l. MESD as estimated by absorption ranged from 0.1 µm to 94 µm, with a mean of 18.4 µm, and by HPLC pigments from 1 µm to 50 µm with a mean of 30.9 µm. Maximal realised quantum yield of photosynthesis (φ_m) was found to range from 0.00035 mol C (mol photons)$^{-1}$ to 0.29 mol C (mol photons)$^{-1}$, with a mean of 0.034 mol C (mol photons)$^{-1}$. Summary statistics of environmental variables can be found in Table 3.1.

3.4.2 Summary of cluster pigment:chl-*a* ratios

Unsupervised Ward's minimum variance hierarchical clustering on phytoplankton pigment concentrations normalised to chl-*a* resulted in 8 distinct clusters (Fig 3.2). Boxplots of temperature, *PE* parameters, stratification and key diagnostic pigments reveal the clusters to be dominated by different phytoplankton populations (Fig 3.3, Table 3.1. Table 3.2, Table 3.3). Clusters 2 and 6 have the highest fuc/chl-*a* levels and dominate in early spring, in addition to having the largest mean cell sizes, along with the highest chl-*a* concentrations, and lowest temperatures and correspond to spring bloom diatoms. The level of β-carotene/chl-*a* is much higher in cluster 6 than in cluster 2, while the mean mixed-layer PAR is higher for cluster 2. The degree of stratification and mean P_m^B are low for both clusters. Cluster 1 also

shows relatively high fuc/chl-*a* levels, though cell size as calculated from both absorption and HPLC pigments is smaller than in either cluster 2 or 6 and occurs later in the season, and mean values of α^B are higher. This cluster may represent either small diatoms or a mixed diatom and prymnesiophyte assemblage. Cluster 3 is dominated by picophytoplankton with mean cell size being small and chlorophyll-*a*-normalised zeaxanthin concentrations are high, although moderate concentrations of per/chl-*a* are also seen, perhaps representing an ecological as opposed to strict taxonomic grouping for this cluster. Cluster 3 also has high mean values of α^B and low φ_m. Cluster 4 has the lowest mean cell size and φ_m along with high zea/chl-*a* and chl-*b*/chl-*a* levels, high P_m^B and high mean mixed-layer PAR, suggesting picophytoplankton form a significant proportion of the total biomass. Large quantities of DVchl-*a* are present, indicating the presence of *Prochlorococcus,* and this cluster appears earlier in the season than cluster 3, to which it is otherwise similar. Cluster 5 consists of nanoflagellates and is characterised by high levels of chl-*b*/chl-*a*, chl-*c*/chl-*a* along with 19'-hex and 19'-but. Very high levels of β-carotene/chl-*a* are also seen despite the estimated PAR being low and this cluster is most abundant late in the year. Both clusters 7 and 8 show a high degree of stratification. They also contain high levels of allo/chl-*a,* perhaps indicating the presence of cryptophytes or photosynthetic ciliates (e.g. *Mesodinium*), although the mean P_m^B and α^B for cluster 7 is much higher. Cluster 8 also has very high levels of per/chl-*a,* indicative of dinoflagellates, and is present throughout the year. Unlike cluster 3, where peridinin is a major pigment in some samples, yet the mean concentration is low, here both the peak and mean concentrations are very high.

3.4.3 Estimates of cell size using HPLC pigments and absorption

A strong correlation was seen between size estimated from HPLC pigment analysis and *in-vivo* specific absorption coefficients (Fig 3.4), ($F_{1391,1}$ = 574, $p < 0.0001$, $R^2 = 0.29$). MESD

was significantly higher when estimated using pigments (30.9 μm), than by absorption (18.4 μm) (W = 1444364, $p < 0.0001$). Mean within-cluster estimates of size (Figs 3.3, 3.4, Table 3.1) reveal that despite an overall correlation between the methods of estimating size, differences exist in the size order of the clusters. Both methods estimate clusters 3 and 4 to be the smallest, and clusters 6, 2 and 1 to be the largest. The pigment-based method of assigning size results in peridinin-dominated cluster 8 being fourth in terms of MESD, instead of sixth. Not only do the estimates of mean size differ, but also the size distributions within clusters (Fig 3.5). The pigment-based approach gives very tight groupings for fucoxanthin-dominated clusters 2 and 6, with the majority of samples between 45 and 50 μm, while the absorption-based approach results in a much broader size spectrum. The opposite is seen for zeaxanthin-dominated cluster 4.

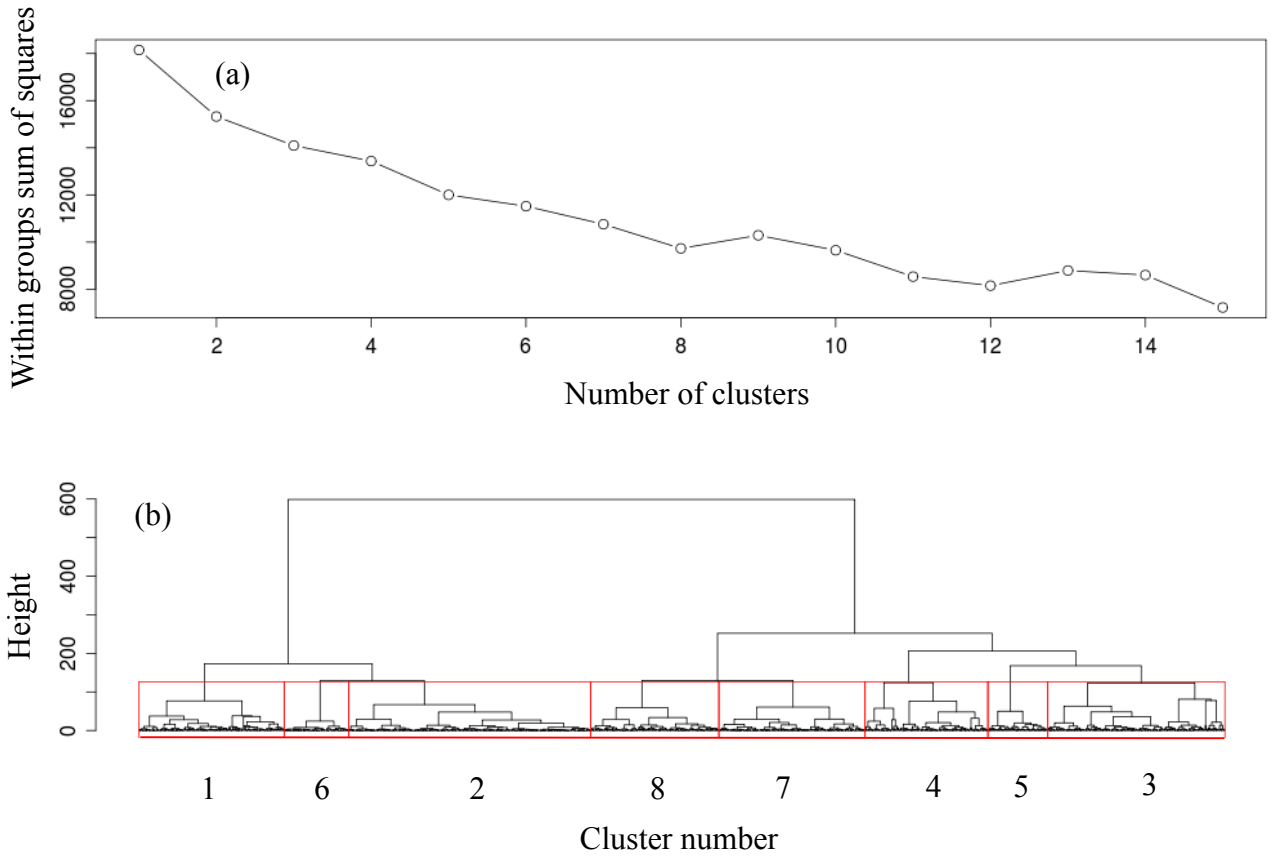

Fig 3.2: Results of Ward's hierarchical cluster analysis using chlorophyll-normalised HPLC pigment concentrations. (a) Descent curve, showing clear elbow at 8 clusters. Clusters numbered according to the order observations appear in the data. (b) Dendrogram showing Euclidian distances between samples, with red boxes surrounding each cluster. **Cluster 1** contains small diatoms and stratification is low. It occurs later than the other two diatom-dominated clusters. **Cluster 2** is also diatom dominated, and found in strong mixing conditions in early spring. **Cluster 3** is dominated by photosynthetic picoeukaryotes, and is characterised by very high levels of stratification during summer, small mean ESD. **Cluster 4** is also dominated by picophytoplankton, both eukaryotic and prokaryotic. It has the lowest mean ESD, very high chlorophyll-normalised zeaxanthin concentrations and is associated with highly-stratified summer conditions. **Cluster 5** consists of nanoflagellates, and is characterised by very high levels of chlorophyll-normalised β-carotene, high levels of chlorophyll-normalised chl-*b*, chl-*c1,2,3* and 19'-hex and 19'-but. **Cluster 6** is the earliest of the diatom-dominated clusters, with very large mean ESD. **Cluster 7** is nanoflagellate-dominated, characterised by highly stratified conditions in autumn. **Cluster 8** consists of dinoflagellates and is found throughout the year.

Table 3.1: Summary of key cluster properties, showing sample temperature, depth, day of year, total HPLC chl-*a, PE* parameters, quantum yield (φ_m), mean-specific absorption between 350 and 700 nm ($\bar{a}^*_{ph}$). Mean phytoplankton ESD was estimated both using absorption (Roy *et al.* 2011) and HPLC pigments (Bricaud *et al.* 2004). The approach of Uitz *et al.* (2008) was used to estimate the proportion of the total biomass due to picophytoplankton, nanophytoplankton and microphytoplankton

		Pigment-based clustering								
	Cluster	**1**	**2**	**3**	**4**	**5**	**6**	**7**	**8**	**All**
	n	187	311	228	158	77	83	188	165	1397
Temp (°C)	Min	-0.9	-1.6	-1.2	-1.5	3.2	-1	1	-0.4	-1.6
	Mean	4.6	3.6	11.6	11.6	9.6	3.2	9.8	7.8	7.9
	Max	19.3	16.1	23.2	26.3	24.2	10.1	19.4	15.7	26.3
	SD	3.6	3.1	5.3	8.4	5.9	3	3.9	3.3	6.0
Depth (m)	Min	0	1	0	1	1	0	1	1	0
	Mean	18.6	13.6	14	21.5	7.8	13.5	8	7.7	13.5
	Max	125	80	130	170	50	51	45	50	170
	SD	19.1	15.4	17.7	29.3	11.6	14.3	10.6	11.3	17.9
Julian day	Min	98	65	84	79	83	65	98	98	65
	Mean	200	133	241.4	173.6	246	111.4	248.7	230.4	197
	Max	355	356	340	340	355	184	353	351	356
	SD	88.4	55.7	62.4	85.6	79.0	27.5	78.0	87.0	87.1
Total Chl-*a* (µg/l)	Min	0.095	0.043	0.073	0.014	0.104	0.35	0.14	0.20	0.014
	Mean	1.24	2.30	0.55	0.36	1.17	4.74	0.94	0.98	1.40
	Max	6.74	13.85	2.42	2.81	7.55	28.0	3.20	4.47	27.97
	SD	1.20	2.63	0.42	0.39	1.29	4.15	0.53	0.63	2.02
P_m^B	Min	0.41	0.42	0.79	0.43	0.74	0.33	0.99	0.57	0.33
	Mean	2.36	2.46	3.3	3.95	3.53	1.87	4.66	3.08	3.10
	Max	6.95	19.73	12.7	12.54	7.69	4.55	9.36	7.46	19.73
	SD	1.29	1.86	2	2.51	2.31	1.02	1.99	1.36	2.02
α^B	Min	0.0043	0.0039	0.0089	0.0029	0.0093	0.0043	0.012	0.0064	0.0029
	Mean	0.034	0.024	0.041	0.034	0.042	0.016	0.047	0.028	0.034
	Max	0.116	0.181	0.088	0.120	0.099	0.040	0.117	0.058	0.181
	SD	0.023	0.021	0.020	0.024	0.029	0.0071	0.022	0.011	0.022
φ_m	Min	0.0050	0.0054	0.0069	0.00036	0.0094	0.0054	0.0073	0.0065	0.00036
	Mean	0.037	0.036	0.022	0.022	0.039	0.030	0.043	0.025	0.034
	Max	0.146	0.291	0.086	0.082	0.098	0.086	0.095	0.123	0.291
	SD	0.027	0.029	0.020	0.021	0.029	0.018	0.023	0.019	0.025
Mean specific	Min	0.0085	0.0051	0.014	0.019	0.010	0.0044	0.011	0.0085	0.0043
	Mean	0.027	0.019	0.034	0.066	0.026	0.014	0.026	0.031	0.030

absorption (400-700 nm)	Max	0.095	0.076	0.099	0.505	0.065	0.054	0.066	0.085	0.505
	SD	0.014	0.011	0.014	0.064	0.0084	0.0081	0.0082	0.013	0.028
Size from absorption (µm)	Min	0.1	0.1	0.1	0.1	0.1	0.1	0.1	0.1	0.1
	Mean	17.8	29.1	12.8	6.7	16.7	31.7	16.8	14	18.4
	Max	61	94	35	24.6	43.2	87.4	46.3	49.8	94.0
	SD	9.5	15.8	6.5	6.3	7.2	16.9	7.3	10.8	13.4
Size from pigments (µm)	Min	12	23.4	1	1	2.1	34.8	11.1	18.5	1
	Mean	37.8	47	17.9	11.7	22	46.9	22.7	34.3	30.9
	Max	50	50	50	38.8	47.5	50	47.3	50	50
	SD	10.7	5.2	7.6	11.1	10.6	3.2	7.5	7.6	15.1
Proportion Pico	Min	0	0	0	0.111	0.024	0	0	0	0
	Mean	0.087	0.032	0.197	0.580	0.231	0.035	0.183	0.107	0.167
	Max	0.356	0.271	1	1	0.722	0.144	0.379	0.493	1
	SD	0.089	0.057	0.147	0.274	0.149	0.026	0.07	0.077	0.204
Proportion Nano	Min	0	0	0	0	0.015	0	0.025	0	0
	Mean	0.176	0.032	0.499	0.219	0.372	0.030	0.407	0.233	0.241
	Max	0.649	0.437	1	0.755	0.652	0.285	0.689	0.550	1
	SD	0.173	0.069	0.156	0.204	0.150	0.058	0.144	0.133	0.220
Proportion Micro	Min	0.180	0.422	0	0	0	0.666	0.159	0.337	0
	Mean	0.738	0.936	0.305	0.201	0.397	0.935	0.410	0.660	0.591
	Max	1	1	1	0.770	0.948	1	0.940	1	1
	SD	0.231	0.112	0.161	0.229	0.225	0.069	0.164	0.165	0.32

Table 3.2: Chlorophyll-normalised HPLC pigment concentrations for the different clusters.

	Pigment-based clustering								**All**
	Cluster	**1**	**2**	**3**	**4**	**5**	**6**	**7**	**8**	**samples**
	n	187	311	228	158	77	83	188	165	1397
allo : chl-*a*	Min	0	0	0	0	0	0	0.019	0	0.
	Mean	0.012	0.008	0.007	0.007	0.025	0.002	0.049	0.048	0.019
	Max	0.095	0.069	0.069	0.129	0.063	0.016	0.129	0.140	0.140
	SD	0.019	0.015	0.015	0.017	0.020	0.003	0.021	0.033	0.026
β-car : chl-*a*	Min	0	0	0	0	0.0070	0.0050	0	0	0
	Mean	0.0001	0.0002	0.0007	0	0.0280	0.0152	0.0001	0.0001	0.0026
	Max	0.0092	0.0092	0.0230	0	0.0760	0.0262	0.0088	0.0122	0.0760
	SD	0.0010	0.0011	0.0035	0	0.0120	0.0039	0.0007	0.0011	0.0078
19'-but : chl-*a*	Min	0	0	0	0	0	0	0	0	0
	Mean	0.026	0.001	0.081	0.012	0.047	0.006	0.037	0.014	0.028
	Max	0.187	0.049	0.314	0.327	0.151	0.043	0.135	0.101	0.327
	SD	0.036	0.006	0.057	0.037	0.041	0.011	0.033	0.025	0.044
chl-*b* : chl-*a*	Min	0	0	0	0	0	0	0	0	0
	Mean	0.063	0.019	0.131	0.202	0.136	0.024	0.115	0.093	0.092
	Max	0.325	0.164	0.654	1.296	0.255	0.101	0.215	0.366	1.296
	SD	0.067	0.034	0.106	0.184	0.057	0.019	0.041	0.066	0.104
Combined	Min	0.066	0	0	0	0	0	0	0.053	0.053

chl-*c1* and chl-*c2* : chl-*a*	Mean	0.193	0.138	0.112	0.056	0.120	0.195	0.095	0.133	0.128
	Max	1.958	0.294	0.287	0.163	0.269	0.430	0.181	0.425	1.958
	SD	0.157	0.057	0.058	0.047	0.056	0.057	0.029	0.046	0.085
chl-*c3* : chl-*a*	Min	0	0	0	0	0	0	0	0	0
	Mean	0.042	0.004	0.033	0.005	0.028	0.013	0.017	0.009	0.018
	Max	0.101	0.036	0.198	0.045	0.086	0.057	0.037	0.043	0.198
	SD	0.023	0.007	0.034	0.011	0.020	0.016	0.012	0.012	0.023
% of total chl-*a* as divinyl	Min	0	0	0	0	0	0	0	0	0
	Mean	0	0	2.82	14.77	1.81	0	0	0	2.50
	Max	0	0	28.12	100	29.73	0	0	0	100
	SD	0	0	6.88	22.73	5.99	0	0	0	10.23
diad : chl-*a*	Min	0	0	0	0	0.010	0.020	0	0	0
	Mean	0.067	0.052	0.084	0.032	0.072	0.048	0.065	0.082	0.063
	Max	0.278	0.163	0.275	0.225	0.160	0.130	0.240	0.207	0.278
	SD	0.044	0.031	0.060	0.041	0.034	0.017	0.034	0.038	0.044
diat : chl-*a*	Min	0	0	0	0	0	0	0	0	0
	Mean	0.008	0.002	0.021	0.039	0.026	0.003	0.010	0.010	0.014
	Max	0.127	0.127	0.128	0.684	0.151	0.021	0.108	0.063	0.684
	SD	0.020	0.010	0.031	0.085	0.034	0.004	0.020	0.017	0.037
fuc : chl-*a*	Min	0.062	0.110	0	0	0	0.318	0.066	0	0
	Mean	0.433	0.449	0.141	0.088	0.210	0.492	0.184	0.264	0.287
	Max	1.397	0.837	0.467	0.404	0.702	0.751	0.490	0.522	1.397
	SD	0.273	0.136	0.083	0.107	0.161	0.086	0.073	0.085	0.202
19'-hex : chl-*a*	Min	0	0	0	0	0	0	0	0	0
	Mean	0.097	0.013	0.288	0.091	0.206	0.017	0.209	0.146	0.131
	Max	0.506	0.229	0.697	0.335	0.368	0.207	0.390	0.504	0.697
	SD	0.098	0.034	0.110	0.090	0.086	0.039	0.098	0.113	0.131
per : chl-*a*	Min	0	0	0	0	0	0	0	0	0
	Mean	0.019	0.001	0.040	0.00001	0.041	0.007	0.026	0.140	0.032
	Max	0.214	0.051	0.291	0.011	0.177	0.056	0.116	0.476	0.476
	SD	0.039	0.005	0.066	0.001	0.051	0.014	0.037	0.064	0.059
zea : chl-*a*	Min	0	0	0	0	0	0	0	0	0
	Mean	0.005	0.003	0.030	0.175	0.038	0.003	0.021	0.003	0.031
	Max	0.154	0.129	0.363	1.947	0.306	0.020	0.192	0.112	1.947
	SD	0.018	0.015	0.051	0.289	0.057	0.005	0.033	0.013	0.114

(a)
Total chl-a µg/l
0
4
8
(b)
Temperature (°C)
0
10
20
(c)
Mixed layer PAR (E m-2 d-1)
0
20
40
(d)
α^B (mg C mg chl-a)-1 h-1 µmol quanta m-2 s-1)-1
0
0.08
(e)
P^B_m mg C (mg chl-a)-1 h-1
0
4
8
(f)
φm (mol C (mol quanta)-1
0
0.08
(g)
MESD - absorption (µm)
0
40
80
(h)
MESD - HPLC (µm)
0
20
40
(i)
Stratification index (°C m-1)
-0.1
0
0.1
(j)
% chl-a divinyl
0
40
80
(k)
Chl-a norm chl-b
0
0.3
(l)
Chl-a norm chl-c1 + c2
0
0.2
1
2
3
4
5
6
7
8
Pigment-based cluster
Pigment-based cluster
Pigment-based cluster

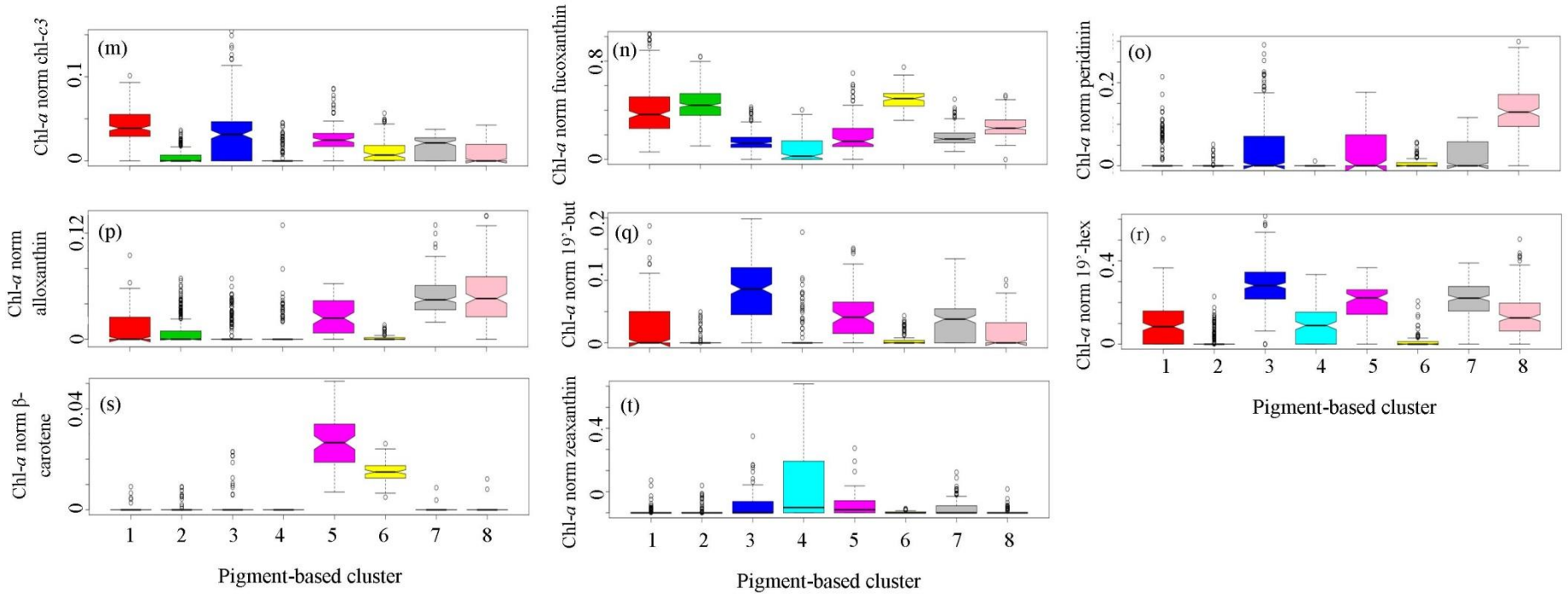

Fig 3.3: Boxplots showing photosynthetic parameters and chlorophyll normalised HPLC pigment concentrations for the different clusters. (a) Total chlorophyll-*a* (µg/l), (b) Temperature (°C), (c) Photosynthetically-active radiation (E m^{-2} d^{-1}), (d) α^B (mg C (mg chl-*a*)$^{-1}$ h^{-1} µmol photons m^{-2} s^{-1})$^{-1}$, (e) P_m^B (mgC (mg chl-*a*)$^{-1}$ h^{-1}), (f) φ_m (mol C mol photons^{-1}), (g) Mean equivalent spherical diameter from absorption (µm), (h) Mean equivalent spherical diameter from pigments (µm), (i) Stratification index, defined as the difference between samples temperature and climatological prediction for the temperature at 100m / offset in depth (°C m^{-1}). (j) Percentage of total chl-*a* which is divinyl, (k) Chl-*a* normalised chl-*b*, (l) Chl-*a* normalised combined chl-*c1* and chl-*c2*, (m) Chl-*a* normalised chl-*c3*, (n) Chl-*a* normalised fucoxanthin, (o) Chl-*a* normalised peridinin, (p) Chl-*a* normalised alloxanthin, (q) Chl-*a* normalised 19'-butanoyloxyfucoxanthin, (r) Chl-*a* normalised 19'-hexanoyloxyfucoxanthin, (s) Chl-*a* normalised β-carotene, (t) Chl-*a* normalised zeaxanthin.

Table 3.3: Summary of pigments present in different clusters and the ecological implications. For the proportion of total accessory pigments: Red = chl-*b*, Green = chl-*c*1*c*2, Dark blue = chl-*c*3, Light blue = fuc, Magenta = per, Yellow = allo, Grey = 19'-but, Black = 19'-hex, Orange = β-carotene, Pink = zea

Proportions of pigments in sample	Cluster number	Important pigments	Ecological implications
	**1**	Fuc, chl-*c*1, *c*2, *c*3	Small diatoms / *Phaeocystis*. Late spring / early summer
	**2**	Fuc, chl-*c*1, *c*2	Large diatoms. Spring, very large MESD
	**3**	Chl-*b*, chl-*c*3, 19'-hex, 19'-but	Picoeukaryotes. Summer, very highly stratified. Some small dino-flagellates, no *Prochlorococcus*
	**4**	Chl-*b*, divinyl chl-*a*, zea. Some 19'-hex, yet 19'-but absent	Picoeukaryotes and prokaryotes. Only cluster with significant pro-portion of *Prochlorococcus*. Summer, stratified
	**5**	Chl-*b*, 19'-hex, 19'-but, β-carotene, some allo	Nanophytoplankton including chrysophytes. Late summer / early autumn. Less stratified than cluster 7.
	**6**	Fuc, chl-*c*1, *c*2, β-carotene	Large diatoms, similar to cluster 2, very large MESD. Early spring.
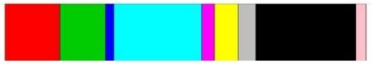	**7**	Chl-*b*, allo, 19'-hex, 19'-but	Nanophytoplankton, more stratified than cluster 5. Very high φ_m and P_m^B.
	**8**	Per, allo	Present throughout the season. Dinoflagellate dominated. Large difference in MESD according to method.

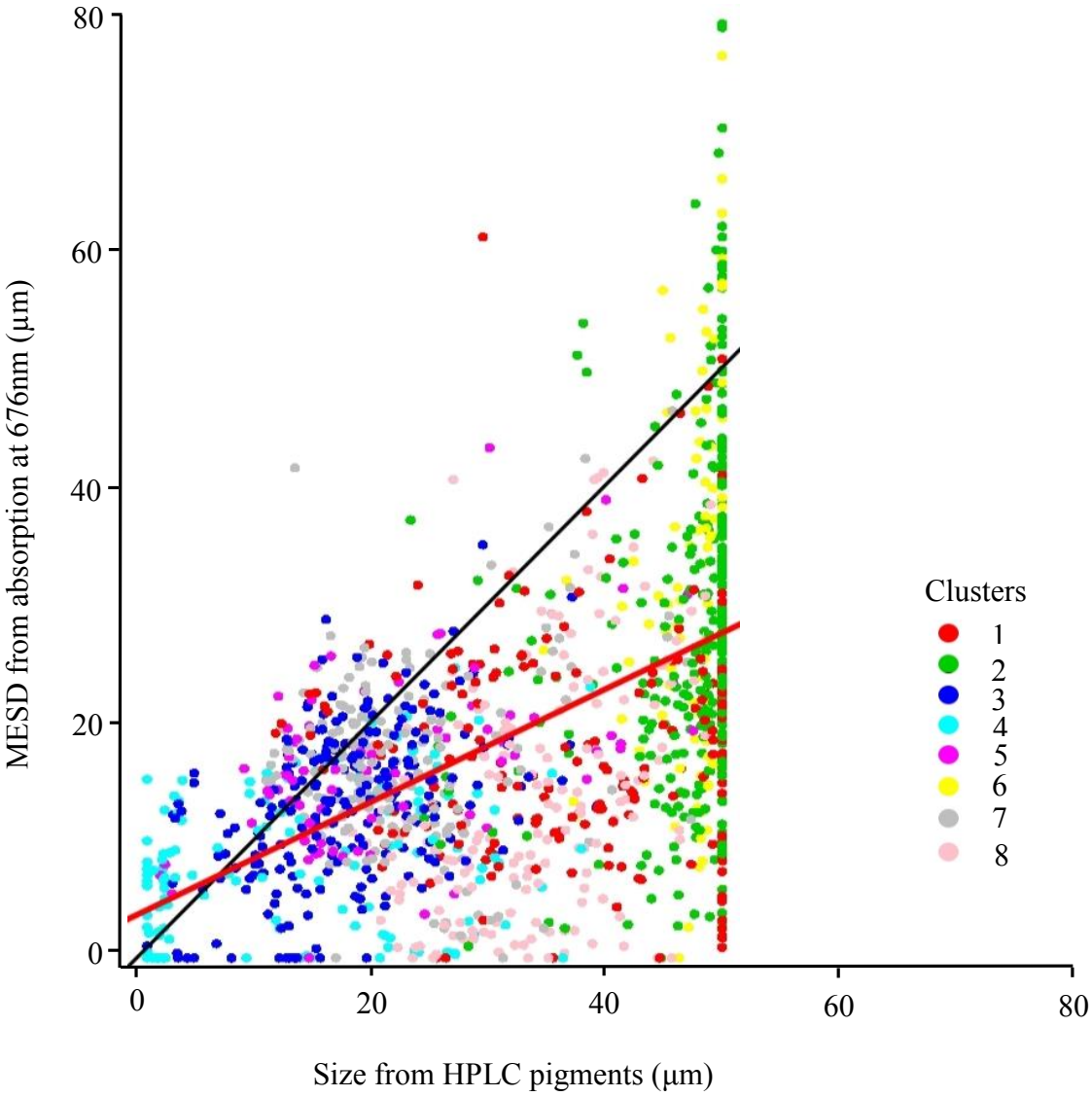

Fig 3.4: A comparison between MESD as estimated using the HPLC pigments-based approach of Bricaud *et al.* (2004) and the absorption-based approach of Roy *et al.* (2011). Black line shows 1:1 relationship, red line the regression on the data.

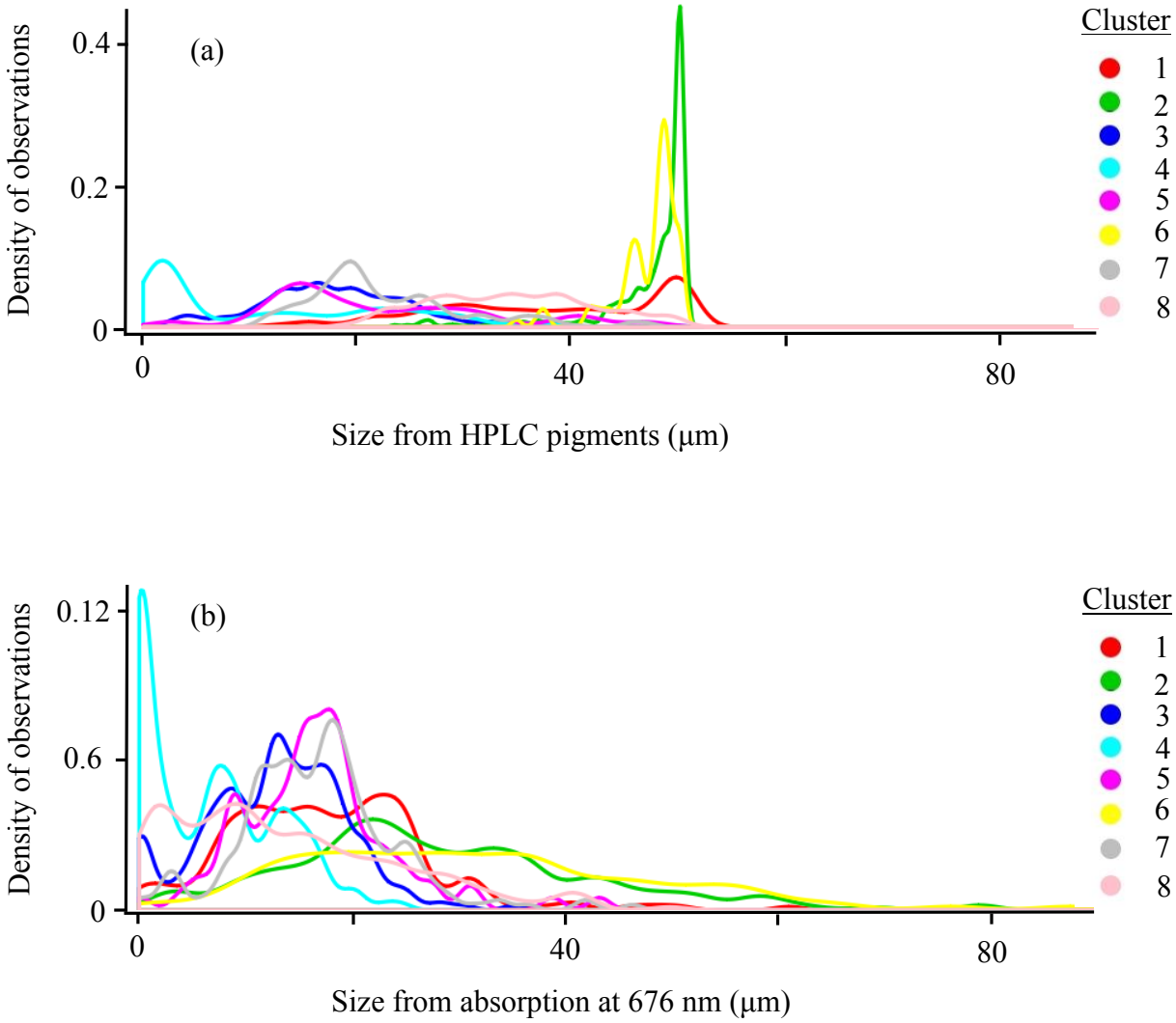

Fig 3.5: Density plots of the size distributions of different phytoplankton populations from hierarchical cluster analysis on chlorophyll normalised HPLC pigment concentrations. Lines coloured according to cluster. (a) Size structure as estimated using HPLC pigments following method of Bricaud *et al.* (2004). (b) Size structure as estimated using absorption at 676 nm.

3.4.4 Relationship between size estimates and environmental variables

A significant positive correlation between MESD and total HPLC chl-*a* concentration was observed (Fig 3.6), for both the pigment-based ($F_{1,1391}$ = 325, R^2 = 0.189, $p < 0.0001$) and the absorption-based method ($F_{1,1391}$ = 570, R^2 = 0.29, $p < 0.0001$) of estimating average cell size. Significant positive relationships are also seen between MESD and temperature for the pigment-based ($F_{1,1050}$ = 1562, R^2 = 0.60, $p < 0.0001$) and the absorption-based method ($F_{1,1052}$ = 259.5, R^2 = 0.20, $p < 0.0001$) of estimating MESD (Fig 3.6). Significant negative correlations between MESD and stratification index are again seen for the pigment-based approach ($F_{1,1049}$ = 526.7, R^2 = 0.33, $p < 0.0001$) and the absorption-based method ($F_{1,1051}$ = 176, R^2 = 0.14, $p < 0.0001$) of estimating MESD (Fig 3.6). Fig 3.7 shows the variation in estimates of size with respect to season, with strong trends being seen for both methods. MESD is highest in spring, before decreasing during the summer months, and then increasing, though not to the same extent, in autumn. A similar trend was seen for both methods, although patterns were slightly distorted for the HPLC pigment-based approach as a great many samples were deemed to be entirely dominated by microphytoplankton, and so have the maximum MESD possible using this method, of exactly 50 µm.

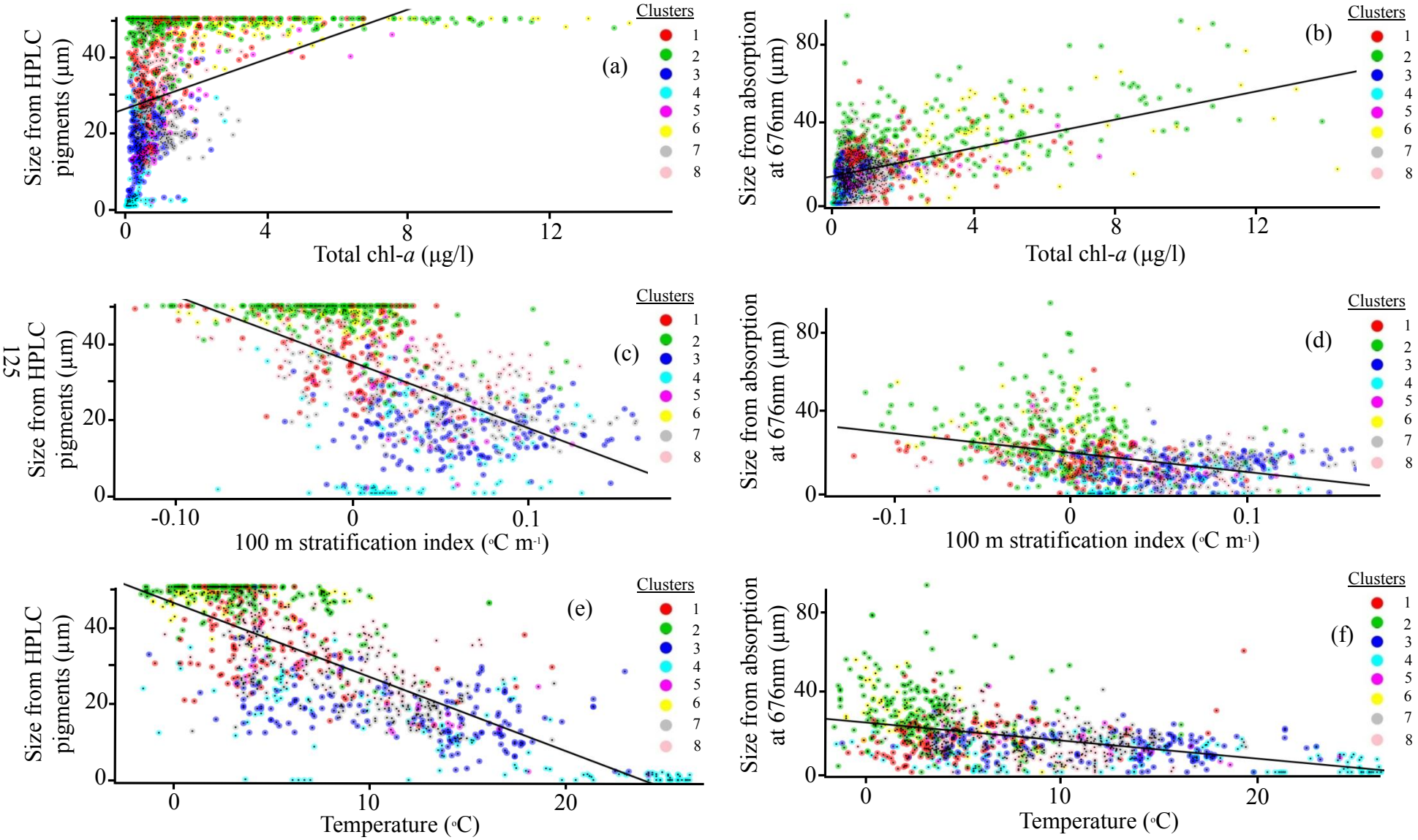
Size from HPLC pigments (µm)
Total chl-a (µg/l)
(a)
Size from absorption at 676nm (µm)
(b)
100 m stratification index (°C m⁻¹)
(c)
(d)
Temperature (°C)
(e)
(f)
Clusters
1
2
3
4
5
6
7
8

Fig 3.6: Relationship between mean equivalent spherical diameter and environmental variables. Points are coloured according to phytoplankton cluster as assigned using chlorophyll normalised hierarchical cluster analysis. (a) Size as estimated using HPLC pigments following method of Bricaud *et al.* (2004) and total chl-*a* (y = 3.25x + 26, $F_{1,1394}$ = 14, R^2 = 0.19, $p < 0.0001$). (b) Size as estimated using absorption at 676 nm and total chl-*a* (y = 3.6x + 13, $F_{1,1395}$ = 570, R^2 = 0.29, $p < 0.0001$). (c) Size as estimated using HPLC pigments following method of Bricaud *et al.* (2004) and the 100 m stratification index (y = -173x + 35, $F_{1,1049}$ = 527, R^2 = 0.33, $p < 0.0001$) (d) Size as estimated using absorption at 676 nm and the 100 m stratification index (y = -95x + 20, $F_{1,1051}$ = 176, R^2 = 0.14, $p < 0.0001$) (e) Size as estimated using HPLC pigments following method of Bricaud *et al.* (2004) and temperature. (y = -1.88x + 46, $F_{1,1050}$ = 1562, $p < 0.0001$) (f) Size as estimated using absorption at 676nm and temperature (y = -0.91x + 25, $F_{1,1052}$ = 260, R^2 = 0.20, $p < 0.0001$).

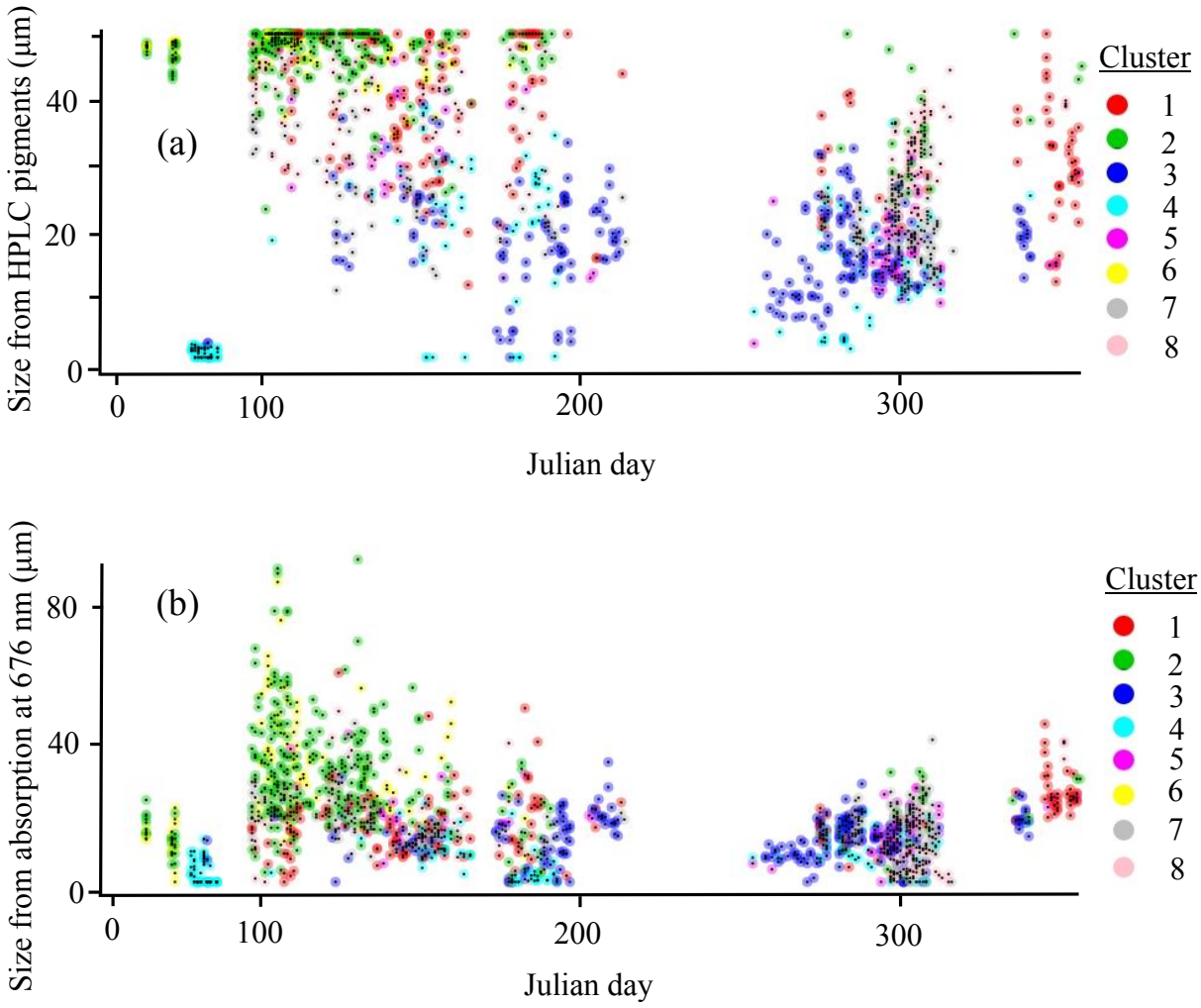

Fig 3.7: Relationship between mean equivalent spherical diameter and Julian day. Points are coloured according to phytoplankton cluster as assigned using chlorophyll-normalised hierarchical cluster analysis. (a) Size as estimated using HPLC pigments following method of Bricaud *et al.* (2004). (b) Size as estimated using absorption at 676 nm.

3.4.5 Successional trends in phytoplankton community structure with respect to season and stratification

In addition to seasonal trends with respect to size, important patterns are seen with respect to the proportion of samples in each cluster (Fig 3.8a). To examine the temporal dynamics of the clusters, I focus on the oceanic province where the majority of samples are found, the North West Atlantic Shelves Province (Longhurst *et al.* 1995). Interannual changes in species succession are accounted for as the dataset covers 8 years of sampling. In early spring, clusters 6 and 2 are the most abundant, accounting for over 2/3 of the samples. These clusters are associated with high chlorophyll-*a*-normalised fucoxanthin concentrations and large cell sizes. By Julian day 150 cluster 6 is absent, and cluster 2 declining in importance. Fucoxanthin is still a major accessory pigment however, as cluster 1 is still strongly represented indicating the presence of small diatoms or *Phaeocystis*, but clusters 3 and 4, associated with high chlorophyll-*a*-normalised zeaxanthin concentrations, now dominate. By Julian day 250 cluster 1 is declining and is less abundant than the dinoflagellate-dominated cluster 8. Around Julian day 275 clusters 3 and 4 decrease rapidly in importance, to be replaced by clusters 5 and 7, indicative of the increasing abundance of β-carotene and alloxanthin as the dominant indicator pigments respectively. These clusters peak in importance around Julian day 300, before decreasing sharply again and are nearly absent by Julian day 325. At this point almost all samples are comprised of a mixed assemblage of clusters 1, 3, 4 and 8 in roughly equal abundance. By winter, around Julian day 350, clusters 3 and 4 have decreased again, while cluster 5 has reappeared.

Similar trends to those seen with respect to seasonality can also be seen as a function of water-column stratification (Fig 3.8b). When the stratification index is low or even negative (where the surface water is colder than the 100 m climatological average) clusters 1, 2 and 6 form the majority of the biomass. As stratification increases, clusters 4 and 5 become

of greater importance, before being replaced by clusters 3 and 7 in very stratified waters. Cluster 8 shows little trend with respect to the degree of water-column stratification, and remains at relatively constant levels throughout. In terms of phytoplankton taxonomic groups, this represents a dominance by large diatoms when the water-column is well mixed during spring to early summer, before being replaced by photosynthetic pico- and nanoeukaryotes in mid to late summer at the system becomes stratified. Towards the autumn the eukaryotes assemblage changes, with nanoflagellates such as chrysophytes coming to dominate, as stratification breaks down. Dinoflagellates are present throughout the season.

The reason for the similarity in patterns seen when considering the relative importance of the different clusters as a function of stratification or seasonality is explained by looking at the relationship between Julian day and stratification (Fig 3.8c). In early spring, the strong wind-driven mixing of the winter months results in weak stratification, with in some cases the low atmospheric temperatures meaning that the surface water is colder than that at depth. As the summer progresses, solar heating causes the surface waters to warm and the degree of wind-induced mixing decreases, resulting in a peak of stratification at around Julian day 250 – 270. Decreased solar heating and stronger winds that follow result in the breakdown of stratification over the winter.

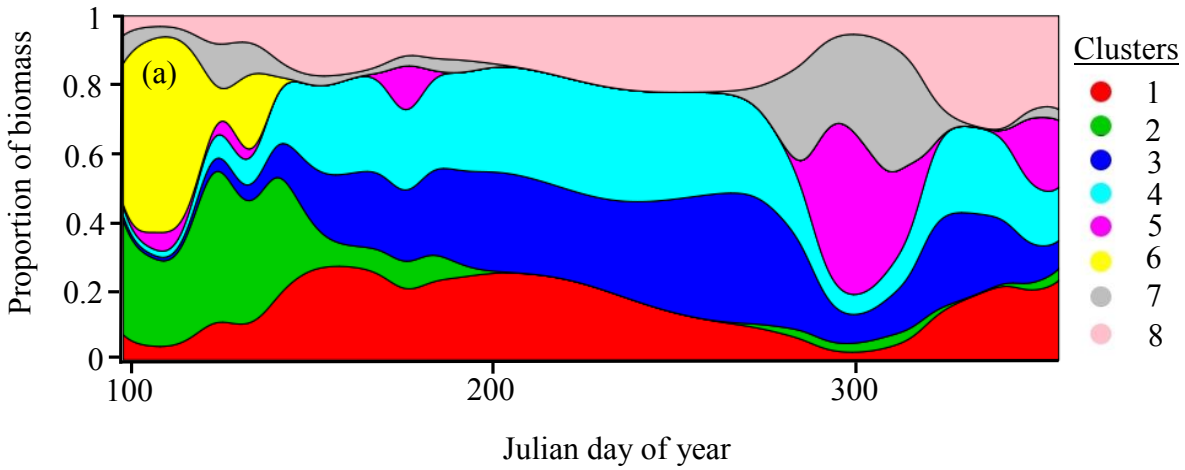
(a)
Proportion of biomass
1
0.8
0.6
0.4
0.2
0
100
200
300
Julian day of year
Clusters
1
2
3
4
5
6
7
8

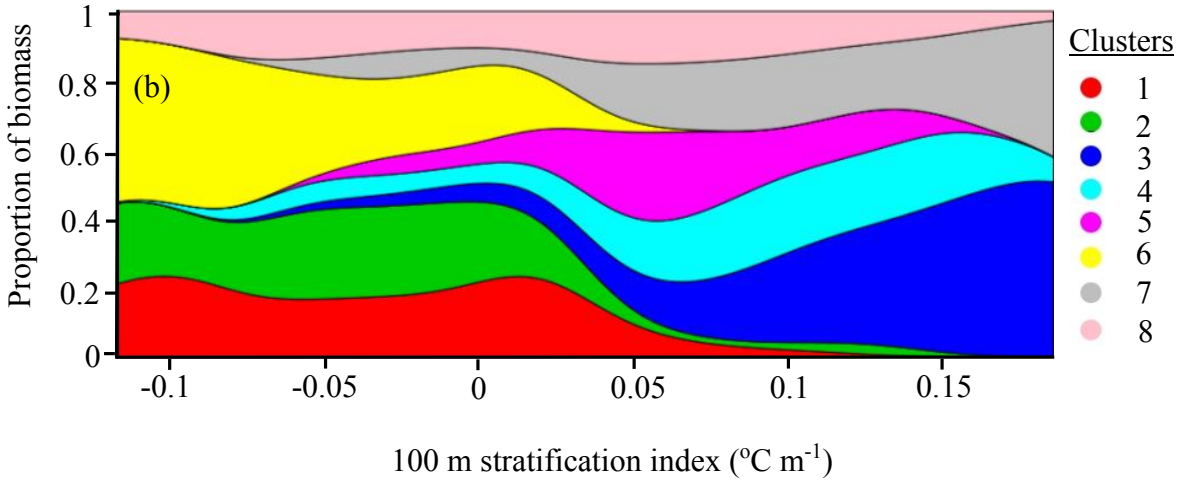
(b)
Proportion of biomass
1
0.8
0.6
0.4
0.2
0
-0.1
-0.05
0
0.05
0.1
0.15
100 m stratification index (°C m-1)
Clusters
1
2
3
4
5
6
7
8

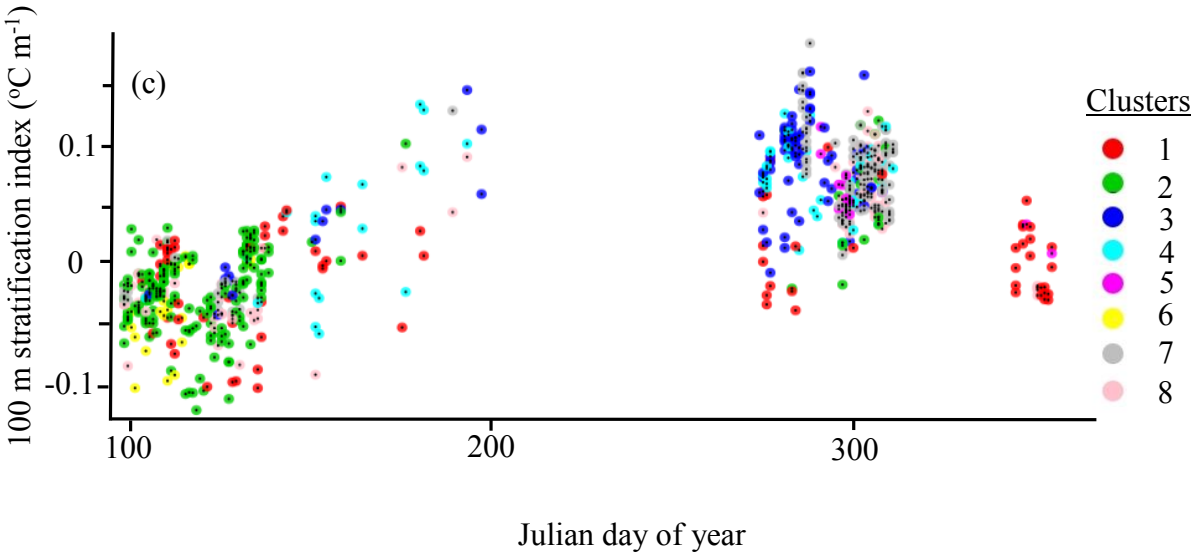
(c)
100 m stratification index (°C m-1)
0.1
0
-0.1
100
200
300
Julian day of year
Clusters
1
2
3
4
5
6
7
8

Fig 3.8: (a) Proportion of samples in each cluster with respect to Julian day in North West Atlantic Shelves Province as defined by Longhurst *et al.* 1995. Clusters assigned using hierarchical cluster analysis on chl-*a* normalised HPLC pigments. (b) Proportion of samples in each cluster with respect to the degree of stratification in the North West Atlantic Shelves Province as defined by Longhurst *et al.* (1995). Clusters assigned using hierarchical cluster analysis on chl-*a* normalised HPLC pigments. (c) Trend in stratification with respect to Julian day of year for North West Atlantic Shelves Province as defined by Longhurst *et al.* (1995). Stratification index defined as the difference between sample temperature and climatological prediction for the temperature at 100 m divided by the offset in depth.

3.4.6 Trends in α^B and φ_m with respect mean daily mixed layer PAR

The seasonal variability in the average light in the mixed layer was reflected in the physiological properties of some of the phytoplankton groups as determined by cluster analysis. Significant negative correlations between in α^B and the climatological mean mixed-layer PAR were seen for cluster 1 ($F_{1,57}$ = 12.9, R^2 = 0.17, p = 0.0006), cluster 4 ($F_{1,34}$ = 9.4, R^2 = 0.19, p = 0.004), cluster 7 ($F_{1,54}$ = 13, R^2 = 0.18, p = 0.0005) and cluster 8 ($F_{1,41}$ = 31, R^2 = 0.42, p <0.0001) (Table 3.2). No relationship was seen for clusters 2, 3, 5, or 6 (Fig 3.9a). Significant positive trends in φ_m with respect to climatological mean mixed-layer PAR were seen for cluster 1 ($F_{1,57}$ = 36, R^2 = 0.38, p < 0.0001), cluster 4 ($F_{1,34}$ = 13.5, R^2 = 0.26, p = 0.0008), cluster 7 ($F_{1,53}$ = 12, R^2 = 0.17, p = 0.001) and cluster 8 ($F_{1,41}$ = 7.4, R^2 = 0.13, p = 0.009) (Table 3.2). No relationship was seen for clusters 2, 3, 5, or 6 (Fig 3.9b). For all groups with a significant relationship, as light intensity increased, the quantum yield decreased.

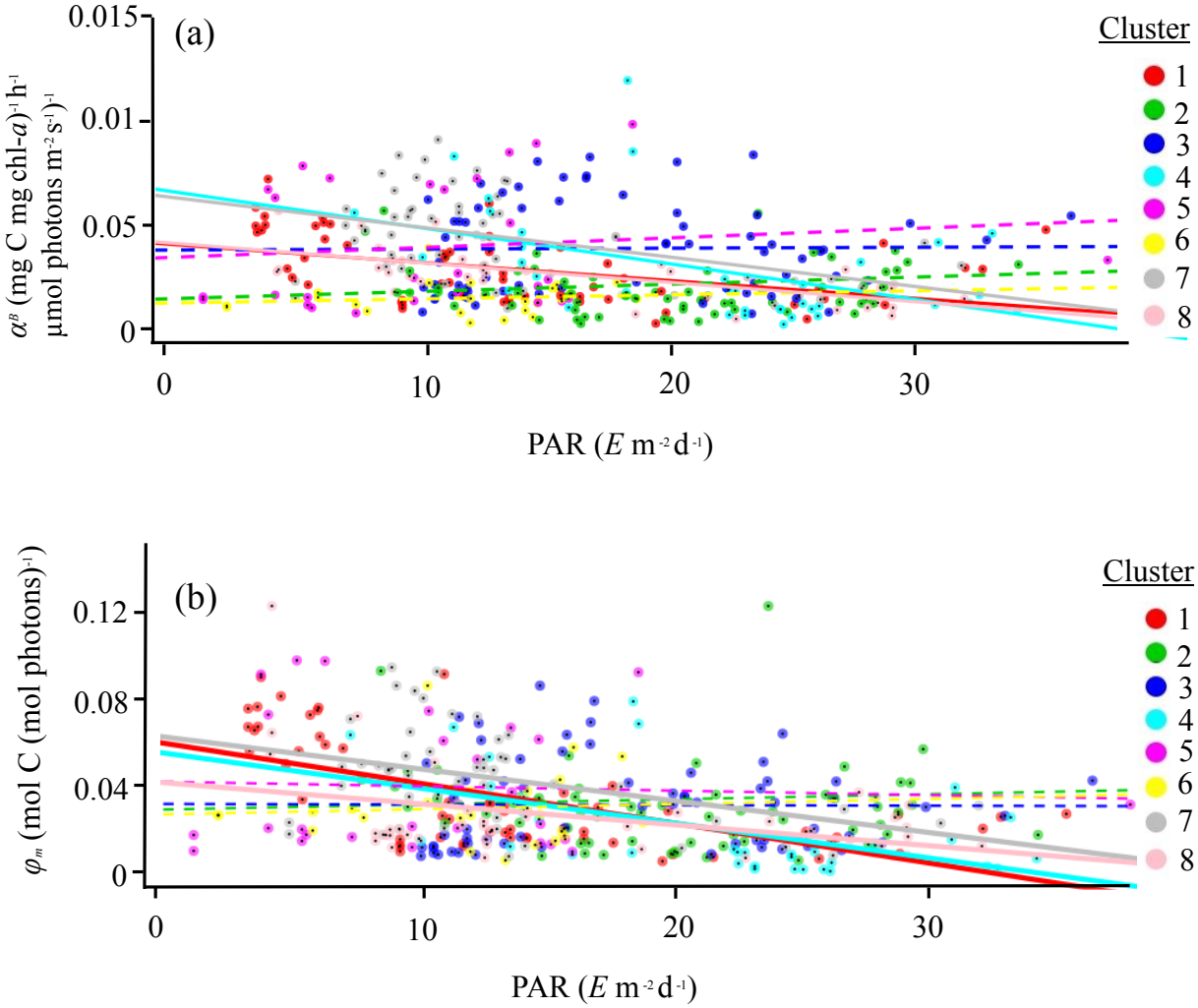

Fig 3.9: Relationship between mean daily PAR in the mixed layer (E m $^{-2}$ d $^{-1}$) estimated from climatology and (a) α^B (mg C mg chl-a)$^{-1}$ h^{-1} µmol quant m^{-2} s^{-1})$^{-1}$ (b) φ_m (mol C (mol photons)$^{-1}$). Points and lines coloured according to hierarchical cluster analysis on chlorophyll-normalised HPLC pigments. Dashed lines show no significant relationship.

3.4.7 Cluster-specific trends in *PE* parameters and absorption

The phytoplankton populations described by the different clusters were characterised by different photosynthetic and absorptive properties. Conventionally these are normalised to biomass so that individual values from different locations of varying chlorophyll

concentrations can be compared. In this study however the aim is to identify trends with respect to clusters of samples, as opposed to single data points. Therefore, the approach of Côté & Platt (1983) was used, where non-biomass-normalised data are plotted against chl-*a* biomass, identifying group-specific relationships. Given that $\bar{a}^*_{ph}$, P_m and α are all functions of biomass, significant relationships are to be expected (Fig 3.10). Cluster 7 shows the highest photophysiological rates (P_m and α) for a given biomass despite a midrange increase in $\bar{a}^*_{ph}$as a function of chl-*a* biomass. Conversely, clusters 3 and 4 have very high specific absorption coefficients, yet differ in the relationship between *PE* parameters and biomass, with the slope of the relationship for cluster 3 *PE* parameters being markedly steeper, as a result of the very low values of φ_m for cluster 4 (Fig 3.3).

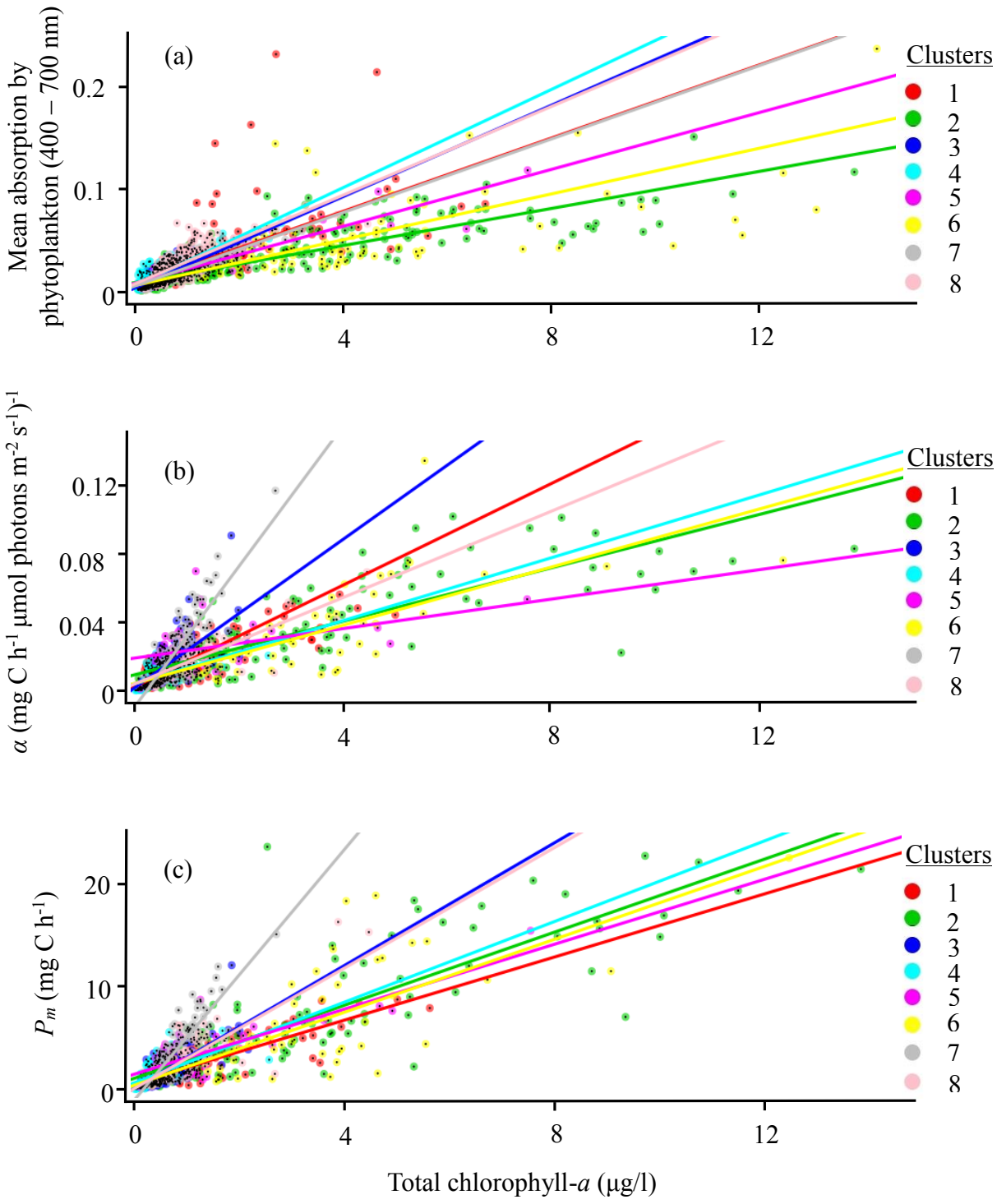

Fig 3.10. Relationships between photophysiological parameters and chlorophyll-*a*. Lines and points coloured according to cluster as ascribed using hierarchical cluster analysis on chlorophyll - normalised HPLC pigment concentrations. (a) Mean specific absorption by phytoplankton between 400 and 700 nm. (b) Light-limited photosynthetic rate (α). (c) Maximal photosynthetic rate (P_m).

3.4.8 Cluster-specific relationships between MESD and φ_m

Significant correlations between MESD as estimated from absorption and φ_m were found for cluster 1 ($F_{1,122}$ = 77.7, R^2 = 0.38, $p < 0.0001$) cluster 2 ($F_{1,151}$ = 5.9, R^2 = 0.03, p = 0.017), cluster 3 ($F_{1,129}$ = 82.9, R^2 = 0.39, $p < 0.0001$), cluster 4 ($F_{1,86}$ = 86.8, R^2 = 0.50, $p < 0.0001$), cluster 6 ($F_{1,44}$ = 14.6, R^2 = 0.23, p = 0.0004), cluster 7 ($F_{1,84}$ = 35.0, R^2 = 0.29, $p < 0.0001$) and cluster 8 ($F_{1,62}$ = 48.6, R^2 = 0.43 $p < 0.0001$). No relationship was observed for cluster 5 ($F_{1,30}$ = *1.5*, R^2 = 0.02, p = 0.23) (Fig 3.11).

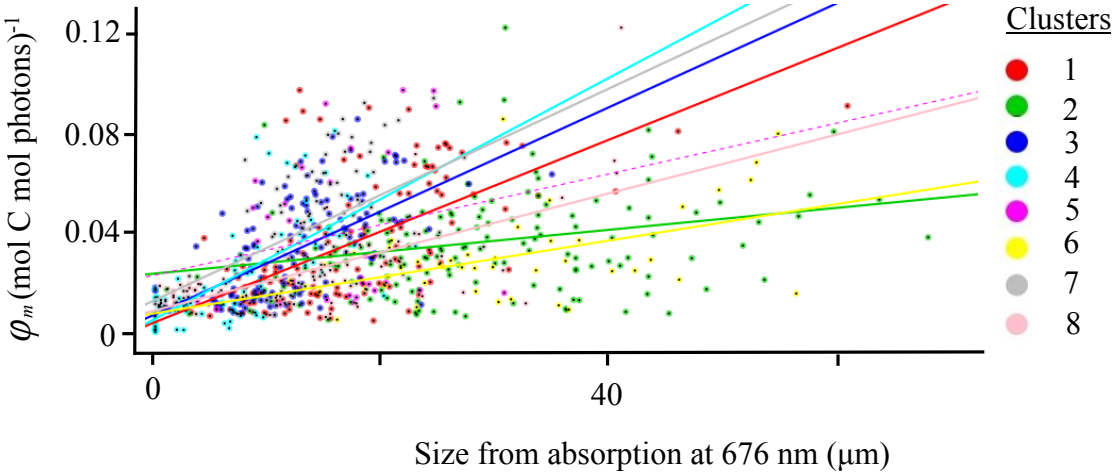

Fig 3.11: Maximum quantum yield (φ_m) as a function of MESD as estimated using absorption. Significant relationships are seen for all clusters (solid lines) except cluster 5 (dashed line).

3.5 Discussion

3.5.1 Benefits of using MESD to assess phytoplankton size

It is important to consider the possible drawbacks of the use of the mean equivalent spherical diameter (MESD) as an indicator of the size structure of the phytoplankton community. MESD is frequently used for convenience in ecological studies since phytoplankton display such a wide range of cell shapes (Chisholm 1992, Montagnes *et al*. 1994), often deviating significantly from spherical. A wide degree of variation in morphology is seen, both within, and between groups, meaning that MESD is a more appropriate measure than absolute size for making comparisons between different taxonomic groups. The benefits of using MESD are particularly pronounced when considering samples across ecological regimes, as it can be used as a relative measure to assess trends in phytoplankton succession, or to estimate cell carbon content, as opposed to trying to obtain an absolute measure of phytoplankton size.

3.5.2 Potential errors in estimating MESD

A significant correlation was seen between size as estimated using the pigment-based taxonomic approach of Bricaud *et al.* (2004) and the absorption-based approach of Roy *et al*. 2011. However, a significant difference in the MESD of phytoplankton estimated using the two methods shows that the two approaches of determining the average cell size of natural samples cannot be treated as identical (Fig 3.4). The benefits and errors associated with the two methods of estimating the MESD are now considered.

A disadvantage to the pigment-based approach is the rigid assignment of phytoplankton size-class according to the indicator pigments present. Potential misclassifications exist for all size-classes. Zeaxanthin is often associated with

picophytoplankton, yet present in high concentrations in the microphytoplankton-sized *Trichodesmium* (Dandonneau *et al.* 2006), and while 19'-hex and 19'-but are commonly used as markers for nanophytoplankton, these pigments can also be found in very small picoflagellates (Aiken *et al.* 2009). Problems are also seen with respect to the assigning cell-size estimates on the basis of a fixed MESD for each size class. Bricaud *et al*. (2004) recognised that not only were pigments not unique to single phytoplankton groups, but also that even within a taxonomic group widespread variation in size was possible. Dandonneau *et al*. (2006) pointed out that in the presence of very small diatoms such as *Chaetoceros socialis* and *Nitzschia* sp., using the Bricaud *et al.* (2004) method led to an underrepresentation of nanophytoplankton since all of the biomass associated with fucoxanthin was assigned to microphytoplankton. The pigment-based approach may also be biased towards the effect of large cells, as a few large cells could contribute significantly towards the pigment biomass, yet form only a low proportion of the total number of cells. Another limitation of the Bricaud *et al.* (2004) approach is that the upper size limit of 50 μm, may be too small to account for large diatoms and dinoflagellates (Hasle & Syvertsen 1997). Large diatom cells are frequently seen during bloom events in the North Atlantic and when combined with the misclassification of fucoxanthin-containing nanophytoplankton, a large proportion of samples are assigned a MESD of between 45 and 50 μm, in this study Fig 3.5a. This artificial peak in the frequency of MESD estimates for this dataset affects the patterns seen with respect to other variables as a function of size (Figs 3.4a, 3.6a, and 3.7a), where size distributions appear to be cut off at the maximum possible MESD of 50 μm. A possible error of the same relative magnitude is also seen by assigning a minimum equivalent spherical diameter of 1 μm for the smallest picophytoplankton, with studies such as Chisholm (1992) estimating *Prochlorococcus* to have a mean equivalent spherical diameter of 0.6 μm. Despite these potential drawbacks, the pigment-based taxonomic approach of Bricaud *et al.* (2004) remains a powerful tool for

assessing the size structure of phytoplankton in the absence of direct measurements of MESD. While some detail will be lost by using such rigid size-classes, the approach has never been intended to be a precise tool, and instead it gives a simple approximation of the dominant size within a population.

Important assumptions are also required for estimating cell size based on the absorptive properties of phytoplankton. The original paper of Roy *et al.* (2011) includes a comparison between size as estimated using absorption by phytoplankton and those measured in cultures and found a very robust 1:1 correlation. As discussed in appendix 3.1, using literature values for the *in-vivo* absorption by chlorophyll-*a* at 676 nm (a^*_{ci} (676)) of 0.0199 (Bidigare *et al.* 1990) or even 0.03, (Moisan & Mitchell 1999), estimates of the absorption by cellular material at 676 nm (a^*_{cm}(676)) resulted in a large number of cells with a package effect index (Q^*_c) of greater than 1. As a consequence the observed *in-situ* absorption coefficient was higher than the predicted value in solution, meaning that a correction factor was required. Values of Q^*_c of greater than 1 have been reported previously (Nelson *et al*. 1993, Bricaud *et al.* 2004), and a range of explanations provided, such as absorption by other cellular material or protein interactions changing pigment absorption properties. The correction used in this study converts chlorophyll-specific a^*_{ci} (676) to a^*_{cm} (676) for whole populations, allows for reliable assessment of Q^*_c and hence representative estimates of the population size structure. While both pigment- and absorption-based approaches have their advantages, important differences in MESD and the shape of the MESD distribution are observed, as described below.

3.5.3 Differences in the shape of the size spectrum according to method

Differences in MESD between the two methods are seen with respect to the distribution of sizes, as well as the overall correlation (Fig 3.5). Most conspicuous is the very sharp peak seen in the density of observations between 40 and 50 μm as estimated using the pigment-based approach. The sharp peak at 40 to 50 μm particularly for clusters 2 and 6 is due to the rigid assignment of all biomass associated with fucoxanthin to diatoms, along with all associated with peridinin to dinoflagellates, and assuming that all diatoms and dinoflagellates have an MESD of 50 μm. Given the significance of seasonality in this temperate region (Dandonneau *et al*. 2004, Henson *et al.* 2009), and the ability of certain diatom species to form high density blooms (Barlow *et al*. 1993), such a sharp peak in the microphytoplankton portion of the size distribution could be possible. However, it has been reported that pico- and nanophytoplankton biomass does not decrease even at the peak of a diatom bloom (Barber & Hiscock 2006), such that the results from the HPLC pigments-based approach which yields only microphytoplankton during a bloom are unlikely. Sheldon & Parsons (1967) suggested that organism abundance (A) per unit volume is inversely related to organism size:

$$A = c_2 V^{\zeta} \tag{19}$$

where ζ is a size scaling exponent and c_2 is the concentration of cells at a reference size of 1 μm. While studies have found wide variation in ζ (Irwin *et al*. 2006), a sharp peak in microphytoplankton abundance as sometimes seen using the pigment-based method would be contrary to expectations, whereas the smoother relationship seen using the absorption-based method of estimating cell size appears more realistic.

3.5.4 Differences in MESD within clusters

Important differences in estimates of MESD are also seen within individual phytoplankton clusters (Fig 3.5, Table 3.1) with especially large discrepancies found for clusters 1 (fucoxanthin dominated) and 8 (peridinin dominated). Cluster 1 is estimated to have a MESD of 38 μm from the Bricaud *et al.* (2004) pigment method and just 18 μm using the absorption-based approach of Roy *et al.* (2011), whereas the MESD for cluster 8 is estimated to be 34 μm from the pigment method and 14 μm from the absorption-based approach. These differences may result from the presence of fucoxanthin amongst nanophytoplankton; it is probable that the low MESD estimated using phytoplankton absorption results from many of the cells containing fucoxanthin being in the nanophytoplankton size range, while the pigments-based approach assigns all biomass associated with fucoxanthin to microphytoplankton. Cluster 8 has very high concentrations of alloxanthin and peridinin, and significant concentrations of chl-*b*. The pigment-based approach results in a large MESD as a result of high concentrations of peridinin (see equation 5). Although peridinin is a reliable indicator of the presence of dinoflagellates, dinoflagellate species as small as 2μm have been recorded (Wright *et al.* 1997), which if present would bias the pigment-based approach. This cluster is present at relatively constant proportions throughout the year (Fig 3.8), a trait that is more usually associated with background populations of nanophytoplankton than microphytoplankton (Marañon *et al*. 2001), hence the absorption-based size estimate may be more representative of the actual size structure.

Cluster 1 shows relatively high chl-*a*-normalised fucoxanthin concentrations along with very high chl-*a*-normalised concentrations of chl-*c1*, *c2* and *c3*, unlike the other clusters with only high concentrations of fucoxanthin (clusters 2 and 6). Chlorophylls-*c1 c2* and *c3* are found in a wide range of phytoplankton groups, including chrysophytes, cryptophytes, prymnesiophytes, dinoflagellates and diatoms, and consequently are not used in the Bricaud

(2004) method as being diagnostic. The association of fucoxanthin and chlorophylls-*c1, c2* and *c3* may indicate the presence of *Phaeocystis* as opposed to diatoms (Vaulot *et al*. 1994). While studies such as that of Vaulot *et al.* (1994) have found 19'-hex and 19'-but to be diagnostic pigments for *Phaeocystis* sp., their low concentrations here do not counter the possible importance of *Phaeocystis* since there are known to be many strains with different pigment compositions, and Stuart *et al.* (2000) found both 19'-hex and 19'-but to be absent from North Atlantic *Phaeocystis* blooms, whereas concentrations of chl-*c3* were high. Alternatively, the biomass linked to the high concentrations of fucoxanthin may be due to small diatoms. In each case, the absorption-based approach identifies these cells as nanophytoplankton sized, while the Bricaud *et al.* 2004 method assigns a MESD in the microphytoplankton range.

3.5.5 Relationships between MESD, season and ecological strategies

As seen in Fig 3.6, there is a significant relationship between cell size and total chlorophyll concentration, agreeing with the strong links identified between increasing cell size and biomass (Yentsch & Phinney 1989, Chisholm 1992, Gibb *et al.* 2000). High concentrations of chl-*a* are associated with an abundant supply of nutrients (Kiørboe 1993), which in turn favours large cells such as diatoms due to their high growth rates (Furnas 1990) since efficient nutrient uptake and use is not required. Large cells will also result in higher chl-*a* concentrations due to the package effect. Self-shading within phytoplankton cells leads to a requirement for higher intracellular chlorophyll concentrations in large cells to harvest the same amount of light than in small cells (Chisholm 1992), strengthening the positive correlation between chl-*a* concentration and MESD.

Seasonality is also strongly linked to trends in MESD, with the highest values found in spring for both methods of estimating MESD (Fig 3.7). While knowing how MESD varies

with time may be of use to those studying downstream processes such as the population dynamics of zooplankton, the focus here is on the underlying selective pressures, which are mainly dictated by nutrient availability, turbulence and light (Estrada & Berdalet 1997).

3.5.5a Competitive advantages to having a large MESD

When the degree of stratification is low, such as after deep winter mixing, the supply of nutrients to the surface waters is high, favouring large celled *r*-strategists such as diatoms, owing to their high growth rates (Furnas 1990) (Fig 3.6). In the North West Atlantic, this corresponds to the early spring, and to a lesser extent, late autumn (Fig 3.7). Under conditions of rapid growth, diatoms have a competitive advantage due to their silicate frustules requiring far less energy to synthesise than an equivalent organic cell wall (Raven 1982), and their ability to tolerate fluctuating conditions by using internal reserves of nutrients (Lomas & Glibert 2001). The dominance of large cells under unstratified, cold, nutrient-replete conditions is seen from field observations (Barlow *et al*. 1993), from bottom-up physiological modelling (Irwin *et al.* 2006), and from remote-sensing ocean-colour studies (Dandonneau *et al*. 2004). The high nutrient flux caused by weak or absent water-column stratification means that competitive disadvantages due the less efficient uptake of nutrients caused by the low surface-area-to-volume ratio of large cells are negated.

3.5.5b Competitive advantages to having a small MESD

Conversely, when waters are warm and highly stratified, nutrient availability is low, favouring small, *K*-strategists (Kiørboe 1993, Raven 1998). In this study such conditions correspond with summer (Julian day 175 to 300; Figs 3.7, 3.8). To use nutrients directly to explain the dynamics in phytoplankton cell size, knowledge of the long-term nutrient fluxes would be required instead of discrete measurements of concentration at a single time. Due to a time lag

of several days in the phytoplankton response to nutrient supply (Omand *et al.* 2011), it is difficult to use point measurements of nutrient concentration to distinguish between a population which has been subjected to nutrient stress over a period of several weeks and one which has recently been nutrient replete and still contains sufficient internal reserves despite low concentrations in the water-column (Barlow *et al.* 1993). In addition to influencing nutrient supply, water-column turbulence also affects phytoplankton populations via losses due to sinking. In a frequently mixed system, sinking cells can be returned to the surface waters, while in a stratified system such cells would be lost permanently, further increasing the benefits of slowly sinking small cells in stratified conditions.

3.5.5c Size and sinking

Cell sinking rate is dependent on cell size (Jiang *et al.* 2005). However in well-mixed environments, rapid sinking rate is not a major disadvantage (Sciascia *et al.* 2012). Upon the onset of stratification, the rate of growth must be greater than the rate of sinking for a population to be sustained (Reynolds 1994) favouring small, slowly sinking cells, or motile species, such as dinoflagellates. This is seen in Fig 3.7, with the very small cells of clusters 3 and 4 along with the peridinin-dominated cluster 8 coming to dominate from day 150 onwards.

3.5.5d Size and predation

Sinking is not the only cause of phytoplankton loss however, with predation also having a major impact. Calbet & Landry (2004) estimated that zooplankton grazing removes over 60% of daily phytoplankton primary production in temperate open-ocean regions. Indeed, at the peak of the spring bloom, predation rates can equal or indeed exceed the maximum theoretical reproductive rate of phytoplankton (Kiørboe 1993). In contrast with nutrient acquisition and

losses due to sinking, large cell size is a competitive advantage when considering the effect of zooplankton grazing (Geider & Osborne 1986, Kiørboe 1993). A wide range of sizes are seen in herbivorous zooplankton, each with relatively specific target sizes (Fenchel 1988), so that small phytoplankton cells are not consumed by large zooplankton and small zooplankton are unable to consume large phytoplankton due to gape limitation. Platt (1985), however, demonstrated that there is a negative slope to the size distribution of individuals within the pelagic environment. Since phytoplankton cells must be smaller than the herbivore that wishes to consume it, the predation pressure decreases as cell size increases. Cell size also affects the growth rate of both phytoplankton and zooplankton, with zooplankton displaying a size-dependent exponential scaling factor for growth of -0.23 (Hansen 1997). Phytoplankton are also affected by this principle, but it would appear to a lesser degree, with Sommer (1989) reporting an exponent of only -0.14 and Finkel *et al.* (2010) reporting an even lower size-dependence at -0.06. The differences in size-specific growth rate between predator and prey further increase the protective advantage of large cell size, and this helps to explain the large MESD observed in spring.

3.5.6 Stratification and patterns in succession

While relationships seen between mean phytoplankton size and both biomass and season (Figs 3.6, 3.7) provide useful insights, a greater understanding of the ecological processes involved can be gained by considering different phytoplankton populations separately and the varying environmental drivers that act on them. Using cluster analysis, seasonal trends in succession can be seen with even greater clarity than using size alone. Unlike pigment-based approaches to taxonomy, such as those of Uitz *et al.* (2008) or Bidigare & Ondrusek (1996), it is important to note that this method makes no attempt to pre-define biological relationships or likely pigment associations, and instead simply identifies samples with similar pigment

compositions. While evidence of successional patterns is seen between clusters in Fig 3.7, the number of samples in each cluster (Fig 3.8), combined with the size and pigment composition of each cluster (Fig 3.3, Table 3.2, Table 3.3), makes patterns of phytoplankton succession far clearer.

Although this study focusses on successional trends in the North West Atlantic Shelves Province (Longhurst *et al*. 1995), previous studies such as Buma *et al.* (1992) (Weddell-Scotia confluence), Dandonneau & Niang (2007) (North Atlantic and tropical Pacific) and Bouman *et al.* (2012) (Eastern Pacific Subantarctic) have used cluster analysis on biomass-normalised pigment concentrations to identify seasonal and spatial trends in phytoplankton distribution. Cluster analysis has shown different patterns in phytoplankton distribution according to province and its associated physiochemical characteristics (Buma *et al.* 1992, Bouman *et al.* 2012) and hence combining different areas, may mask trends. Due to the interplay between latitude and seasonality, trends in both abiotic forcing factors and phytoplankton distributions may be seen later in the year at higher latitudes (Buma *et al.* 1992).

Successional patterns are further emphasised by considering how water-column stratification varies throughout the year (Fig 3.8c). One of the most important factors controlling abiotic conditions and the niches available to phytoplankton is the extent of water-column stratification. Margalef (1978) proposed a mandala to divide phytoplankton groups according to the levels of turbulence and nutrient availability, and more recent studies such as Buma *et al.* (1992), Li (2002) and Bouman *et al.* (2003, 2011) have confirmed the importance of temperature and water-column stability for determining phytoplankton community structure. Such changes have major implications for the rate of export of carbon fixed. Where populations are dominated by small pico- and nanophytoplankton, the low rate of sinking and tight coupling between phytoplankton and grazer populations means that the flux of carbon to deep waters is far lower than in upwelling or well mixed systems dominated by

microphytoplankton (Cermeño *et al.* 2006). Changes in the dominant phytoplankton size-class and to the phenology of the successional patterns will have both short- and long-term implications for the carbon flux, with studies such as Platt *et al.* (2003) and Genner *et al.* (2010) identifying the tight links between the seasonality of phytoplankton blooms and fish larval recruitment. It has been reported that already changes in phytoplankton phenology and increased water temperature as a result of recent climate change might be compromising cod larval survival rates (Beaugrand *et al.* 2003). In addition to seasonal changes in recruitment and distribution of fish populations, climate change will also act on a longer time scale. Bown (2005) reports that during warm periods of the Mesozoic, small *K*-selected nanoflagellates predominated, while diatoms were favoured following the Eocene cooling. Since the export characteristics of phytoplankton populations are tightly linked to size and community structure (Legendre & Rassoulzadegan 1996), an equivalent shift in dominant species as a result of climate change would therefore decrease the ability of the oceans to sequester carbon, and potentially accelerate the rise of global atmospheric CO_2 concentrations (Hoegh-Guldberg *et al.* 2010).

3.5.7 Succession and ecological properties of clusters

The successional trends seen are consistent with previous studies of the North Atlantic system (Barlow *et al*. 1993, Lochte *et al.* 1993, Li 2002, Bouman *et al.* 2003) with MESD being large during the spring, when stratification is absent, and associated with high concentrations of fucoxanthin, predominantly from clusters 2 and 6, implying diatom dominance. The importance of fucoxanthin in phytoplankton clusters identified in the North Atlantic in spring confirms the trends seen in Dandonneau & Niang (2007). Clusters 2 and 6 appear almost identical in terms of size, with the only visible difference being the far greater concentration of β-carotene found in cluster 6. Given the important role β-carotene plays in photoprotection

(Llewellyn *et al.* 2005) it seems surprising that mean mixed-layer PAR is higher for cluster 2 than 6, although Dimier *et al*. (2007) found an almost three-fold range in chlorophyll-normalised β-carotene concentrations between different diatom species grown at the same irradiance.

For the three fucoxanthin-dominated clusters, while cluster 1 has a lower MESD and is of greater importance later in the year than clusters 2 or 6, no difference is seen in the relationship to stratification. This decrease in MESD fits with the successional trends identified by Margalef (1978), Barlow *et al.* (1993), Lochte *et al.* (1993), Savidge *et al.* (1995), Irigoien *et al.* (2004) and Llewellyn *et al*. (2005). Such a decrease in MESD could be due to the increased importance of small diatoms, such as *Nanoneis hasleae,* which Savidge *et al.* (1995) found important following the initial spring bloom in the North East Atlantic. Alternatively, it could be as a result of the replacement of diatoms by *Phaeocycstis*, a trend which would be predicted by the seasonal succession described by Wassmann *et al.* (2005), where *Phaeocystis* blooms follow those of diatoms as silicate becomes depleted, with further evidence provided by the high levels of chl-*c3* seen in cluster 1 (Stuart *et al.* 2000). By Julian day 150 in addition to the increased presence of cluster 1, the large-celled fucoxanthin-dominated clusters 2 and 6 have been replaced by clusters 3 and 4, with cell size decreasing. This succession also fits with the results of cluster analysis reported for the Southern Ocean by Buma *et al.* (1992), where diatoms decreased in abundance as water-column stability increased while the proportion of nanophytoplankton increased.

Clusters 3 and 4 appear dominated by small eukaryotes, as suggested by the high levels of 19'-hex and 19'-but, and form the greatest proportion of the total biomass under highly stratified conditions. The presence of peridinin in cluster 4 suggests the replacement of non-motile diatoms with dinoflagellates capable of regulating their position in the water-column (Margalef 1978).

The next important successional event comes at around Julian day 275 with the sudden appearance of clusters 5 and 7 fitting with the remotely-sensed trends seen by Dandonneau *et al*. (2004) and Demarcq *et al*. (2012) who report increases in average surface chl-*a*, from which they infer an increase in mean cell size, as larger eukaryotic groups experience a second, smaller bloom, and the autumnal decline in prokaryotic phytoplankton (Olson *et al*. 1990). The presence of 19'-hex, 19'-but, chl-*b,* and alloxanthin suggests that this bloom is a result of a mixture of nano- and picophytoplankton species, such as prasinophytes, chlorophytes, and chrysophytes. While clusters 5 and 7 appear at the same time, their relative importance appears to depend on the degree of stratification, with cluster 7 thriving under more highly-stratified conditions than cluster 5. Since the autumnal mixing is not as intense as in spring, the more taxonomically-mixed populations reflect the link between intermediate disturbance and diversity reported by Li (2002). By Julian day 325, this small bloom is no longer present and the population appears to be an even mix of all groups apart from the two large-celled diatom clusters.

When trying to understand the phytoplankton dynamics of the North West Atlantic, it is important to also examine the non-bloom-forming taxa that comprise the ambient background biomass (Barber & Hiscock 2006). Cluster 8 appears to remain at fairly constant proportions throughout the seasonal cycle, with high concentrations of alloxanthin, and even higher levels of peridinin, unlike the trends seen in Dandonneau & Niang (2007) where peridinin was associated with the spring cluster and only present at low concentrations during the summer. The persistence of cluster 8 throughout the year supports the idea that the majority of changes in phytoplankton species distribution can be considered as the addition of certain groups to a background phytoplankton population (Yentsch & Phinney 1989, Sieracki *et al*. 1993, Li 2002, Barber & Hiscock 2006).

3.5.8 Trends in α^B and φ_m with respect mean daily mixed-layer PAR

Knowing the groups present in a system and their size distributions however only describes part of the ecological dynamics, since phytoplankton groups can be very diverse in their physiological characteristics, in particular in their light-harvesting, absorptive and photoprotective properties. Given that the production of light-harvesting pigments is energetically costly for phytoplankton (Raven 1984, Geider *et al.* 1996), cells that are subjected to higher irradiances would be expected to invest less energy in the synthesis of light-harvesting pigments, and have lower values of α^B. Significant negative relationships between mean daily PAR in the mixed layer and the light-limited rate of photosynthesis are seen for clusters 1, 4, 7 and 8 (Fig 3.9a), suggesting that selection with respect to light-harvesting is acting on these populations. Clusters 2, 3, 5 and 6, however, show no such response. The mean values for α^B in those clusters which do not show a relationship with mean daily mixed-layer PAR are all lower than those for clusters 1,4,7 and 8 which do show a relationship (Fig 3.3). The same pattern is seen for φ_m, with again clusters 1, 4, 7 and 8 displaying negative relationships between φ_m and light intensity, and clusters 2, 3, 5 and 6 showing no such relationship (Fig 3.9b).

Negative relationships between φ_m and mean daily mixed-layer PAR may be caused by an increase in the concentration of photoprotective pigments (Wilk-Woźniak *et al.* 2002, Babin *et al.* 1996). Since light absorbed by photoprotective pigments is dissipated as heat, the energy cannot be used for carbon fixation, and so cannot contribute towards the observed φ_m. Alternatively the relationships may be as a result of a reduction of functional photosynthetic reaction centres due to photoinhibition (Long *et al*. 1994), or as a result of nutrient stress (Babin *et al*. 1996). Given that clusters 2 and 3, neither of which shows light-dependent relationships in φ_m, are found in areas with high daily averaged irradiances over the mixed-layer (Fig 3.3), nutrient limitation would appear the more likely explanation for these clusters.

3.5.9 Cluster specific trends in *PE* parameters and absorption

When trying to compare trends between clusters, variability within the data can result in difficulties in differentiating between relationships using mean values. Instead a comparison of the slope of the relationship between a non-biomass-normalised variable and chl-*a* concentration can be used, as in Côté & Platt (1983). To consider how the different clusters use light, the regressions against chl-*a* are considered for the non-biomass normalised absorption by phytoplankton between 400 and 700 nm ($\bar{a}_{ph}$), α, and P_m in Fig 3.10. Diatom-dominated clusters 2 and 6 have the largest MESD, and this is reflected in the shallow slopes seen in the relationship between $\bar{a}_{ph}$ and total chl-*a*. The low values of $\bar{a}_{ph}$ as a function of biomass are further decreased since these groups are found in highly turbulent and non-stratified conditions, meaning that photoprotective pigments which would otherwise increase $\bar{a}_{ph}$ are absent. Since α is a function of $\bar{a}_{ph}$ and φ_m, the shallow slope of the relationship between $\bar{a}_{ph}$ and biomass means the slope of the relationship between α and chl-*a* is also low. Conversely the gradient of the relationship between $\bar{a}_{ph}$ and total chl-*a* is very steep for clusters 3, 4 and 8 (Fig 3.10). Clusters 3 and 4 have very small MESD as estimated using either pigments or absorption at 676 nm, with further evidence that cluster 4 is dominated by very small cells, indicated by the high concentrations of divinyl chlorophyll-*a* suggesting the presence of *Prochlorococcus*. Due to the low package effect, small cell size will result in a high $\bar{a}_{ph}$ as a function of biomass. Clusters 3 and 4 also have high levels of photoprotective pigments including zeaxanthin, which will further steepen the gradient of the relationship between $\bar{a}_{ph}$ and total chl-*a*.

The shallowest slope on the relationship between α and chl-*a* is seen for cluster 5, which may seem surprising given the low mean localised levels of PAR and the presence of high concentrations of pigments indicative of nanophytoplankton, a size-class which generally

displays high photosynthetic efficiencies (Fig 3.10). This result may be due to the positive offset on the y axis seen for this cluster which will greatly decrease the slope of the relationship. A comparison of mean values for α^B between clusters (Fig 3) reveals that the average for cluster 5 is in fact lower only than that for cluster 7.

The steepest gradients on the relationship between α and chl-*a* are seen for clusters 3 and 7 (Fig 3.10). The MESD of both these clusters is low when estimated using either pigments or absorption, and they both contain high levels of 19'-hex and 19'-but. These pigments are associated with nanophytoplankton, which are known to have high values of α^B (Bouman *et al.* 2005). In the case of cluster 3, this trend would appear to be driven by the very steep regression between $\bar{a}_{ph}$ and total chl-*a*, while in the case of cluster 7 the steep gradient of the relationship between α and chl-*a* is due to the high values of φ_m this cluster displays (Fig 3.3). Such efficiency is likely to be due to the strongly stratified conditions for both these clusters, meaning that light-harvesting can be optimised for maximal efficiency as cells are well acclimated to a relatively stable light environment.

Cluster 7 also shows the steepest relationship between P_m and chl-*a*, due to the high temperature of these samples (Fig 3.10). Due to the kinetics of enzyme-catalysed reactions an increase in temperature will result in an increase in the rate of carbon fixed by Rubisco and hence increased values of P_m (Davison 2004). Clusters 3 and 4 have an even higher mean temperature, however these are associated with highly-stratified conditions during the summer months, where nutrient availability is low (Dandonneau *et al*. 2004), hence the gradient between P_m and chl-*a* is more shallow. Conversely clusters 1, 2 and 6 are associated with low temperatures and as a result have very shallow relationships between P_m and chl-*a*. The correlation between P_m and chl-*a* has a shallow gradient for cluster 5 which reflects the low mean values of climatological PAR for this group, which would promote very high intracellular chlorophyll concentrations are required in order for the reaction centres to be

saturated (Dubinsky & Stambler 2009).

3.5.10 Size and maximal quantum yield

While the efficiency of light absorption by phytoplankton decreases as MESD increases, the opposite trend is seen with respect to φ_m, with all clusters apart from cluster 5 displaying positive relationships between φ_m and size (Fig 3.11 This is in contrast to the trends predicted by Geider & Osborne (1986) where φ_m was deemed not to vary according to light regime, or species. Similarly Finkel (2001) further suggests that φ_m is independent of cell size and finds the quantum yield of photosynthesis (φ_p) to decrease as cell size increases, although admits that this may be due to an artefact of experimental design. Other studies however such as that of Ignatiades *et al.* (2002), have also reported decreases in φ_m as cell size increases. The results seen here could be a consequence of greater investment by phytoplankton in the efficiency of photosynthesis as size increases, to compensate for the decreased efficiency of light-harvesting. Alternatively it could be as a result of the trend for large values of MESD to be associated with high nutrient concentrations, a factor known to increase φ_m (Babin *et al.* 1996).

3.6 Conclusions

Using a dataset of HPLC phytoplankton pigments and absorption predominantly from the North West Atlantic, important trends in phytoplankton distribution and succession were identified and two methods of estimating phytoplankton MESD could be compared. A significant correlation was seen between the estimates of the MESD of phytoplankton as estimated by the HPLC pigment-based approach of Bricaud *et al.* (2004) and the absorption-based method of Roy *et al.* (2011). The overall size spectrum produced by the absorption-based approach was closer to that seen in previous studies of the North Atlantic, whereas the pigment-based method led to an abrupt peak in MESD at 50µm. High values of MESD were associated with high chl-*a* concentrations, and a highly mixed water-column, as found in early spring, while smaller cells are found during the summer period, when the water-column was strongly stratified.

Cluster analysis on chlorophyll-a-normalised accessory pigment concentrations revealed 8 distinct populations of phytoplankton with succession between the clusters dictated by seasonality and stratification. Fucoxanthin-dominated clusters, indicating the presence of diatoms, dominated in spring when turbulence was high. As stratification increased, the MESD decreased, indicating the presence of photosynthetic picophytoplankton, while in autumn, the strength of stratification decreased, and nanoflagellates increased in importance.

In addition to differences in pigment concentrations between the clusters, trends in light-harvesting properties are also seen. Clusters where stratification is high display a strong negative relationship between φ_m and climatological mixed-layer PAR, while those from turbulent systems show no relationship, while for all apart from one cluster a significant relationship between MESD and φ_m was seen, reflecting greater quantum efficiency as the

efficiency of light absorption decreased due to self-shading. Differences in the slope of the relationship between key photophysiological variables and chl-*a* biomass were found according to phytoplankton cluster. Clusters where stratification is weak and MESD large were less efficient at harvesting and using light, corresponding to shallow gradients on the relationship between $\bar{a}_{ph}$ and total chl-*a*, between α and chl-*a* and between P_m and chl-*a*, than those from highly stratified areas with low values of MESD, reflecting the gains in efficiency possible for species adapted to a static environment as opposed to one characterised by regular disturbance.

Reliable means of estimating phytoplankton size are highly relevant to studies of phytoplankton ecology or biogeography due to impact changes in phytoplankton population structure has on the range of trophic interactions supported, with both the pigments- and the absorption-based methods of calculating MESD having a wide range of potential applications. HPLC measurements of phytoplankton accessory pigment concentrations are routinely made, while there is the potential for the absorption-based approach to be applied to remotely-sensed ocean colour data. Given the importance of models of phytoplankton primary production to estimating global fluxes of carbon, particularly when predicting responses to a warming ocean, refinements to techniques for estimating phytoplankton size are essential to improve both estimates of net phytoplankton production, and of that export.

3.7 Appendix: Calculating mean equivalent spherical diameter from phytoplankton absorption at 676nm

3.7.1 Calculating the package effect

When phytoplankton are approximated to homogeneous spheres (Duysens 1956, Morel & Bricaud 1981) the absorption characteristics of the cell can be shown to be a function of ρ, which is a product of the intracellular absorption coefficient of the pigments inside the cell (a_{cm}) at a particular wavelength and the cell diameter (d):

$$\rho = d \; a_{cm} \tag{1}$$

The quantity a_{cm} can in turn be expressed as a product of the specific absorption coefficient of the absorbing pigments inside the cell at the same wavelength (a^*_{cm}) and the intracellular concentration of these pigments (p_i).

$$a^*_{cm} = a_{cm} / p_i \tag{2}$$

Since absorption due to pigments other than chl-*a* is minimal at 676 nm, this wavelength is preferred to examine the effect of pigment packaging. For the absorbing material of N cells in solution, Sathyendranath *et al.* (1987) state the absorption coefficient would be:

$$a_{sol} = \frac{\pi}{4} d^3 N a_{cm} \tag{3}$$

Following Duysens (1956), ρ can also be used to describe the dimensionless absorption

efficiency of a cell (Q_a), which is defined as the ratio between the light absorbed by a cell and the light incident on it:

$$Q_a(\rho) = 1 + \frac{2\exp(-\rho)}{\rho} + \frac{\exp(-\rho)\text{-}1}{\rho^2} \quad . \tag{4}$$

The absorption coefficient a_{ph} of a suspension of N particles in the same medium is given by:

$$a_{ph} = \frac{4}{\pi} d^2 N Q_a(\rho), \tag{5}$$

where $\frac{4}{\pi} d^2$ is the cross-sectional area of a cell. From equations 3 and 5, it can be seen that the absorption coefficient of a pigment dissolved in a medium (a_{sol}) is greater than the absorption coefficient of the same pigment packaged in the form of discrete particles. This ratio defines the flattening effect (F).

$$F(\rho) = \frac{a_{ph}}{a_{sol}} = \frac{3Q_a(\rho)}{2\rho} \tag{6}$$

The specific absorption coefficient (a^*_{ph}) of intact phytoplankton cells in water can therefore be written as:

$$a^*_{ph}(\rho) = a^*_{cm} F(\rho) = \frac{3a^*_{cm}Q_a(\rho)}{2\rho}. \tag{7}$$

In the method of Roy *et al.* (2010), size is estimated from the ratio of absorption by phytoplankton to the absorption by the same concentration of pigments in a hypothetical

solution at 676 nm, where all absorption by phytoplankton pigments is as a result of chl-*a*. Therefore a^*_{ph} can be rewritten as $\rho = d \times a_{pi}$ where *pi* is the intracellular pigment concentration of chl-*a*. This leads to:

$$a^*_{ph}(\rho) = a^*_{pi} F(\rho) = \frac{3a^*_{ci}Q_a(\rho_c)}{2\rho} \quad (8)$$

Whereas the *in-vivo* chlorophyll-specific absorption coefficient a^*p_i contains information about cell size, before *d* can be obtained, the intracellular chlorophyll concentration p_i needs to be found. Based on Marañon *et al*. (2007), Roy et al. (2010) expressed p_i as a function of diameter:

$$p_i = c_0 d^{-m} \quad (9)$$

where c_0 is the proportionality constant and *m* the size scaling exponent. Roy *et al*. (2011) used intracellular chlorophyll concentrations from Marañon *et al*. (2007) to calculate that $m = 0.06$, and $p_i = 1.68 \times 10^6$. From equation 8,

$$a^*_{ph}(\rho) = a^*_{pi} F(\rho) = \frac{3a^*_{ci}Q_a(\rho_c)}{2\rho} \quad (10)$$

and

$$a^*_{ph}(\rho_c) = a^*_{pi} F(\rho_c) = \frac{3a^*_{ci}Q_a(\rho_c)}{2\rho_c} \quad . \quad (11)$$

Since:

$$Q^*_c = \frac{3Qa}{2\rho} = \frac{a^*_{ph}}{a^*_{pi}}, \quad (12)$$

using measured values of a^*_{ph} and a^*_{pi}, d can be calculated. Roy *et al*. (2011) used a Newton-Raphson scheme to solve for *d*. Here a lookup table was created to generate corresponding values of ρ for d ranging from 0 to 500 μm, to enable approximate values for d to be calculated for given values of a^*_{ph} and a^*_{pi}. As cells with $d = 0$ are clearly not possible, where $Q^*_c \geq 1$, d was set to 0.1 μm (Cheung *et al.* unpublished).

3.7.2 Correcting for values of Q^*_c greater than 1

Using $a^*_{pi}(676) = 0.0199$ for $a^*_{cm}(676)$ (Bidigare *et al*. 1990), large numbers of samples were found to have values of $Q^*_c \geq 1$, implying that as with Nelson *et al*. (1993), Bissett *et al*. (1997) and Bricaud *et al*. (2004), either other material apart from chl-*a* is contributing significantly to absorption by phytoplankton yet which cannot be measured using HPLC, or the absorption by chlorophyll is being modified by protein associations within the cell. Bricaud *et al*. (2004) explicitly calculated this missing term by analysing samples extracted in methanol both spectrophotometrically and using HPLC, but in the absence of such data, this approach was not possible. Instead the correct value for $a^*_{cm}(676)$ was back calculated by setting the 95% quantile of Q^*_c to 1, leading to a value for $a^*_{cm}(676)$ of 0.0584.

Chapter 4: Assessment of the environmental controls of phytoplankton photosynthesis in different size-classes

4.1 Abstract

Phytoplankton productivity represents the efficiency of carbon uptake and is determined by the species present and the integrated growth environment: a combination of light, nutrients and temperature. Here the largest ever database of *in-situ* photosynthesis-irradiance (*PE*) measurements is used to compare two different approaches to ascribing phytoplankton size-class using HPLC pigment data, before identifying how class-specific trends in *PE* parameters relate to abiotic forcing. The methods of Uitz *et al.* (2008) and Sathyendranath *et al.* (2009) were used to ascribe the size-classes based on diagnostic pigments. Uitz *et al.* (2008) was more suited to apportioning biomass in mixed populations, whereas Sathyendranath *et al.* (2009) identified samples principally dominated by one group and was therefore better for assessing class-specific trends in phytoplankton assemblages. For the Uitz *et al.* (2008) method, samples classified as either picophytoplankton or microphytoplankton occurred over a much wider temperature range than with the Sathyendranath *et al.* (2009) method. As in previous studies a strong relationship between the photosynthetic parameters (maximum photosynthetic rate (P_m^B) and the light-limited photosynthetic rate (α^B)) and temperature was found, but weaker relationships with

nutrients and mean daily mixed layer irradiance. This study describes an "envelope" approach to identifying trends in phytoplankton photosynthetic parameters where quantile plots on the large dataset are used to assess relationships with respect to temperature under 'optimal' conditions. Within-class relationships reveal that the size of the dominant phytoplankton group decreases as temperature increases: microphytoplankton dominate in cold to temperate environments (below 7.5 ^{o}C), nanophytoplankton from 7.5 ^{o}C to 17.5 ^{o}C and picophytoplankton from 17.5 ^{o}C to the maximum temperature in this study of 26.3 ^{o}C. P_m^B for both nanophytoplankton and microphytoplankton is strongly and positively correlated with temperature, whereas picophytoplankton display the opposite pattern. Using the Sathyendranath *et al.* (2009) approach of estimating phytoplankton size class, microphytoplankton P_m^B ranged from 0.33 to 9.33 mg C (mg chl-*a*)$^{-1}$ h^{-1} , with a mean of 2.3, and α^B from 0.004 to 0.057 mg C (mg chl)$^{-1}$ h^{-1} (μmol photons m^{-2}s^{-1})$^{-1}$, with a mean of 0.017, nanophytoplankton P_m^B from 1.12 to 8.4, with a mean of 4.15 and α^B from 0.018 to 0.75, with a mean of 0.043 and picophytoplankton P_m^B ranged from 0.67 to 8.4 with a mean of 4.1 while α^B ranged from 0.0029 to 0.083 with a mean of 0.021. Principle component analysis (PCA) was used to assess the main abiotic factors governing variability in the photosynthetic parameters of the different size-groups. Microphytoplankton were found to dominate in areas of high turbulence, nutrient availability and chlorophyll-*a* concentration, whereas nano- and picophytoplankton were more abundant under stable stratified conditions. The proportion of the biomass due to picophytoplankton was found to be most closely linked with high temperatures and irradiances, and the proportion of the biomass due to nanophytoplankton with high values of P_m^B and α^B.

4.2 Introduction

4.2.1 The importance of phytoplankton photophysiology

Phytoplankton are responsible for more than 98.5% of marine carbon fixation (Middleburg 2011), so an understanding of their dynamics and the processes by which they are governed is a key aspect when assessing marine ecosystems and biogeochemical cycles. With increasing interest in predicting future effects of climate change, there has been a concerted effort to understand how large-scale trends in phytoplankton photosynthesis vary according to environmental conditions, which influence carbon draw-down and capture in the oceans (Le Quéré *et al.* 2005). *In-situ* observations of the physiological status of phytoplankton from ^{14}C-uptake experiments, however, only provide a snapshot of photosynthesis in the marine environment (Behrenfeld & Falkowski 1997b).

Ocean-colour remote-sensing is increasingly being used to provide synoptic information on both phytoplankton biomass and abiotic forcing factors such as temperature and irradiance (Joint *et al.* 2000). To date, a range of models have been developed to estimate primary production from space (e.g. Platt *et al.,* 1988; Platt *et al.,* 1995, Antoine & Morel 1996, Behrenfeld & Falkowski 1997a, Behrenfeld *et al.* 2005, Smyth *et al*. 2005, Uitz 2008, Westberry *et al.* 2008). Here the factors responsible for the variability seen in phytoplankton photosynthesis are considered and group-specific relationships between temperature and photosynthetic rates identified which could be used in conjunction with remote-sensing models to estimate primary production in different phytoplankton size-classes. To do this requires information on the photosynthetic biomass present, the underwater light field and the photosynthetic response of phytoplankton to light. Surface phytoplankton biomass in the form of chlorophyll-*a* (chl-*a*) concentration and surface irradiance can both be measured, either *in-*

situ or by remote-sensing. Since the total absorption of light in the water-column co-varies with the chlorophyll concentration, the attenuation of photosynthetically active radiation (PAR) with depth can be calculated from surface values and estimated biomass profiles (Platt & Sathyendranath 1988, Uitz *et al.* 2006). The only information for the estimation of primary production which cannot be derived from remote-sensing observables is the photosynthetic response of phytoplankton, hence the need for a greater understanding of the processes by which it is controlled.

4.2.2 The effect of temperature and nutrient availability on phytoplankton primary production

The photosynthetic response of phytoplankton to available light may be described using two parameters; the light-limited photosynthetic rate (α^B) and the maximal photosynthetic rate (P_m^B), both of which are normalised to chl-*a* biomass and are, known together as the *PE* (photosynthesis-irradiance) parameters. To estimate primary productivity on basin scales, it is necessary to have a large-scale understanding of how these parameters vary, as opposed to just point measurements. Extrapolation over space and season based on biogeography is instructive (Longhurst *et al.*1995, Sathyendranath *et al.* 1995), but a more predictive approach is required as even if remote-sensing is used to assign dynamic boundaries to biogeographical provinces, assigning uniform properties to entire regions cannot account for the spatial and temporal variability seen in a dynamic ocean. A key controlling factor, which like chl-*a* concentration can be observed via remote-sensing, is temperature (Antoine & Morel 1996, Behrenfeld & Falkowski 1997a, Uitz *et al.* 2008, Bouman *et al.* 2005). While studies such as that of Eppley (1972) have demonstrated that temperature can on its own have a major effect on phytoplankton growth rate, it must be noted that in nature many other variables such as light and nutrient availability co-vary with temperature (Bouman e*t al.* 2005). Temperature

can be used as a proxy for nutrient availability since as the surface waters are warmed, they become less dense, preventing mixing with deeper waters and so become nutrient depleted (see Chapter 3 for further details). Bouman *et al.* (2003) found that 65% of the variation in P_m^B for the Scotian Shelf could be described by temperature alone. Below 20 ^oC, increasing temperature results in an increase in P_m^B due to linear reaction kinetics (Raven & Geider 1988). At temperatures above 20 ^oC however, which are associated with high irradiance and stratified oligotrophic conditions, photosynthesis becomes restricted since increased investment in photoprotection and the repair of photodamage is energetically costly (Raven 2011), and nutrient availability limiting. While the intensity of light that phytoplankton experience has a major effect on the gross photosynthetic rate, approaches such as that of Platt & Sathyendranath (1988), or Uitz *et al.* (2006) which link surface chlorophyll concentrations to biomass profiles mean that it is possible to obtain reliable climatological estimates of irradiance at depth. Photoacclimatory status will also have an effect on phytoplankton P_m^B. Since maximum photosynthetic rate is normalised to the concentration of chl-*a*, higher intracellular concentrations of chl-*a* will result in lower values of P_m^B than for a population with the same gross photosynthetic rate, but having a lower intracellular concentration of chl-*a* (Geider *et al.* 1997).

The effect of temperature on growth and photosynthetic rates has been extensively studied in cultures (Eppley 1972, Raven & Geider 1988). These studies have shown species to be acclimated to a narrow temperature band with sharp decreases in rate either side of this optimum (Eppley 1972). The value of culture-based studies to examine temperature-dependent changes in microalgal physiology is limited since in nature sub-optimal conditions for one species result in its replacement by another. In addition to temperature, nutrient supply also has a strong impact on controlling both the type of phytoplankton assemblage and the photosynthetic efficiency. Under nutrient-limited conditions, phytoplankton species capable of

efficient nutrient uptake are selected for, and under very heavily oligotrophic conditions P_m^B will be limited for all species (Geider *et al.* 1997). Unfortunately, nutrient availability within the surface ocean is not directly accessible via remote-sensing. While attempts have been made to model nutrient distribution using season-specific relationships between sea surface temperature and nitrate concentration, which can then be used to obtain an estimate of the phytoplankton groups present (Kamykowski & Zentara 2003), such approaches require large datasets to validate and are applicable only for a single ecological province. Overall variability in biomass normalised photosynthetic rates may be accounted for by differences in taxonomic structure, modified by temperature, nutrients and light.

4.2.3 The importance of phytoplankton size and taxa

Just as temperature can be thought of as an important environmental variable accessible via remote-sensing for predicting phytoplankton photophysiology, cell size is considered to be a useful indicator of the physiological and ecological functioning of phytoplankton. Phytoplankton display a greater than 1000-fold difference in cell volume from the smallest cyanobacterium to the largest diatom (with equivalent spherical diameters of ~0.6 to >1000 μm (Jiang *et al.* 2005)), which has important implications for nutrient uptake (Sournia 1982), and light absorption (Duysens 1956, Friebele *et al.* 1978, Morel & Bricaud 1981). Physiological differences due to size or taxonomic group are reflected in variation in photophysiology and rates of carbon fixation (Tilstone *et al.* 1999, Bouman *et al.* 2005, Uitz *et al.* 2010). By determining the responses to abiotic forcing of phytoplankton of different size-classes it will be possible to predict not only the amount of carbon fixed, but also its fate (Geider *et al.* 1998). For example, large cells such as diatoms sink rapidly and result in carbon and nutrients being removed from the photic zone to depth (Riegman *et al.* 1993), whereas smaller cells such as cyanobacteria and other picophytoplankton sink slowly and they are

efficiently remineralised via the microbial loop, meaning net export is greatly reduced (Legendre & Rassoulzadegan 1995).

4.2.4 Methods of identifying phytoplankton groups

In order to ascribe photophysiological parameters by size-class (i.e. P_m^B and α^B), such as estimated by Uitz *et al.* 2008, *in-situ* measurements are required of *PE* data along with information on the taxonomic or functional groups of phytoplankton present. There are a range of methods that can be used to determine the dominant phytoplankton groups within a sample. Direct cell counts allow for very precise identification of some species. These are problematic however, being exceedingly time consuming and expensive to carry out, and cannot account for the entire phytoplankton community (Claustre 1994). Flow cytometry allows greater throughput, but is limited by an inability to detect larger cells, or distinguish algal classes, as opposed to just optically-distinct groups (see Chapter 2 for further details).

By using high pressure liquid chromatography (HPLC) the pigment composition of samples can be accurately and rapidly measured. Since different taxonomic groups contain different pigment concentrations, this can be used to estimate the taxonomic make up of a sample (Gieskes *et al.* 1988, Everitt *et al.* 1990, Letelier *et al*. 1993, Mackey *et al*. 1996, Bidigare & Ondrusek 1996, Vidussi *et al*. 2001, Uitz *et al*. 2006, 2008, Van den Meersche *et al.* 2008, Sathyendranath *et al*. 2009). Diagnostic pigments alone however do not allow the precise identification of phytoplankton. Firstly, even within a group pigment ratios can vary significantly according to environmental conditions. This means that any pigment-based approach needs to combine culture-based work with natural observations to account for changes in pigment composition due to differing temperature, nutrient availability (Henriksen *et al.* 2002) or photoacclimatory status (Laviale & Neveux 2011). Moreover, pigments are not unique to taxonomic groups, for example fucoxanthin is present in both *Phaeocystis* and

diatoms (Wright & Jeffrey 1997, Stuart *et al.* 2000), and it is therefore possible to misclassify samples.

Here two different pigment-based approaches used to estimate phytoplankton taxonomic composition are compared. Uitz *et al.* (2008) divides the total biomass of all samples into three size categories according to the relative abundances of certain indicator pigments. Samples where the percentage of total biomass due to a single size-class is above a threshold value can then be taken as representative of that size-class. Sathyendranath *et al.* (2009) instead identifies samples where indicator pigment ratios suggest that they are comprised of a mixed population, and rejects them, leaving only samples dominated by a single taxonomic group. These groups of samples dominated by individual taxonomic groups can then be combined to give a collection of samples dominated by a single size-class, and are thus directly comparable with the output resulting from applying the Uitz *et al.* (2008) approach, which assigns biomass on a size class as opposed to taxonomic basis.

4.2.4 Aims of chapter

This chapter compares two different pigment-based approaches towards ascribing phytoplankton size-class, aiming to identify samples dominated by a single size-class which are then used to assess size-class specific relationships between phytoplankton *PE* parameters and environmental variables. The size-class-specific *PE* relationships are discussed in relation to the parameterisation of remote-sensing models that differentiate by size, and the fate of fixed carbon within the pelagic ecosystem.

4.3 Methods

4.3.1 Study areas

Vertical profiles of temperature were acquired from CTD profile data. Water samples were collected from 3 to 9 depths in the upper 200 m during 47 cruises in the Atlantic Ocean (Fig 4.1). The data originated from sampling programmes from three institutes: from Bedford Institute of Oceanography (BIO), from the Eumeli series of cruises conducted by the Observatoire Océanologique de Villefranche sur Mer (LOV) and data from Plymouth Marine Laboratory (PML).

Table 4.1: Summary of cruises included in the database, showing the geographic location, Chl-*a* range (µg / l), and the number of samples for HPLC pigments and ^{14}C measured *PE* parameters, and the protocol followed for analysis.

Dataset	**Location**	**Date**	**[Chl-*a*] range (µg / l)**	**n *PE* parameters**	**n HPLC**	**Analysis protocol**
Amt6	N-S Atlantic transect	1998	0.019 – 8.3	55	275	PML
Irish Sea	NE Atlantic	2001	0.33 – 7.06	60	52	PML
Eumeli 4	Tropical N Atlantic	1992	0 – 3.25	194	162	LOV
BIO	NW Atlantic	1996 – 2003	0.014 – 27.98	767	1873	BIO

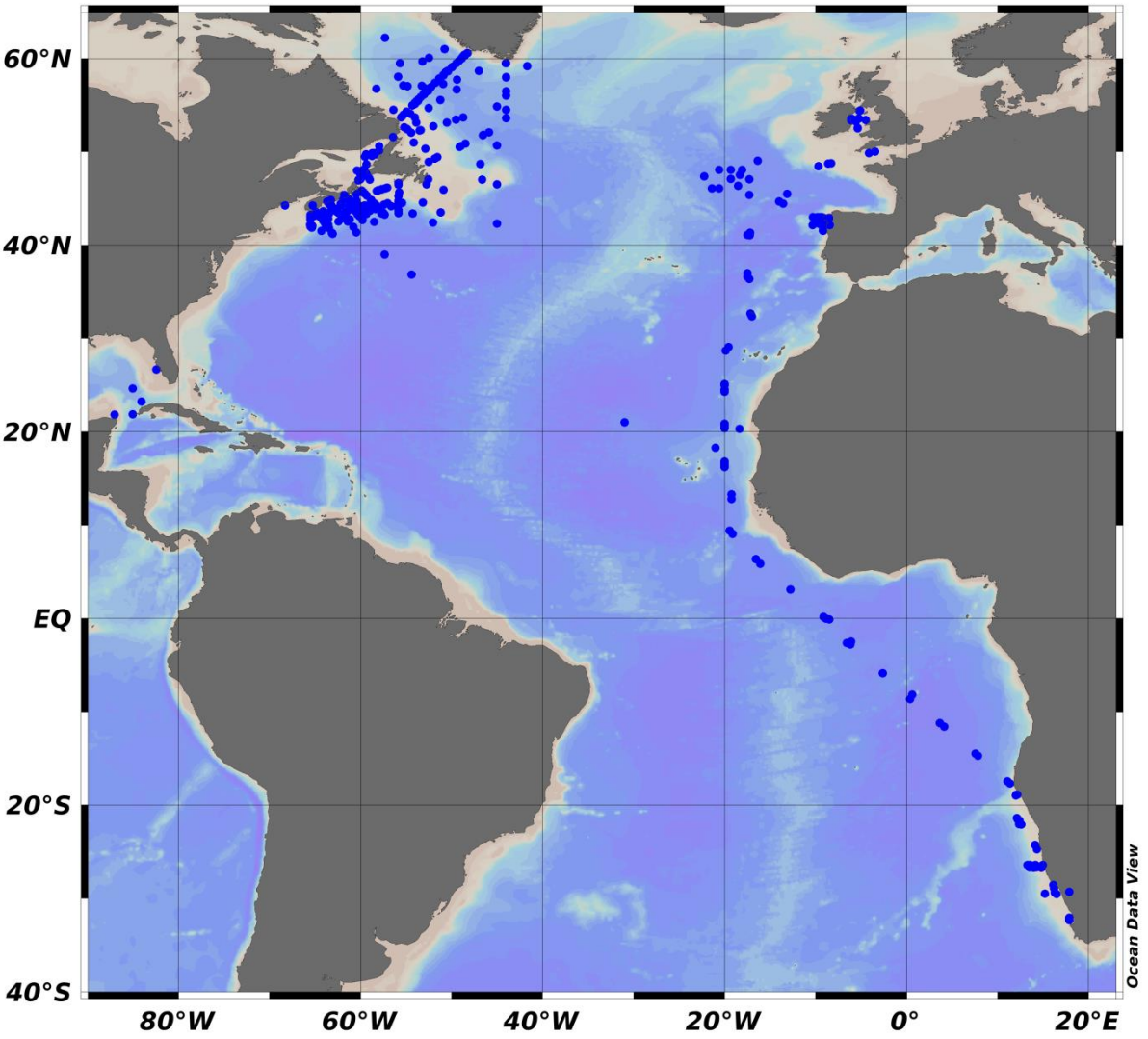

Fig 4.1: Locations of the stations included in the analysis for Chapter 4.

Environmental Variables

4.3.2 Temperature

Temperatures corresponding to the sample depths were obtained using in situ profiling conductivity, temperature, depth (CTD) sensors.

4.3.3 Irradiance

Average surface irradiance was estimated using MODIS-Aqua monthly climatology (OeanColour level 3) which was combined with estimates of the vertical attenuation

coefficient from chl-*a* of 0.016 m^2 (mg chl-*a*)$^{-1}$ (Schanz *et al.* 1997) and from seawater of 0.043 m^{-1} (Platt *et al.* 2003) to obtain mean mixed layer photosynthetically active radiation (PAR) and the euphotic depth (z_e, where the light intensity is 1% of surface irradiance). Mixed-layer data (z_m) came from the World Ocean Atlas (Locarnini *et al.* 2009) and temperature salinity and potential density were taken from Jackett *et al.* (2006), and used to calculate the ratio between euphotic and mixed-layer depth (z_e/z_m). Given the potential errors in assuming chlorophyll profiles and possible deep chlorophyll maxima, values of PAR for samples below the estimated mixed-layer depth were not calculated. Linear interpolation was used to derive estimates of daily irradiance from the monthly climatology. Natural neighbour interpolations were used to estimate mixed-layer depth.

4.3.4 Nutrients

Samples for nutrient analysis were frozen at -20 ºC before being analysed for nitrate and phosphate using a Technicon Autoanalyzer®, and the methods of Murphy & Reiley (1962) and Raimbault *et al.* (1990) respectively (LOV), an Alpkem RF-300 Autoanalyser (Stuart *et al.* 2000) (BIO), or a Skalar SANplus Segmented Flow Autoanalyser following Strickland & Parsons (1972) (PML).

Biological variables

4.3.5 Fluorometric chlorophyll-*a*

Chlorophyll-*a* concentrations were measured using a Turner Designs fluorometer before and after acidification using the method of Holm-Hansen *et al.* (1965) (BIO), Yentsch & Menzel (1963), adapted by Holm-Hansen & Rieman (1978) (LOV), or the non-acidification method of Welschmeyer (1994) (PML) and was used to normalise the *PE* parameters to biomass. 100 ml samples (Holm-Hansen 1965) or 80 ml samples (Yentsch & Menzel 1963) were filtered

onto GF/F filters and immediately extracted overnight in 90% acetone, or methanol in the case of Parsons *et al.* (1984). Concentrations were then quantified using the equations of either Lorenzen (1967) (LOV), Jeffrey & Humphrey (1975) (PML) or Tahey *et al.* (1994) (BIO).

4.3.6 HPLC pigments

Chl-*a* and accessory pigments were also measured on a subset of samples using high performance liquid chromatography (HPLC) following the procedure described by Head & Horne (1993) (BIO), Barlow *et al.* (1997) (PML) or Claustre & Marty (1995) (LOV). A comparison of different methods of HPLC analysis by Claustre *et al.* (2004) found an average of no more than 21.5% difference in pigment concentrations as measured by 4 laboratories each running a different HPLC protocol, meaning that comparison between samples analysed using different protocols is appropriate, and tests on this dataset demonstrated a close correlation between HPLC and fluorometric chl-*a* concentrations. Water samples were filtered onto a GF/F filter before being flash frozen in liquid nitrogen and stored at -80 ^{o}C until analysis. Frozen filters were either homogenized in 90% acetone (PML & BIO), centrifuged and diluted aqueous ammonium acetate added (Sathyendranath *et al.* 2005, Gibb *et al.* 2000, Barlow *et al*. 1997) or 100% methanol (LOV) (Claustre & Marty 1995). Standards from Sigma chemical company were used for the identification of chl-*a*, chl-*b*, and β-carotene. Chl-*c*, 19′-butanoyloxyfucoxanthin, fucoxanthin, 19′-hexanoyloxyfucoxanthin and diadinoxanthin were identified using standards from Dr R. Bidigare (BIO) (Stuart *et al.* 2000), or from VKI Denmark (PML) (Gibb *et al.* 2000).

4.3.7 Photosynthesis - irradiance (*PE*) parameters

The protocol for the determination of *PE* parameters is described in Babin *et al.* (1994) (LOV), Tilstone *et al*. (2003) (PML) and Bouman *et al.* (2005) (BIO). In brief, seawater samples were collected to characterise the fluorescence profile in the water-column from between 3 to 8 depths. For the BIO samples, 30 bottles were inoculated with 185 to 370 kBq (5 to 10 μCi) of ^{14}C-labelled bicarbonate and incubated for 2 - 3 hours. Tilstone *et al.* (2003) used 15 light levels (PML), whereas Babin *et al.* (1994) used 12 (EUM) before incubating for 1 - 2 hours. After the incubation, the water was filtered through 25 mm glass fibre filters (Whatman GF/F) at a vacuum pressure of < 20 cm Hg. The filters were exposed to concentrated HCl fumes to remove any inorganic carbon present, immersed in scintillation cocktail and the disintegration time per minute of ^{14}C was counted on a liquid scintillation counter. The *PE* parameters, P_m^B and α^B, were estimated by fitting the data to the model of Platt *et al.* (1980) (BIO, PML), or Jassby & Platt (1976) (LOV). Fluorometric as opposed to HPLC chl-*a* was used to normalise to biomass for greater consistency.

4.3.8 Pigment-based classification of phytoplankton types

To classify phytoplankton type, two approaches were used based on Uitz *et al.* (2008) and Sathyendranath *et al.* (2009), which are described below.

4.3.8a Size-class method (Uitz *et al.* 2008)

This approach assigns the proportion of total chlorophyll-*a* to each of 3 size-classes (microphytoplankton 20-200 μm, nanophytoplankton 2-20 μm, picophytoplankton <2 μm) using 7 diagnostic pigments (fucoxanthin (fuc), peridinin (per), alloxanthin (allo) 19'-butanoyloxyfucoxanthin (19'-but), 19'-hexanoyloxyfucoxanthin (19'-hex), zeaxanthin (zea) and the monovinyl chlorophyll *b* and divinyl chlorophyll *b* (chl-*b*)). A weighted sum of these

diagnostic pigments (wDP) was calculated as follows:

$$\text{wDP} = 1.41[\text{fuc}] + 1.41[\text{per}] + 0.6[\text{allo}] + 0.35[\text{19'-but}] + 1.27[\text{19'-hex}] + 0.86[\text{zea}] + 1.011[\text{chl-}b]. \quad (1)$$

The ratio of the weighted sum of group-specific diagnostic pigments to wDP provides the proportion of total biomass in each size-class, meaning that both dominant and rare pigments can be used as indicators so long as they are found only in a single group (Uitz *et al.* 2006, 2008).

$$f_{micro} = (1.41[\text{fuc}] + 1.41[\text{per}])/\text{wDP} \quad (2)$$

$$f_{nano} = (0.6[\text{allo}] + 0.35[\text{19'-but}] + 1.27[\text{19'-hex}])/\text{wDP} \quad (3)$$

$$f_{pico} = (0.86[\text{zea}] + 1.01[\text{chl-}b])/\text{wDP} \quad (4)$$

As previously acknowledged (Vidussi *et al.* 2001, Uitz *et al.* 2006, Uitz *et al.* 2008) an indicator pigment-based approach can lead to discrepancies as some diagnostic pigments are found in more than one group. Potential errors by using pigment markers may be reduced by looking at combinations of pigments. In addition, intra-group size variation can mean that some groups can cover more than one size range (e.g. some tropical diatoms will fall within the nanoplankton size-range (Hasle & Booth 1984). In this study samples were defined as being dominated by a single size-class if more than 70% of the total biomass was assigned to that size-class.

4.3.8b Sathyendranath *et al.* (2009) method.

Following the approach of Sathyendranath *et al.* (2009), samples dominated by any one of 6 phytoplankton groups (Prymnesiophytes, *Prochlorococcus*, diatoms, other cyanobacteria, green algae and dinoflagellates) were selected using the following diagnostic pigments: chl-*c,* DV chl-*a*, monovinyl chl-*b* (MVchl-*b*), DV chl-*b*, zea, per, allo, diadinoxanthin (diad), fuc, 19'-but and 19'-hex. Instead of trying to apportion chl-*a* for each size-class, ratios of diagnostic pigments with respect to chl-*a* are used to omit all samples containing mixed populations (see Sathyendranath *et al.* (2009) for details). By considering only samples dominated by a single algal group, much of the uncertainty of apportioning biomass in mixed samples associated with the method of Uitz *et al.* (2008) is avoided, albeit at a large cost to dataset size as up to 90% of samples were classified as mixed populations. In order to compare directly with the results obtained from the Uitz *et al.* (2008) approach, these taxonomic classes were then converted into the same 3 size-classes. Uitz *et al.* (2008) assigned all biomass associated with chl-*b* to the picophytoplankton size-class due to its presence in picophytoplankton such as *Micromonas* (Not *et al.* 2004) and *Prochlorococcus* (Chisholm *et al.* 1988). For this study however, due to the importance of chl-*b* containing flagellates to nanophytoplankton in the North Atlantic (Wright *et al.* 2010, Eker-Develi *et al.* 2011), and the definition of picophytoplankton as those smaller than 2 μm, as opposed to 3 μm in some studies, such as Bouman *et al.* (2012), chl-*b* containing samples found to consist predominantly of green flagellates using the Sathyendranath *et al.* (2009) are categorised as nanophytoplankton-dominated.

Table 4.2: Output categories for Sathyendranath *et al.* (2009) approach and Uitz *et al.* (2008) approach. For the purposes of analysis the output from Sathyendranath *et al.* (2009) was converted into size-classes equivalent to those produced by Uitz *et al.* 2008. (microphytoplankton 20-200 μm, nanophytoplankton 2-20 μm, picophytoplankton <2 μm)

Sathyendranath *et al.* 2009 class	**Uitz *et al.* 2008 class**
Diatoms	Microphytoplankton
Dinoflagellates	Microphytoplankton
Prymnesiophytes	Nanophytoplankton
Green algae	Nanophytoplankton
Prochlorococcus	Picophytoplankton
Other cyanobacteria	Picophytoplankton

4.3.9 Statistical analysis

All data analysis was performed using CRAN R statistical software; with package "reshape" 0.8.4 used to process the data. Principle component analysis was performed using the prcomp command within "stats" package 2.5.1. All data were plotted using package "ggplot2" version 0.8.9.

4.4 Results

4.4.1 Environmental variability

Temperature varied between -1.6 ºC and 26.3 ºC with a mean of 10.7 ºC, nitrate concentration from -0.6 to 26.1 µmol/l with a mean of 2.15 and mean estimated mixed-layer PAR from 3.21 to 51.8 Einsteins/m^2/day with a mean of 24.7.

Table 4.3: Mean values and ranges for key environmental variables.

Temperature and nitrate concentration were measured *in-situ*, mean mixed-layer PAR estimated for those samples in the mixed-layer from MODIS-aqua with mixed-layer data from the World Ocean Atlas (2009) and temperature salinity and potential density from Jackett *et al.* (2006).

	Minimum	Mean	Maximum
Temperature (°C)	-1.6	11.5	26.3
Nitrate (µmol / l)	-0.6	2.15	26.1
MLD PAR (E/m^2/day)	3.21	24.7	52.8
Chl-*a* (µg/l)	0	1.37	27.97

4.4.2 Variability in P_m^B

4.4.2a By size-class, for all sampling depths combined

P_m^B varied from 0.33 to 19.7 mg C (mg chl-*a*)$^{-1}$ h^{-1}, with a mean of 3.49 mg C (mg chl-*a*)$^{-1}$ h^{-1}. When values of P_m^B were compared with respect to size-class and classification method, P_m^B varied according to the phytoplankton size-class, with highest values corresponding to pico-

and nanophytoplankton-dominated samples (Fig. 4.2a, Table 4.4). There was no significant difference between pico- and nanophytoplankton P_m^B when considering samples from all depths according to either classification method. Microphytoplankton P_m^B as estimated by the Uitz *et al.* (2008) approach was significantly lower than that for either picophytoplankton ($W = 5597, p < 0.0001$) or nanophytoplankton ($W = 4149, p < 0.0001$). Microphytoplankton P_m^B as estimated using the Sathyendranath *et al.* (2009) approach was also significantly lower than that for both picophytoplankton ($W = 851, p = 0.008$) and nanophytoplankton ($W = 1061, p < 0.0001$) There was no significant difference in P_m^B between the size-classes defined by the Uitz *et al.* (2008) and Sathyendranath *et al.* (2009) methods ($F_{1, 496} = 0.4, p = 0.53$)

4.4.2b Differences in P_m^B between surface and deep samples

No difference was seen in P_m^B between surface (<5 m) and deep (>40 m) samples for any size-class as ascribed following Uitz *et al.* (2008) (Fig 4.3a). Differences according to depth were however observed for microphytoplankton- and picophytoplankton-dominated samples as identified by the Sathyendranath *et al.* (2009) method. Surface microphytoplankton P_m^B was significantly lower than at depth ($W = 7.5, p = 0.009$), while P_m^B was significantly higher for surface picophytoplankton-dominated samples than deep ($W = 18, p = 0.02$). P_m^B was significantly higher for surface microphytoplankton-dominated samples as estimated by Uitz *et al.* (2008) compared to those estimated by the Sathyendranath *et al.* (2009) method ($W = 51, p = 0.0018$). The sample size was too small to assess potential differences in nanophytoplankton P_m^B (n = 1 for Sathyendranath *et al.* (2009) deep nanophytoplankton, n = 2 for Sathyendranath *et al.* (2009) shallow nanophytoplankton and Uitz *et al.* (2008) deep nanophytoplankton). No difference in P_m^B was seen between size-classes as estimated following Uitz *et al.* (2008) and Sathyendranath *et al.* (2009) for other size-classes of surface

samples or any size-class for deep samples.

4.4.3 Variability in α^B

4.4.3a By size-class for all sampling depths combined

α^B ranged from 0.002 to 0.59 mg C (mg chl)$^{-1}$ h^{-1} (µmol photons m^{-2} s^{-1})$^{-1}$ with a mean of 0.033 mg C (mg chl)$^{-1}$ h^{-1} (µmol photons m^{-2} s^{-1})$^{-1}$ (Table 4.4). When considering samples from all depths, there was no significant difference in α^B between pico- and microphytoplankton (Fig 4.2b) for both classification methods. α^B was significantly higher for nanophytoplankton than microphytoplankton using both the Uitz *et al.* (2008) approach ($W = 461$, $p < 0.0001$) and the Sathyendranath *et al.* (2009) method ($W = 93$, $p < 0.0001$). α^B was also significantly higher for nanophytoplankton than for picophytoplankton using both methods (Uitz *et al.,* (2008) ($W = 21$, $p < 0.0001$) Sathyendranath *et al.* (2009) ($W = 41$, $p = 0.003$). There was no significant difference in α^B between the size-classes defined by the Uitz *et al*.(2008) and Sathyendranath *et al.* (2009) approaches ($F_{1, 448} = 2.02$, $p = 0.16$)

4.4.3b Differences in α^B between surface and deep samples

For microphytoplankton, mean α^B was significantly higher in deep samples than shallow samples for both the Uitz *et al.* (2008) ($W = 779$, $p = 0.012$) and Sathyendranath *et al.* (2009) methods ($W = 0.0047$) (Fig 4.3b). Significantly higher values of α^B were also seen for deep picophytoplankton than shallow using the Sathyendranath *et al.* (2009) method ($W = 18$, $p = 0.024$). The sample size was too small to assess potential differences in nanophytoplankton α^B (n = 1 for Sathyendranath *et al.* (2009) deep nanophytoplankton, n = 2 for Sathyendranath *et al.* (2009) shallow nanophytoplankton and Uitz *et al.* (2008) deep nanophytoplankton). Mean microphytoplankton α^B in surface samples was found to be higher amongst microphytoplankton as defined by Uitz *et al.* (2008) than by Sathyendranath *et al.* (2009) (*W*

= 52, p = 0.005). No other differences between classification methods were observed.

4.4.4 Variability in E_k

4.4.4a By size-class for all sampling depths combined

E_k varied from 11.5 to 1257 µmol photons m^2 s^{-1}, with a mean of 127.5 (Table 4.4). Picophytoplankton E_k for all depths as defined by Uitz *et al.* (2008) was significantly higher than either nanophytoplankton (*W = 28, p = 0.006*) or microphytoplankton (*W = 236, p = 0.0009*) (Fig 4.2). Picophytoplankton E_k as determined using the Sathyendranath *et al.* (2009) approach for samples from all depths was also significantly higher than for nanophytoplankton (*W = 185, p = 0.003*), and microphytoplankton (*W = 964, p = 0.0001*). No significant differences were seen between nano- and microphytoplankton-dominated samples according to either classification method

4.4.4b Differences in E_k between surface and deep samples

Surface microphytoplankton-dominated samples as defined by Uitz *et al.* (2008) were found to have a significantly higher mean E_k than deep samples (*W = 1676, p < 0.0001*) (Fig 4.3). No other significant depth dependent differences were observed. E_k for surface microphytoplankton as defined by Sathyendranath *et al.* (2009) was found to be higher (*W = 328, p = 0.024*) than for Uitz *et al.* (2008).

Table 4.4: *PE* parameters for 3 size-classes of phytoplankton (picophytoplankton <2µm, nanophytoplankton 2-20µm, microphytoplankton >20µm as estimated by 2 pigment-based approaches for identifying samples dominated by a single phytoplankton size-class, where P_m^B is the chlorophyll-normalised maximal photosynthetic rate (mg C (mg chl-*a*)$^{-1}$ h^{-1}, α^B the initial slope of the *PE* mg C (mg chl)$^{-1}$ h^{-1} (µmol photons m^{-2} s^{-1})$^{-1}$ and E_k (µmol photons m^{-2} s^{-1}). Results from Sathyendranath *et al.* (2009) converted from taxonomic group to equivalent size-class for ease of comparison.

	Size-class	**Micro**	**Nano**	**Pico**
$\boldsymbol{P_m^B}$	Uitz *et al.* (2008)	2.3	4.34	3.25
	Sathyendranath *et al.* (2009)	1.97	4.15	4.1
$\boldsymbol{\alpha^B}$	Uitz *et al.* (2008)	0.022	0.052	0.028
	Sathyendranath *et al.* (2009)	0.17	0.43	0.021
$\boldsymbol{E_k}$	Uitz *et al.* (2008)	110.3	85.9	275.6
	Sathyendranath *et al.* (2009)	125.8	126.3	291.9

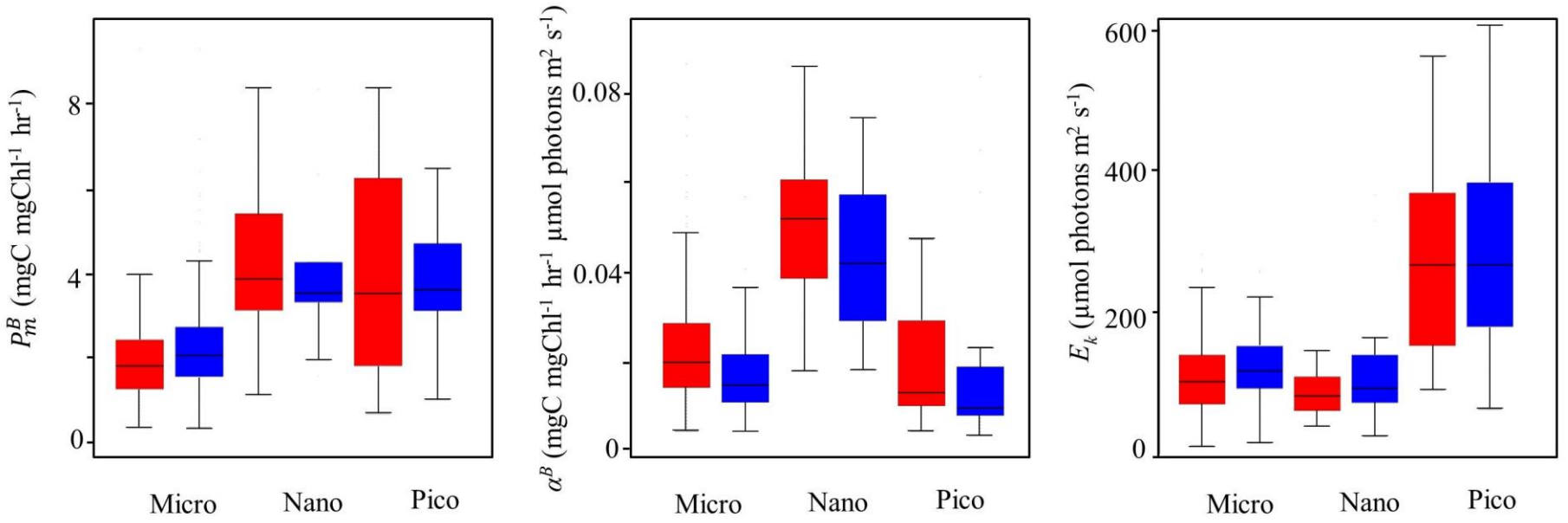

Fig 4.2: *PE* parameters by phytoplankton size. (a) P_m^B , (b) α^B, and (c) E_k all normalised to total HPLC chlorophyll-*a* Uitz *et al.* (2008) approach shown in red, Sathyendranath *et al.* (2009) approach shown in blue. Microphytoplankton >20 µm, Nanophytoplankton 2-20 µm, Picophytoplankton <2 µm. Microphytoplankton P_m^B was significantly lower than the other groups. Nanophytoplankton α^B was significantly higher than for the other groups. Picophytoplankton E_k was significantly high than for the other groups. Other differences were non-significant. No significant difference in mean values was seen according to size-class classification method.

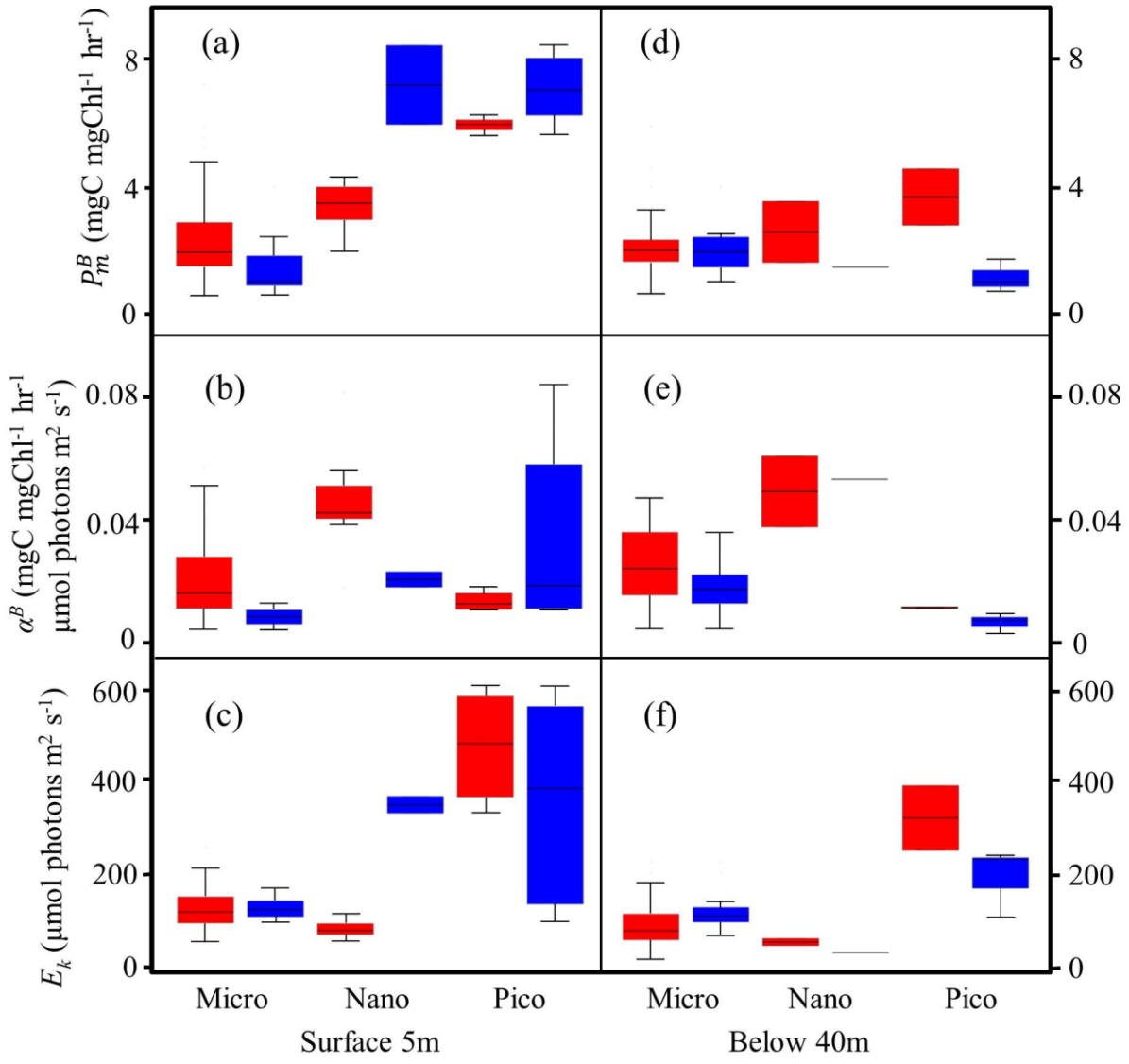

Fig 4.3: *PE* parameters for shallow (< 5m) and deep (> 40m) samples according to classification method. Uitz *et al.* (2008) in red, Sathyendranath *et al.* (2009) in blue. Microphytoplankton >20 µm, Nanophytoplankton 2-20 µm, Picophytoplankton <2 µm. (a) P_m^B, shallow. (b) α^B, shallow. (c) E_k, shallow. (d) P_m^B, deep. (e) α^B, deep. (f))E_k deep. Significant differences in P_m^B as a function of depth were seen for micro and pico size-classes for Sathyendranath *et al.* (2009). Significant differences in α^B were seen for the micro class for both classification methods, as well as the pico class for Sathyendranath *et al.* (2009). There was a significant difference in E_k with respect to depth only for the Uitz *et al.* (2008) micro class. Significant differences according to classification method were seen in P_m^B for the shallow nano and micro classes. Shallow microphytoplankton also differed in α^B and according to the classification method used. All other differences were non-significant. Note: there were insufficient deep nanophytoplankton-dominated samples from Sathyendranath *et al.* (2009) for analysis (n=1).

4.4.5 Effect of temperature on *PE* parameters

When comparing P_m^B and temperature (Fig. 4.4a and 4.4d), there appears to be an upper bound of the scatter of points which shows a general increase in P_m^B with increasing temperature until 15 ºC before decreasing at temperatures above 20 ºC. α^B also displayed a strong relationship with temperature (Figs 4.4b and 4.4e), with an increase in α^B at low temperatures before a decrease above 20ºC. Trends with respect to temperature are also seen for E_k . This remains stable for temperatures from 0 ºC to 15 ºC, before increasing sharply from 15 ºC to 27.5 ºC (Figs 4.4c and 4.4f). In all cases the samples dominated by a single size-class display a greater temperature range when following the approach of Uitz *et al.* (2008) than that of Sathyendranath *et al.* (2009).

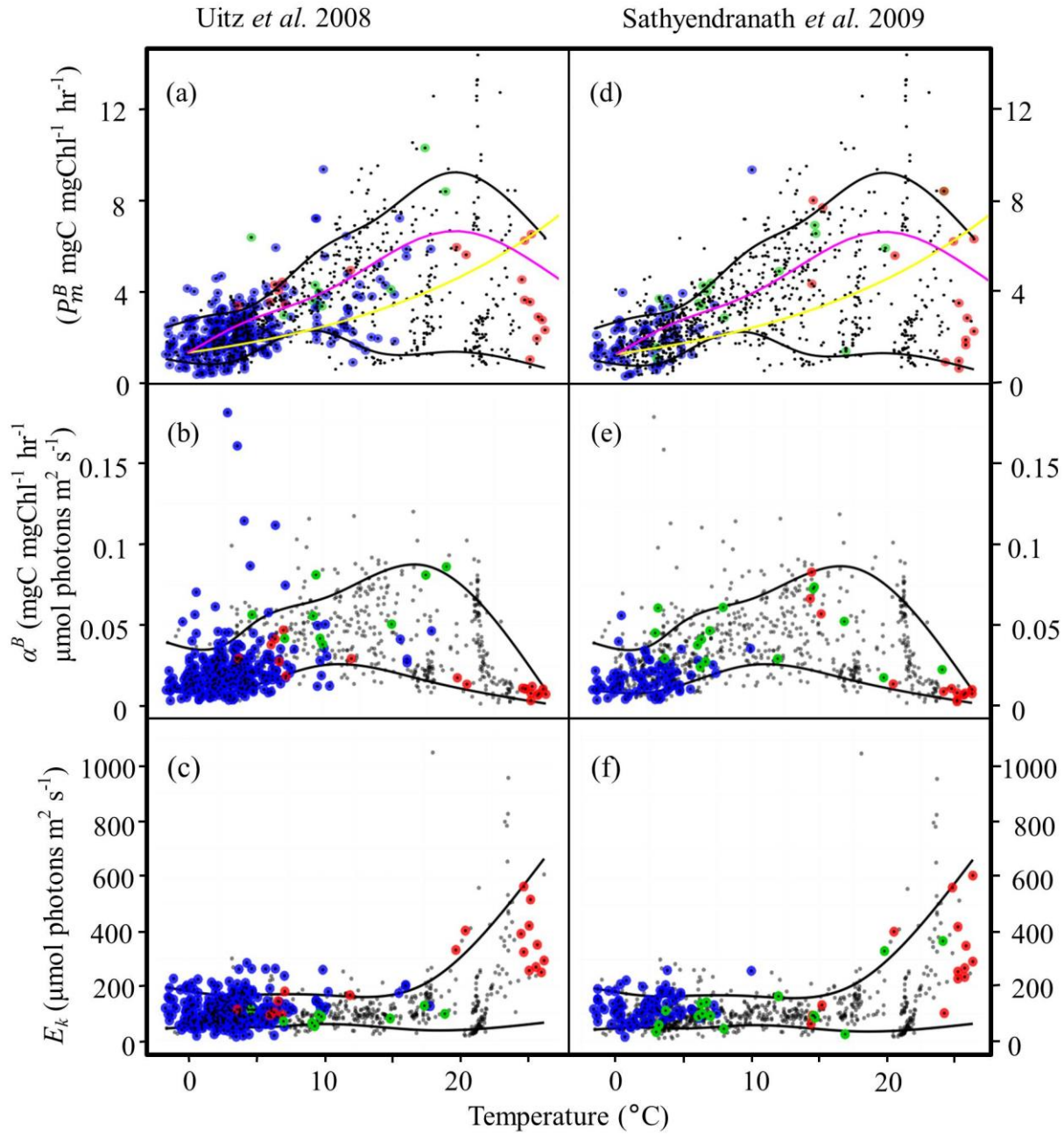

Fig 4.4: Envelope plots of the relationships between phytoplankton *PE* parameters and temperature. Blue points signify microphytoplankton-dominated samples (>20 µm), green nanophytoplankton (2-20 µm), red picophytoplankton (<2 µm). Grey points signify mixed populations. Black lines shown are the 10 and 90% quantiles fitted using a running average over all samples. For (a) and (b) the yellow line shows the relationship between P_m^B and temperature from Eppley (1972) and the pink line the 7th order polynomial relationship from Behrenfeld & Falkowski (1997a). (a) P_m^B, samples classified according to Uitz *et al.* (2008). (b) α^B, Uitz *et al.* (2008). (c) E_k, Uitz *et al.* (2008). (d) P_m^B, samples classified according to Sathyendranath *et al.* (2009). (e) α^B, Sathyendranath *et al.* (2009). (f) E_k, Sathyendranath *et al.* (2009).

4.4.6 Group-specific relationships between environmental variables and *PE* parameters

4.4.6a Temperature

To assess the within-group responses, the relationship between *PE* parameters and temperature for samples estimated to be dominated by a single phytoplankton size-class were examined.

Diagnostic pigments, such as fucoxanthin, associated with diatoms and other microphytoplankton, dominate samples at temperatures below 10 ^{o}C. Above 20 ^{o}C chlorophyll-*b* and zeaxanthin found in *Prochlorococcus* and other picophytoplankton dominate. With both methods, the size of the dominant group decreases as temperature increases, although there is greater overlap between the size-classes when following the approach of Uitz *et al.* (2008) (Fig 4.4).

A significant relationship between P_m^B and temperature is seen for samples dominated by each size-class (Fig. 4.5). The values of P_m^B for microphytoplankton have a strong positive correlation with temperature for both the Uitz *et al.* (2008) ($p < 0.0001$, $R^2 = 0.15$) and Sathyendranath *et al.* (2009) approaches ($p < 0.0001$, $R^2 = 0.22$). Samples dominated by nanophytoplankton as defined by the Sathyendranath *et al.* (2009) method also display a positive relationship between temperature and P_m^B ($p = 0.003$, $R^2 = 0.45$), though no relationship is seen for nanophytoplankton-dominated samples as defined using the Uitz *et al.* (2008) approach. Samples which are found to be dominated by picophytoplankton using the Sathyendranath *et al.* (2009) approach are found to have a significant negative relationship with temperature ($p = 0.04$, $R^2 = 0.24$), whereas no relationship is seen between those classified as picophytoplankton-dominated according to the Utiz *et al.* (2008) method ($p = 0.67$, $R^2 = -0.05$).

Size-dependent differences were also observed for α^B, with nanophytoplankton being

the most photosynthetically efficient, which suggests that this group is adapted to low light levels (Table 4.5). A weak positive linear correlation between α^B and temperature is seen for samples found to be dominated by microphytoplankton using the approach of Uitz *et al.* (2008) ($p = 0.0005$, $R^2 = 0.036$), but using the Sathyendranath *et al.* (2009) method of classification no significant relationship is found. A negative relationship between α^B and temperature is observed for picophytoplankton-dominated samples using both the Uitz *et al.* (2008) ($p < 0.0001$, $R^2 = 0.78$) and the Sathyendranath *et al.* (2009) approaches ($p < 0.0001$, $R^2 = 0.89$). There is no correlation between nanophytoplankton α^B and temperature.

Within group relationships are also found between E_k and temperature (Fig 4.7). Samples classified as dominated by microphytoplankton using the Uitz *et al.* (2008) approach show a significant positive relationship between E_k and temperature ($p = 0.002$, $R^2 = 0.03$), though there is no significant relationship between E_k and for microphytoplankton-dominated samples as classified using the Sathyendranath *et al.* (2009) method. No relationship between E_k and temperature is observed for samples dominated by nanophytoplankton according to the Uitz *et al.* (2008) approach, however a significant positive relationship between E_k and temperature is seen for samples found to be dominated by nanophytoplankton using the Sathyendranath *et al.* (2009) method ($p = 0.006$, $R^2 = 0.41$). There is a significant negative relationship between *Ek* and temperature for samples found to be dominated by picophytoplankton using either the Uitz *et al.* (2008) ($p < 0.0001$, $R^2 = 0.61$) or the Sathyendranath *et al.* (2009) approach ($p = 0.02$, $R^2 = 0.30$).

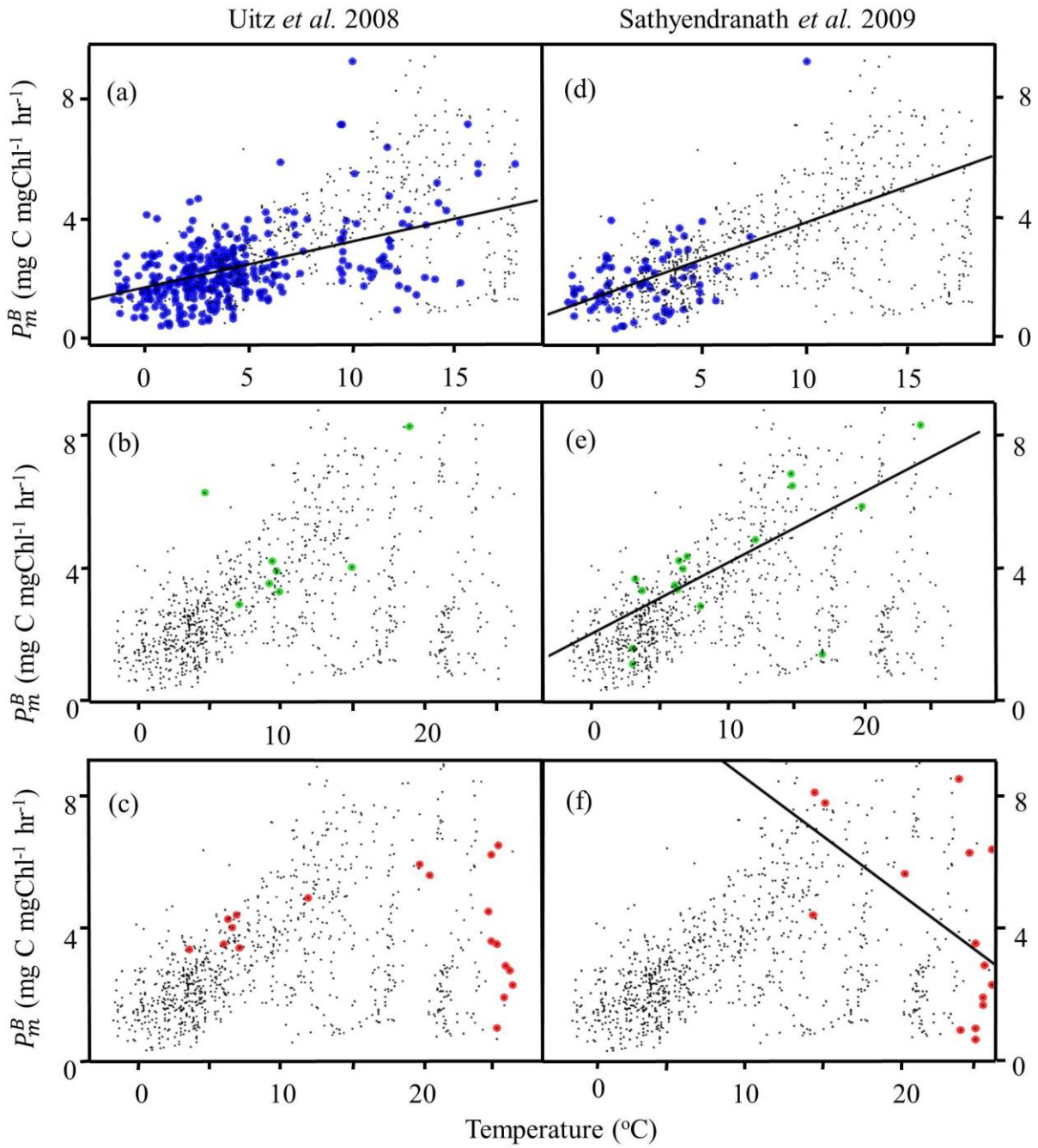

Fig 4.5: Relationships between P_m^B and temperature for samples dominated by a single size-class for Microphytoplankton (>20 µm) blue, Nanophytoplankton (2-20µm) green, Picophytoplankton (<2µm) red. Grey points show mixed populations. (a) Microphytoplankton as defined by Uitz *et al.* (2008). y = 0.15 x + 1.68, R^2 = 0.15, p < 0.0001. (b) Nanophytoplankton, (Uitz *et al.* 2008). y = 0.19 x + 2, R^2 = 0.02, p = 0.27. (c) Picophytoplankton, (Uitz *et al.* 2008). y = 0.047 x + 2.6, R^2 = 0.02, p = 0.12. (d) Microphytoplankton as defined by Sathyendranath *et al.* (2009). y = 0.25 x + 1.45, R^2 = 0.22, p = < 0.0001. (e) Nanophytoplankton (Sathyendranath *et al.* 2009). y = 0.216 x + 2, R^2 = 0.45, p = 0.003. (f) Picophytoplankton (Sathyendranath *et al.* 2009). y = 11.7 - 0.33 x, R^2 = 0.24, p = 0.037.

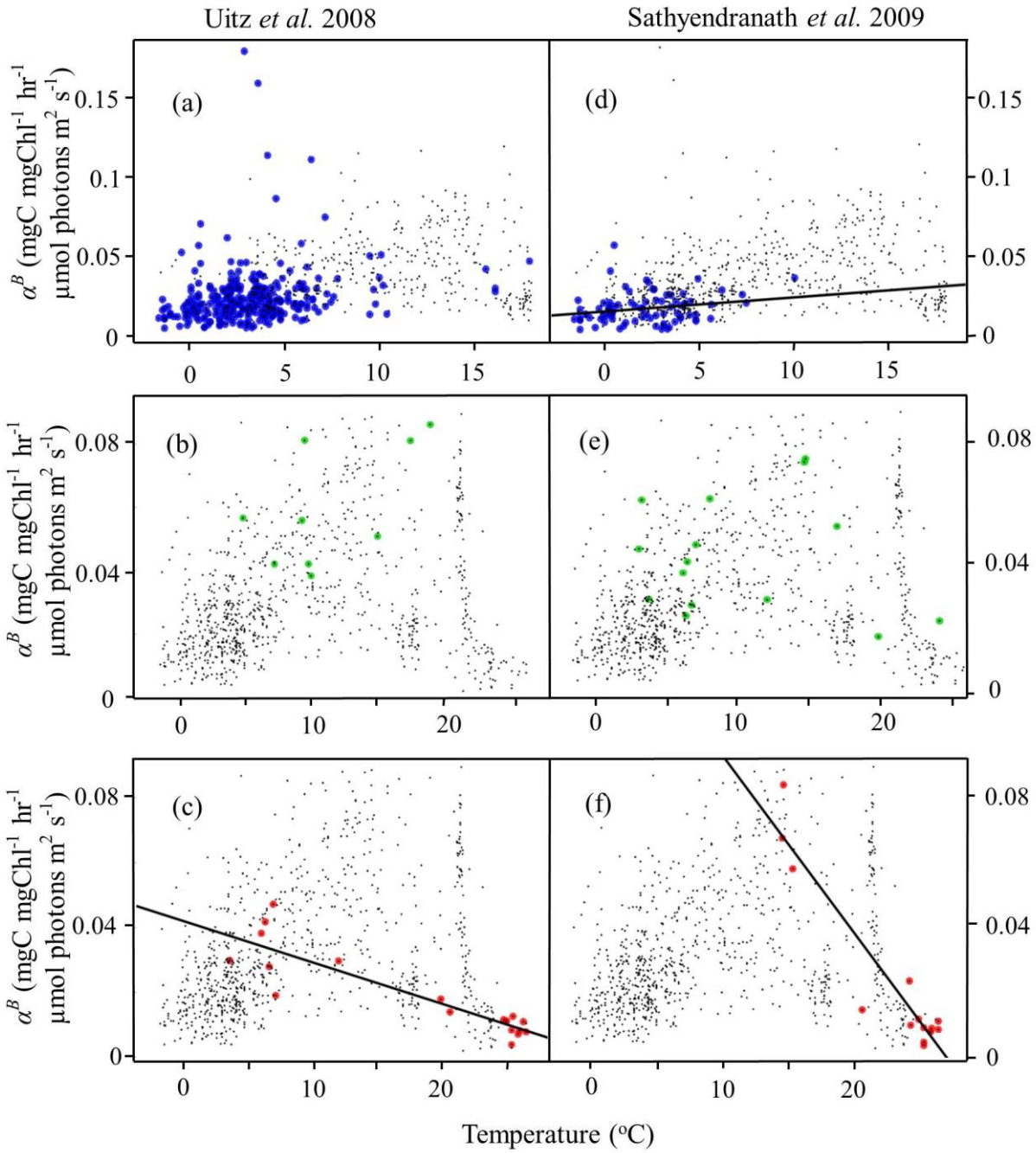

Fig 4.6: Relationship between α^B and temperature for samples dominated by a single size-class. Microphytoplankton, blue (>20 µm), Nanophytoplankton, green (2-20µm), Picophytoplankton, red (<2µm). Grey points show mixed samples. (a) Microphytoplankton as defined by Uitz *et al.* (2008). y = 0.00044 x + 0.02, R^2 = 0.0068, p = 0.068. (b) Nanophytoplankton (Uitz *et al.* 2008): y = 0.0009 x + 0.04, R^2 =- 0.0, p = 0.55. (c) Picophytoplankton (Uitz *et al.* 2008). y = 0.04 – 0.0001 x, R^2 = 0.17, p = 0.0001. (d) Microphytoplankton as defined by Sathyendranath *et al.* (2009). y = 0.00089 x + 0.015, R^2 = 0.035, p = 0.055. (e) Nanophytoplankton (Sathyendranath *et al.* 2009). y = 0.046 - 0.00029 x, R^2 = - 0.07, p = 0.72. Picophytoplankton (Sathyendranath *et al.* (2009). y = 0.15 - 0.005 x, R^2 = 0.89, p < 0.0001.

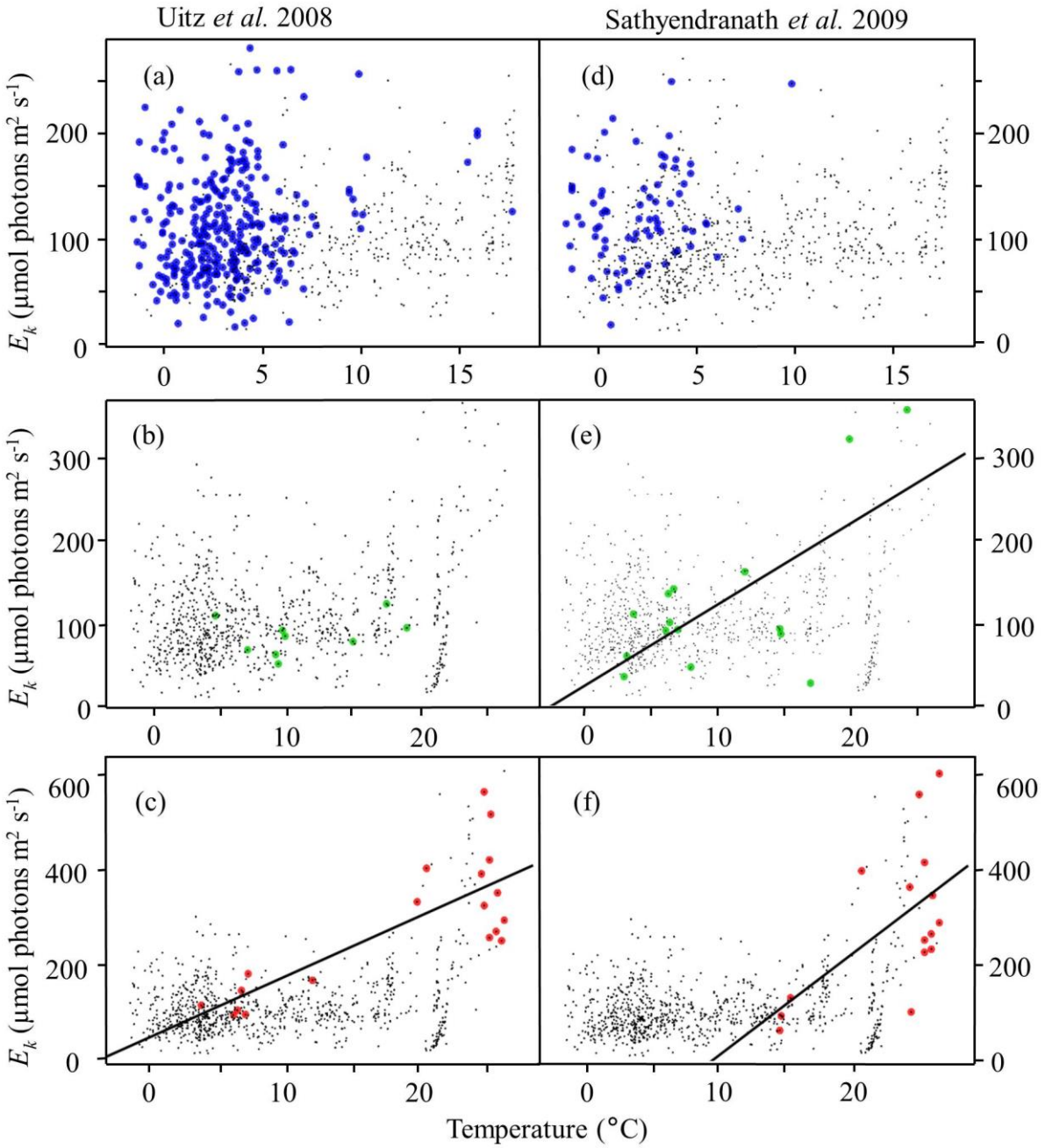

Fig 4.7: Relationship between E_k and temperature for samples dominated by a single size. Microphytoplankton, blue (>20 µm), Nanophytoplankton, green (2-20 µm), Picophytoplankton, red (<2 µm). Grey points show mixed populations. (a) Microphytoplankton as defined by Uitz *et al.* (2008). y = 2.4 x + 103, R^2 = 0.018, p = 0.01. (b) Nanophytoplankton (Uitz *et al.* 2008). y = 1.67 x + 65, R^2 = -0.03, p = 0.45. (c) Picophytoplankton (Uitz *et al.* 2008). y = 10.7 x + 25, R^2 = 0.29, p < 0.0001. (d) Microphytoplankton as defined by Sathyendranath *et al.* (2009). y = 4.2 x + 117, R^2 = 0.03, p = 0.069. (e) Nanophytoplankton (Sathyendranath *et al.* 2009). y = 10 x + 23, R^2 = 0.41, p < 0.0001. (f) Picophytoplankton (Sathyendranath *et al.* 2009). y = 21 x - 200, R^2 = 0.3, p = 0.02.

4.4.6b Ratio between the euphotic depth and the depth of mixing

A very weak positive relationship is seen between P_m^B and the ratio between the depth at which light is 1% of that at the surface and mixing depth (z_e/z_m) (Fig 4.8). Samples that routinely experience mixing below the euphotic zone (i.e. z_e/z_m <1) tend to be dominated by microphytoplankton, corresponding to their prevalence under conditions of turbulent mixing or upwelling. Values of P_m^B are higher for the stations where z_e/z_m >1 than when z_e/z_m <1 at 3.55 as compared with 2.33 mg C (mg chl-*a*)$^{-1}$ h^{-1} ($W = 6603$, $p < 0.0001$).

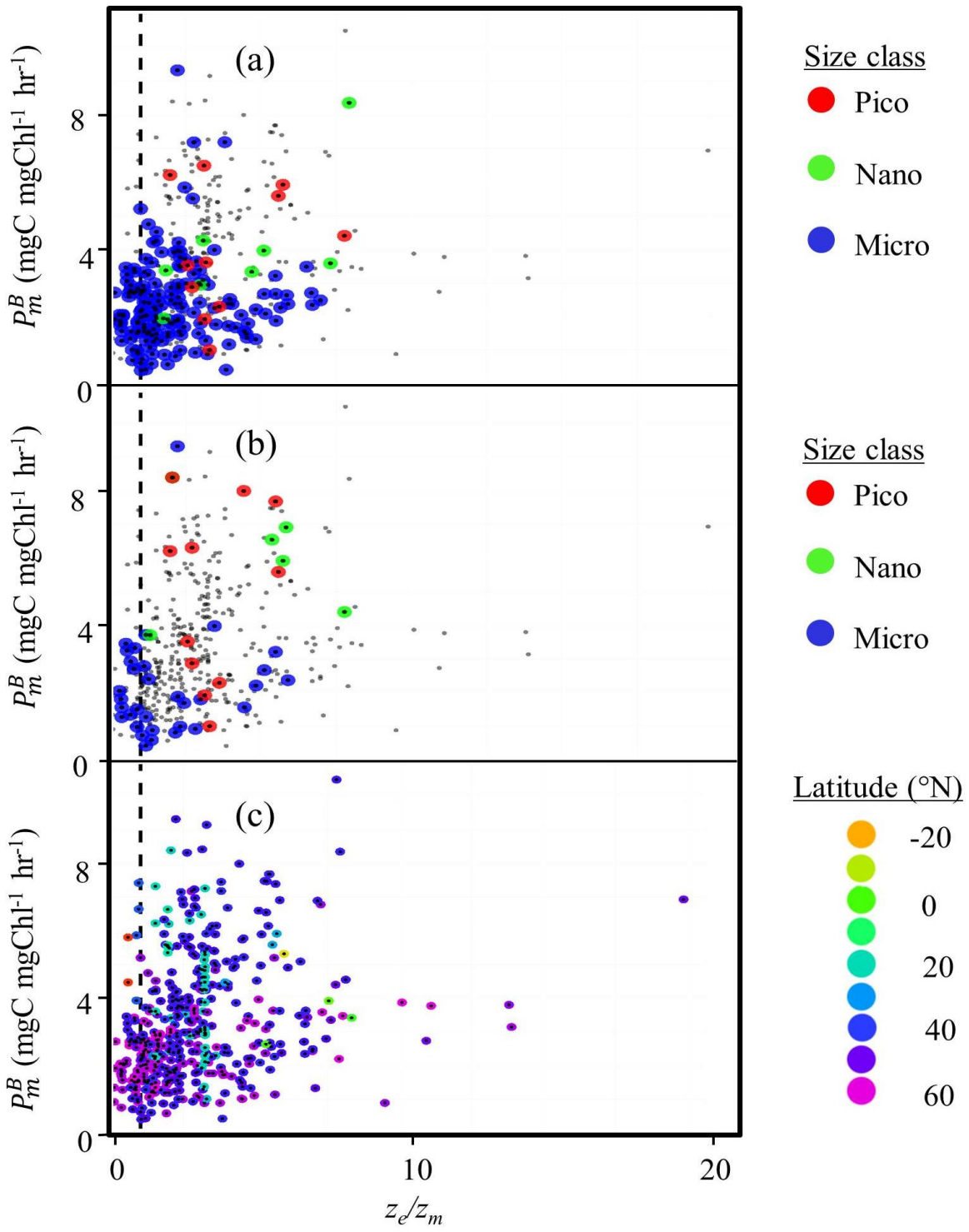

Fig 4.8: Correlation between phytoplankton P_m^B and z_e/z_m. For (a) and (b) blue points signify microphytoplankton-dominated samples (>20 µm), green nanophytoplankton (2-20 µm) and red picophytoplankton (<2 µm). Grey points correspond to mixed populations. Dashed line marks when euphotic depth equals the depth of mixing. (a) following Uitz *et al.* (2008) (b) following Sathyendranath *et al.* (2009). (c) Points coloured according to latitude.

4.4.6c Nutrients

While a strong relationship between n the *PE* parameters and temperature was observed, only a weak relationship between P_m^B and nutrient status was seen (Fig.4.9). At high nutrient concentrations P_m^B was consistently low. Much greater variation was seen at low nutrient levels with an almost 10-fold variation observed.

A very weak relationship between α^B and nutrient status was also seen (Fig. 4.9). At high nutrient concentrations α^B was consistently low. As with P_m^B, much greater variation was seen at low nutrient levels yet the overall trend is likely to be masked by the complex interplay of other variables, such as temperature and light.

As E_k is a function of P_m^B and α^B, the same lack of nutrient dependent trend is seen in Ek as in P_m^B and α^B. A wide range in E_k is seen at very low nitrate concentrations, with lower, and less varied values seen at higher (above 1.5 μmol/l) nitrate concentrations, perhaps representing depth dependent variability in photoacclimation in stratified, low nutrient regions.

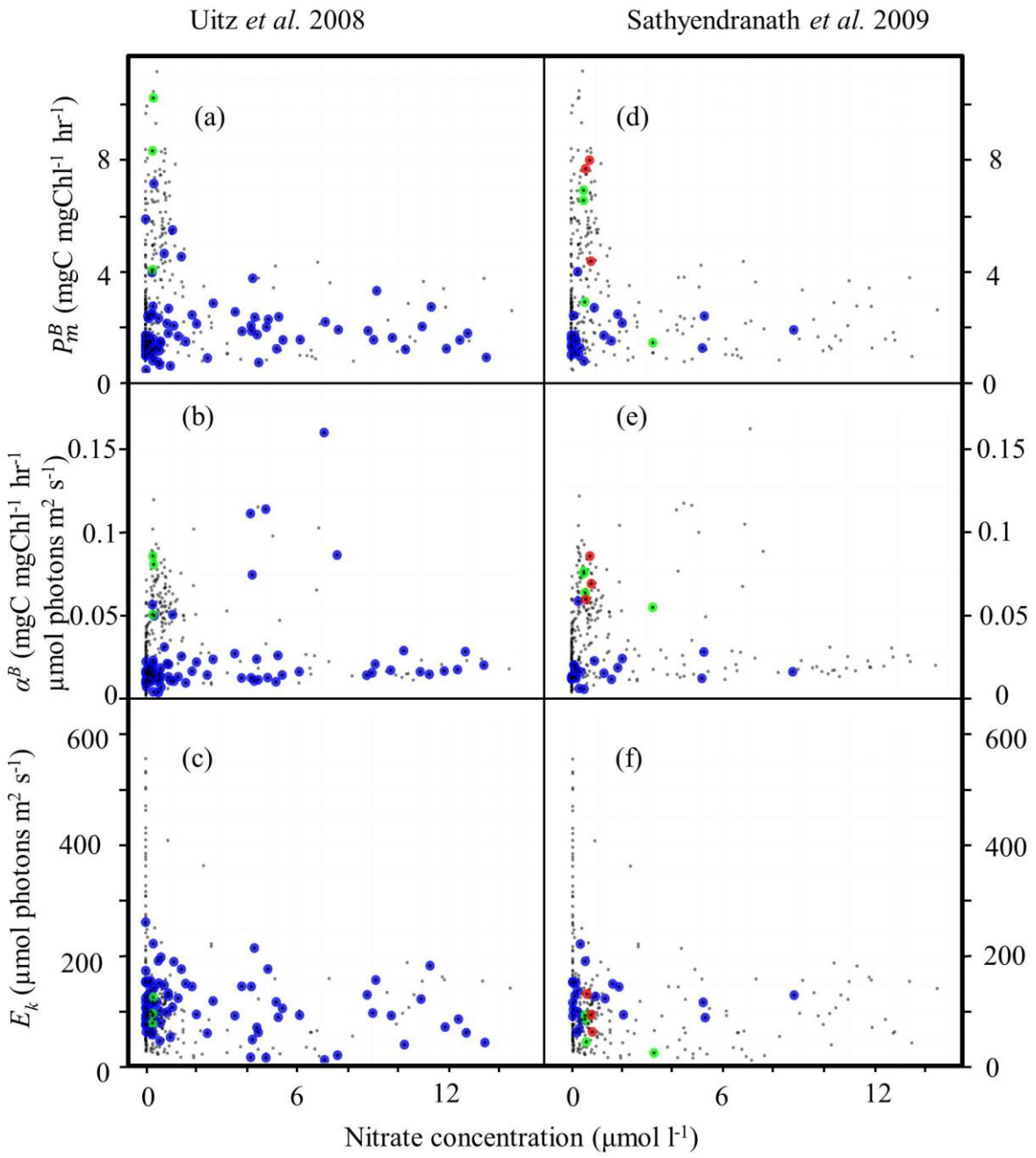

Fig 4.9: Trends in *PE* parameters with respect to ambient nitrate concentration. Blue points signify microphytoplankton-dominated samples (>20 µm), green nanophytoplankton (2-20 µm) and red picophytoplankton (<2 µm). Grey points correspond to mixed populations. (a) P_m^B, size-classes assigned following Uitz *et al.* (2009). (b) α^B(Uitz *et al* 2008). (c) E_k (Uitz *et al.* 2008). (d) P_m^B, size-classes assigned following Sathyendranath *et al.* (2009). (e) α^B (Sathyendranath *et al.* 2009). (f) E_k (Sathyendranath *et al.* 2009).

4.4.7 Principal component analysis

The relationship between phytoplankton physiology and environmental variables was further investigated using a principal component analysis (PCA) performed on the *PE* database (Fig. 4.10). This allows us to assess not only which environmental parameters co-vary with the photosynthetic parameters, but also the relationships between the environmental variables themselves. The data matrix consisted of 373 observations of 10 variables (environmental variables: temperature, depth, nitrate concentration and localised PAR; biological variables: chl-*a*, the proportion of biomass due to each phytoplankton size-class and the photophysiological parameters of P_m^B and α^B). The first two eigenvalues of the data matrix account for over 65% of the variance, so the analysis will be limited to the first factorial plane.

The main variables contributing to the first principle component are temperature, the proportion of microphytoplankton and chl-*a*. The proportion of microphytoplankton and chl-*a* concentration are closely linked and inversely correlated with temperature, while an inverse relationship between the proportion of picophytoplankton and the chl-*a* concentration demonstrates that picophytoplankton generally dominate in low biomass areas. Trends are also seen when considering the relationship between chl-*a* concentration and light intensity: high light samples are correlated with low chl-*a* since a lower concentration of pigment is required to saturate the light-harvesting complexes at high irradiances. There are four main variables which control the second component with the available light and proportion of the biomass due to picophytoplankton operating in the opposite direction to α^B and chl-*a*.

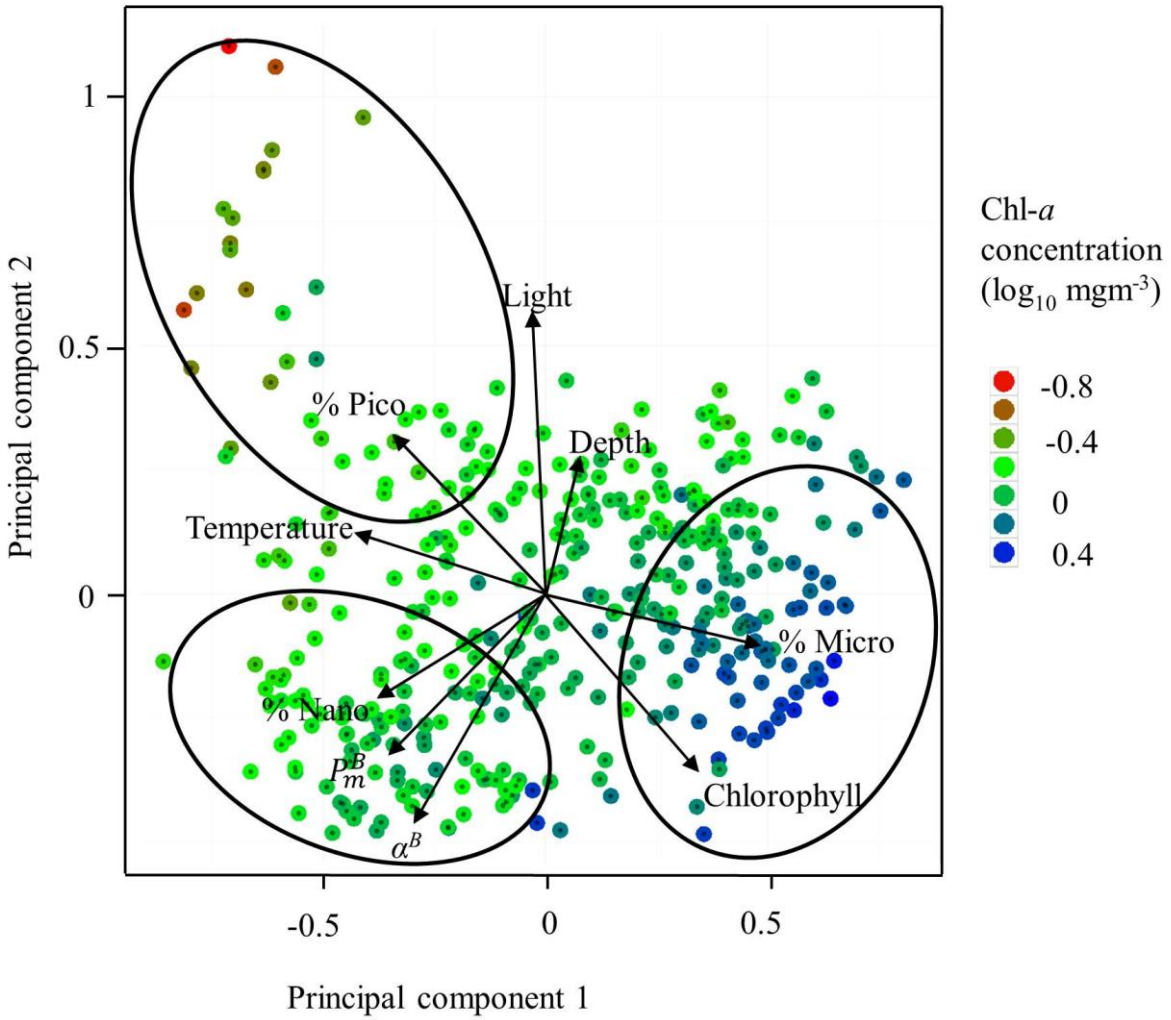

Fig 4.10: Graphical representation of PCA results showing a projection of the individual samples in the plane formed by the two first principle components, which describe 66% of the total variation. The points are coloured according to the concentration of total HPLC chl-*a*. 3 ecological groupings are circled: a high biomass cluster associated with the vectors for chlorophyll concentration and % microphytoplankton, a high light region linked to the vectors for % picophytoplankton, and mean mixed layer PAR and a high efficiency group associated with the vectors for % nanophytoplankton, α^B and P_m^B.

4.5 Discussion

4.5.1 Comparison of classification methods

This study aims to compare two different pigment-based methods of assessing phytoplankton size-class to help understand how phytoplankton *PE* parameters relate to abiotic variables not only for the entire assemblage, but also within fixed size-classes. To understand any potential differences in the classification methods that we tested, we must first consider the way in which the approaches were intended to be used and consequent differences in their methodologies. The Uitz *et al.* (2008) method was developed to estimate the size distribution of all samples to investigate links between community structure and photophysiology, whereas the Sathyendranath *et al.* (2009) method was designed to investigate group-specific trends in phytoplankton properties, and uses a series of criteria to discard samples which may represent mixed populations of phytoplankton. Thus, in the Sathyendranath *et al.* (2009) approach, samples are selected that are dominated by a single group and so a large dataset is required, as the majority of samples are excluded. It should be noted however that many phytoplankton groups, especially in the nanophytoplankton size range, rarely form blooms (Hirata *et al*. 2010) and assessing only samples dominated by marker pigments of a single phytoplankton group could result in omission of certain phytoplankton communities from the analysis. Uitz *et al.* (2008) is much less restrictive, and if a cut-off point of 70% is used to define samples as being dominated by a single size-class, fewer samples are found to have mixed populations than when following the Sathyendranath *et al.* (2009) approach. Consequently, the two approaches differ in the range of temperature for each size-class. Using the Uitz *et al.* (2008) method, samples for this dataset were estimated to be dominated by picophytoplankton at temperatures as low as 3.7 ^{o}C, whereas the coldest

picophytoplankton-dominated sample as defined by Sathyendranath *et al.* (2009) was 12.8 ºC. According to the Uitz *et al.* (2008) approach, biomass is assigned to the picophytoplankton size-class as a result of the presence of either zeaxanthin of chl-*b*, with the low temperature samples which the Uitz *et al* (2008) approach classifies as picophytoplankton dominated having high chl-*b* concentrations, yet little zeaxanthin. While this may indicate the presence of picoeukaryotes such as *Micromonas*, it could be as a result of chl-*b* containing nanoflagellates being wrongly identified as picophytoplankton. Similarly, the temperature range for microphytoplankton-dominated samples is larger when using the Uitz *et al.* (2008) method, with the highest temperature at which microphytoplankton dominated being 10 ºC when following Sathyendranath *et al.* (2009) as compared with 17.9 ºC using Uitz *et al.* (2008). The decrease in cell size as temperature increases confirms the trends seen in studies such as Marañon *et al.* (2001), Bouman *et al.* (2003), Finkel *et al.* (2010). While this relationship is not directly caused by temperature, and high temperature samples dominated by large cells can be found (Marañon *et al.* 2012) for open oceans, temperature is a strong predictor of cell size as it co-varies with so many other environmental variables such as light (Finkel *et al.* 2010), stratification and nutrient supply (Sathyendranath *et al.* 1991, Kamykowski *et al.* 2002). The Sathyendranath *et al.* (2009) approach allocates samples dominated by a single group over a small subset of the total sample number, whereas the Uitz *et al.* (2008) represents a more inclusive approach, producing a larger sample size, at the risk of including more mixed populations. It should also be noted that the methods were developed over different study areas, with Uitz *et al.* (2008) containing many warm samples from the Mediterranean and Sathyendranath *et al.* (2009) focussed more on the North West Atlantic, potentially meaning that the pigment:chl-*a* ratios used in the Uitz *et al.* (2008) approach may be less suited to this study area either due to differences in the phytoplankton groups present, or as a result of differences in photoprotective pigment concentration as a

result of photoacclimation.

4.5.2 Phytoplankton size and *PE* parameters

Relationship between P_m^B and size-class are seen in Fig 4.2a, with microphytoplankton having lower mean values for P_m^B than the other two groups, with no significant differences found between the two methods. Size dependency of P_m^B is consistent with the trends reported in Geider *et al.* (1997) and Le Quéré *et al.* (2005), with small cells generally having higher biomass-normalised rates of photosynthesis which is caused by both direct and indirect effects. Size indirectly affects P_m^B due to basic-scale trends in phytoplankton distributions. Small cells are more likely to be found in warm conditions, and the kinetics of enzyme-catalysed reactions means that reaction rates and hence P_m^B will increase under warm conditions Raven & Geider (1988). Cell size can also directly affect P_m^B via changes in the efficiency of resource usage, with small cells being able to take up nutrients more efficiently than larger cells (Kiørboe 1993) reducing the possibility that P_m^B will be limited by nutrient availability. Small cells are also more efficient at harvesting light due to lower pigment packaging than large cells, since the potential for pigments in cells to absorb light is decreased as cell size increases (Duysens 1956, Kirk 1976, Morel & Bricaud 1981, Sathyendranath *et al.* 1996, Ciotti *et al.* 2002). As self-shading is lower in small cells than in large ones, a small cell is capable of harvesting more light per unit of pigment, meaning lower pigment concentrations are required to harvest sufficient light. It should be noted that while the package effect would appear not to have an effect on P_m^B as by definition light is saturating at this point, small cells will have had to invest less energy in the production of costly light-harvesting pigments (Behrenfeld *et al.* 2008, Key *et al.* 2010), and therefore be able to use this saved energy for other processes which may potentially be P_m^B limiting, such

as nutrient accumulation (Howarth *et al.* 1988).

Higher maximal photosynthetic rates for small cells are not seen in all studies however, with Uitz *et al.* (2008) finding the highest values of P_m^B to be from samples dominated by large cells (microphytoplankton). This discrepancy may be due to differences in the geographical distribution of the two datasets, as in this study samples which were estimated by be dominated by microphytoplankton were mostly located in the temperate North West Atlantic, whereas for the study by Uitz *et al.* (2008) a greater fraction of the data was collected at lower latitudes and the Mediterranean. As temperature is known to strongly affect P_m^B, (Eppley 1972, Raven & Geider 1988, Behrenfeld & Falkowski 1997a) and no warm microphytoplankton-dominated samples were found in this study a direct comparison is therefore not possible. Cermeño *et al.* (2005) also observed higher biomass normalised photosynthetic rates for large cells, however this study used carbon as opposed to chlorophyll for normalisation. Since the package effect means that small cells require lower intracellular concentrations of chlorophyll, the ratio of carbon-to-chlorophyll decreases as cell size increases. By measuring biomass in terms of carbon as opposed to chlorophyll, the biomass specific photosynthetic rates of small cells will be decreased and those of large cells increased.

Strong size-dependent trends are also seen in α^B. Since α^B is dependent on the proportion of incident photons harvested large cells have a major competitive disadvantage (Key *et al.* 2010) due to higher pigment packaging, which means that less light can be harvested per unit of pigment. Since chl-*a* concentration is used as a measure of biomass when normalising α, any increase in the concentration of chl-*a* required to harvest the same amount of light will result in lower values of α^B, and hence the low values of α^B found for microphytoplankton (Fig 4.2b). Nanophytoplankton α^B is much higher than for microphytoplankton, which reflects the increased efficiency of light harvesting and nutrient

uptake that their smaller cell size allows (Morel & Bricaud 1981, Howarth *et al.* 1988). Nanophytoplankton, such as prymnesiophytes, are known to form a large proportion of the biomass around the deep chlorophyll maximum (Gibb *et al.* 2001) where irradiances are very low, meaning that there is strong selective pressure to maximise photosynthetic rates under limiting light. Due to their even smaller size it could be expected that picophytoplankton would have mean values of α^B which were even higher than nanophytoplankton. However, in this study, samples dominated by picophytoplankton are often found at low latitudes, where nutrient concentrations are extremely low and irradiances high. Low nutrient availability is known to decrease α^B (Platt *et al.* 1992, Sosik 1996), while at high light levels, efficient use of light by phytoplankton cells is not selected for (Sosik & Mitchell 1994). High irradiances are also potentially harmful to cells at the sea surface, meaning that photoprotective pigments are required to prevent damage to the photosystems (Dimier *et al.* 2007). Energy absorbed by photoprotective pigments is dissipated as heat, and so cannot contribute towards photosynthesis (Raven 2011), further lowering α^B in samples dominated by picophytoplankton.

Phytoplankton E_k a gives an indication as to the photoacclimatory status of phytoplankton and underwater light environment to which the sample is adapted (Raven 1998). Significant differences according to phytoplankton size-class are also seen for E_k (Fig 4.2c). Since E_k is defined as P_m^B / α^B, size-class specific trends in E_k can be driven either by changes in P_m^B or in α^B. No significant difference is seen between micro- and nanophytoplankton E_k due to P_m^B and α^B co-varying (Behrenfeld *et al.* 2004, Huot *et al.* 2013), so that while nanophytoplankton P_m^B may be higher than that for microphytoplankton, the increase in α^B means that E_k is unchanged. Picophytoplankton however have a high mean P_m^B, combined with a low α^B, and therefore a very high E_k, which reflects the fact that samples

dominated by picophytoplankton are likely to be found at low latitudes, and experience high irradiance (Raven 1998, Marañon *et al.* 2001).

4.5.3 *PE* parameters and depth

Differences in P_m^B between shallow and deep samples for the different size-classes can be explained by the different environmental conditions under which the samples dominated by a single size-class are likely to be found (Fig 4.3). Due to light levels being much lower for deep samples than for those collected from the surface, phytoplankton adapted to conditions deep in the water-column contain much higher intracellular chlorophyll concentrations than those acclimated to surface irradiances (Veldhuis & Kraay 2004). Since P_m is normalised to chlorophyll biomass to obtain P_m^B, an increase in the intracellular chlorophyll levels for the same value of P_m lowers the P_m^B, meaning that changes in the photoacclimatory status with respect to depth would be reflected in the vertical variability of photosynthetic parameters (Babin *et al.* 1996, Bouman *et al.* 2000). A greater difference between surface and deep samples is seen for picophytoplankton than for microphytoplankton as microphytoplankton are more likely to be dominant at higher latitudes, with stronger mixing regimes, than picophytoplankton. Areas with deep mixing result in more uniform populations with respect to depth, as all cells are exposed to a wide range of irradiances, while in highly-stratified waters such as in the Subtropical Gyres, differently acclimated surface and deep populations are found (Moore *et al.* 1995, Moore & Chisholm 1999, Rocap *et al.* 2003, Veldhuis & Kraay 2004). As picophytoplankton dominance is associated with stratified conditions, the difference in P_m^B for shallow and deep samples is greater for picophytoplankton than for microphytoplankton. There are insufficient samples to determine if such differences would be found in areas dominated by nanophytoplankton. The lack of nanophytoplankton-dominated

samples reflects important aspects both about the ecology nanophytoplankton and the assumptions made in this study. Nanophytoplankton are very taxonomically diverse (Bouman *et al.* 2012) and contain a diverse array of pigments, making identification using pigment-based approaches difficult. In addition, while nanophytoplankton may form a large proportion of the total biomass (Hirata *et al.* 2010), unlike pico- or microphytoplankton, blooms rarely form (Li 2002, Uitz *et al.* 2006).

4.5.4 P_m^B and temperature

4.5.4a P_m^B and temperature – for all samples

The data presented show a clear envelope for the relationship between temperature and P_m^B for all samples, with the samples thought to be dominated by a single phytoplankton size-class differing slightly according to the classification method used (Fig 4.4). The overall shape of the curves and distributions of the points are the same, the difference being which samples are deemed to be dominated by a single size-class. As one traverses from the tropics to temperate regions there is a change from highly-stratified, warm oligotrophic waters dominated by prokaryotic picophytoplankton to more turbulent, eutrophic colder conditions dominated by larger eukaryotes, in particular the diatoms (Platt *et al.* 2005, Nair *et al.* 2008, Brewin *et al.* 2010), and this is reflected in this study with the progression from picophytoplankton dominance at high temperatures to microphytoplankton-dominated samples at low temperature. The growth rate curve of an individual species obtained from culture experiments shows narrow temperature tolerances, displaying initially an increase from the point at which growth is first possible up to an optimal level, before rapidly decreasing again (Eppley 1972), meaning that the overall relationship between growth and temperature is as a result of changes in the phytoplankton species present, not changes in the response of a single species. Growth rates are distinct from P_m^B as they concern the rate of

cell divisions as opposed to carbon fixation. A conversion between the two is possible however (Antoine & Morel 1996b) by normalising the growth curve to a fixed value for P_m^B at a given temperature.

The logarithmic relationship between temperature and optimum growth rate obtained from Eppley (1972) used a range of phytoplankton species in culture and found growth rates increased with increasing temperature. Since the study of Eppley (1972) was performed using cultures however, it may not have captured the variability in conditions natural populations experience, as many other factors such as nutrient availability and irradiance co-vary with temperature. The general pattern of the Eppley growth curve corresponds reasonably well with the temperature dependence of P_m^B obtained in this study until about 18 ºC (Fig 4.4). At higher temperatures, however, there is a divergence between the field and culture data. The increase in P_m^B at low temperatures (< 15 °C) can be explained by the kinetics of enzyme-catalysed reactions, in this case the activity of Rubisco, increases with temperature due to the increased collision rate. Complicating effects though come from the different forms of Rubisco present in different phytoplankton groups (Tortell *et al.* 2000). Rubisco is a highly conserved, inefficient enzyme, capable of using both CO_2 and O_2 as a substrate, though the forms seen in most eukaryotic phytoplankton display higher CO_2 specificities than those see in terrestrial plants (Macintyre *et al.* 2000). Some groups, such as cyanobacteria, use a form that is less selective for CO_2, however increased investment in carbon-concentrating mechanisms means this is not reflected in decreased carbon fixation at higher temperatures (Raven 1991). Raven & Geider (1988) reported a Q_{10} of between 1.5 and 2.6, which agrees with the 2 to 2.5 fold increase seen with our data at temperatures below 15 ºC. Using global *in-situ* data Behrenfeld & Falkowski (1997a) suggested a 7th-order polynomial relationship between temperature and P_{opt}^B which allowed the reduction in biomass-normalised

productivity at high temperatures to be included. It should be noted that P_{opt}^{B} is distinct from P_{m}^{B} in that the P_{opt}^{B} parameter is derived from longer *in-situ* incubations (from 2 to 24 hours (Behrenfeld & Falkowski 1997a)) and it describes the optimum value for the water-column instead of that for a given depth and instantaneous point in time like P_{m}^{B}. As such the values for each cannot easily be directly compared although the overall trends can, with the shape of the relationship found in the study of Behrenfeld & Falkowski (1997a) fitting midway between the 10% and 90% quantiles from this study.

The line showing the 90% quantile for P_{m}^{B} should be regarded as the phytoplankton response under ideal conditions for which the species present are optimised, just as Eppley (1972) used peak growth rate for each species. However, it should be noted that in natural assemblages, such optimal conditions are rarely observed. The majority of production rates are far lower than this upper bound due to the effect of nutrient or light-limitation or changes in the community structure. Alternatively ATP and NADPH can be diverted into direct usage such as cell maintenance, without the photosynthate ever passing through a carbon form. This effect is particularly pronounced at low temperatures (Behrenfeld *et al.* 2004).

4.5.4b Size-specific relationships between P_{m}^{B} and temperature

In addition to considering the effect of temperature on the response of the overall assemblage, the relationship between P_{m}^{B} and temperature can be assessed for samples dominated by a single phytoplankton size-class. Figure 4.5 shows the different relationships between P_{m}^{B} and temperature for the each of the phytoplankton size-classes, for both classification methods. A strong, positive, linear correlation between P_{m}^{B} and temperature is seen for samples estimated to be dominated by microphytoplankton using either method. The Uitz *et al.* (2008) method however identifies samples as being dominated by microphytoplankton at much higher

temperatures than that of Sathyendranath *et al.* (2009). For samples dominated by nanophytoplankton, the trends differ according to the classification strategy used, with the Uitz *et al.* (2008) method showing no trend while a positive linear relationship between P_m^B and temperature is seen following the Sathyendranath *et al.* (2009) approach. The lack of a significant relationship may result from the Uitz *et al.* (2008) approach wrongly identifying mixed populations as dominated by nanophytoplankton. Alternatively the Uitz *et al.* (2008) approach may be incorrectly classifying samples as being dominated by microphytoplankton when in fact they consist of nanophytoplankton, an issue which was seen in Chapter 3 when comparing the pigment-based method of estimating phytoplankton MESD with an absorption-based approach. Samples categorised as being dominated by picophytoplankton also show different responses according to the method used, with a strong negative linear relationship observed when following the Sathyendranath *et al.* (2009) method and a very weak trend using the Uitz *et al.* (2008) approach. While similar samples were identified at temperatures over 15 ^{o}C, when using the Uitz *et al.* (2008) method any trends may be masked by a large number of surprisingly low-temperature samples which were found to be picophytoplankton-dominated. It is likely that this reflects the difficulty in correctly apportioning biomass within mixed samples, owing to a lack of unique indicator pigments for most groups. Thus when using a large dataset, the Sathyendranath *et al.* (2009) method provides a more accurate representation of samples dominated by a particular taxon or size-class owing to its strict exclusion-based approach towards mixed assemblages.

The positive relationship between P_m^B and temperature for samples identified as dominated by microphytoplankton using classification methods and those found to be dominated by nanophytoplankton using the Sathyendranath *et al.* (2009) approach may be caused by enzymatic effects on the dark reactions of photosynthesis. Increasing temperature results in an increased P_m^B due to standard reaction kinetics with a Q_{10} of 2.47 for

microphytoplankton, and 2.16 for nanophytoplankton, agreeing with Raven & Geider (1988), who found it to be between 1.5 and 2.6. Samples dominated by picophytoplankton, however are found to show a negative relationship between P_m^B and temperature, probably reflecting the strong negative correlation between temperature and nutrient supply in the open ocean (Sathyendranath *et al.* 1991, Kamykowski *et al.* 2002). Behrenfeld & Falkowksi (1997) confirm that temperature is unlikely to cause this effect directly. Instead the low values of P_m^B for very high temperature samples are a result of extreme nutrient limitation in very warm stratified conditions (Geider *et al.* 1997), coupled with increased energetic costs of photoprotection (Raven 2011).

The clear and linear positive relationship between P_m^B and temperature seen in this study for samples dominated by microphytoplankton may help to account for the fact that Uitz *et al.* (2008) found microphytoplankton-dominated samples to have the higher values of P_m^B than those dominated by smaller cells. While microphytoplankton P_m^B was low in this study, no samples were found to be dominated by microphytoplankton at high temperatures. The relationship observed between temperature and microphytoplankton P_m^B would however predict high values of P_m^B if such high-temperature, high-irradiance, microphytoplankton-dominated samples were to be found (Fig 4.5). The disparity in mean P_m^B values for samples dominated by microphytoplankton between this study and that of Uitz *et al.* (2008) therefore results from a difference in the regime in which the samples are found combined with the different species of microphytoplankton present. Uitz *et al.* (2008) recorded values of microphytoplankton P_m^B of up to 4.26 mg C (mg chl-*a*)$^{-1}$ h^{-1}, which would be predicted at a temperature of 11.2 ^{o}C using the relationship seen between microphytoplankton P_m^B and temperature following the Sathyendranath *et al.* (2009) approach, or 17.2 ^{o}C using that of Uitz *et al.* (2008).

4.5.5 α^B and temperature

4.5.5a α^B and temperature – for all samples

Temperature-dependent trends in α^B for all samples are of a similar shape to those for P_m^B, with minima at extremes of temperature and increased mean levels and variability at intermediate temperatures (Fig 4.4). α depends on the amount of light absorbed by phytoplankton and the maximum quantum yield φ_m (MacIntyre *et al.* 2002).

$$\alpha^B = (\varphi_m \, \bar{a}^*_{ph\,(400\text{-}700)})/0.0231, \quad (5)$$

where $\bar{a}^*_{ph\,(400\text{-}700)}$ is the mean chlorophyll-specific absorption coefficient of phytoplankton, between 400 and 700nm, and the constant 0.0231in the numerator converts grams to moles and hours to seconds. In trying to understand the relationship between temperature and α^B it should be noted that trends in P_m^B and α^B are tightly linked. Various studies such as Behrenfeld *et al.* (2004) have implicated nutrients and photoadaptation, with increases in both α^B and P_m^B across the nutricline. Temperature is also closely linked to irradiance and stratification, with warm subtropical regions being far more stratified and receiving much higher irradiances averaged across the mixed layer than cold temperate areas. Nutrients alone cannot be responsible for variations in α^B however as otherwise α^B for low temperature stations would be higher due to the high nutrient concentrations resulting from mixing. When light intensity is strong, efficient harvesting of light is of low importance meaning that α^B will be lower at high temperatures. Alternatively as suggested by Platt *et al.* (1992) parallel changes in α^B and P_m^B might both as a result of changes in quantum yield, implying that φ_m may be varying as a result of changes in temperature or phytoplankton type. Cold waters tend to be dominated by large microphytoplankton such as diatoms, while in warmer waters smaller cells predominate

with higher mean values of $\bar{a}^*_{ph\ (400\text{-}700)}$, causing lowered values of α^B at low temperatures. φ_m is also strongly dependent on nutrient status and the highly oligotrophic conditions found in the very warm, stratified areas will result in a low quantum yield (Platt *et al.* 1992, Falkowski & Wilson 1992, Sosik & Mitchell 1994, Sosik 1996) therefore further contributing to the low levels of α^B seen at high temperatures.

4.5.5b Size-specific relationships between α^B and temperature

Trends in the relationship between α^B and temperature can be seen even more clearly when considering the responses of an individual size-class (Fig 4.6). A positive linear relationship between temperature and α^B is seen for microphytoplankton-dominated samples for both pigment-based classification methods, which may be due to the increased importance of light-dependent mitochondrial synthesis of ATP at low temperatures, which can consume a large proportion of the photosynthetic reductant, without carbon fixation (Behrenfeld *et al.* 2004). Alternatively the positive relationship may be due co-variation in P_m^B and α^B as proposed by Platt *et al.* (1992) and Behrenfeld *et al.* (2004), with increased temperatures resulting in higher values of φ_m. Samples dominated by nanophytoplankton show consistently high values for α^B with both classification methods, reflecting the *k*-strategist ecological role of nanophytoplankton, which specialise in maximising efficiency, including of light harvesting (Chisholm 1992). Nanophytoplankton also are known to form a large proportion of the biomass at the deep chlorophyll maximum (Gibb *et al.* 2001) where low irradiances mean high values of α^B will be selected for. Samples found to be dominated by picophytoplankton using the Sathyendranath *et al.* (2009) method show a strong negative relationship between α^B and temperature caused by the link between high temperatures, damaging light levels and extreme nutrient limitation in highly stratified waters. The same pattern is again visible for the very warm samples found to be dominated by

picophytoplankton using the approach of Uitz *et al.* (2008), but overall the trend masked by the large number of colder stations.

4.5.6 E_k and temperature

The majority of the samples display E_k-independent variation, with increases in E_k being seen only for the warmest stations (Fig 4.4), a relationship which confirms the results of previous studies such as Marañon & Holligan (1999) and Behrenfeld *et al.* (2004) where the highest values of E_k were also found to be associated with warm, subtropical waters. As E_k is correlated with the light intensity to which a phytoplankton population is adapted (Barlow *et al.* 2010), one can use the idea of ecological specialisation when considering the trends seen in E_k. The relationships are made even clearer when considering only samples dominated by a single phytoplankton size-class (Fig 4.7). Increases in E_k represent a strategy of acclimation to high light levels (Geider 1996, Behrenfeld *et al.* 2004), since in the highly-stratified subtropics efficient harvesting of light is not a high priority for phytoplankton, unlike efficient nutrient use. It is thought that E_k-independent variation is driven by changes in the quantum yield and not α^B (Platt *et al.* 1992). Since the increase in Ek at high temperatures is seen for samples where P_m^B is decreasing, this change must be driven by a decrease in α^B. The increase in E_k at high temperatures therefore demonstrates a major shift from maximising φ_m to prioritising photoprotection, especially as the proportion of samples dominated by picophytoplankton increases with temperature, and these smaller cells will have higher values of $\bar{a}^*_{ph\,(400\text{-}700)}$ due to the package effect.

4.5.7 *PE* parameters and nutrients

There appears to be little trend in P_m^B with respect to nutrient concentration either for a population as a whole or within samples dominated by a single phytoplankton size-class according to either classification method (Fig 4.9). NO_3^- is generally considered the one of the main limiting nutrients in the North Atlantic (Levitus *et al.* 1993). At high nutrient concentrations (above 10 μmol/l) there is little variability in P_m^B, although the rates of P_m^B are low. Samples under mesotrophic conditions ($NO3^-$ concentrations between 1-10 μmol/l) display a much wider range of P_m^B, with the mean value being more than twice what is found in waters with higher concentrations, before values of P_m^B drop again when nutrient levels are very low ($NO3^-$ below 1 μmol/l), as even the most efficient cells become nutrient limited. The trends seen here are as a result of the nutrient data consisting of instantaneous values, which are a poor indicator of nutrient status (Barlow *et al.* 1993), as opposed to long term fluxes. Since the lag time on nutrient assimilation may be several days (Omand *et al.* 2011) it is therefore difficult to distinguish between a population that has recently been nutrient replete and still has sufficient internal reserves, even though the outside concentration is low, and one which has been subjected to nutrient stress for weeks or months.

While it would be expected that there would be a strong correlation between nutrient levels and α^B due to the nutrient dependence of φ_m (Platt *et al.* 1992), this is not seen, (Fig 4.9) for the same reason that little relationship was seen between P_m^B and nutrient concentration, namely that instantaneous measurements of nutrient concentration do not provide information on nutrient flux to the surface layer. Similarly, no relationship is seen for E_k.

4.5.8 z_e/z_m and P_m^B

The ratio of the depth where light is 1% of that found at the surface to the depth of mixing is a key indicator for the light regime to which a phytoplankton population is adapted (Uitz *et al.* 2008). Samples at stations where the depth of mixing is close to or greater than the euphotic depth will be adapted to low light conditions, even if the sample itself is taken from near the surface. Samples estimated to be dominated by microphytoplankton following either the Sathyendranath *et al.* (2009) or the Uitz *et al.* (2008) classification approach were more prevalent at low values of z_e/z_m, confirming the results of previous studies which have found microphytoplankton to dominate in well mixed areas (Fig 4.8) (Margalef 1968, Key *et al.* 2010, Sciascia *et al.* 2012). In particular, of the samples where z_e/z_m is less than 1, almost all are microphytoplankton-dominated. Overall however, much stronger relationships are seen between the *PE* parameters and temperature than with z_e/z_m, implying that temperature is a better descriptor of general environmental conditions than z_e/z_m.

4.5.9 Principal component analysis of forcing factors affecting *PE* parameters

By using PCA, all input variables are considered simultaneously and their interrelationships can be examined. Temperature is confirmed as the dominant variable, and is responsible for the largest portion of the variation on the first PCA axis, reflecting how well temperature is correlated with the overall environmental conditions. If temperature is the most important of the physical forcing components, the corresponding biological response comes from changes in the size structure of the phytoplankton population. The change in the size structure is shown by the vector concerning the proportion of the biomass due to microphytoplankton, which is in almost exactly the opposite direction to that for temperature. The proportion of the biomass due to microphytoplankton is in turn positively correlated with chl-*a* concentration, as seen in Uitz *et al.* (2008). The association of high biomass with

microphytoplankton is indeed reflected in the trends seen in Figure 4.4, where high temperatures are associated with highly stratified, stable systems dominated by picophytoplankton and low temperature samples are dominated by microphytoplankton. In the ecological space displayed by PCA ordination analysis samples dominated by microphytoplankton are seen in the bottom right hand corner of the plot, with the highest chlorophyll concentrations, showing that in this dataset microphytoplankton are the size class responsible for blooms. There is however almost no link with the maximising the efficiency of light usage as would be shown by a correlation between microphytoplankton biomass and α^B, or with P_m^B. Nanophytoplankton cluster in the bottom left hand corner of the plot along with both α^B and P_m^B showing their high photosynthetic efficiency, and their adaptation to a stable environment, where photosynthetic efficiency is more important than peak biomass (Estrada & Berdalet 1997, Cullen *et al.* 2002). Relationships between forcing factors can also be considered with respect to α^B, with the bottom left hand portion of the plot showing those samples with the highest values of α^B. α^B is seen to be acting in the opposite direction from PAR, suggesting that phytoplankton optimised to low light levels will display high light-harvesting efficiencies and that those optimised for high light conditions are not investing in optimising light-harvesting, but may also require photoprotection to avoid damage, leading to lower values of α^B. Samples dominated by picophytoplankton are clustered in the top left of the plot, and are associated with high temperatures and irradiances along with low chlorophyll concentrations, reflecting the warm, high-light, low-biomass conditions in which they are dominant.

For the purposes of estimating net carbon fixation, temperature in conjunction with phytoplankton size-class, which in turn reflects overall phytoplankton biomass, is by far the most informative of the remotely-sensed variables as an indicator of photosynthetic performance. Even when considering *in-situ* data where pigment-based methods of ascribing

phytoplankton class can be applied, this additional information appears to remove only a limited amount of the total variation as compared with temperature alone. What pigment-based taxonomic identification approaches do allow however is the assessment of the effect of a changing environment within a phytoplankton group. Changes in the groups present may not alter the overall rate of carbon fixation but will greatly alter its fate. Large cells contribute more to export out of the photic zone due to their high rates of sinking, whereas small cells are likely to be remineralised *in-situ*. The zooplankton predators present will also depend on the prey available and in turn the energy will be channelled into different trophic pathways. In addition to aiding with quantitative estimates of the contributions of each taxonomic group and hence the fate of the fixed carbon, the dynamic ranges of *PE* parameters seen within groups here illustrate the limitations of using a single parameter per size or taxonomic class.

This study has important implications for both remote-sensing of phytoplankton primary production and *in-situ* studies. As remote-sensing retrieval of phytoplankton functional type improves (Sathyendranath *et al.* 2001, 2004, Nair *et al.* 2008) these group-specific relationships between *PE* parameters and temperature can be applied to remotely-sensed chlorophyll data providing not only for an accurate assessment of overall rates of primary production, but also the size-classes responsible, allowing a greater understanding of the energy dynamics of the different trophic webs. The trends in size-class-specific production can also be applied in more general biogeochemical models of the pelagic system such as dynamic green ocean models (LeQuéré *et al.* 2005), while i*n-situ* studies will also benefit from improved estimates of productivity. Since the *PE* parameters are expensive and time consuming to assess owing to the need to use radioactive material, in many cases they are not measured. The approach presented here of estimating P_m^B using a combination of HPLC pigments and easily measured environment variables will help to extrapolate class-specific estimates of phytoplankton primary production from ^{14}C-based data.

4.6 Conclusions

This study has used an extensive database of *PE* parameters and HPLC pigment concentrations to first compare two pigment-based approaches for estimating phytoplankton population structure, and then to examine the effect of abiotic forcing on different size-classes of phytoplankton. For the purpose of identifying samples dominated by a single phytoplankton size-class, the method of Sathyendranath *et al.* (2009) was found to be more suitable provided the sample size was sufficiently large as the majority of samples are excluded due to being mixed populations. The approach of Uitz *et al.* (2008) however may be more appropriate if sample sizes were small as it instead provides estimates of the proportion of the total biomass in each three size classes, for all samples. Both methods found the mean phytoplankton size decreased as temperature increased, however the temperature ranges for samples dominated by each size class were wider when using the Uitz *et al.* (2008) method than the Sathyendranath *et al.* (2009) approach.

Temperature was found to be the best predictor of *PE* parameters in mixed populations. P_m^B and α^B increased with temperature until plateauing at 15 ^oC, and decreasing above 17.5 ^oC. E_k was found to be constant for most of the temperature range before increasing sharply above 17.5 ^oC. Only weak relationships were seen with respect to the *PE* parameters and both nitrate concentration, and the ratio between the depth of the1% light level and the depth of mixing.

Mean microphytoplankton P_m^B was found to be significantly lower than for the other size-classes, for both classification methods. No difference was observed in P_m^B between samples dominated by picophytoplankton and those dominated by nanophytoplankton. Nanophytoplankton α^B was also found to be significantly higher than the other size-classes.

The low values for microphytoplankton α^B are likely to be due to their large size, as the package effect means that higher intracellular chlorophyll concentrations are required to harvest the same quantity of light. Picophytoplankton α^B values are also low, due to the very high irradiances they experience, meaning that investment in the efficient harvesting of light is superfluous. This is confirmed by the size-related trends seen in E_k as picophytoplankton show significantly higher values, a result of their very low mean α^B value.

Within-group trends in *PE* parameters with respect to temperature were investigated, with microphytoplankton demonstrating a significant, positive linear relationship between temperature and both P_m^B and α^B for both classification methods. For the Sathyendranath *et al.* (2009) approach picophytoplankton P_m^B was negatively correlated with temperature, perhaps owing to photodamage or investment in photoprotection. Nanophytoplankton *PE* parameters display only weak trends with respect to temperature. A positive relationship with respect to temperature is seen for E_k in all size-classes. Other environmental variables such as nitrate concentration and z_e/z_m were found to show little relationship with the *PE* parameters. Trends in phytoplankton size and *PE* parameters with respect to environmental forcing are confirmed using a PCA, which demonstrates that the proportion of microphytoplankton correlates with high biomass and low temperatures, the proportion of nanophytoplankton with efficiency of light-harvesting and P_m^B. Picophytoplankton abundance is associated with high temperatures and high light intensities.

The size-class specific relationships between *PE* parameters and temperature are suited to being used in remote-sensing models of primary production. By relating the *PE* parameters to temperature as opposed to using a fixed value for each phytoplankton class, more accurate estimates will be possible. While it may be possible to obtain remotely-sensed estimates of primary production without considering the different size-classes of phytoplankton, dividing primary production estimates according to size-class will allow a

more detailed understanding of the energy flows through the pelagic system as the type of trophic pathway supported depends strongly on the size-class of phytoplankton responsible for the production.

Chapter 5: Conclusions and future work

5.1 Conclusions of study

The work presented in this thesis addresses three distinct stages in understanding the ecological functioning of phytoplankton in the Atlantic Basin. The first stage develops a method to determine the taxonomic composition of mixed phytoplankton populations. The second applies this method to improve our understanding of how these populations change as a result of seasonal succession. The third assesses how the photophysiological response of each size-class of phytoplankton is dictated by environmental forcing. To this end, the simple and widely-applied approach of Uitz *et al.* (2008) for dividing phytoplankton biomass into three size-classes was applied to a database of phytoplankton pigments, photophysiology and environmental variables from the Atlantic, and in each results chapter was compared with more specialised or complex methods. While a great range of tools are available for researchers studying phytoplankton distributions and dynamics, the results from this work demonstrate that each approach has its merits and shortcomings, but that clear biogeochemical, ecological and successional patterns emerge using each method.

Chapter 2 addressed the question of how to use bulk pigment data to identify phytoplankton groups present within a sample, with specific reference to the Atlantic Gyres. To this end, three methods of using HPLC accessory pigment data to estimate phytoplankton taxonomic distributions were evaluated, with the chlorophyll based biomass estimates from each method being compared with flow cytometry data. The results were then used to identify depth-dependent trends in phytoplankton size, community structure and photoacclimation, from which the following conclusions can be drawn.

- Variations in the carbon-to-chlorophyll ratio in phytoplankton mean that any comparison between chlorophyll-based estimates of biomass and those using either carbon or cell abundance will inevitably propagate considerable errors. The depth-dependent trends in carbon-to-chlorophyll ratios for different phytoplankton groups that were identified in this chapter will be of considerable use in biogeochemical models.
- Both the size-based approach of Uitz *et al.* (2008) and the taxa-based approach of Bidigare & Ondrusek (1996) consistently overestimated the importance of microphytoplankton, while the taxa-based approach also produced significant samples with a negative prokaryotic biomass. These errors were likely caused by using the methods outside the areas where they were initially calibrated.
- Variable pigment:chl-*a* approaches such as CHEMTAX are highly sensitive to the conditions under which they are run, and users must be careful to ensure that both the starting values of the pigment:chl-*a* ratio matrix and the eventual outputs are biologically plausible. The iterative nature of CHEMTAX means that it is occasionally possible for pigment:chl-*a* ratios to increase indefinitely as opposed to converging on the correct value. Another important finding of the CHEMTAX analyses is that unexplained residual errors arising from CHEMTAX can be low, even if the pigment:chl-*a* ratios are unrealistically constrained in the initial set up.
- The relative importance of *Prochlorococcus* and *Synechococcus* using CHEMTAX can be subject to significant errors in the model outputs, with estimates of cell biomass being markedly different from those observed using flow cytometry.

Chapter 3 examined how the composition of phytoplankton populations is related to the environmental controls that govern phytoplankton taxonomic succession in temperate marine

systems. Whereas Chapter 2 focussed solely on the Atlantic Gyres, Chapter 3 focussed on the North West Atlantic where the seasonal range of cell sizes is much greater. It also addressed the successional patterns seen in both pigment markers and the absorptive properties of phytoplankton, which may be considered as indicators of the size structure of the entire phytoplankton population. From these results the following conclusions can be made:

- While the HPLC-based method of Bricaud *et al.* (2004) for estimating mean equivalent spherical diameter (MESD) is simple and quick to implement, anomalous spikes in the size spectrum were found at the upper size limit of the method (50 μm). The absorption-based method of Roy *et al.* (2011) produced results which fitted more closely to the size structure predicted by previous theoretical and experimental studies.
- Using cluster analysis trends in succession were seen to be strongly linked to season and stratification. Under well-mixed conditions in spring, populations were dominated by large fucoxanthin-containing cells. Fucoxanthin remained important during early summer, but MESD decreased. During summer when stratification was at the most intense samples were dominated by very small picoeukaryotes, which were replaced in autumn by nanoflagellates and chrysophytes in autumn as stratification decayed. A population of dinoflagellates was found to be present throughout the year.
- Strong positive relationships were seen between MESD and chlorophyll concentration, while strong negative correlations are found between MESD and both the intensity of stratification and temperature. Such relationships have the potential to improve the retrieval of phytoplankton size from remote-sensing variables.
- A positive relationship is seen between MESD and φ_m. This increased efficiency of light usage may be to compensate for the decreased efficiency of light-harvesting. Negative relationships were seen for mean daily mixed-layer PAR and both α^B and φ_m.

While the main focus of Chapters 2 and 3 was on the distributions and successional trends of phytoplankton, Chapter 4 aims to relate phytoplankton photosynthetic parameters to environmental variables, both for mixed assemblages, and for those dominated by a single phytoplankton size class. The following conclusions were obtained from these results.

- The approach of using diagnostic pigments (Sathyendranath *et al.* 2009) is effective at identifying samples dominated by a single phytoplankton size-class in the North Atlantic. These samples can then be used to analyse group-specific properties using field observations.
- Temperature is the best predictor of phytoplankton *PE* parameters, although it is unlikely to be the sole cause of the variability observed. Instead, temperature provides a proxy for the overall environmental conditions (light, nutrients, stratification) to which phytoplankton communities are adapted.
- P_m^B and E_k increase as average cell size decreases, while α^B is highest for the nanophytoplankton size-class.
- Positive correlations between P_m^B and temperature were observed for the micro- and nanophytoplankton size-classes, while picophytoplankton show a negative correlation. A positive correlation between temperature and α^B is seen for microphytoplankton, and a negative relationship for picophytoplankton. E_k increases with temperature for all size classes. The size-specific trends between temperature (an environmental variable that can be observed from remote sensing) and phytoplankton photophysiology can be used to improve out estimate of the relative contributions each size-class makes to primary production on a global scale using ocean-colour remote sensing. Moreover, these results highlight that considerable variability in photophysiology exists within phytoplankton size or taxonomic groups which may

lead to significant errors in assessing their contributions to primary production (especially on a regional or seasonal basis) if fixed values are used.

5.2 Future work

This thesis has identified a series of important spatial and temporal patterns in the size structure and physiological functioning of natural phytoplankton populations. These patterns can be explained by the abiotic factors governing phytoplankton growth, namely temperature, light, nutrient availability and stratification. Yet further work is required on refining methods that use HPLC pigments for chemotaxonomy, since although results from Chapter 2 show promising agreement between flow cytometry counts and pigment-based biomass estimates for Gyre, validation datasets for higher latitudes, where larger cells dominate and microscope counts are required, are lacking. Such validation datasets are also required to test the models that estimate MESD from phytoplankton absorption coefficients as used in Chapter 3. Given that *in-situ* absorption was estimated to be greater than the predicted absorption in solution, there is a need to obtain better estimates of the absorptive properties of pigment-protein complexes in suspension across a range of phytoplankton groups. Finally, the size-specific trends in *PE* parameters identified in Chapter 4 should be further resolved to include different phytoplankton functional types, since while size provides a valuable first approximation to phytoplankton ecological properties, many cells with similar sizes can fill very different biogeochemical roles, especially within the nanophytoplankton, where the greatest differences occurred between methods. To achieve this goal would require a combination of techniques to physically separate cells in the field and probe their physiological properties, such as the use of fast-sorting flow cytometers, combined with ^{14}C methods.

While some further work is required to refine the techniques and relationships seen in this study, the results on the size-specific relationships between phytoplankton size and photophysiology arising from this thesis can be directly applied to the next generation of remote-sensing primary productivity studies, particularly if the relationships between

temperature, stratification and phytoplankton succession are included. In addition, the relationships between MESD and temperature will aid understanding of the impact of climate and phytoplankton biogeography on the ocean carbon cycle, both on a seasonal, and a longer-term basis, with implications for climate-change studies and fisheries management.

References

AIKEN, J., HARDMAN-MOUNTFORD, N.J., BARLOW, R., FISHWICK, J., HIRATA, T. and SMYTH, T., 2008. Functional links between bioenergetics and bio-optical traits of phytoplankton taxonomic groups: an overarching hypothesis with applications for ocean colour remote-sensing. *Journal of Plankton Research,* **30**(2), pp. 165-181.

AIKEN, J., PRADHAN, Y., BARLOW, R., LAVENDER, S., POULTON, A., HOLLIGAN, P., & HARDMAN-MOUNTFORD, N. 2009. Phytoplankton pigments and functional types in the Atlantic Ocean: A decadal assessment, 1995—2005. *Deep-sea research. Part 2. Topical Studies in Oceanography*, **56**(15), 899-917.

AKSNES, D. and EGGE, J., 1991. A theoretical model for nutrient uptake in phytoplankton. *Marine Ecology Progress Series,* **70**(1), pp. 65-72.

ALLDREDGE, A.L. and GOTSCHALK, C., 1988. In Situ Settling Behavior of Marine Snow. *Limnology and Oceanography,* **33**(3), pp. 339-351.

ALLEN, W., 1921. Some work on marine phytoplankton in 1919. *Transactions of the American Microscopical Society,* **40**(4), pp. 177-181.

ALVAIN, S., MOULIN, C., DANDONNEAU, Y. and BRÉON, F.M., 2005. Remote sensing of phytoplankton groups in case 1 waters from global SeaWiFS imagery. *Deep Sea Research Part I: Oceanographic Research Papers,* **52**(11), pp. 1989-2004.

ANTOINE, D. and MOREL, A., 1996. Oceanic primary production: 1. Adaptation of a spectral light-photosynthesis model in view of application to satellite chlorophyll observations. *Global Biogeochemical Cycles,* **10**(1), pp. 43-55.

ÁLVAREZ, E., LÓPEZ-URRUTIA, Á., NOGUEIRA, E. and FRAGA, S., 2011. How to effectively sample the plankton size spectrum? A case study using FlowCAM. *Journal of Plankton Research,* **33**(7), pp. 1119-1133.

ANTONOV, J.I., SEIDOV, D., BOYER, T.P., LOCARNINI, R.A., MISHONOV, A.V., GARCIA, H.E., BARANOVA, O.K., ZWENG, M.M. and JOHNSON, D.R., 2010. *World Ocean Atlas 2009, Volume 2: Salinity.* U.S. Government Printing Office,.

AZAM, F., FENCHEL, T., FIELD, J.G., GRAY, J.S., MEYER-REIL, L.A. and THINGSTEAD, F., 1983. The ecological role of water column microbes in the sea. *Marine Ecology Progress Series,* **10**(3), pp. 257-263.

BABIN, M., MOREL, A., CLAUSTRE, H., BRICAUD, A., KOLBER, Z. and FALKOWSKI, P.G., 1996. Nitrogen-and irradiance-dependent variations of the maximum quantum yield of carbon fixation in eutrophic, mesotrophic and oligotrophic marine systems. *Deep Sea Research Part I: Oceanographic Research Papers*, **43**(8), pp. 1241-1272.

BABIN, M., MOREL, A. and GAGNON, R., 1994. An Incubator Designed for Extensive and Sensitive Measurements of Phytoplankton Photosynthetic Parameters. *Limnology and Oceanography,* **39**(3), pp. 694-702.

BACH, L., RIEBESELL, U., SETT, S., FEBIRI, S., RZEPKA, P., & GEORG SCHULZ, K. 2012. An approach for particle sinking velocity measurements in the 3—400 μm size range and considerations on the effect of temperature on sinking rates. *Marine*

Biology, **159**(8), 1853-1864.

BARBER, R.T. and HISCOCK, M.R., 2006. A rising tide lifts all phytoplankton: Growth response of other phytoplankton taxa in diatom-dominated blooms. *Global Biogeochemical Cycles*, **20**(4), GB4S03.

BARLOW, R.G., MANTOURA, R.F.C., GOUGH, M.A. and FILEMAN, T.W., 1993. Pigment signatures of the phytoplankton composition in the northeastern Atlantic during the 1990 spring bloom. *Deep Sea Research Part II: Topical Studies in Oceanography*, **40**(1–2), pp. 459-477.

BARLOW, R. G., AITKEN, J., HOLLIGAN, P. M., CUMMINGS, D. G., MARITORENA, S., & HOOKER, S. 2002. Phytoplankton pigment and absorption characteristics along meridional transects in the Atlantic Ocean. *Deep Sea Research Part I: Oceanographic Research Papers*, **49**(4), 637-660

BARLOW, R.G., CUMMINGS, D.G. and GIBB, S.W., 1997. Improved resolution of mono- and divinyl chlorophylls *a* and *b* and zeaxanthin and lutein in phytoplankton extracts using reverse phase C-8 HPLC. *Marine Ecology Progress Series*, **161**, pp. 303-307.

BARLOW, R., LAMONT, T., KYEWALYANGA, M., SESSIONS, H., & MORRIS, T. 2010. Phytoplankton production and physiological adaptation on the southeastern shelf of the Agulhas ecosystem. *Continental Shelf Research*, **30**(13), 1472-1486.

BEAUGRAND, G., BRANDER, K. M., LINDLEY, J. A., SOUISSI, S., & REID, P. C. 2003. Plankton effect on cod recruitment in the North Sea. *Nature*, **426**(6967), 661-664.

BEHRENFELD, M. J., & FALKOWSKI, P. G. 1997a. Photosynthetic rates derived from

satellite-based chlorophyll concentration. *Limnology and Oceanography*, **42**(1), 1-20.

BEHRENFELD, M. J., & FALKOWSKI, P. G. 1997b. Photosynthetic rates derived from satellite-based chlorophyll concentration. *Limnology and Oceanography*, **42**(1), 1-20.

BEHRENFELD, M. J., PRASIL, O., BABIN, M., & BRUYANT, F. 2004. In search of a physiological basis for covariations in light-limited and light-saturated photosynthesis. *Journal of Phycology*, *40*(1), 4-25.

BEHRENFELD, M.J., BOSS, E., SIEGEL, D.A. and SHEA, D.M., 2005. Carbon-based ocean productivity and phytoplankton physiology from space. *Global Biogeochemical Cycles,* **19**(1), pp. GB1006.

BEHRENFELD, M.J., HALSEY, K.H. and MILLIGAN, A.J., 2008. Evolved physiological responses of phytoplankton to their integrated growth environment. *Philosophical transactions of the Royal Society of London. Series B, Biological sciences,* (**1504**), pp. 2687-2703.

BEL HASSEN, M., DRIRA, Z., HAMZA, A., AYADI, H., AKROUT, F. and ISSAOUI, H., 2008. Summer phytoplankton pigments and community composition related to water mass properties in the Gulf of Gabes. *Estuarine, Coastal and Shelf Science,* **77**(4), pp. 645-656.

BERGESCH, M., & ODEBRECHT, C., 2001. Characteristics and importance of planktonic flagellates in marine coastal and oceanic ecosystems. *Oecologia Brasiliensis*, **9**(1), 12.

BIDIGARE, R.R. and ONDRUSEK, M.E., 1996. Spatial and temporal variability of phytoplankton pigment distributions in the central equatorial Pacific Ocean. *Deep Sea Research Part II: Topical Studies in Oceanography*, **43**(4–6), pp. 809-833.

BIDIGARE, R.R., ONDRUSEK, M.E., MORROW, J.H. and KIEFER, D.A., 1990. In vivo absorption properties of algal pigments, *Proceedings of SPIE - The International Society for Optical Engineering* 1990, pp. 290-302.

BISSETT, W.P., PATCH, J.S., CARDER, K.L. and LEE, Z.P., 1997. Pigment packaging and Chl a-specific absorption in high-light oceanic waters. *Limnology and Oceanography*, **42**(5 I), pp. 961-968.

BLANCHOT, J., ANDRÉ, J.-., NAVARETTE, C., NEVEUX, J. and RADENAC, M., 2001. Picophytoplankton in the equatorial Pacific: vertical distributions in the warm pool and in the high nutrient low chlorophyll conditions. *Deep Sea Research Part I: Oceanographic Research Papers*, **48**(1), pp. 297-314.

BOUMAN, H., PLATT, T., KRAAY, G.W., SATHYENDRANATH, S. and IRWIN, B., 2000. Bio-optical properties of the subtropical North Atlantic. I. Vertical variability. *Marine Ecology Progress Series*, **200**, pp. 3-18.

BOUMAN, H., PLATT, T., SATHYENDRANATH, S. and STUART, V., 2005. Dependence of light-saturated photosynthesis on temperature and community structure. *Deep Sea Research Part I: Oceanographic Research Papers*, **52**(7), pp. 1284-1299.

BOUMAN, H.A., LEPÈRE, C., SCANLAN, D.J. and OSVALDO, U., 2012. Phytoplankton community structure in a high-nutrient, low-chlorophyll region of the eastern Pacific

Subantarctic region during winter-mixed and summer-stratified conditions. *Deep Sea Research Part I: Oceanographic Research Papers*, **69**, pp. 1-11

BOUMAN, H.A., PLATT, T., SATHYENDRANATH, S., LI, W.K.W., STUART, V., FUENTES-YACO, C., MAASS, H., HORNE, E.P.W., ULLOA, O., LUTZ, V. and KYEWALYANGA, M., 2003. Temperature as indicator of optical properties and community structure of marine phytoplankton: Implications for remote-sensing. *Marine Ecology Progress Series,* **258**, pp. 19-30.

BOUMAN, H.A., ULLOA, O., BARLOW, R., LI, W.K.W., PLATT, T., ZWIRGLMAIER, K., SCANLAN, D.J. and SATHYENDRANATH, S., 2011. Water-column stratification governs the community structure of subtropical marine picophytoplankton. *Environmental Microbiology Reports,* **3**(4), pp. 473-482.

BOWN, P. R. 2005. Calcareous nannoplankton evolution: a tale of two oceans. *Micropaleontology*, **51**(4), 299-308.

BREWIN, R.J.W., SATHYENDRANATH, S., HIRATA, T., LAVENDER, S.J., BARCIELA, R.M. and HARDMAN-MOUNTFORD, N.J., 2010. A three-component model of phytoplankton size class for the Atlantic Ocean. *Ecological Modelling*, **221**(11), pp. 1472-1483.

BRICAUD, A., BABIN, M., CLAUSTRE, H., RAS, J. and TIÈCHE, F., 2010. Light absorption properties and absorption budget of Southeast Pacific waters. *Journal of Geophysical Research,* **115**, C08009.

BRICAUD, A., CLAUSTRE, H., RAS, J. and OUBELKHEIR, K., 2004. Natural variability of phytoplanktonic absorption in oceanic waters: Influence of the size structure of algal populations. *Journal of Geophysical Research,* **109**, C11010.

BROWN, S.L., LANDRY, M.R., CHRISTENSEN, S., GARRISON, D., GOWING, M.M., BIDIGARE, R.R. and CAMPBELL, L., 2002. Microbial community dynamics and taxon-specific phytoplankton production in the Arabian Sea during the 1995 monsoon seasons. *Deep Sea Research Part II: Topical Studies in Oceanography,* **49**(12), pp. 2345-2376.

BUCK, K., CHAVEZ, F., & CAMPBELL, L. 1996. Basin-wide distributions of living carbon components and the inverted trophic pyramid of the central gyre of the North Atlantic Ocean, summer 1993. *Aquatic Microbial Ecology*, **10**(3), 283-298.

BUMA, A., GIESKES, W. and THOMSEN, H.A., 1992. Abundance of Cryptophyceae and chlorophyll b-containing organisms in the Weddell-Scotia Confluence area in the spring of 1988. *Polar Biology,* **12**(1), pp. 43-52.

CALBET, A. and LANDRY, M.R., 2004. Phytoplankton growth, microzooplankton grazing, and carbon cycling in marine systems. *Limnology and Oceanography,* **49**(1), pp. 51-57.

CANFIELD, D.E., 2005. The early history of atmospheric oxygen: homage to Robert M. Garrels. *Annual Review of Earth Planetary Sciences,* **33**, pp. 1-36.

CHAVEZ, F.P., BUCK, K.R., SERVICE, S.K., NEWTON, J. and BARBER, R.T., 1996. Phytoplankton variability in the central and eastern tropical Pacific. *Deep Sea Research Part II: Topical Studies in Oceanography,* **43**(4–6), pp. 835-870.

CARR, M. E., FRIEDRICHS, M. A., SCHMELTZ, M., AITA, M. N., ANTOINE, D., ARRIGO, K. R., ... & YAMANAKA, Y. 2006. A comparison of global estimates of marine primary production from ocean color. *Deep-sea research. Part 2. Topical studies in oceanography*, **53**(5-7), 741-770.

CERMENO, P., MARANON, E., PEREZ, V., SERRET, P., FERNANDEZ, E., & CASTRO, C. G. 2006. Phytoplankton size structure and primary production in a highly dynamic coastal ecosystem (Ría de Vigo, NW-Spain): seasonal and short-time scale variability. *Estuarine, Coastal and Shelf Science*, **67**(1), 251-266.

CERMENO, P., DUTKIEWICZ, S., HARRIS, R. P., FOLLOWS, M., SCHOFIELD, O., & FALKOWSKI, P. G. 2008. The role of nutricline depth in regulating the ocean carbon cycle. *Proceedings of the National Academy of Sciences of the United States of America*, **105**(51), 20344-20349.

CHARLSON, R.J., LOVELOCKL, J.E., ANDREAEI, M.O. and WARREN, S.G., 1987. Oceanic phytoplankton, atmospheric sulphur, cloud. *Nature,* **3526**, pp. 16.

CHAVEZ, F., BUCK, K., NEWTON, J., & BARBERS, R. (1996). Phytoplankton variability in the central and eastern tropical Pacific. *Deep Sea Research. Part 2. Topical Studies in Oceanography*, **43**(4-6), 835-870.

CHISHOLM, S., OLSON, R., ZETTLER, E., GOERICKE, R., WATERBURY, J., & WELSCHMEYER, N. 1988. A novel free-living prochlorophyte abundant in the oceanic euphotic zone. *Nature*, **334**(6180), 340-343.

CHISHOLM, S.W., 1992. Phytoplankton size. In: P.G. FALKOWSKI and A.D. WOODHEAD, eds, *Primary productivity and biogeochemical cycles in the sea.* Springer, pp. 213-237.

CIOTTI, Á.M., LEWIS, M. R., and CULLEN, J.J., 2002. Assessment of the Relationships between Dominant Cell Size in Natural Phytoplankton Communities and the Spectral Shape of the Absorption Coefficient. *Limnology and Oceanography,* **47**(2), pp. 404-417.

CLAUSTRE, H., 1994. The Trophic Status of Various Oceanic Provinces as Revealed by Phytoplankton Pigment Signatures. *Limnology and Oceanography,* **39**(5), pp. 1206-1210.

CLAUSTRE, H., HOOKER, S.B., VAN HEUKELEM, L., BERTHON, J., BARLOW, R., RAS, J., SESSIONS, H., TARGA, C., THOMAS, C.S., VAN DER LINDE, D. and MARTY, J., 2004. An intercomparison of HPLC phytoplankton pigment methods using *in-situ* samples: application to remote-sensing and database activities. *Marine Chemistry,* **85**(1–2), pp. 41-61.

CLAUSTRE, H., BABIN, M., MERIEN, D., RAS, J., PRIEUR, L., DALLOT, S., PRASIL, O., DOUSOVA, H. and MOUTIN, T., 2005. Toward a taxon-specific parameterization of bio-optical models of primary production: A case study in the North Atlantic. *Journal of Geophysical Research,* **110**, C07S12.

CLAUSTRE, H. and MARTY, J., 1995. Specific phytoplankton biomasses and their relation to primary production in the tropical North Atlantic. *Deep Sea Research Part I: Oceanographic Research Papers,* **42**(8), pp. 1475-1493.

COESEL, S., OBORNÃK, M., VARELA, J., FALCIATORE, A. and BOWLER, C., 2008. Evolutionary Origins and Functions of the Carotenoid Biosynthetic Pathway in Marine Diatoms. *PLoS ONE,* **3**(8), pp. e2896.

COTE, B. and PLATT, T., 1983. Day-to-Day Variations in the Spring-Summer Photosynthetic Parameters of Coastal Marine Phytoplankton. *Limnology and Oceanography,* **28**(2), pp. 320-344.

CULLEN, J. J., FRANKS, P. J., KARL, D. M., & LONGHURST, A. 2002. Physical influences on marine ecosystem dynamics. *The Sea*, **12**, 297-336.

DANDONNEAU, Y. and NIANG, A., 2007. Assemblages of phytoplankton pigments along a shipping line through the North Atlantic and tropical Pacific. *Progress in Oceanography,* **73**(2), pp. 127-144.

DANDONNEAU, Y., DESCHAMPS, P., NICOLAS, J., LOISEL, H., BLANCHOT, J., MONTEL, Y., THIEULEUX, F. and BÉCU, G., 2004. Seasonal and interannual variability of ocean color and composition of phytoplankton communities in the North Atlantic, equatorial Pacific and South Pacific. *Deep-Sea Research Part II: Topical Studies in Oceanography,* **51**(1-3), pp. 303-318.

DANDONNEAU, Y., MONTEL, Y., BLANCHOT, J., GIRAUDEAU, J. and NEVEUX, J., 2006. Temporal variability in phytoplankton pigments, picoplankton and coccolithophores along a transect through the North Atlantic and tropical southwestern Pacific. *Deep Sea Research Part I: Oceanographic Research Papers,* **53**(4), pp. 689-712.

DAVISON, I. R. (2004). Environmental effects on algal photosynthesis: temperature. *Journal*

of Phycology, **27**(1), 2-8.

DEMARCQ, H., REYGONDEAU, G., ALVAIN, S. and VANTREPOTTE, V., 2012. Monitoring marine phytoplankton seasonality from space. *Remote Sensing of Environment*, **117**, pp. 211-222.

DIMIER, C., CORATO, F., TRAMONTANO, F. and BRUNET, C., 2007. Photoprotection and xanthophyll-cycle activity in three marine diatoms. *Journal of Phycology*, **43**(5), pp. 937-947.

DUBINSKY, Z., & STAMBLER, N. 2009. Photoacclimation processes in phytoplankton: mechanisms, consequences, and applications. *Aquatic Microbial Ecology*, **56**(2-3), 163-176.

DUYSENS, L.N.M., 1956. Energy Transformations in Photosynthesis. *Annual Review of Plant Physiology*, **7**(1), pp. 25-50.

EKER-DEVELI, E., BERTHON, J., CANUTI, E., SLABAKOVA, N., MONCHEVA, S., SHTEREVA, G. and DZHUROVA, B., 2012. Phytoplankton taxonomy based on CHEMTAX and microscopy in the northwestern Black Sea. *Journal of Marine Systems*, **94**(0), pp. 18-32.

EMILIANI, C., 1993. Extinction and viruses. *Biosystems*, **31**(2), 155-159.

EPPLEY, R.W., 1972. Temperature and phytoplankton growth in the sea. *Fishery Bulletin*, **70**(4), pp. 1063-1085.

ESTRADA, M. and BERDALET, E., 1997. Phytoplankton in a turbulent world. *Scientia Marina*, **61**(SUPPL.1), pp. 125-140.

EVERITT, D.A., WRIGHT, S.W., VOLKMAN, J.K., THOMAS, D.P. and LINDSTROM, E.J., 1990. Phytoplankton community compositions in the western equatorial Pacific determined from chlorophyll and carotenoid pigment distributions. *Deep Sea Research Part A.Oceanographic Research Papers*, **37**(6), pp. 975-997.

FALKOWSKI, P.G., 1980. *Primary productivity in the sea.* New York: Plenum press.

FALKOWSKI, P.G. and WILSON, C., 1992. Phytoplankton productivity in the North Pacific ocean since 1900 and implications for absorption of anthropogenic CO2. *Nature*, **358**(6389), pp. 741-743.

FALKOWSKI, P.G. and OLIVER, M.J., 2007. Mix and match: how climate selects phytoplankton. *Nature Reviews Microbiology*, **5**(10), pp. 813-819.

FENCHEL, T., 1988. Marine Plankton Food Chains. *Annual Review of Ecology and Systematics*, **19**(1), pp. 19-38.

FENCHEL, T., 2008. The microbial loop – 25 years later. *Journal of Experimental Marine Biology and Ecology*, **366**(1–2), pp. 99-103.

FIELD, C.B., BEHRENFELD, M.J., RANDERSON, J.T. and FALKOWSKI, P., 1998. Primary production of the biosphere: integrating terrestrial and oceanic components. *Science*, **281**(5374), pp. 237-240.

FINKEL, Z.V., 2001. Light absorption and size scaling of light-limited metabolism in marine diatoms. *Limnology and Oceanography*, pp. 86-94.

FINKEL, Z.V., BEARDALL, J., FLYNN, K.J., QUIGG, A., REES, T.A.V. and RAVEN, J.A., 2010. Phytoplankton in a changing world: Cell size and elemental stoichiometry. *Journal of Plankton Research,* **32**(1), pp. 119-137.

FOGG, G.E., 1986. Review Lecture: Picoplankton. *Proceedings of the Royal Society of London.Series B.Biological Sciences,* **228**(1250), pp. 1-30.

FOLLOWS, M. J., & DUTKIEWICZ, S. 2011. Modelling diverse communities of marine microbes. *Annual Review of Marine Science*, **3**, 427-451.

FRIEBELE, E.S., CORRELL, D.L. and FAUST, M.A., 1978. Relationship between phytoplankton cell size and rate of orthophosphate uptake: In situ observations of an esturine population. *Marine Biology,* **45**(1), pp. 39-52.

FRIEDRICHS, M. A., CARR, M. E., BARBER, R. T., SCARDI, M., ANTOINE, D., ARMSTRONG, R. A., & WINGUTH, A. 2009. Assessing the uncertainties of model estimates of primary productivity in the tropical Pacific Ocean. *Journal of Marine Systems,* **76**(1), 113-133.

FURNAS, M.J., 1990. In situ growth rates of marine phytoplankton: Approaches to measurement, community and species growth rates. *Journal of Plankton Research,* **12**(6), pp. 1117-1151.

GAARDER, T. and GRAN, H.H., 1927. *Investigations of the production of plankton in the Oslo Fjord.* Conseil permanent international pour l'exploration de la mer.

GEIDER, R. and OSBORNE, B., 1986. Light absorption, photosynthesis and growth of *Nannochloris atomus* in nutrient-saturated cultures. *Marine Biology,* **93**(3), pp. 351-360.

GEIDER, R.J., MACINTYRE, H.L. and KANA, T.M., 1996. A dynamic model of photoadaptation in phytoplankton. *Limnology and Oceanography,* , pp. 1-15.

GEIDER, R.J., MACINTYRE, H.L. and KANA, T.M., 1997. Dynamic model of phytoplankton growth ant acclimation: responses of the balanced growth rate and the chlorophyll *a*:carbon ratio to light, nutrient-limitation and temperature. *Marine Ecology Progress Series,* **148**, pp. 187-200.

GEIDER, R., MACINTYRE, H.L. and KANA, T.M., 1998. A Dynamic Regulatory Model of Phytoplanktonic Acclimation to Light, Nutrients, and Temperature. *Limnology and Oceanography,* **43**(4), pp. 679-694.

GENNER, M. J., HALLIDAY, N. C., SIMPSON, S. D., SOUTHWARD, A. J., HAWKINS, S. J., & SIMS, D. W. 2010. Temperature-driven phenological changes within a marine larval fish assemblage. *Journal of Plankton Research*, **32**(5), 699-708.

GIBB, S.W., BARLOW, R.G., CUMMINGS, D.G., REES, N.W., TREES, C.C., HOLLIGAN, P. and SUGGETT, D., 2000. Surface phytoplankton pigment distributions in the Atlantic Ocean: An assessment of basin scale variability between 50°N and 50°S. *Progress in Oceanography,* **45**(3-4), pp. 339-368.

GIBB, S.W., CUMMINGS, D.G., IRIGOIEN, X., BARLOW, R.G., FAUZI, R. and MANTOURA, C., 2001. Phytoplankton pigment chemotaxonomy of the northeastern

Atlantic. *Deep Sea Research Part II: Topical Studies in Oceanography,* **48**(4–5), pp. 795-823.

GIESKES, W.W. and KRAAY, G.W., 1986. Analysis of phytoplankton pigments by HPLC before, during and after mass occurrence of the microflagellate Corymbellus aureus during the spring bloom in the open northern North Sea in 1983.*Marine Biology*, **92**, pp 45-52.

GIESKES, W.W.C., KRAAY, G.W., NONTJI, A., SETIAPERMANA, D. and SUTOMO, 1988. Monsoonal alternation of a mixed and a layered structure in the phytoplankton of the euphotic zone of the banda sea (Indonesia): a mathematical analysis of algal pigment fingerprints. *Netherlands Journal of Sea Research*, **22(**2), pp. 123-137.

GREVE, W., & PARSONS, T. R. 1977. Photosynthesis and fish production: hypothetical effects of climatic change and pollution. *Helgoland Marine Research*, **30(**1), 666-672.

GOERICKE, R., & WELSCHMEYER, N. 1993. The marine prochlorophyte Prochlorococcus contributes significantly to phytoplankton biomass and primary production in the Sargasso Sea. *Deep Sea Research. Part 1. Oceanographic Research Papers*, **40**(11-12), 2283-2294.

GOES, J., SAINO, T., OAKU, H. and JIANG, D., 1999. A method for estimating sea surface nitrate concentrations from remotely sensed SST and chlorophyll a - A case study for the North Pacific Ocean using OCTS/ADEOS data . *IEEE Transactions on Geoscience and Remote Sensing,* **37 pt 2**(3), pp. 1633-1644.

GÓMEZ-BAENA, G., LÓPEZ-LOZANO, A., GIL-MARTÍNEZ, J., LUCENA, J.M., DIEZ, J., CANDAU, P. and GARCÍA-FERNÁNDEZ, J.M., 2008. Glucose uptake and its effect on gene expression in Prochlorococcus. *PloS ONE,* **3**(10), pp. e3416.

GROB, C., ULLOA, O., CLAUSTRE, H., HUOT, Y., ALARCÃN, G. and MARIE, D., 2007. Contribution of picoplankton to the total particulate organic carbon concentration in the eastern South Pacific. *Biogeosciences,* **4**, pp 837-852.

GROB, C., HARTMANN, M., ZUBKOV, M.V. and SCANLAN, D.J., 2011. Invariable biomass-specific primary production of taxonomically discrete picoeukaryote groups across the Atlantic Ocean. *Environmental Microbiology,* **13**(12), pp. 3266-3274.

GROBEN, R., JOHN, U., ELLER, G., LANGE, M. and MEDLIN, L., 2004. Using fluorescently-labelled rRNA probes for hierarchical estimation of phytoplankton diversity - a mini review. *Nova Hedwigia,* **79**, pp. 313-320.

GRUBER, N., & GALLOWAY, J. N. 200). An Earth-system perspective of the global nitrogen cycle. *Nature*, **451**(7176), 293-296.

HAMM, C., MERKEL, R., SPRINGER, O., JURKOJC, P., MAIER, C., PRECHTEL, K., & SMETACEK, V. 2003. Architecture and material properties of diatom shells provide effective mechanical protection. *Nature*, **421**, 841-843.

HANSEN, B.W., 1997. Zooplankton grazing and growth: Scaling within the 2-2,000-~ III body size range. *Limnology and Oceanography*, **42**, pp. 687-704.

HARDY, A., HENDERSON, G., LUCAS, C. and FRASER, J., 1936. The ecological relations between the herring and the plankton investigated with the plankton indicator. *Journal of the Marine Biological Assosciation of the UK,* **21**, pp. 147-291.

HASLE, G.R. and BOOTH, B.C., 1984. *Nitzschia cylindroformis* sp. nov., a common and abundant nanoplankton diatom of the eastern subarctic Pacific. *Journal of Plankton Research,* **6**(3), pp. 493-503.

HASLE, G. and SYVERTSEN, E., 1997. Marine Diatoms. Tomas C R. Identifying Marine Phytoplankton.

HAVSKUM, H., SCHLUTER, L., SCHAREK, R., BERDALET, E. and JACQUET, S., 2004. Routine quantification of phytoplankton groups - microscopy or pigment analyses. *Marine Ecology Progress Series,* **273**, pp. 31-42.

HAYS, G., RICHARDSON, A., and ROBINSON, C. 2005. Climate change and marine plankton. *Trends in ecology & evolution*, **20**(6), 337-344.

HEAD, E.J.H. and HORNE, E.P.W., 1993. Pigment transformation and vertical flux in an area of convergence in the North Atlantic. *Deep Sea Research Part II: Topical Studies in Oceanography,* **40**(1-2), pp. 329-346.

HENSON, S.A., DUNNE, J.P. and SARMIENTO, J.L., 2009. Decadal variability in North Atlantic phytoplankton blooms. *Journal of Geophysical Research,* **114**, pp. C04013.

HERBLAND, A., LE BOUTEILLER, A. and RAIMBAULT, P., 1985. Size structure of phytoplankton biomass in the equatorial Atlantic Ocean. *Deep Sea Research Part A.Oceanographic Research Papers,* **32**(7), pp. 819-836.

HENRIKSEN, P., RIEMANN, B., KAAS, H., SØRENSEN, H. M., & SØRENSEN, H. L. 2002. Effects of nutrient-limitation and irradiance on marine phytoplankton pigments. *Journal of Plankton Research*, **24**(9), 835-858.

HEYWOOD, J.L., ZUBKOV, M.V., TARRAN, G.A., FUCHS, B.M. and HOLLIGAN, P.M., 2006. Prokaryoplankton standing stocks in oligotrophic Gyre and equatorial provinces of the Atlantic Ocean: Evaluation of inter-annual variability. *Deep Sea Research Part II: Topical Studies in Oceanography,* **53**(14–16), pp. 1530-1547.

HIRATA, T., HARDMAN-MOUNTFORD, N. J., BREWIN, R. J. W., AIKEN, J., BARLOW, R., SUZUKI, K.., & YAMANAKA, Y. 2010. Synoptic relationships quantified between surface Chlorophyll-a and diagnostic pigments specific to phytoplankton functional types. *Biogeosciences Discussions*, **7**(5), 6675-6704.

HOEGH-GULDBERG, O., & BRUNO, J. F. 2010. The impact of climate change on the world's marine ecosystems. *Science*, **328**(5985), 1523-1528.

HOEPFFNER, N. and SATHYENDRANATH, S., 1992. Bio-optical characteristics of coastal waters:absorption spectra of phytoplankton and pigment distribution in the western North Atlantic. *Limnology and Oceanography*, **37**(8), pp. 1660-1679.

HOEPFFNER, N., & SATHYENDRANATH, S. 1993. Determination of the major groups of phytoplankton pigments from the absorption spectra of total particulate matter. *Journal of Geophysical Research*, **98**(C12), 22789-22803.

HOLM-HANSEN, O., LORENZEN, C.J., HOLMES, R.W. and STRICKLAND, J.D.H., 1965. Fluorometric Determination of Chlorophyll. *Journal du Conseil*, **30**(1), pp. 3-15.

HOWARTH, R.W., MARINO, R. and LANE, J., 1988. Nitrogen fixation in freshwater, estuarine, and marine ecosystems. 1. Rates and importance. *Limnology and Oceanography,* **33**, pp. 669-687.

HUOT, Y., BABIN, M., & BRUYANT, F. 2013. Photosynthetic parameters in the Beaufort Sea in relation to the phytoplankton community structure. *Biogeosciences Discussions*, **10**, 1551-1576.

IGLESIAS-RODRIGUEZ, M.D., HALLORAN, P.R., RICKABY, R.E.M., HALL, I.R., COLMENERO-HIDALGO, E., GITTINS, J.R., GREEN, D.R.H., TYRRELL, T., GIBBS, S.J. and VON DASSOW, P., 2008. Phytoplankton calcification in a high-CO2 world. *Science,* **320**(5874), pp. 336-340.

IGNATIADES, L., PSARRA, S., ZERVAKIS, V., PAGOU, K., SOUVERMEZOGLOU, E., ASSIMAKOPOULOU, G. and GOTSIS-SKRETAS, O., 2002. Phytoplankton size-based dynamics in the Aegean Sea (Eastern Mediterranean). *Journal of Marine Systems,* **36**(1–2), pp. 11-28.

IRIGOIEN, X., MEYER, B., HARRIS, R. and HARBOUR, D., 2004. Using HPLC pigment analysis to investigate phytoplankton taxonomy: The importance of knowing your species. *Helgoland Marine Research,* **58**(2), pp. 77-82.

IRWIN, A.J., FINKEL, Z.V., SCHOFIELD, O.M.E. and FALKOWSKI, P.G., 2006. Scaling-up from nutrient physiology to the size-structure of phytoplankton communities. *Journal of Plankton Research,* **28**(5), pp. 459-471.

JACKETT, D.R., MCDOUGALL, T.J., FEISTEL, R., WRIGHT, D.W. and GRIFFITES, S.M., 2006. Algorithms for density, potential temperature, conservative temperature,

and the freezing temperature of seawater. *Journal of Atmospheric and Oceanic Technology*, **23**(12), pp. 1709.

JASSBY, A.D. and PLATT, T., 1976. Mathmatical formulation of the relationship between photosynthesis and light for phytoplankton. *Limnology and Oceanography*, **21**(4), pp. 540-547.

JEFFREY, S. and HUMPHREY, G.F., 1975. New spectrophotometric equations for determining chlorophylls a, b, c1 and c2 in higher plants, algae and natural phytoplankton. *Biochemie und Physiologie der Pflanzen*, **167**, pp. 191-194.

JENNINGS, S., & BRANDER, K. 2010. Predicting the effects of climate change on marine communities and the consequences for fisheries. *Journal of Marine Systems*, **79**(3), 418-426.

JIANG, L., SCHOFIELD, O.M. and FALKOWSKI, P.G., 2005. Adaptive evolution of phytoplankton cell size. *American Naturalist*, pp. 496-505.

JOINT, I. and GROOM, S.B., 2000. Estimation of phytoplankton production from space: current status and future potential of satellite remote-sensing. *Journal of Experimental Marine Biology and Ecology*, **250**(1), pp. 233-255.

KAMYKOWSKI, D., ZENTARA, S. J., MORRISON, J. M., & SWITZER, A. C. 2002. Dynamic global patterns of nitrate, phosphate, silicate, and iron availability and phytoplankton community composition from remote sensing data. *Global Biogeochemical Cycles*, **16**(4), 25-1.

KAMYKOWSKI, D., & ZENTARA, S. J. 2003. Can phytoplankton community structure be

inferred from satellite-derived sea surface temperature anomalies calculated relative to nitrate depletion temperatures? *Remote Sensing of Environment*, **86**(4), 444-457.

KEY, T., MCCARTHY, A., CAMPBELL, D.A., SIX, C., ROY, S. and FINKEL, Z.V., 2010. Cell size trade-offs govern light exploitation strategies in marine phytoplankton. *Environmental Microbiology*, **12**(1), pp. 95-104.

KIØRBOE, T., 1993. Turbulence, water column structure and phytoplankton cell size. *Advances in Marine Biology*, **29**, pp. 1-72.

KIRK, J.T., 1976. A theoretical analysis of the contribution of algal cells to the attenuation of light within natural waters. III. Cylindrical and spheroidal cells. *New Phytologist*, **77**, pp. 341-358.

KIRK, J.T., 2011. *Light and photosynthesis in Aquatic Ecosystems.* 3 edn. Cambridge University Press.

KISHINO, M., TAKAHASHI, M. and ICHIMURA, S., 1985. Estimation of the spectral absorption coefficients of phytoplankton in the sea. *Bulletin of Marine Science*, **37**(2), pp. 634-642.

LANDRY, M. R. 1977. A review of important concepts in the trophic organization of pelagic ecosystems. *Helgoländer Wissenschaftliche Meeresuntersuchungen*, **30**(1-4), 8-17.

LATASA, M., 2007. Improving estimations of phytoplankton class abundances using CHEMTAX. *Marine Ecology Progress Series*, **329**, pp. 13-21.

LAVIALE, M., & NEVEUX, J. 2011. Relationships between pigment ratios and growth irradiance in 11 marine phytoplankton species. *Marine Ecology. Progress Series* **425**,

63-77.

LAW, R., PLANK, M. J., JAMES, A., & BLANCHARD, J. L. 2009. Size-spectra dynamics from stochastic predation and growth of individuals. *Ecology*, **90**(3), 802-811.

LAWS, E.A., FALKOWSKI, P.G., SMITH, W., O., DUCKLOW, H. and MCCARTHY, J.J., 2000. Temperature effects on export production in the open ocean. *Global Biogeochemical Cycles*, **14**(4), pp. 1231-1246.

LE BOUTEILLER, A. and BLANCHOT, J., 1991. Size distribution and abundance of phytoplankton in the Pacific Equatorial upwelling. *La Mer*, **29**, pp. 175-179.

Le QUÉRÉ, C., HARRISON, S.P., PRENTICE, C. I., BUITENHUIS, E.T., AUMONT, O., BOPP, L., CLAUSTRE, H., COTRIM DA CUNHA, L., GEIDER, R., GIRAUD, X., KLAAS, C., KOHFELD, K.E., LEGENDRE, L., MANIZZA, M., PLATT, T., RIVKIN, R.B., SATHYENDRANATH, S., UITZ, J., WATSON, A.J. and WOLF-GLADROW, D., 2005. Ecosystem dynamics based on plankton functional types for global ocean biogeochemistry models. *Global Change Biology*, **11**(11), pp. 2016-2040.

LEGENDRE, L. and RASSOULZADEGAN, F., 1995. Plankton and nutrient dynamics in marine waters. *Ophelia*, **41**, pp. 153-172.

LEGENDRE, L. and RASSOULZADEGAN, F. 1996. Food-web mediated export of biogenic carbon in oceans: hydrodynamic control. *Marine Ecology Progress Series*, **145**(1), 179-193.

LETELIER, R.M., BIDIGARE, R.R., HEBEL, D.V., ONDRUSEK, M., WINN, C.D. and KARL, D.M., 1993. Temporal Variability of Phytoplankton Community Structure Based on Pigment Analysis. *Limnology and Oceanography,* **38**(7), pp. 1420-1437.

LEVITUS, S., CONKRIGHT, M.E., REID, J.L., NAJJAR, R.G. MANTYLA, A., 1993. Distribution of nitrate, phosphate and silicate in the world oceans. *Progress in Oceanography,* **31**(3), pp. 245-273.

LI, W.K.W., 2002. Macroecological patterns of phytoplankton in the northwestern North Atlantic Ocean. *Nature,* **419**(6903), pp. 154-157.

LITCHMAN, E. and KLAUSMEIER, C., 2008. Trait-Based Community Ecology of Phytoplankton. *Annual Review of Ecology, Evolution, and Systematics,* **39**(1)

LITCHMAN, E., KLAUSMEIER, C. A., & YOSHIYAMA, K. 2009. Contrasting size evolution in marine and freshwater diatoms. *Proceedings of the National Academy of Sciences*, **106**(8), 2665-2670.

LLEWELLYN, C.A., FISHWICK, J.R. and BLACKFORD, J.C., 2005. Phytoplankton community assemblage in the English Channel: A comparison using chlorophyll a derived from HPLC-CHEMTAX and carbon derived from microscopy cell counts. *Journal of Plankton Research,* **27**(1), pp. 103-119.

LOCARNINI, R.A., MISHONOV, A.V., ANTONOV, J.I., BOYER, T.P. and GARCIA, H.E., 2009. *World Ocean Atlas 2009,Volume 1, Temperature.*

LOCHTE, K., DUCKLOW, H.W., FASHAM, M.J.R. and STIENEN, C., 1993. Plankton succession and carbon cycling at 47°N 20°W during the JGOFS North Atlantic Bloom

Experiment. *Deep Sea Research Part II: Topical Studies in Oceanography*, **40**(1–2), pp. 91-114.

LOMAS, M. W., GLIBERT, P. M., CLOUGHERTY, D. A., HUBER, D. R., JONES, J., ALEXANDER, J., & HARAMOTO, E. 2001. Elevated organic nutrient ratios associated with brown tide algal blooms of Aureococcus anophagefferens (Pelagophyceae). *Journal of Plankton Research*, **23**(12), 1339-1344.

LONG, S., HUMPHRIES, S. and FALKOWSKI, P.G., 1994. Photoinhibition of photosynthesis in nature. *Annual Review of Plant Biology*, **45**(1), pp. 633-662.

LONGHURST, A., SATHYENDRANATH, S., PLATT, T. and CAVERHILL, C., 1995. An estimate of global primary production in the ocean from satellite radiometer data. *Journal of Plankton Research*, **17**(6), pp. 1245-1271.

LORENZEN, C.J., 1967. Determination of chlorophyll and phaeo-pigments: Spectrophotometric equations. *Limnology and Oceanography*, **12**(2), pp. 343-346.

MACINTYRE, H. L., KANA, T. M., & GEIDER, R. J. 2000. The effect of water motion on short-term rates of photosynthesis by marine phytoplankton. *Trends in Plant Science*, **5**(1), 12-17.

MACINTYRE, H.L., KANA, T.M., ANNING, T. and GEIDER, R.J., 2002. Photoacclimation of photosynthesis-irradiance response curves and photosynthetic pigments in microalgae and. *Journal of Phycology*, **38**(1), pp. 17-38.

MACKEY, M.D., MACKEY, D.J., HIGGINS, H.W. and WRIGHT, S.W., 1996. CHEMTAX - a program for estimating class abundances from chemical markers: application to

HPLC measurements of phytoplankton. *Marine Ecology Progress Series,* **144**, pp. 265-283.

MANTOURA, R.F.C., and LLEWELLYN C.A., 1983. The rapid determination of algal chlorophyll and carotenoid pigments and their breakdown products in natural waters by reverse-phase high-performance liquid chromatography. *Analytica Chimica Acta*, **151**, pp. 297-314.

MARAÑON, E. and HOLLIGAN, P., 1999. Photosynthetic parameters of phytoplankton from 50°N to 50°S in the Atlantic Ocean . *Marine Ecology Progress Series*, **176**, pp. 191-203.

MARAÑÓN, E., HOLLIGAN, P.M., VARELA, M., MOURIÑO, B., & BALE, A. J. (2000). Basin-scale variability of phytoplankton biomass, production and growth in the Atlantic Ocean. *Deep Sea Research Part I: Oceanographic Research Papers*, **47**(5), 825-857.

MARAÑÓN, E., HOLLIGAN, P.M., BARCIELA, R., GONZÁLEZ, N., MOURIÑO, B., PAZÓ, M.J. and VARELA, M., 2001. Patterns of phytoplankton size structure and productivity in contrasting open-ocean environments. *Marine Ecology Progress Series,* **216**, pp. 43-56.

MARAÑON, E., BEHRENFELD, M.J., GONZALEZ, N., MOURINO, B. and ZUBKOV, M.V., 2003. High variability of primary production in oligotrophic waters of the Atlantic Ocean: uncoupling from phytoplankton biomass and size structure. *Marine Ecology Progress Series,* **257**, pp. 1-11.

MARAÑÓN, E., 2005. Phytoplankton Growth Rates in the Atlantic Subtropical Gyres. *Limnology and Oceanography,* **50**(1), pp. 299-310.

MARAÑÓN, E., CERMEÑO, P., RODRÍGUEZ, J., ZUBKOV, M.V. and HARRIS, R.P., 2007. Scaling of phytoplankton photosynthesis and cell size in the ocean. *Limnology and Oceanography,* **52**(5), pp. 2190-2198.

MARGALEF, R., 1978. Life-forms of phytoplankton as survival alternatives in an unstable environment. *Oceanologica acta,* **134**, pp. 493-509.

MAURY, O., FAUGERAS, B., SHIN, Y. J., POGGIALE, J. C., ARI, T. B., & MARSAC, F. 2007. Modeling environmental effects on the size-structured energy flow through marine ecosystems. Part 1: the model. *Progress in Oceanography*, **74**(4), 479-499.

MCMANUS, G. B., & DAWSON, R. 1994. Phytoplankton pigments in the deep chlorophyll maximum of the Caribbean Sea and the western tropical Atlantic Ocean. *Marine Ecology Progress Series*, **113**(1), 199-206.

MENDES, C.R., SÁ, C., VITORINO, J., BORGES, C., TAVANO GARCIA, V.M. and BROTAS, V., 2011. Spatial distribution of phytoplankton assemblages in the Nazaré submarine canyon region (Portugal): HPLC-CHEMTAX approach. *Journal of Marine Systems,* 87(1), pp. 90-101.

MIDDLEBURG, J. J. 2011. Chemoautotrophy in the ocean. *Geophysical Research Letters*, **38**(24), L24604.

MITCHELL, B.G. and KIEFER, D.A., 1984. Determination of absorption and fluorescence excitation spectra for phytoplankton. Washington, DC: AGU, pp. 157-169.

MOISAN, T.A. and MITCHELL, B.G., 1999. Photophysiological acclimation of Phaeocystis antarctica Karsten under light limitation. *Limnology and Oceanography,* **44**(2), pp. 247-258.

MOISAN, J. R., MOISAN, T. A., & LINKSWILER, M. A. 2011. An inverse modelling approach to estimating phytoplankton pigment concentrations from phytoplankton absorption spectra. *Journal of Geophysical Research: Oceans ,* **116**(C9).

MONTAGNES, D.J.S., BERGES, J.A., HARRISON, P.J. and TAYLOR, F.J.R., 1994. Estimating carbon, nitrogen, protein, and chlorophyll alpha from volume in marine phytoplankton. *Limnology and Oceanography,* **39**(5), pp. 1044-1060.

MOORE, C., BARNARD, A., FIETZEK, P., LEWIS, M.R., SOSIK, H.M., WHITE, S. and ZIELINSKI, O., 2009. Optical tools for ocean monitoring and research. *Ocean Science,* **5**, pp. 661-684.

MOORE, L., GOERICKE, R. and CHISLHOLME, S., 1995. Comparative physiology of *Synechococcus* and *Prochlorococcus*: influence of light and temperature on growth, pigments, fluorescence and absorptive propertie. *Marine Ecology Progress Series,* **116**, pp. 259-275.

MOORE, L. and CHISHOLM, S.W., 1999. Photophysiology of the Marine Cyanobacterium *Prochlorococcus*: Ecotypic Differences among Cultured Isolates. *Limnology and Oceanography,* **44**(3, Part 1), pp. 628-638.

MOREL, A., 1991. Light and marine photosynthesis: a spectral model with geochemical and climatological implications. *Progress in Oceanography,* **26**(3), pp. 263-306.

MOREL, A. and BRICAUD, A., 1981. Theoretical results concerning light absorption in a discrete medium, and application to specific absorption of phytoplankton. *Deep Sea Research Part A, Oceanographic Research Papers,* **28**(11), pp. 1375-1393.

MURPHY, J. and RILEY, J.P., 1962. A modified single solution method for the determination of phosphate in natural waters. *Analytica Chimica Acta,* **27**, pp. 31-36.

MURRAY, C. and WILSON, T., 1997. Marine carbonate formations: Their role in mediating long-term ocean-atmosphere carbon dioxide fluxes—A review. *Energy Conversion and Management,* **38**, pp. S287-S294.

NAIR, A., SATHYENDRANATH, S., PLATT, T., MORALES, J., STUART, V., FORGET, M., DEVRED, E. and BOUMAN, H., 2008. Remote sensing of phytoplankton functional types. *Remote Sensing of Environment,* **112**(8), pp. 3366-3375.

NELSON, N.B., PREZELIN, B.B. and BIDIGARE, R.R., 1993. Phytoplankton light absorption and the package effect in California coastal waters. *Marine Ecology Progress Series,* **94**(3), pp. 217-227.

NIELSEN, E. S., & HANSEN, V. K. 1959. Measurements with the carbon-14 technique of the respiration rates in natural populations of phytoplankton. *Deep Sea Research (1953), 5*(2), 222-233.

NOT, F., LATASA, M., MARIE, D., CARIOU, T., VAULOT, D., & SIMON, N. 2004. A single species, *Micromonas pusilla* (Prasinophyceae), dominates the eukaryotic picoplankton in the western english channel. *Applied and Environmental Microbiology*, **70**(7), 4064-4072.

OLSON, R.J., CHISHOLM, S.W., ZETTLER, E.R., ALTABET, M.A. and DUSENBERRY, J.A., 1990. Spatial and temporal distributions of prochlorophyte picoplankton in the North Atlantic Ocean. *Deep Sea Research Part A.Oceanographic Research Papers,* **37**(6), pp. 1033-1051.

OMAND, M. M. 2011. Physical controls on episodic nearshore phytoplankton blooms in Southern California. *University of California*

ORGANELLI, E., NUCCIO, C., MELILLO, C. and MASSI, L., 2011. Relationships between phytoplankton light absorption, pigment composition and size structure in offshore areas of the Mediterranean Sea. *Advances in Oceanography and Limnology*, **2**(2), pp. 107-123.

PARSONS, T. and LALLI, C., 2002. Jellyfish population explosions: revisiting a hypothesis of possible causes. *La Mer,* **40**, pp. 111-121.

PARSONS, T.R., YOSHIAKI, M. and LALLI, C.M., 1984. *A manual of chemical and biological methods for seawater analysis.*

PARTENSKY, F., HOEPFFNER, N., LI, W. K., ULLOA, O., & VAULOT, D. 1993. Photoacclimation of Prochlorococcus sp.(Prochlorophyta) strains isolated from the North Atlantic and the Mediterranean Sea. *Plant Physiology*, **101**(1), 285-296.

PARTENSKY, F., BLANCHOT, J., LANTOINE, F., NEVEUX, J. and MARIE, D., 1996. Vertical structure of picophytoplankton at different trophic sites of the tropical northeastern Atlantic Ocean. *Deep Sea Research Part I: Oceanographic Research Papers,* **43**(8), pp. 1191-1213.

PARTENSKY, F., HESS, W.R. and VAULOT, D., 1999. Prochlorococcus, a Marine Photosynthetic Prokaryote of Global Significance. *Microbial and Molecular Biology Reviews,* **61**(1), pp. 106-127.

PICHARD, S., CAMPBELL, L. and PAUL, J., 1997. Diversity of the ribulose bisphosphate carboxylase/oxygenase form I gene (rbcL) in natural phytoplankton communities. *Applied and Environmental Microbiology,* **63**(9), pp. 3600-3606.

PLATT, T., GALLEGOS, C. and HARRISON, W., 1980. Photoinhibition of photosynthesis in natural assemblages of marine phytoplankton. *Journal of Marine Research,* **38**.

PLATT, T., & HERMAN, A. W. 1983. Remote sensing of phytoplankton in the sea: surface-layer chlorophyll as an estimate of water-column chlorophyll and primary production. *International Journal of Remote Sensing*, **4**(2), 343-351.

PLATT, T., 1985. PHYTOPLANKTON PRODUCTION IN OLIGOTROPHIC MARINE ECOSYSTEMS: THE MEDITERRANEAN SEA. *Mediterranean Marine Ecosystems,* **8**, pp. 231.

PLATT, T., SATHYENDRANATH, S., CAVERHILL, C., & LEWIS, M. 1988. Ocean primary production and available light: further algorithms for remote-sensing. *Deep-Sea Research. Part A. Oceanographic Research Papers*, **35**(6), 855-879.

PLATT, T., SATHYENDRANATH, S., ULLOA, O., HARRISON, W.G., HOEPFFNER, N. and GOES, J., 1992. Nutrient control of phytoplankton photosynthesis in the Western North Atlantic. *Nature,* **356**(6366), pp. 229-231.

PLATT, T., SATHYENDRANATH, S., LONGHURST, A., WILSON, T.R.S., WOODS, J. and TAKAHASHI, T., 1995. Remote Sensing of Primary Production in the Ocean: Promise and Fulfilment [and Discussion]. *Philosophical Transactions of the Royal Society of London.Series B: Biological Sciences*, **348**(1324), pp. 191-202.

PLATT, T., BROOMHEAD, D.S., SATHYENDRANATH, S., EDWARDS, A.M. and MURPHY, E.J., 2003. Phytoplankton biomass and residual nitrate in the pelagic ecosystem. *Proceedings of the Royal Society of London.Series A: Mathematical, Physical and Engineering Sciences*, **459**(2033), pp. 1063-1073.

PLATT, T. and FUENTES-YACO, C K.T.F., 2003. Marine ecology: spring algal bloom and larval fish survival. *Nature*, **423**(6938), pp. 398-399.

PLATT, T., BOUMAN, H., DEVRED, E., FUENTES-YACO, C. and SATHYENDRANATH, S., 2005. Physical forcing and phytoplankton distributions. *Scientia Marina*, **69**, pp. 55-73.

PLATT, T., SATHYENDRANATH, S., FORGET, M. H., WHITE, G. N., CAVERHILL, C., BOUMAN, H., & SON, S. 2008. Operational estimation of primary production at large geographical scales. *Remote Sensing of Environment*, **112**(8), 3437-3448.

POLOVINA, J.J., HOWELL, E.A. and ABECASSIS, M., 2008. Ocean's least productive waters are expanding. *Geophysical Research Letters*, **35**(3), pp. 03618.

QUIROGA, I. and CHRÉTIENNOT-DINET, M., 2004. A new species of Minidiscus (Diatomophyceae, Thalassiosiraceae) from the eastern English Channel, France. *Botanica Marina*, **47**(4), pp. 341-348.

R CORE DEVELOPMENT TEAM 2009. R: A language and environment for statistical computing. R foundation for Statistical Computing, Vienna, Austria. ISBN 3-900051-07-0, URL http://www.R-project.org

RAIMBAULT, P., SLAWYK, G., COSTE, B. and FRY, J., 1990. Feasibility of using an automated colorimetric procedure for the determination of seawater nitrate in the 0 to 100 n*M* range: Examples from field and culture. *Marine Biology*, **104**(2), pp. 347-351.

RAVEN, J.A., 1982. The Energetics of Freshwater Algae; Energy Requirements for Biosynthesis and Volume Regulation. *New Phytologist*, **92**(1), pp. 1-20.

RAVEN, J.A., 1984. Physiological correlates of the morphology of early vascular plants. *Botanical Journal of the Linnean Society*, **88**(1-2), pp. 105-126.

RAVEN, J. A. 1991. Physiology of inorganic C acquisition and implications for resource use efficiency by marine phytoplankton: relation to increased CO2 and temperature. *Plant, Cell & Environment*, **14**(8), 779-794.

RAVEN, J., 1998. The twelfth Tansley lecture: Small is beautiful: The picophytoplankton. *Functional Ecology*, **12**(4), pp. 503-513.

RAVEN, J. A. 2011. The cost of photoinhibition. *Physiologia Plantarum*, *142*(1), 87-104.

RAVEN, J. and GEIDER, R.J., 1988. Temperature and algal growth. *New Phytologist*, **110**(4), pp. 441-461.

RAVEN, J. and FALKOWSKI, P., 2002. Oceanic sinks for atmospheric CO2. *Plant, Cell & Environment*, **22**(6), pp. 741-755.

RAVEN, J. A., & WAITE, A. M. 2004. The evolution of silicification in diatoms: inescapable sinking and sinking as escape? *New Phytologist*, **162**(1), 45-61.

REDALJE, D. G., & LAWS, E. A. 1981. A new method for estimating phytoplankton growth rates and carbon biomass. *Marine Biology*, **62**(1), 73-79.

REYNOLDS, C. S. 1994. The long, the short and the stalled: on the attributes of phytoplankton selected by physical mixing in lakes and rivers. *Hydrobiologia*, **289**(1), 9-21.

RIEBESELL, U., ZONDERVAN, I., ROST, B.È., TORTELL, P.D., ZEEBE, R.E. and MOREL, F.Ë.M.M., 2000. Reduced calcification of marine plankton in response to increased atmospheric CO_2. *Nature*, **407**(6802), 364-367.

RIEGMAN, R., KUIPERS, B.R., NOORDELOOS, A.A.M. and WITTE, H.J., 1993. Size-differential control of phytoplankton and the structure of plankton communities. *Netherlands Journal of Sea Research,* **31**(3), pp. 255-265.

ROCAP, G., LARIMER, F.W., LAMERDIN, J., MALFATTI, S., CHAIN, P., AHLGREN, N.A., ARELLANO, A., COLEMAN, M., HAUSER, L., HESS, W.R., JOHNSON, Z.I., LAND, M., LINDELL, D., POST, A.F., REGALA, W., SHAH, M., SHAW, S.L., STEGLICH, C., SULLIVAN, M.B., TING, C.S., TOLONEN, A., WEBB, E.A., ZINSER, E.R. and CHISHOLM, S.W., 2003. Genome divergence in two Prochlorococcus ecotypes reflects oceanic niche differentiation. *Nature,* **424**(6952), pp. 1042-1047.

RODRIGUEZ, F., GARRIDO, J.L., CRESPO, B.G., ARBONES, B. and FIGUEIRAS, F.G., 2006. Size-fractionated phytoplankton pigment groups in the NW Iberian upwelling

system: impact of the Iberian Poleward Current. *Marine Ecology Progress Series,* **323**, pp. 59-73.

ROY, S., SATHYENDRANATH, S. and PLATT, T., 2011. Retrieval of phytoplankton size from bio-optical measurements: theory and applications. *Journal of The Royal Society Interface*, **8**(58), pp. 650-660.

RYTHER, J. H. 1969. Photosynthesis and fish production in the sea. *Science*, **166**(3901), 72-76.

SABA, V. S., FRIEDRICHS, M. A. M., ANTOINE, D., ARMSTRONG, R. A., ASANUMA, I., BEHRENFELD, M. J., & WESTBERRY, T. K. 2010. An evaluation of ocean color model estimates of marine primary productivity in coastal and pelagic regions across the globe. *Biogeosciences Discussions*, **7**(5), 6749-6788.

SARMIENTO, J.L., HUGHES, T.M.C., STOUFFER, R.J. and MANABE, S., 1998. Simulated response of the ocean carbon cycle to anthropogenic climate warming. *Nature,* **393**(6682), pp. 249.

SATHYENDRANATH, S., LAZZARA, L., & PRIEUR, L. 1987. Variations in the spectral values of specific absorption of phytoplankton. *Limnology and Oceanography*, **32**(2), 403-415.

SATHYENDRANATH, S., PRIEUR, L. and MOREL, A., 1987. An evaluation of the problems of chlorophyll retrieval from ocean colour, for case 2 waters. *Advances in Space Research,* **7**(2), pp. 27-30.

SATHYENDRANATH, S., GOUVEIA, A.D., SHETYE, S.R., RAVINDRAN, P. and PLATT, T., 1991. Biological control of surface temperature in the Arabian Sea. *Nature*, **349**(6304), pp. 54-56.

SATHYENDRANATH, S., LONGHURST, A., CAVERHILL, C.M. and PLATT, T., 1995. Regionally and seasonally differentiated primary production in the North Atlantic. *Deep Sea Research Part I: Oceanographic Research Papers*, **42**(10), pp. 1773-1802.

SATHYENDRANATH, S., PLATT, T., STUART, V., IRWIN, B., VELDHUIS, M.J., KRAAY, G.W. and HARRISON, W.G., 1996. Some bio-optical characteristics of phytoplankton in the NW Indian Ocean . *Marine Ecology Progress Series*, **132**, pp. 299-311.

SATHYENDRANATH, S. and PLATT, T., 1998. Ocean-Color Model Incorporating Transspectral Processes. *Applied Optics*, **37**(12), pp. 2216-2227.

SATHYENDRANATH, S., COTA, G., STUART, V., MAASS, H. and PLATT, T., 2001. Remote sensing of phytoplankton pigments: A comparison of empirical and theoretical approaches. *International Journal of Remote Sensing*, **22**(2-3), pp. 249-273.

SATHYENDRANATH, S., STUART, V., PLATT, T., BOUMAN, H., ULLOA, O. and MAASS, H., 2005. Remote sensing of ocean colour: Towards algorithms for retrieval of pigment composition. *Indian Journal of Marine Sciences*, **34**(4), pp. 333-340.

SATHYENDRANATH, S., STUART, V., NAIR, A., OKA, K.N.,T., BOUMAN, H., FORGET, M., MAASS, H. and PLATT, T., 2009. Carbon-to-chlorophyll ratio and growth rate of phytoplankton in the sea. *Marine Ecology Progress Series*, **383**, pp. 73-84.

SAVIDGE, G., BOYD, P., POMROY, A., HARBOUR, D. and JOINT, I., 1995. Phytoplankton production and biomass estimates in the northeast Atlantic Ocean, May-June 1990. *Deep-Sea Research Part I: Oceanographic Research Papers,* **42**(5), pp. 599-617.

SCHLITZER, R. 2002. Ocean Data View, http://www.awi-bremerhaven.de/GEO/ODV

SCIASCIA, R., DE MONTE, S., & PROVENZALE, A. 2012. Physics of sinking and selection of plankton cell size. *Physics Letters A*. **337**, 467-472

SHALAPYONOK, A., OLSON, R. J., & SHALAPYONOK, L. S. 2001. Arabian Sea phytoplankton during Southwest and Northeast Monsoons 1995: composition, size structure and biomass from individual cell properties measured by flow cytometry. *Deep Sea Research Part II: Topical Studies in Oceanography*, **48**(6), 1231-1261.

SCHANZ, F., SENN, P., & DUBINSKY, Z. 1997. Light absorption by phytoplankton and the vertical light attenuation: ecological and physiological significance. *Oceanography and marine biology*, **35**, 71-96.

SHELDON, R. and PARSONS, T., 1967. A continuous size spectrum for particulate matter in the sea. *Journal of the Fisheries Board of Canada,* **24**(5), pp. 909-915.

SIERACKI, M.E., VERITY, P.G. and STOECKER, D.K., 1993. Plankton community response to sequential silicate and nitrate depletion during the 1989 North Atlantic spring bloom. *Deep-Sea Research Part II,* **40**(1-2), pp. 213-225.

SIMÓ, R., 2001. Production of atmospheric sulfur by oceanic plankton: biogeochemical, ecological and evolutionary links. *Trends in Ecology & Evolution,* **16**(6), pp. 287-294.

SIMON, N., LEBOT, N., MARIE, D., PARTENSKY, F. and VAULOT, D., 1995. Fluorescent *in-situ* hybridization with rRNA-targeted oligonucleotide probes to identify small phytoplankton by flow cytometry. *Applied and Environmental Microbiology*, **61**(7), pp. 2506-2513.

SMAYDA, T. J., & REYNOLDS, C. S. 2001. Community assembly in marine phytoplankton: application of recent models to harmful dinoflagellate blooms. *Journal of Plankton Research*, **23**(5), 447-461.

SMYTH, T.J., - TILSTONE, G.H. and - GROOM, S.B., 2005. Integration of radiative transfer into satellite models of ocean primary production. *Journal of Geophysical Research: Oceans* (1978-2012, **110**(C10).

SOMMER, U., 1989. Maximal growth rates of Antarctic phytoplankton: only weak dependence on cell size. *Limnology & Oceanography*, **34**(6), pp. 1109-1112.

SOSIK, H.M., 1996. Bio-optical modeling of primary production: consequences of variability in quantum yield and specific absorption. *Marine Ecology Progress Series*, **143**, pp. 225-238.

SOSIK, H.M. and MITCHELL, B.G., 1994. Effects of temperature on growth, light absorption and quantum yield in *Dunaliella tertiolecta* (Chlorophyceae). *Journal of Phycology*, **30**(5), pp. 833-840.

SOURNIA, A., 1982. FORM AND FUNCTION IN MARINE PHYTOPLANKTON. *Biological Reviews*, **57**(3), pp. 347-394.

SOURNIA, A., CHRDTIENNOT-DINET, M.J. and RICARD, M., 1991. Marine phytoplankton: how many species in the world ocean? *Journal of Plankton Research,* **13**(5), pp. 1093-1099.

STRICKLAND, J. D. H., & PARSONS, T. R. 1972. Inorganic micronutrients in sea water. *Stevenson, J. Ed., A*.

STUART, V., SATHYENDRANATH, S., HEAD, E.J.H., PLATT, T., IRWIN, B. and MAASS, H., 2000. Bio-optical characteristics of diatom and prymnesiophyte populations in the Labrador Sea. *Marine Ecology Progress Series,* **201**, pp. 91-106.

STUART, V., SATHYENDRANATH, S., PLATT, T., MAASS, H. and IRWIN, B.D., 1998. Pigments and species composition of natural phytoplankton populations: Effect on the absorption spectra. *Journal of Plankton Research,* **20**(2), pp. 187-217.

SUNDA, W. and HARDISON, D., 2010. Evolutionary tradeoffs among nutrient aquisition, cell size, and grazing defense in marine phytoplankton promote ecosystem stability. *Marine Ecology Progress Series,* **401**, pp. 63-76.

SUNDA, W. G., & HUNTSMAN, S. A. 1997. Interrelated influence of iron, light and cell size on marine phytoplankton growth. *Nature*, **390**(6658), 389-392.

SVEDRUP, H. U. 1953. On conditions for the vernal blooming of phytoplankton. *Journal du Conseil*, **18**(3), 287-295.

TAHEY, T.M., DUINEVELD, G.C.A., BRGHUIS, E.M. and HELDER, W., 1994. Relationship between sediment-water fluxes of oxygen and silicate and faunal

abundance at continental shelf, slope and deep water stations in the northwest Mediterranean. *Marine Ecology Progress Series,* **104**, pp. 119-130.

TARRAN, G.A., HEYWOOD, J.L. and ZUBKOV, M.V., 2006. Latitudinal changes in the standing stocks of nano- and picoeukaryotic phytoplankton in the Atlantic Ocean. *Deep Sea Research Part II: Topical Studies in Oceanography,* 53(14–16), pp. 1516-1529.

TAYLOR, A.H., GEIDER, R.J. and GILBERT, F.J.H., 1997. Seasonal and latitudinal dependencies of phytoplankton carbon-to-chlorophyll a ratios: results of a modelling study. *Marine Ecology Progress Series,* **152**, pp. 51-66.

TETT, P., & BARTON, E. D., 1995. Why are there about 5000 species of phytoplankton in the sea?. *Journal of plankton research*, **17**(8), 1693-1704.

TILSTONE, G., FIGUEIRAS, F., FERMIN, E., & ARBONES, B. 1999. Significance of nanophytoplankton photosynthesis and primary production in a coastal upwelling system (Ría de Vigo, NW Spain). *Marine Ecology. Progress Series*, **183**, 13-27.

TILSTONE, G., FIGUEIRAS, F.G., LORENZO, L.M. and ARBONES, B., 2003. Phytoplankton composition, photosynthesis and primary production during different hydrographic conditions at the Northwest Iberian upwelling system. *Marine Ecology Progress Series,* **252**, pp. 89-104.

TILSTONE, G., SMYTH, T., POULTON, A. and HUTSON, R., 2009. Measured and remotely sensed estimates of primary production in the Atlantic Ocean from 1998 to 2005. *Deep Sea Research Part II: Topical Studies in Oceanography,* **56**(15), pp. 918-930.

TORTELL, P., RAU, G. and MOREL, A., 2000. Inorganic carbon acquisition in coastal Pacific phytoplankton communities. *Limnology and Oceanography,* **45**(7), pp. 1485-1500.

TOZZI, S., SCHOFIELD, O., & FALKOWSKI, P. 2004. Historical climate change and ocean turbulence as selective agents for two key phytoplankton functional groups. *Marine Ecology Progress Series*, **274**, 123-132.

UITZ, J., CLAUSTRE, H., MOREL, A. and HOOKER, S., 2006. Vertical distribution of phytoplankton communities in open ocean: An assessment based on surface chlorophyll. *Journal of Geophysical research,* **111**(C8)

UITZ, J., HUOT, Y., BRUYANT, F., BABIN, M., CLAUSTRE, H. and CLAUSTRE, H., 2008. Relating Phytoplankton Photophysiological Properties to Community Structure on Large Scales. *Limnology and Oceanography,* **53**(2), pp. 614-630.

UITZ, J., CLAUSTRE, H., GENTILI, B. and STRAMSKI, D., 2010. Phytoplankton class specific primary production in the world's oceans: Seasonal and interannual variability from satellite observations. *Global Biogeochemical Cycles,* **24**(3),.

UITZ, J., CLAUSTRE, H., GRIFFITHS, F. B., RAS, J., GARCIA, N., & SANDONI, V. 2009. A phytoplankton class-specific primary production model applied to the Kerguelen Islands region (Southern Ocean). *Deep Sea Research Part I: Oceanographic Research Papers*, **56**(4), 541-560.

VAN DEN MEERSCHE, K., SOETAERT, K. and MIDDELBURG, J., 2008. A Bayesuan Compositional Estimator for microbial taxonomy based on biomarkers. *Limnology and Oceanography Methods,* **6**, pp. 190-199.

VAULOT, D., COURTIES, C. and PARTENSKY, F., 1989. A simple method to preserve oceanic phytoplankton for flow cytometric analyses. *Cytometry*, **10**, pp. 629-635.

VAULOT, D., PARTENSKY, F., NEVEUX, J., MANTOURA, R.F.C. and LLEWELLYN, C.A., 1990. Winter Presence of Prochlorophytes in Surface Waters of the Northwestern Mediterranean Sea. *Limnology and Oceanography*, **35**(5), pp. 1156-1164.

VAULOT, D., BIRRIEN, J., MARIE, D., CASOTTI, R., VELDHUIS, M.J.W., KRAAY, G.W. and CHRÉTIENNOT-DINET, M., 1994. Morphology, ploidy, pigment composition and genome size of cultured strains of Phaeocystis (Prymnesiophyceae). *Journal of Phycology*, **30**(6), pp. 1022-1035.

VELDHUIS, M.J. and KRAAY, G.W., 1990. Vertical distribution and pigment composition of a picoplanktonic prochlorophyte in the subtropical North Atlantic: a combined study of HPLC-analysis of pigments and flow cytometry. *Marine Ecology Progress Series*, **68**(1), pp. 121-127.

VELDHUIS, M.J.W. and KRAAY, G.W., 2004. Phytoplankton in the subtropical Atlantic Ocean: towards a better assessment of biomass and composition. *Deep Sea Research Part I: Oceanographic Research Papers*, **51**(4), pp. 507-530.

VIDUSSI, F., CLAUSTRE, H., MANCA, B.B., LUCHETTA, A. and MARTY, J., 2001. Phytoplankton pigment distribution in relation to upper thermocline circulation in the eastern Mediterranean Sea during winter. *Journal of Geophysical Research*, **106**, pp. 19939-19956.

WARD, B., DUTKIEWICZ, S., JAHN, O. and FOLLOWS, M., 2012. A size-structured food-web model for the global ocean. *Limnology and Oceanography,* **57**(6), pp. 1877.

WARNER, A. and HAYS, G., 1994. Sampling by the continuous plankton recorder survey. *Progress in Oceanography,* **34**(2), pp. 237-256.

WASSMANN, P., RATKOVA, T. and REIGSTAD, M., 2005. The contribution of single and colonial cells of Phaeocystis pouchetii to spring and summer blooms in the north-eastern North Atlantic. *Harmful Algae,* **4**(5), pp. 823-840.

WESTBERRY, T., BEHRENFELD, M., SIEGEL, D., & BOSS, E. 2008. Carbon-based primary productivity modeling with vertically resolved photoacclimation. *Global Biogeochemical Cycles*, **22**(2).

WELSCHMEYER, N. A. 1994. Fluorometric analysis of chlorophyll a in the presence of chlorophyll b and pheopigments. *Limnology and Oceanography*, 1985-1992.

WHITMAN, W.B., COLEMAN, D.C. and WIEBE, W.J., 1998. Prokaryotes: the unseen majority. *Proceedings of the National Academy of Sciences*, **95**(12), pp. 6578-6583.

WICKHAM, H., 2009. ggplot2: Elegant Graphics for Data Analysis. 2nd edn. *Springer Publishing Company, Incorporated*.

WILK-WOŹNIAK, E., POCIECHA, A. and BUCKA, H., 2002. Phytoplankton-zooplankton interactions, size relations and adaptive responses. A short review. *Ecohydrology and Hydrobiology,* **1**(4), pp. 511-517.

WRIGHT, S., JEFFREY, S. and MANTOURA, R., 1997. *Phytoplankton pigments in oceanography: guidelines to modern methods.* Unesco Pub.

WRIGHT, S.W. and VAN DEN ENDEN, R.L., 2000. Phytoplankton community structure and stocks in the East Antarctic marginal ice zone (BROKE survey, January–March 1996) determined by CHEMTAX analysis of HPLC pigment signatures. *Deep Sea Research Part II: Topical Studies in Oceanography,* 47(12–13), pp. 2363-2400.

WRIGHT, S.W. and VAN DEN ENDEN, R.L., PEARCE, I., DAVIDSON, A. T., SCOTT, F. J., & WESTWOOD, K. J. (2010). Phytoplankton community structure and stocks in the Southern Ocean (30–80 E) determined by CHEMTAX analysis of HPLC pigment signatures. *Deep Sea Research Part II: Topical Studies in Oceanography*, *57*(9), 758-778.

WRIGHT, S.W., 2005. Analysis of phytoplankton populations using pigment markers, *Workshop on pigment analysis of Antarctic microorganisms* 2005.

YENTSCH, C.S. and MENZEL, D.W., 1963. A method for the determination of phytoplankton chlorophyll and phaeophytin by fluorescence. *Deep Sea Research and Oceanographic Abstracts,* **10**(3), pp. 221-231.

YENTSCH, C.S. and PHINNEY, D.A., 1989. A bridge bewteen ocean optics and microbial ecology. *Limnology & Oceanography,* **34**(8), pp. 1649-1705.

YENTSCH, C.S., 1962. Measurement of Visible Light Absorption by Particulate Matter in the Ocean. *Limnology and Oceanography,* **7**(2), pp. 207-217.

ZUBKOV, M.V., SLEIGH, M.A., BURKILL, P.H. and LEAKEY, R.J.G., 2000. Picoplankton community structure on the Atlantic Meridional Transect: a comparison between seasons. *Progress in Oceanography,* **45**(3–4), pp. 369-386.

ZUBKOV, M.V., SLEIGH, M.A., TARRAN, G.A., BURKILL, P.H. and LEAKEY, R.J.G., 1998. Picoplanktonic community structure on an Atlantic transect from 50°N to 50°S. *Deep Sea Research Part I: Oceanographic Research Papers*, **45**(8), pp. 1339-1355.